

The dynamic mechanical properties of keratin fibres

Author:

Danilatos, Gerasimos Daniel

Publication Date:

1977

DOI:

<https://doi.org/10.26190/unsworks/4861>

License:

<https://creativecommons.org/licenses/by-nc-nd/3.0/au/>

Link to license to see what you are allowed to do with this resource.

Downloaded from <http://hdl.handle.net/1959.4/56156> in <https://unsworks.unsw.edu.au> on 2024-04-27

THE DYNAMIC MECHANICAL PROPERTIES
OF KERATIN FIBRES

by

GERASIMOS D. DANILATOS

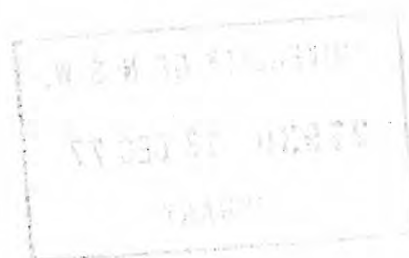
A thesis presented for the degree of

Doctor of Philosophy

in the School of Textile Technology

University of New South Wales

May 1977



THE UNIVERSITY OF NEW SOUTH WALES

DECLARATION RELATING TO DISPOSITION OF THESIS

This is to certify that I G. D. DANILATOS being a candidate for the degree of DOCTOR OF PHILOSOPHY am fully aware of the policy of the University relating to the retention and use of higher degree theses, namely that the University retains the copies of any thesis submitted for examination, "and is free to allow the thesis to be consulted or borrowed. Subject to the provisions of the Copyright Act (1968) the University may issue the thesis in whole or in part, in photostat or microfilm or other copying medium."

In the light of these provisions I grant the University Librarian permission to publish, or to authorise the publication of my thesis, in whole or in part, as he deems fit.

I also authorize the publication by University Microfilms of a 600 word abstract in Dissertation Abstracts International (D.A.I.).

This is to certify that the work herein has been carried out by the undersigned in the School of Textile Technology, University of New South Wales, and has not been submitted previously for any other award or degree.

G. DANILATOS

ACKNOWLEDGEMENTS

The author wishes to thank Professor M. Feughelman for the valuable discussions, encouragement and the overall help which he has given throughout the course of these studies; Professor R. Postle for the encouragement and help, and Mr. O. Zubzanda for his useful advice on problems of electronics.

Further, the author wishes to acknowledge the award of a Dean's Scholarship for postgraduate research in the Faculty of Applied Science.

ABSTRACT

The complex modulus of single keratin fibres has been studied at various extensions or times as well as at different relative humidities, temperatures and frequencies. Two parameters of the complex modulus were measured, namely the dynamic modulus and the loss angle.

To carry out measurements for the above studies a dynamic mechanical tester was designed and constructed. By using a piezoelectric element the apparatus allows for measurements to be taken in the frequency range 6 Hz to 1500 Hz, while with an environment conditioning chamber the full range of relative humidities and the range of -100°C to $+50^{\circ}\text{C}$ for temperatures can be covered. Fine fibre samples can be extended in the apparatus and tested at each extension. Considerable precautions were taken in the apparatus to reduce noise because of the small values of the signals detected.

By using the above equipment it was found that the modulus of wool fibres decreases with strain up to intermediate extensions of about 20% and then increases with higher extensions. The loss angle variation with extension is inverse to the modulus changes. The complex modulus was also measured while fibres were extension cycled or relaxed at fixed strains. More measurements were taken under other specific conditions of strain. All of these results, it was shown, could be explained by the application of the two-phase structure model of keratin: one phase C being relatively impenetrable to water and possessing elastic properties at all extensions, and the other phase M being water penetrable and acting mechanically as a viscoelastic solid.

Measurements on fibres were carried out during abrupt relative humidity changes at a constant frequency and temperature. For an abrupt

relative humidity increase it was found that the loss angle vs time exhibits an overshoot at the time when the absorption is nearly completed, while the modulus curve is changing markedly at the same time. This result was compatible with the suggestion that the structural mobility of the keratin fibre reaches a maximum at the time when absorption is almost complete.

The complex modulus of wet keratin fibres was measured in the frequency range of 6 - 1500 Hz at different temperatures between 0.2 and 45°C. Some measurements were taken at different relative humidities. These results together with results of other workers indicated the presence of a characteristic transition process in keratin dependent strongly on the water content. This process was attributed to the main chain motion in the M phase.

LIST OF SYMBOLS

a	amplitude of a-c strain
a*	complex strain
a ₀	constant static strain
a _T	shift factor
A	amplitude of displacement for propagating wave or cross-sectional area
B	amplitude of displacement for reflected wave
c	phase velocity
c*	complex velocity
c ₁ , c ₂	constants in the WLF equation
C, C _p	capacitance or $C = E_r \frac{\xi l}{\xi l_r}$
C _p	specific heat at constant pressure
C _a	specific heat at constant strain
d _v	diametral variation in percent
D	$D = \frac{1}{2} \tan \delta$
E	magnitude of complex modulus
E*	complex modulus
E'	dynamic (storage) modulus; the component of complex modulus in-phase with the displacement
E''	loss modulus; the component of complex modulus in- quadrature with the displacement
E ₁	component of dynamic modulus associated with relaxation
E _m	relaxation modulus, or complex modulus of phase M
E _c	dynamic modulus of the elastic phase C
E _u	unrelaxed (instantaneous or initial) modulus
E _r	relaxed (equilibrium or final) modulus
E _a	apparent modulus

f	frequency
f	static (d-c) stress
F	$F = \omega l / c$
g_1	geometrical correction factor at 100% R.H.
g_2	geometrical correction factor at 0% R.H.
i	intercept or $i = \sqrt{-1}$
k	wave number
l	length
m	mass
n	number of moles
N	magnitude of transducer ratio
N^*	complex transducer ratio
$\left. \begin{matrix} p \\ p' \\ p'' \end{matrix} \right\}$	amplitudes of various a-c forces
σ_r	amplitude of reference a-c stress
σ_r^*	complex reference stress
P	ambient pressure
P_i, P_f	initial and final partial vapour pressure
P_{si}, P_{sf}	initial and final saturation vapour pressure
r	regain
r_i, r_f	initial and final regain
R	frictional element or electrical resistance
RH	relative humidity
RH_i, RH_f	initial and final relative humidity
s	stiffness or slope
t	time
T	absolute temperature
T_i, T_f	initial and final temperature

u	amplitude of velocity
u^*	complex velocity
V	volume or a-c voltage
V^*	complex voltage
V_r	amplitude of a-c reference voltage
V_i, V_f	initial and final volume
W	weight
x	thickness
Z^*	complex mechanical impedance
Z_0	characteristic mechanical impedance of a medium
Z_{in}	input mechanical or electrical impedance.
Z_t	terminal mechanical impedance
Z_p	electrical impedance
α	attenuation coefficient or $\alpha \langle \ln \tau \rangle$
β	thermal expansion coefficient or the width of the log-normal distribution function
γ	amplitude of acceleration
Δn	g-moles of water leaving the buffer wool
ΔW	energy absorbed per cycle per unit volume
δ	loss angle
δ_m	loss angle of the phase M
δ_p	loss angle of the p-z element
ϵ	static strain in percent
η	viscosity
θ	measured angle
κ	strain rate
μ	linear density
ξ, ξ'	amplitude of a-c displacement
ξ^*	complex displacement

ρ	density
σ	amplitude of a-c stress
σ^*	complex stress
Σ	resultant a-c free
τ	relaxation time constant
ϕ	angle
χ	distance
$\psi(t)$	normalised relaxation function
ω	angular frequency

CONTENTS

<u>CHAPTER 1</u>	<u>Page No.</u>
<u>The Structure and Properties of Keratin</u>	1
1.1 Introduction	1
1.2 The Histology	1
1.3 The Fine Structure	2
1.4 The Chemical Composition	4
1.5 The Mechanical Properties	4
1.5.1 Extension	4
1.5.2 Sorption	6
1.5.3 Temperature-Time Effects, Complex Modulus	7
1.6 Experimental Techniques	10
1.7 Terminology Used	11
1.8 Summary	11
 <u>CHAPTER 2</u>	
<u>The Building of a Dynamic Mechanical Tester</u>	12
2.1 Introduction	12
2.2 Propagation of Acoustical Waves in a Loss Free Medium	12
2.3 Measured Angle and Loss Angle	15
2.4 Measurement of the Alternating Force	18
2.5 The Instruments Used	23
2.6 Conditioning of the Sample	27
2.6.1 Conditioning Chamber	28
2.6.2 Temperature Control	29
2.6.3 Humidity Control	30

	<u>Page No.</u>	
2.7	Noise	31
	2.7.1 Mechanical Noise	32
	2.7.2 Electrical Noise	32
2.8	Calibration of the Apparatus	33
2.9	Errors	35
2.10	Conclusion	35

CHAPTER 3

	<u>The Complex Modulus of Keratin Against Extention</u>	37
3.1	Introduction	37
3.2	Preparation of Samples	37
3.3	Measurements at Low Extensions - Unit Modulus	38
3.4	The Effect of Strain on the Complex Modulus of Wool in Water	41
3.5	The Effect of Strain on Complex Modulus at Different Relative Humidities.	42
3.6	The Effect of Rate of Static Strain at Different Relative Humidities	43
3.7	The Two Phase Model	44
	3.7.1 The Phase C	46
	3.7.2 The Phase M	49
3.8	Application of the Two Phase Model	53
	3.8.1 Integration of the Elastic Term	53
	3.8.2 Integration of the Viscoelastic Term	56
	3.8.3 Discussion of the Experimental Results	58
3.9	Energy Considerations - Loss Modulus	61
3.10	Measurement of Complex Modulus of a Fibre Relaxing in Water at Fixed Extensions	62
	3.10.1 Discussion	63

	<u>Page No.</u>	
3.11	The X-Y Series Zone Model	66
3.12	The Effects of Extension Cycling	68
3.13	Relaxation During Retraction of an Extension Cycle	71
3.14	The Effect of Strain at Various Frequencies	72
3.15	The Effect of Strain on Different Polymers	73
	3.15.1 Terylene	73
	3.15.2 Nylon	74
	3.15.3 Cupresa	74
	3.15.4 Discussion	75
3.16	Conclusion	76
 <u>CHAPTER 4</u>		
	<u>The Complex Modulus During Sorption</u>	78
4.1	Introduction	78
4.2	Transient Phenomena During Absorption of Water by Keratin Fibres	78
4.3	The Complex Modulus at Low Extensions Following Changes in Relative Humidity	79
	4.3.1 Tests on Horse Hair	80
	4.3.2 Tests on Lincoln Wool	83
4.4	Qualitative Explanation of the Results	84
4.5	Corroborative Evidence from Published Work	88
	4.5.1 Experiments with D ₂ O	88
	4.5.2 Stresses Developed Due to Regain Change by Absorption	88
	4.5.3 Kinetic Studies of the Wool-Water System	90
4.6	The Complex Modulus During Absorption and Desorption at Fixed Extensions	93
	4.6.1 Desorption	94
	4.6.2 Absorption	96
4.7	Conclusion	98

<u>CHAPTER 5</u>	<u>Page No.</u>
<u>The Time-Temperature Dependence of the Complex Modulus of Keratin Fibres</u>	101
5.1 Introduction	101
5.2 The Modulus of Keratin Fibres as a Function of Time	101
5.3 Experimental Results	103
5.4 Analysis of the Results	105
5.5 Comparison with Published Data	109
5.6 Theoretical Fit	113
5.7 The Loss Angle	115
5.8 Discussion	115
5.9 Conclusion	118
 <u>CHAPTER 6</u>	
<u>Conclusion</u>	120
6.1 Summary	120
6.2 The Experimental Technique	120
6.3 The Keratin as a Viscoelastic Material	121
6.4 The Keratin Under Extension	121
6.5 Transient Phenomena in Keratin	122
6.6 Future Work	123
 <u>APPENDIX A</u>	124
The Apparent Modulus	124
 <u>APPENDIX B</u> Drawings of Apparatus	125
 <u>APPENDIX C</u>	126
C.1 Solutions for Maintaining Constant Relative Humidity	126
C.2 Calculation of the Required Quantity of Buffer Wool	127
 REFERENCES	129

CHAPTER 1

THE STRUCTURE AND PROPERTIES OF KERATIN

1.1 Introduction

Natural proteins occur in two forms, globular and fibrous. Keratins are a class of fibre proteins in which wool, hair and horn constitute a subdivision, the hard mammalian keratins.

Because relatively little work has been done on the study of the dynamic mechanical properties of keratin, in this thesis the main objective of the research is concerned both with the construction of a dynamic tester and the study of the complex modulus of hard mammalian keratins in order to further understand and elucidate the structural features of keratins in terms of these measurements. A review of the structure as well as of some physical and chemical properties of this latter form of keratin is presented below as an introduction to the present work.

1.2 The Histology

Lincoln wool and horse hair were used for the tests in the present work and therefore a brief review of the important elements of the histology of keratin fibres, following Bendit and Feughelman¹² is given below; detailed description of the histology of keratin fibres is given by Fraser et al⁵².

In general, keratin fibres have three major components, cuticle, cortex and medulla, the first two of which are shown in figure (1-1)⁸⁰. The cortex, which forms the bulk of the fibre, consists of spindle-shaped keratinized cells $\approx 100\mu$ long and $\approx 5\mu$ across. The internal structure of these cortical cells is highly complex.

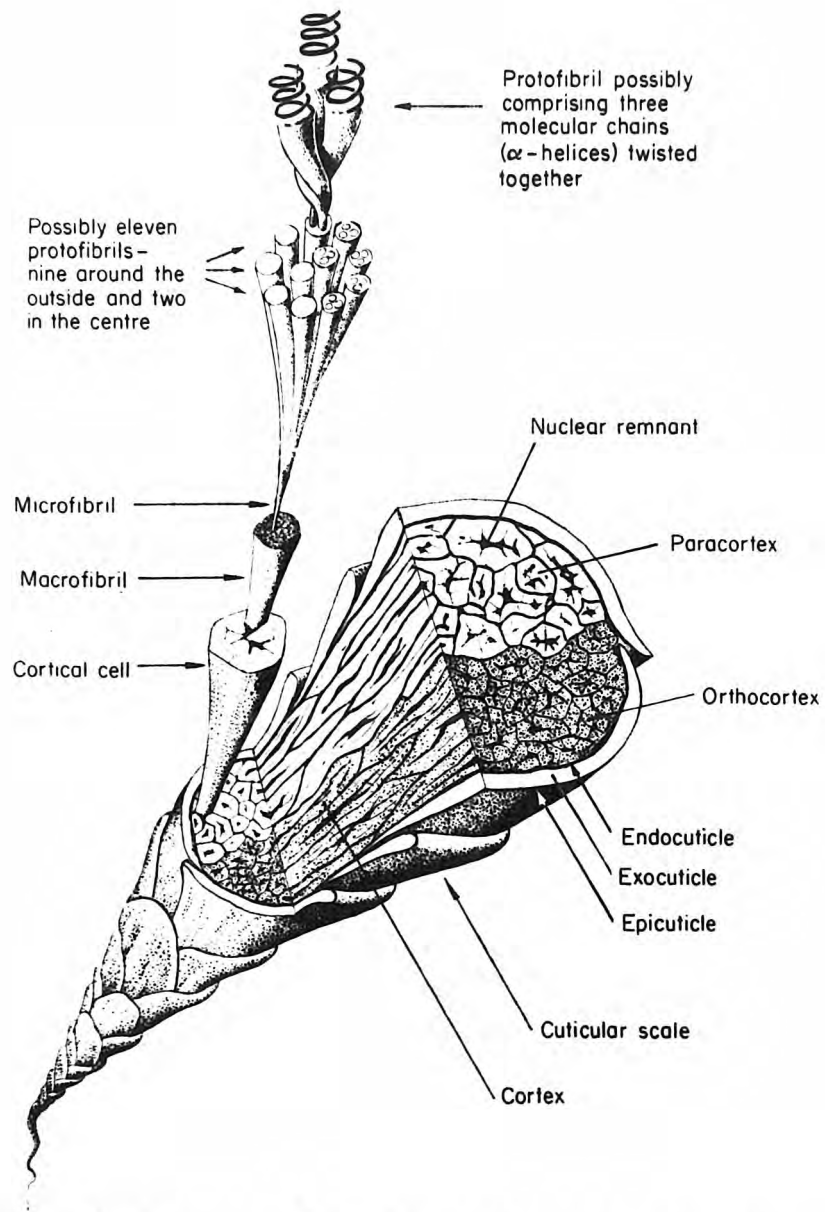


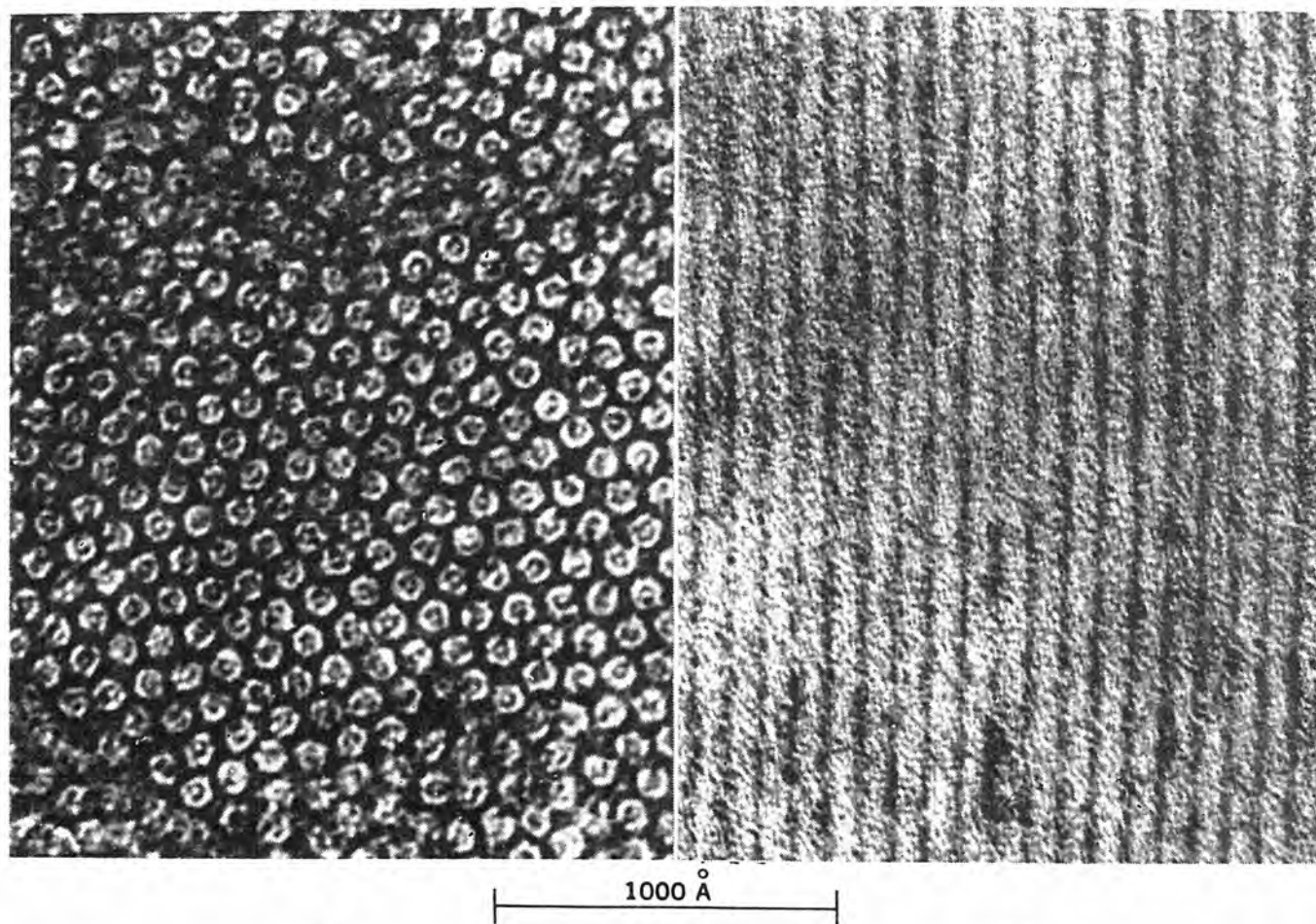
FIG.1-1. Diagram showing one possible way in which the α -helix molecules and protofibrils are grouped within the microfibrils of wool. (After Ryder and Stephenson.)

The cortex is enclosed by layers of protein material referred to as the cuticle, which forms an envelope of overlapping scales surrounding the fibre. Each scale or scale cell consists of an outer keratinous layer (the exocuticle) and an inner nonkeratinous layer (the endocuticle). These cuticular layers are bounded on the outside by a very resistant membrane, the epicuticle, which is only about 100 \AA thick. Coarse fibres usually have a cuticle many scale cells thick. The third main component is the medulla, an axial region consisting of cavities formed by large cells, which is generally found only in coarse fibres, or in structures such as quills, and is usually absent in fine animal hairs. In addition to these major components, keratin fibres generally contain lipids, melanin pigments, nuclear remnants and other nonkeratinous inclusions.

There are two types of cortical cells termed ortho and para cells and may be distinguished by histological staining techniques or by their appearance in electron micrographs. The cells in the paracortex are more highly keratinized (hardened) than those in the orthocortex. The former are found for crimped Merino wool fibres in the concave half of the crimp wave, whereas the latter are found in the convex half. In contrast to the so-called bilateral structure found in Merino wool, some almost straight or slightly wavy fibres (e.g. Lincoln wool) have a radial distribution of cells, with the para-like cells in an annular region around a central core consisting of ortho-like cells.

1.3 The Fine Structure

Electron microscopy bridges the gap between molecular dimensions and objects visible with the light microscope. In transverse sections of wool fibres examined with the light microscope



(a)

(b)

Fig. 1-2 Electron micrographs (50) of porcupine quill tip (*Hystrix cristata*). (a) Cross section of cortex; (b) longitudinal section of cortex.

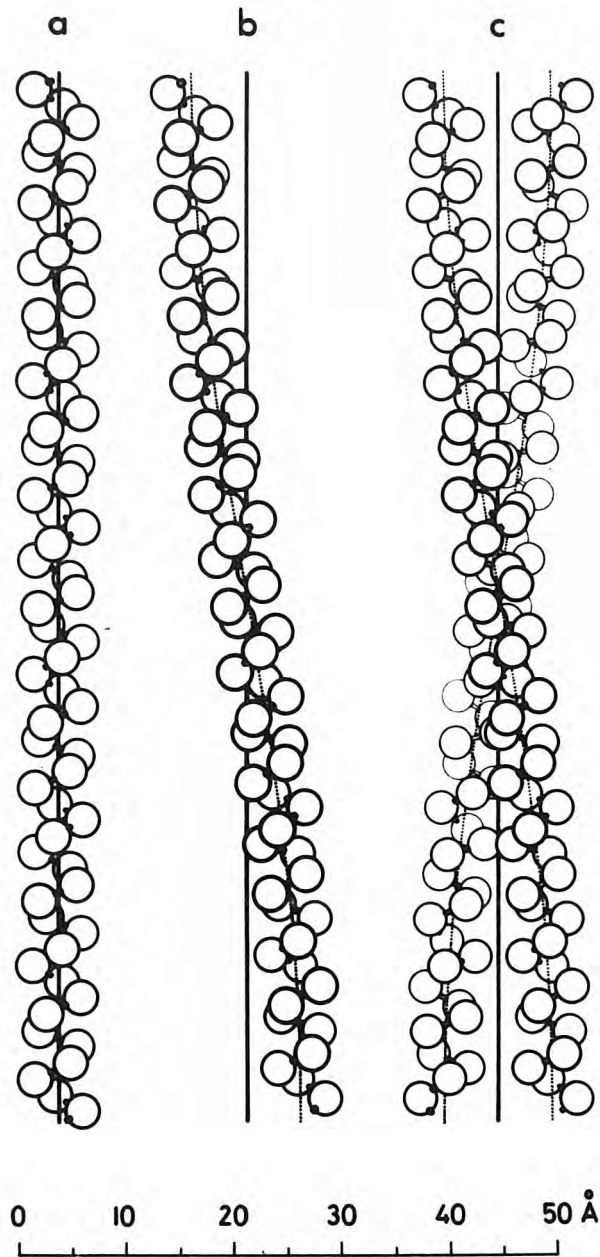


Figure 1-3 The two-strand coiled coil rope model for the regular secondary structure in α -keratin. (a) Right-handed α -helix; each residue has been represented by a sphere centered on the α -carbon atom. The diameter of the sphere is arbitrary and has no physical significance. (b) The same α -helix distorted into a coiled coil. The original axis, shown dotted, is distorted into a left-hand helix of pitch 186 Å. (c) A two-strand rope in which a pair of coiled coils are so positioned relative to each other that "knob-hole" packing of the residues is achieved in the interior of the rope along its entire length.

fibrillar structures known as macrofibrils are just visible within the cortical cells (fig. 1-1). Electron microscopy has shown that these are built up from smaller aligned filaments, rodlike structures of indefinite length - the microfibrils, embedded in nonaligned material - the matrix (fig. 1-2).^{26, 59, 78, 79} The diameter of the microfibrils has been estimated to be $\approx 80 \text{ \AA}$, their centre-to-centre distance in the range $85\text{-}100 \text{ \AA}$ depending on the type of keratin. The mode of packing of the microfibrils was found to vary according to species, and also depended on the type of cortical cell: the packing ranges from near perfect hexagonal arrays to totally irregular packing or whorl arrangements. Every microfibril is constituted of still smaller units, the protofibrils, with diameter $\approx 20 \text{ \AA}$. Nine of the protofibrils in a microfibril are arranged in an outer ring (fig. 1-1) and two in the centre. However, there is some controversy about the presence of the protofibrils in the centre, but the total number must be about ten¹⁹. The microfibrils also exhibit longitudinal fine structure with 200 \AA periodicity, consisting of a lightly stained region $\approx 160 \text{ \AA}$ long and a more heavily stained region $\approx 40 \text{ \AA}$ long²⁰. The protofibrils (fig. 1-1) split into smaller units (two or three) of $\approx 10 \text{ \AA}$ diameter, which are believed to be macromolecular helices, the α -helices (see fig. 1-3). Crick¹⁷ suggested that two or three α -helices could pack together at an angle, which would allow the side chains of one helix to fit into the space between side chains of another, forming the so called coiled-coils.

The matrix consists of amorphous material in general. Globular material⁸² has been reported to exist in the matrix and some polypeptide helices may be present but not in an organized form³⁷.

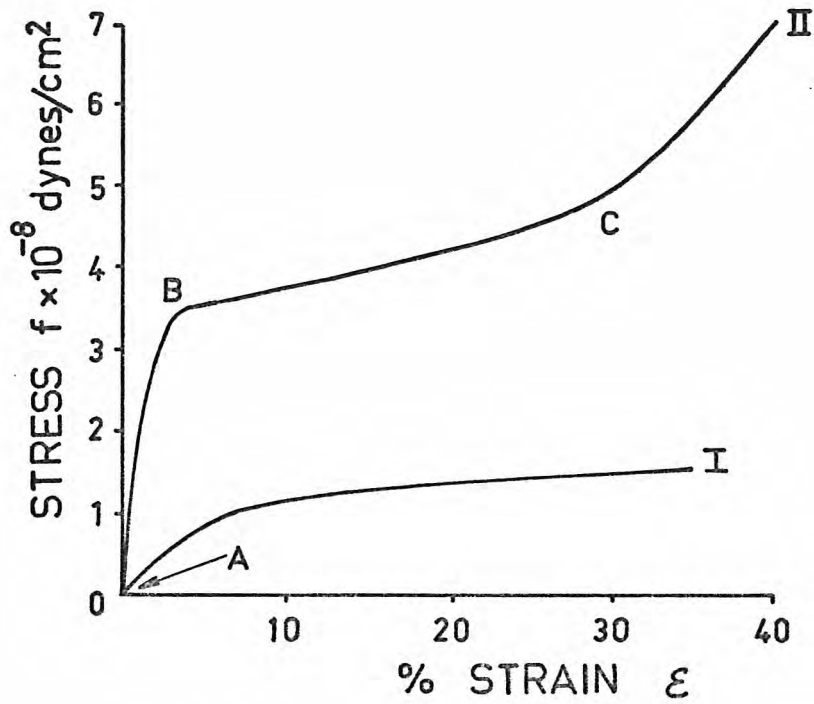
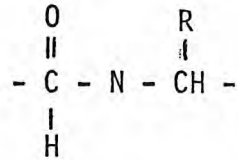


Fig. 1-4 The stress-strain relationship for an African porcupine quill in water at 20° C in (I) the direction perpendicular to growth (II) the direction parallel to growth.

1.4 The Chemical Composition

Keratin, as a protein, consists of polypeptide chains, the repeat unit of which is



where R denotes the side chain of the respective amino acid residue.

At present, twenty different residues have been identified¹².

Chemical reduction of native keratin yields two main protein fractions, namely, the low sulfur group SCMKA and the high-sulfur group SCMKB⁵².

The low-sulfur fraction SCMKA has a high helix content and contains proteins with molecular weights in the range 45000 to 63000. The high-sulfur fraction has a much lower range of molecular weights 14000 to 18000. It has been suggested¹² that the main proportion of these fractions originate from different regions of the native keratin.

1.5 The Mechanical Properties

Some mechanical properties of keratin fibres relating to the present work are presented below.

1.5.1 Extension

If a keratin fibre is stretched and the (static) stress f plotted against strain ϵ at a constant rate of strain, we obtain a curve similar to the curve (II) in fig. 1-4. The general shape of the curve is the same irrespective of regain and temperature (in a wide range). There are three well-defined regions whose names - "Hookean", "yield", and "post-yield" - were given by early workers in the field. This omits the initial decrimping region corresponding to the straightening of the fibre, which varies considerably depending on the initial crimp of the fibre under test.

In the Hookean region the extension is nearly proportional to the load as required by Hooke's law. The slope of the straight-line portion of the Hookean region gives the Young's modulus according to the relation

$$\text{Young's modulus} = \frac{\text{stress}}{\text{strain}} = \frac{\text{load/cross-sectional area}}{\text{extension/original length}}$$

However, the behaviour is not truly spring-like because the Young's modulus of this polymer (keratin is a biopolymer) is not independent of the rate at which the fibre is stretched. The concept of incremental or slope modulus is very often used for extensions beyond the Hookean region. We find that for a fibre in water the slope moduli in the Hookean, yield and post-yield regions are approximately in the ratio of 100:1:10. The Hookean region lies approximately between 0 and 2% strain with a Young's modulus of the order of 10^{10} dynes/cm², and the yield region is between approximately 2 and 30% strain. The effect of temperature increase is to reduce the slope modulus at all strains; similarly, the increase of water content in keratin also reduces the slope at all strains. The amount by which the temperature or the water content affect the slope modulus at any particular strain depends on the applied rate of strain: increasing the rate of straining generally increases the slope modulus¹².

The stress-strain relationship for an African porcupine quill in water at 20°C was obtained by Feughelman and Druhala⁹⁹ in (I) the direction perpendicular to growth (II) the direction parallel to growth (fig. 1-4). The curve (II) as pointed out above is a representative curve for any keratin fibre for longitudinal extension. The curve (I) does not have the three distinct regions of curve (II). Thus keratin is highly anisotropic.

The mechanical properties of keratin fibres are closely related to their molecular or near molecular structure. Thus curve (I) is associated mainly with the matrix, while curve (II) for a fibre in water reflects mainly the properties of the microfibrillar structure. The unextended microfibrils contain the α -helices, which proceeding from a few percent extension onwards⁷ are transformed into β -form (pleated-sheet structures¹²). The $\alpha \rightarrow \beta$ transformation combined with the series-zone model (X-Y zones)³⁵ provide a satisfactory explanation of the stress-strain curve with longitudinal extension.

Except for Mason⁶⁹ who measured the incremental modulus for some fixed strains and Woo and Postle who measured the sonic modulus of wool at discrete strains and room conditions, no work has been reported on the modulus against the complete continuous range of extension at various humidities. For this reason a considerable part of the present work is aimed at fulfilling this deficiency.

1.5.2 Sorption

Keratin can absorb (or desorb) water from (or to) the environment in relatively large quantities depending on the relative humidity. The amount of moisture in a specimen may be expressed in terms of regain r , which is defined as⁷³.

$$r = \frac{\text{mass of absorbed water in specimen}}{\text{mass of dry specimen}} \times 100\%$$

The unextended fibre is penetrable by water mainly in the matrix while the microfibrillar structure takes up only small quantities of water³⁰.

Numerous studies have been done on the kinetics of the wool-water system by Watt, Mackay and Downes and others^{89,90,100,21}. These studies have been concerned mainly with the measurement of water content during absorption or desorption.

The static stress during sorption has been examined extensively by Feughelman but no work has been done on the measurement of the

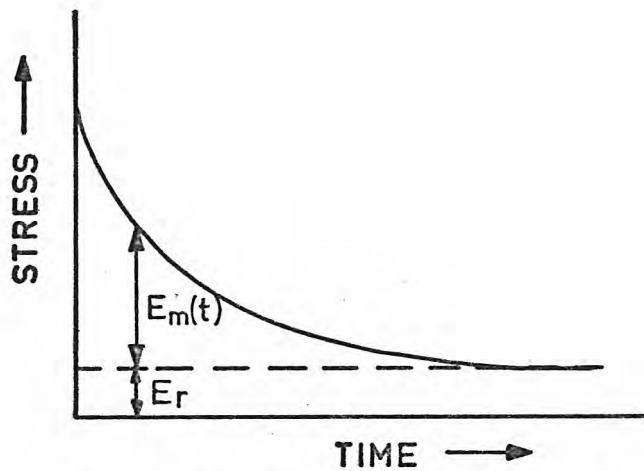


Fig. 1-5 Stress-Time relationship for unit strain applied at $t=0$.

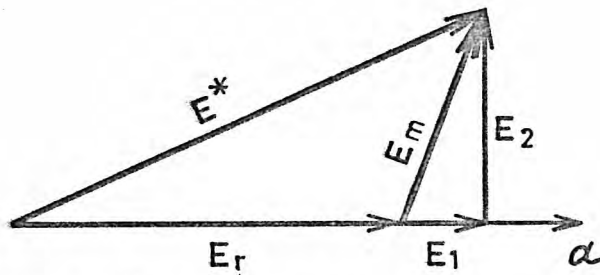


Fig. 1-6 The vector diagram relating the complex modulus to its component moduli.

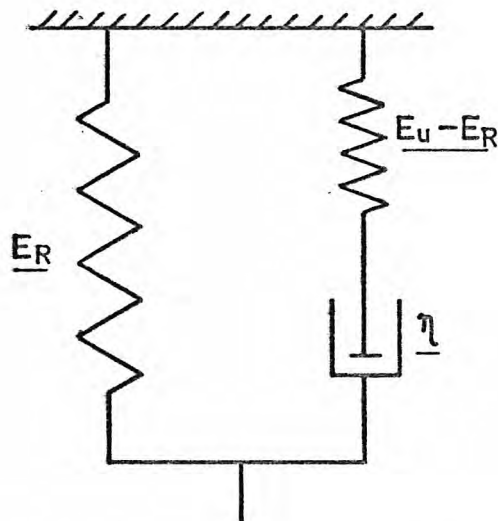


Fig. 1-7 The "standard linear solid" model. E_R and $E_U - E_R$ are the moduli of the two springs and η the viscosity of the dashpot.

modulus during absorption or desorption. This present work seeks to overcome to some extent this lack of information.

1.5.3 Temperature-Time Effects, Complex Modulus

It was pointed out previously that the modulus of keratin depends on the rate of strain and the temperature. This dependence is characteristic of all viscoelastic materials, which exhibit behaviour combining both liquid-like and solid-like characteristics. Some fundamental concepts of the viscoelastic theory is given below⁵⁴.

Application of a constant strain a_0 on a viscoelastic material produces a stress $f(t)$ given by (fig. 1-5)

$$f(t) = E(t)a = [E_r + E_m(t)] a \quad a = \begin{cases} 0 & t < 0 \\ a_0 & t > 0 \end{cases} \quad (1-1)$$

where E_r is the relaxed (equilibrium) elastic modulus, $E_u = E_r + E_m(0)$ the unrelaxed (instantaneous) elastic modulus and $E_m(t)$ the relaxation function, with $E_m(\infty) = 0$

Application of alternating strain with amplitude a and angular frequency ω produces in the steady state a sinusoidal stress, which is part in phase and part in quadrature with the strain. Therefore, the complex stress σ^* can be written

$$\sigma^* = E^* a^* \quad \text{where } a^* = a \exp(i\omega t) \quad (1-2)$$

and E^* the complex modulus. Reducing E^* into real and imaginary components one gets (fig. 1-6).

$$E^* = E' + i E'' \quad (1-3)$$

where E' is the dynamic (storage) modulus and E'' the loss modulus. The dynamic modulus E' can be considered as the sum of two moduli, namely E_r the relaxed modulus independent of time together with a

modulus E_1 which is dependent on the viscoelastic nature of the fibre under test i.e. $E' = E_r + E_1$. We further define a modulus E_m given by $E_m = E_1 + iE''$ and is therefore associated with the viscoelastic properties of the fibre.

Throughout this present work, for simplicity, the term dynamic modulus or, simply, modulus will be used to imply the in-phase component E' of the complex modulus. Any modulus other than E' will be specified accordingly. A useful quantity which can be measured experimentally with relative ease is the $\tan \delta$, the loss tangent given

$$\text{by } \tan \delta = \frac{E''}{E'}$$

or the loss angle δ given by

$$\delta = \tan^{-1} \frac{E''}{E'} \quad (1-4)$$

This angle δ denotes the angle by which the stress σ^* leads the strain a^* , i.e.

$$\sigma^* = \sigma \exp(i\omega t + \delta) \quad (1-5)$$

where σ is the amplitude of the alternating stress which is given by

$$\sigma = E a \quad (1-6)$$

where $E = |E^*|$ the amplitude of complex modulus. When δ is relatively small, then it can be considered that $E' \approx |E^*|$.

The complex modulus is generally a function of the applied frequency. In the particular case of the "standard linear solid" model in which the mechanical properties of a viscoelastic material is replaced by a spring in parallel with a spring and dashpot in series, the dependence of the various components of the complex modulus is given below^{88,98}.

$$E' = \frac{E_r + \omega^2 \tau^2 E_u}{1 + \omega^2 \tau^2} \quad (1-7)$$

$$E'' = \frac{(E_u - E_r) \omega \tau}{1 + \omega^2 \tau^2} \quad (1-8)$$

$$\tan \delta = \frac{(E_u - E_r) \omega \tau}{E_r + \omega^2 \tau^2 E_u} \quad (1-9)$$

where $\tau = \frac{\eta}{E_u - E_r}$

The relaxed modulus E_r , the unrelaxed modulus E_u and their relation to the springs of the model as well as the viscosity η of the dashpot are shown in fig. 1-7.

One of the objectives of the present work is to measure the complex modulus of keratin fibres with change of frequency, in a frequency range where very little is known. Makinson⁶⁵, Chaikin¹⁴ and Mason^{68 69} measured the modulus of keratin at single frequencies under different conditions. Thus there is lack of information about the complex modulus of keratin fibres for a wide range of frequencies at a particular relative humidity.

In order to expand the frequency range, in which the complex modulus is measured, the time-temperature equivalence²⁷ can be applied for many polymers. Time-temperature equivalence in its simplest form implies that the viscoelastic behaviour at one temperature can be related to that at another temperature by a change in the time scale only.

A more detailed presentation of the existing data will be presented along with the results of the measurement of complex modulus against frequency at various temperatures, at a fixed relative humidity, in chapter 5.

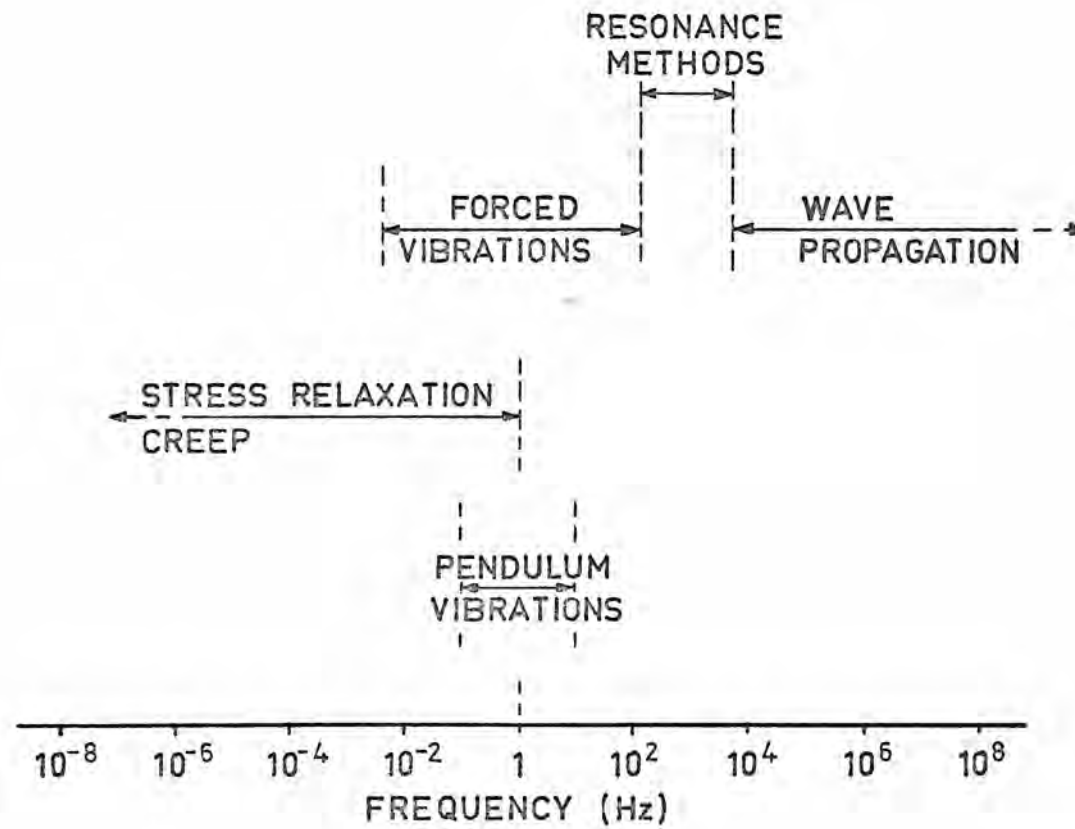


Fig. 1-8 Approximate frequency scales for different experimental techniques (after Becker).

The measurement of complex modulus provides a powerful tool in looking at the material under varying external conditions. Thus, in fact, it will be the complex modulus against strain which will be studied in chapter 3 and the complex modulus during sorption in chapter 4.

1.6 Experimental Techniques

In order to study the viscoelasticity in polymers a very large number of techniques have been employed^{27,64,88}.

A satisfactory understanding of the viscoelastic behaviour can only be achieved usually if data can be obtained over a wide range of frequency (or time) and temperature. The coverage of a wide range of frequencies at a constant temperature can only be done by combining a wide variety of techniques, the approximate time scale of which is shown in fig. 1-8.⁶ The techniques fall into five main classes

- (a) Transient measurements: creep and stress relaxation.
- (b) Low-frequency vibrations: free oscillation methods.
- (c) High-frequency vibrations: resonance methods.
- (d) Forced-vibration non-resonance methods.
- (e) Wave-propagation.

Although the nonresonant vibration type of measurement has much in its favour, it is not free from disadvantages. Since it is a nonresonance experiment, the vibrations are usually small and spurious equipment oscillations can become a problem. In addition, the measurement techniques are not simple, since it consists of measuring the magnitude and phase of forces and displacements. It is for these reasons that such techniques have not been as widely applied as measurements of creep and stress relation. In this work the forced-vibration technique was used. The development and construction of an apparatus utilizing this technique together with a conditioning chamber

to control humidity and temperature and an extensometer will be the topic of chapter 2.

1.7 Terminology Used

Very frequently in this work two types of quantities are considered i.e. oscillatory or non-oscillatory. The oscillatory quantities are associated with the term "dynamic" or "a-c". The non-oscillatory quantities are often termed "static" or "d-c". Thus a stress can be an alternating stress, an a-c stress or a dynamic stress as compared with the continuous stress, d-c stress or static stress. Likewise, strain and many other quantities can be considered in the same way. The terms Young's modulus, slope modulus or incremental modulus imply a static modulus; the terms loss modulus and complex modulus are dynamic quantities but the term dynamic modulus or simply modulus are reserved in the present work to imply only the in-phase component of the complex modulus. In addition measurements can also be distinguished as static or dynamic; for example the stress-strain relationship, as obtained with an extensometer, is a static measurement as compared with the measurement of the stress-strain relationship when an oscillatory strain is compared with the resultant oscillatory stress.

1.8 Summary

Keratins are a class of biopolymers made up of polypeptide chains. The polypeptide chains exist either in an orderly configuration in the microfibrils or in a more disordered configuration in the matrix. Little is known as to how the complex modulus of keratin varies with extension, frequency, temperature, humidity and during sorption. The remainder of this thesis is concerned with the study of these phenomena.

C H A P T E R 2

THE BUILDING OF A DYNAMIC MECHANICAL TESTER

2.1 Introduction

An apparatus capable of measuring the magnitude and loss angle of the complex moduli of fibrous materials has been developed. The apparatus allows for measurements to be made at different frequencies under varying conditions of extension, rate of extension, humidity, temperature and against time.

The design and construction of the apparatus was preceded by a theoretical investigation of the propagation of longitudinal mechanical waves in solids. The complex modulus of a "standard linear solid" does not depend on the geometry of the system (see equations (1-7), (108), (1-9)). However, in an actual experiment, in which we are interested in measuring the modulus and loss angle in a certain range of frequencies, we find that the measured angle between stress and strain does not coincide with the loss angle, as is shown in this chapter. The measured angle is generally a function of the loss angle, the length of the system and the applied frequency. To simplify measurement it would be convenient if the measured angle were equal to the actual loss angle of the material. Details of the relation between the two parameters is therefore developed in the following sections.

2.2 Propagation of acoustical waves in a loss free medium

Let us consider for example a fibrous material of length ℓ . One end of the sample is attached to a rod of a different material and of infinite length. On the other end of the sample, which is free, we apply a sinusoidal displacement of angular frequency ω . The two media are assumed to be perfectly elastic, so that there is no absorption of

energy by the material during the wave propagation. The motion of a particle in the sample at a distance χ from its free end at a time t can be described by the general wave equation

$$\xi^* = A \exp [i(\omega t - k\chi)] + B \exp [i(\omega t + k\chi)] \quad (2-1)$$

where A is the amplitude of a wave travelling towards the clamped end, B is the amplitude of the reflected wave from the clamped end, ξ^* is the displacement of the particle from its equilibrium position and k is the wave number, which is a real number in this case. There is also a wave transmitted along the clamping rod.

The particle velocity u^* is

$$u^* = \frac{\partial \xi^*}{\partial t} = i\omega A \exp [i(\omega t - k\chi)] + i\omega B \exp [i(\omega t + k\chi)] \quad (2-2)$$

The stress σ^* , or force per unit cross-sectional area in the medium is given by

$$\sigma^* = -E \frac{\partial \xi^*}{\partial \chi} = ikEA \exp [i(\omega t - k\chi)] - ikEB \exp [i(\omega t + k\chi)] \quad (2-3)$$

where E is the Young's modulus of the sample.

The mechanical impedance then at any point in the medium may be written as

$$Z^* = \frac{\sigma^*}{u^*} = Z_0 \frac{A \exp(-ik\chi) - B \exp(ik\chi)}{A \exp(-ik\chi) + B \exp(ik\chi)} \quad (2-4)$$

where we have substituted

$$Z_0 = \frac{kE}{\omega} = \rho c \quad (2-5)$$

The product ρc is the characteristic impedance of the medium with ρ its density and c the phase velocity of the wave.

Let the medium be terminated at $\chi=l$ by an impedance Z_t .

Then from equation (2-4)

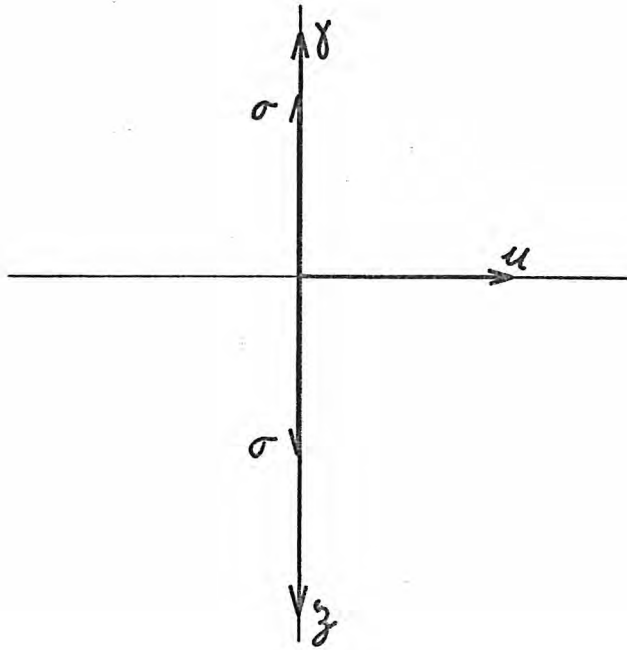


Fig. 2-1a In a loss free material the velocity u leads the displacement ξ by $\pi/2$ radians, the acceleration γ leads the velocity by $\pi/2$ radians. The stress σ is in phase with either the displacement or the acceleration.

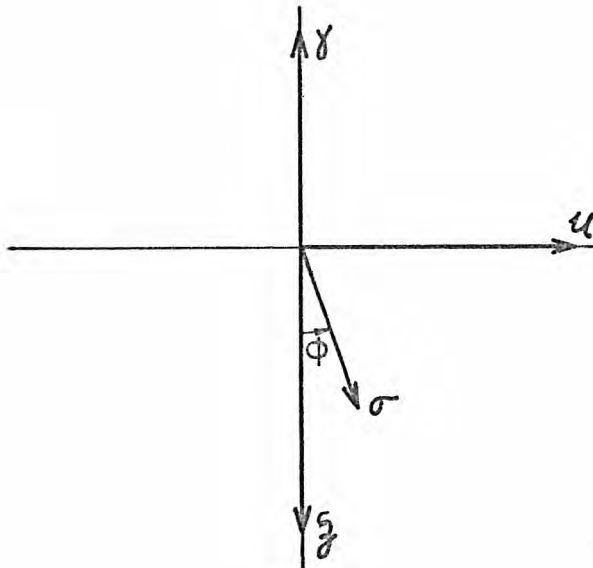


Fig. 2-1b In the presence of mechanical loss the applied stress leads the displacement by an angle ϕ .

$$Z_t = Z_0 \frac{A \exp(-ik\ell) - B \exp(ik\ell)}{A \exp(-ik\ell) + B \exp(ik\ell)} \quad (2-6)$$

from which

$$\frac{Z_0 - Z_t}{Z_0 + Z_t} = \frac{B}{A} \exp(2ik\ell) \quad (2-7)$$

The input impedance Z_{in} , i.e. the impedance at $x = 0$, is given by

$$Z_{in} = Z_0 \frac{A - B}{A + B} \quad (2-8)$$

Combining the relations (2-7) and (2-8) we find the general expression for the input impedance²⁵

$$Z_{in} = Z_0 \frac{Z_0 \sinh(ik\ell) + Z_t \cosh(ik\ell)}{Z_0 \cosh(ik\ell) + Z_t \sinh(ik\ell)} \quad (2-9)$$

In the case where the terminating impedance of the sample is a rigid backing rod

$$\text{i.e. } Z_t = \infty$$

the input impedance becomes

$$Z_{in} = Z_0 \coth(ik\ell) = -Z_0 i \cot(k\ell) \quad (2-10)$$

The relation (2-10) indicates that the velocity at the free end of the sample is out of phase with the applied stress by an angle of $\pi/2$ radians (Fig. 2-1a). The displacement and the stress are in phase at that end for frequencies, for which

$$2n \frac{\pi}{2} < k\ell < (2n+1) \frac{\pi}{2} \quad n = 1, 2, 3 \dots$$

or out of phase by π radians for frequencies, for which

$$(2n+1) < k\ell < 2(n+1) \frac{\pi}{2} \quad n = 1, 2, 3 \dots$$

We see that the medium acts as a pure reactance, since there is no

energy dissipated or net energy flux in either direction. For very low frequencies the input impedance has the limiting value

$$Z_{in} = -i \frac{\rho c}{k \ell} = -i \frac{E}{\omega \ell} \quad (2-11)$$

which is identical with the input impedance of a simple spring having a stiffness constant $s = E/\ell$.

2.3 Measured angle and loss angle

The corresponding mathematical analysis for a sample with mechanical loss is similar, except that the wave number k and the phase velocity c become complex quantities. The wave number is expressed as

$$k^* = k - i\alpha \quad (2-12)$$

where α is the attenuation coefficient of the propagating wave.

The velocity is calculated from the complex modulus:

$$c^* = \sqrt{\frac{E^*}{\rho}}$$

where E^* can be written as

$$E^* = E' (1 + i \tan \delta)$$

and thus approximately

$$c^* = c \left(1 + \frac{i}{2} \tan \delta\right) \quad (2-13)$$

In the same way the relation between the loss $\tan \delta$ and the attenuation coefficient is found to be

$$\alpha = \frac{k}{2} \tan \delta \quad (2-14)$$

since $k^* = \frac{\omega}{c^*} \approx k \left(1 - \frac{i}{2} \tan \delta\right)$

by comparison with (2-12).

From the relationships (2-10), (2-13) and (2-14) we find for the input impedance:

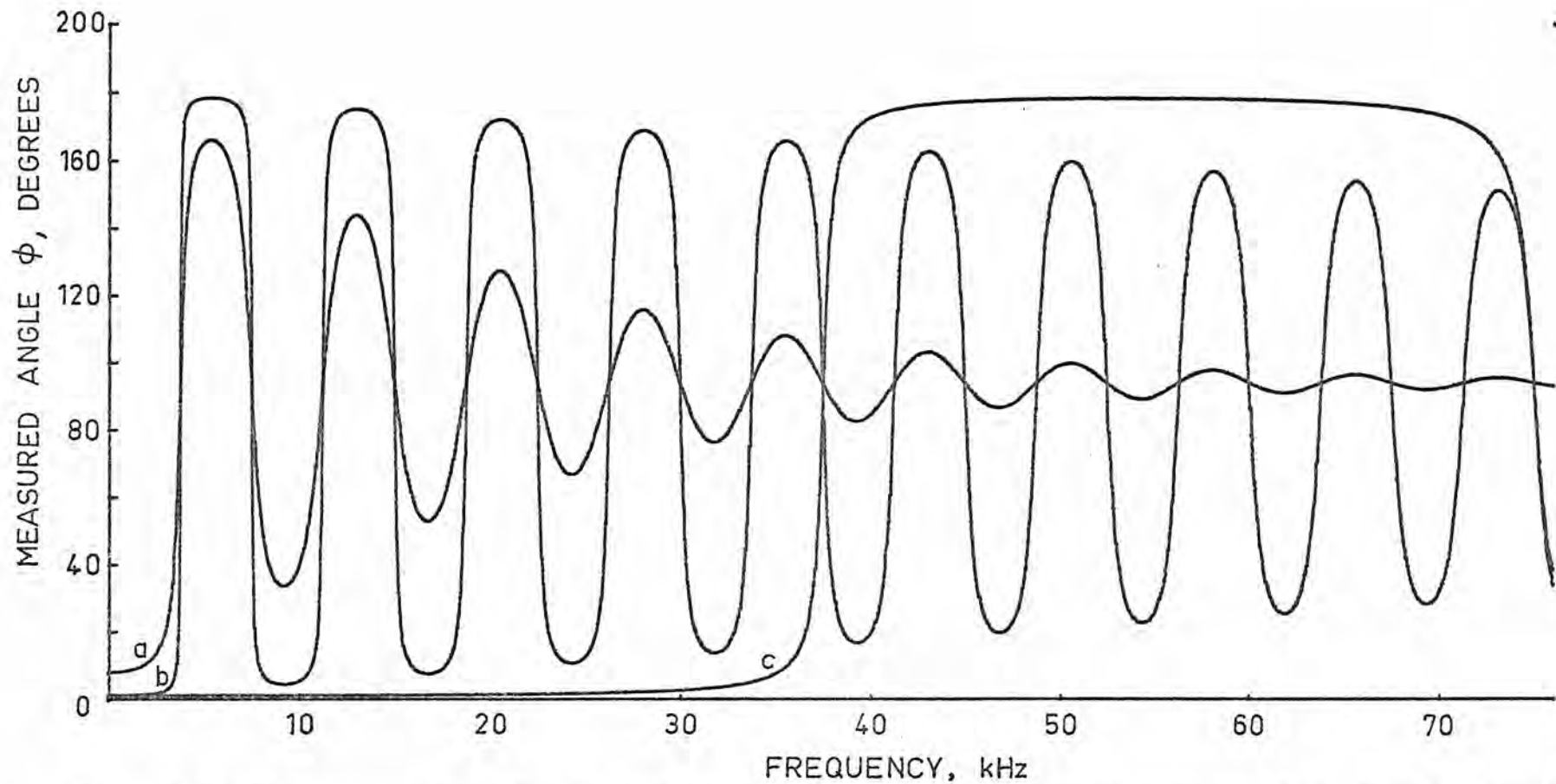


Fig. 2-2 The measured angle ϕ against frequency for different values of c , l and δ as follows: Curve (a), $c=1500$ m/sec, $l=10$ cm, $\delta=8^\circ$. Curve (b), $c=1500$ m/sec, $l=10$ cm, $\delta=1^\circ$. Curve (c), $c=1500$ m/sec, $l=1$ cm, $\delta=1^\circ$.

$$Z_{in} = \rho c \left(1 + \frac{i}{2} \tan \delta\right) \coth i \left[\frac{\omega \ell}{c} \left(1 - \frac{i}{2} \tan \delta\right)\right] \quad (2-15)$$

It must be mentioned that the quantities c (real part of the complex phase velocity) and the loss angle δ are both functions of frequency, which are characteristic of the material.

The stress and displacement at the free end of the medium (since by definition $Z_{in} = \sigma^*/u^*$) are related as follows

$$\sigma^* = Z_{in}^* i\omega \xi^* \quad (2-16)$$

where $i\omega \xi^*$ is equal to the velocity u^* . The phase difference ϕ between stress and displacement is found by separating the quantity $Z_{in}^* i\omega$ into real and imaginary parts and then finding its argument. The argument is given as follows

$$\phi = \tan^{-1} \frac{D \sin(2F) + \sinh(2FD)}{\sin(2F) - D \sinh(2FD)} \quad (2-17)$$

where $D = \frac{1}{2} \tan \delta$ and $F = \frac{\omega \ell}{c}$.

The quantities ξ , u , γ , σ , and ϕ are depicted in a vector diagram in fig. (2-1b).

From equation (2-17) it is obvious that the measured angle between applied force and displacement is generally a function of frequency, of length and the nature of the material

$$\phi = \phi \{ \omega, \ell, \delta(\omega), c(\omega) \}$$

To compare the measured angle ϕ with the loss angle δ , we assume fixed values for δ and c and plot ϕ versus frequency f ($2\pi f = \omega$) for a fibre of length ℓ . Figure (2-2) shows the results for three different cases: curve (a) for $c = 1500$ m/sec, $\ell = 10$ cm, $\delta = 8^\circ$, curve (b) for $c = 1500$ m/sec, $\ell = 10$ cm, $\delta = 1^\circ$ and curve (c) for $c = 1500$ m/sec, $\ell = 1$ cm, $\delta = 1^\circ$. We observe from all the curves as well as from formula (2-17) that

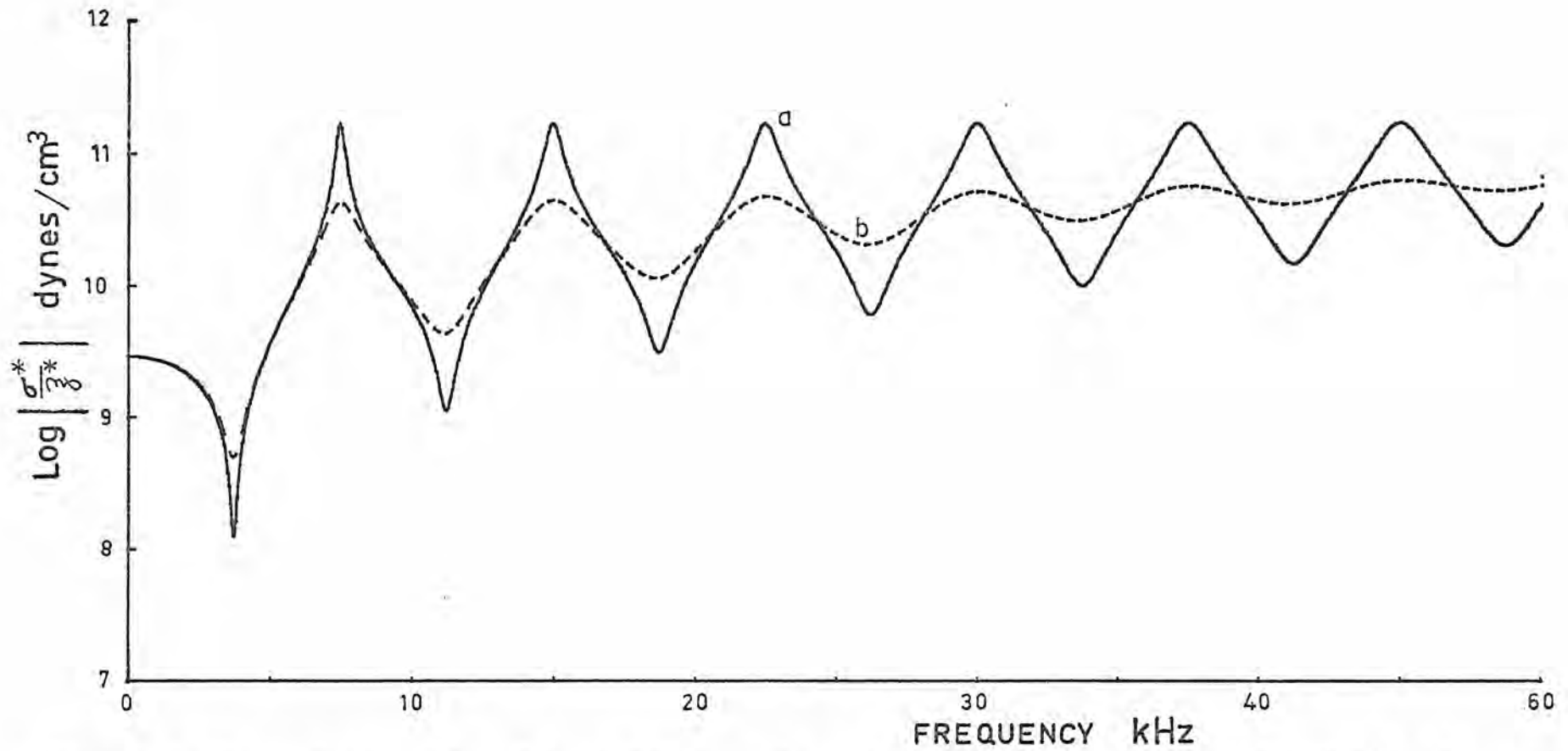


Fig. 2-3 The relationship of $\log|\sigma^*/\xi^*|$ against frequency. Curve (a) is for $\delta=2^\circ$ and curve (b) for $\delta=8^\circ$; both are for $c=1500$ m/sec, $\rho=1.3$ gr/cm and $l=10$ cm.

$$\lim_{f \rightarrow 0} \phi = \delta \quad \ell = \text{fixed}$$

or
$$\lim_{\ell \rightarrow 0} \phi = \delta \quad f = \text{fixed}$$

There is a resonance for frequencies

$$v = n \frac{c}{4\ell} \quad n = 1, 2, 3 \dots$$

At any resonance frequency the change of ϕ for a lossy material is always less than 180° in contradistinction to an ideally elastic material, in which the phase ϕ jumps by 180° . In a visco-elastic medium the magnitude of the change of ϕ decreases with increasing frequency or length so that we have from (2-17)

$$\lim_{f \rightarrow \infty} \phi = 90^\circ + \frac{\delta}{2} \quad \ell = \text{fixed}$$

or
$$\lim_{\ell \rightarrow \infty} \phi = 90^\circ + \frac{\delta}{2} \quad f = \text{fixed}$$

The measured stress per unit displacement can be calculated from the relationship (2-16) likewise by taking the absolute value of the quantity $Z_{in} i\omega$. The result obtained is as follows

$$\left| \frac{\sigma^*}{\xi^*} \right| = |Z_{in} i\omega| = \frac{\omega \rho c \sqrt{[(1+D^2)(\sinh^2(2FD) + \sin^2(2F))]} }{\cosh(2FD) - \cos(2F)} \quad (2-18)$$

A plot of (2-18) is given in fig. 2-3 for two cases: curve (a) for $\delta = 2^\circ$ and curve (b) for $\delta = 8^\circ$. Both are for $c = 1500$ m/sec, $\rho = 1.3$ gm/cm and $\ell = 10$ cm. The plot is on a log-linear scale.

For sufficiently low frequencies using equation (2-18) the stress per unit strain is found to be

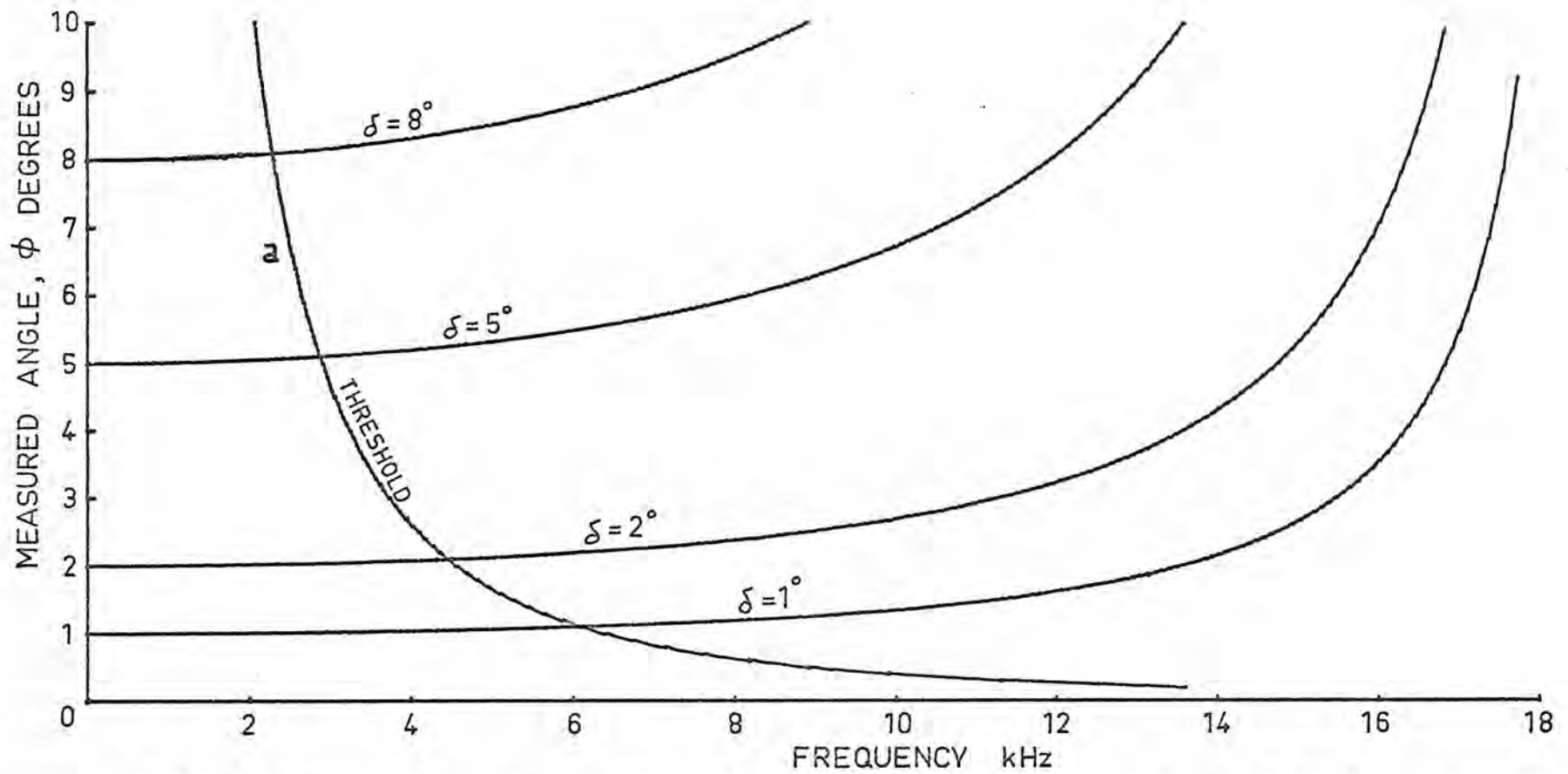


Fig. 2-4 The measured angle ϕ against frequency for different values of δ , for a sample of 2 cm length. Curve (a) gives the upper limit of frequencies for which $\phi - \delta < 0.1^\circ$.

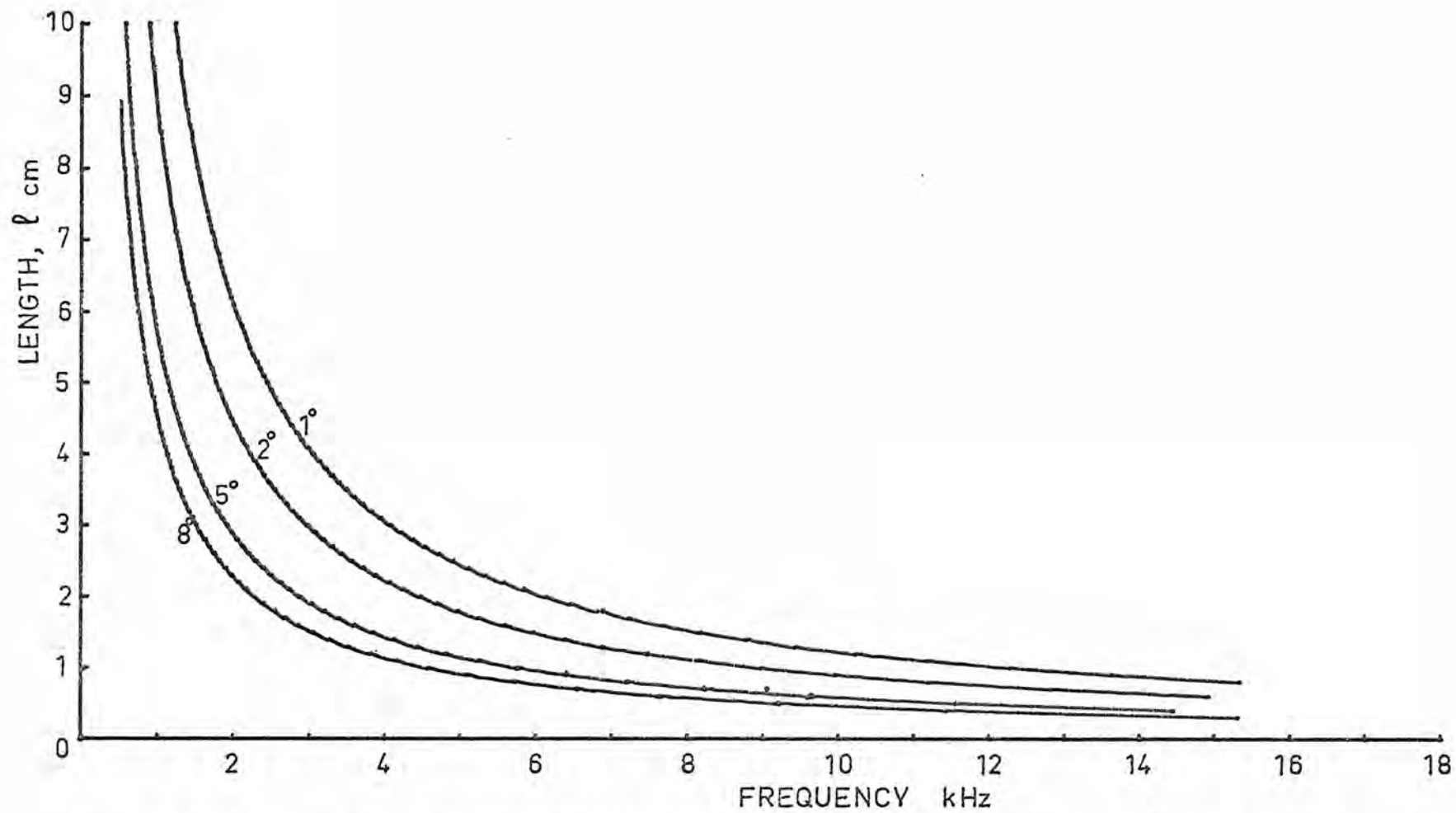


Fig. 2-5 The sample length l plotted against the limiting frequencies for different values of δ (see text).

$$\lim_{f \rightarrow 0} \left| \frac{\ell \sigma^*}{\xi^*} \right| = \rho c^2 \sqrt{(1+D^2)} \approx E \quad (2-19)$$

for small δ . In other words the measured oscillatory force corresponds to the modulus of the material only for low frequencies. An overall picture of how the measured angle and force change with frequency is presented in Appendix A.

Now, the conditions, under which $\phi \approx \delta$, will be established. From fig. 2-2 it is apparent that the relationship $\phi \approx \delta$ must be sought at sufficiently low frequencies in the range before the first resonance occurs. The definition of a sufficiently low frequency depends on the expected change of the loss angle, or equivalently, on the material. For wool in particular it may be sufficient to tolerate a maximum difference of 0.1° i.e.

$$\phi - \delta < 0.1^\circ \quad (2-20)$$

Figure 2-4 shows a set of curves for different values of δ for a sample of 2 cm length. Curve (a) gives the threshold of frequencies which must not be exceeded for the different values of δ . Figure 2-5 gives the same limiting frequencies against sample length for different δ 's.

The measured force decreases as the first resonance is approached (Fig. 2-2). When the measured angle has increased by 0.1° above the loss angle, the measured force has decreased by 8% below the expected value of E/ℓ (for $\delta < 10^\circ$).

2.4 Measurement of the alternating force

Up to now we have considered factors which restrict the frequency range, in which we can directly measure the mechanical loss in a material. These factors originate from the nature of the material alone and impose a theoretical limit on the high frequency side.

However, the equipment, with which we might attempt the measurement, incorporates factors which impose a limit on the high as well as on the low frequency side, as it will be shown in the following analysis. Therefore, the superposition of both the internal (related with the nature of the medium) and the external factors (related with the measuring system) define the frequency range, in which we can directly measure the dynamic mechanical parameters e.g. the complex modulus.

For frequencies below the resonance frequency it is interesting to note that the angle ϕ (phase difference between stress and strain at the same point of the sample i.e. the free end) is equal to the phase difference between the strain at the free end and the stress at the clamped end of the sample. This is, because in the case of standing waves any oscillating quantity (e.g. velocity, force, displacement etc.) has the same phase at any point between two consecutive nodes. The amplitude of force varies between two nodes, but for frequencies below the threshold defined by the curves of fig. 2-5 it can be considered the same at both ends of the sample.

Let us consider the application of a sinusoidal force to a fibrous sample. That force can be measured with a stress gauge, which may be regarded as consisting of an electrical component, which converts mechanical stress into an electrical signal, a clamping mechanism with a mass m , a spring with stiffness s and a frictional element R (fig.2-6a). The stiffness s must be very high so that the motion at the point B is very small compared with the amplitude of oscillation at the point A of the sample. The mass m of the clamp interferes with the measurement of the force exerted by the sample with an inertia force

$$\Sigma = i\omega^2 m \xi'$$

where ξ' is the amplitude of oscillation at the point B and ω is the frequency of oscillation. The complete vector diagram of forces acting

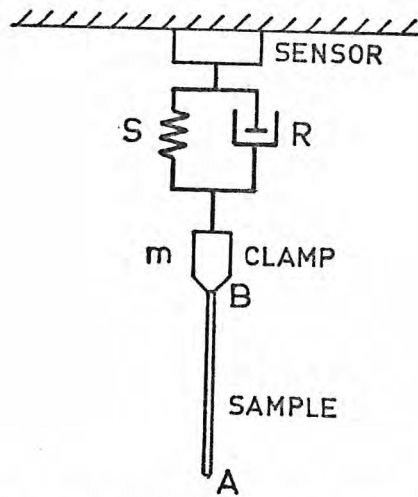


Fig. 2-6a A stress gauge consists of a clamping mass m , a spring with stiffness s , a frictional element R , and a sensor that converts the applied stress on it into an electrical output.

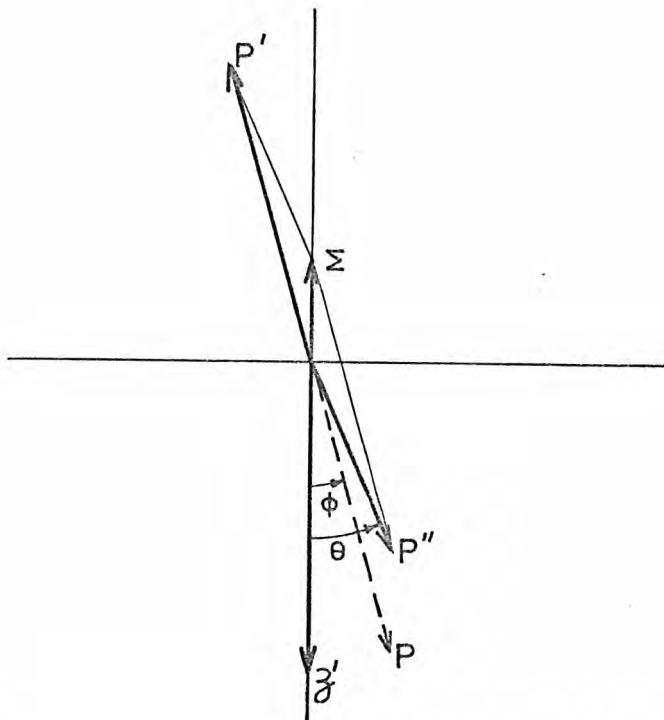


Fig. 2-6b Vector diagram of the forces p' and p'' acting upon the mass m with their sum Σ ; θ is the new measured angle.

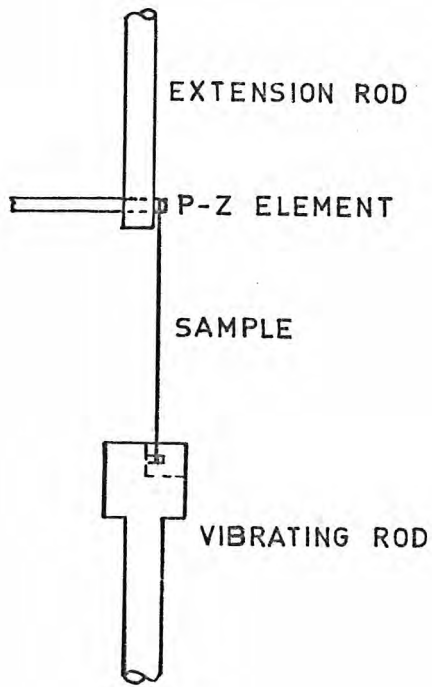


Fig. 2-7a Sample mounted between vibrating rod and piezoelectric element.

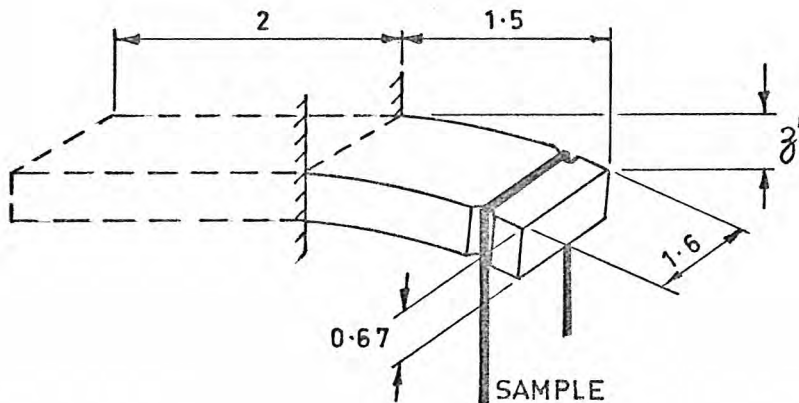


Fig. 2-7b Sample mounted around the piezoelectric element. About two-thirds of the element is cemented; exact dimensions are shown.

on the mass m is shown in fig. 2-6b. The force Σ is the vectorial sum of all external forces acting on the mass and is 180° out of phase with the displacement ξ' . The fibre acts with a force p' upon the mass m , p is equal and opposite to p' and would be the force measured by the sensor in the case where $m = 0$ (in this case the diagram in fig. 2.6b would reduce to that of fig. 2-1b), while p'' is the force exerted by the sensor on the mass m and is the quantity we measure. It can be seen further that we no longer measure the angle ϕ but another angle θ . It can be shown in complex form that the measured force p'' and displacement ξ' are related as follows

$$p'' = \left[\left(\frac{S}{\omega} - \omega m \right) + iR \right] \omega \xi' \quad (2-21)$$

from which it follows for the angle that

$$\theta = \tan^{-1} \frac{R}{\frac{S}{\omega} - \omega m} \quad (2-22)$$

From the latter we conclude that

$$\lim_{\omega \rightarrow 0} \theta = \phi \quad (2-23)$$

or $m \rightarrow 0$

or $S \rightarrow \infty$

Therefore, the relationship $\theta \approx \phi$ is a good approximation at any desired frequency, provided the mass m is made small enough and/or the stiffness s is made sufficiently large.

Practically we can obtain the necessary condition for $\theta \approx \phi$ by using a piezoelectric element as a stress measuring device. The fibre can even be mounted directly on it by forming a loop around it as shown in fig. 2-7a and 2-7b. Two tiny slots on the element ensure that the sample does not slip off. The element acts as a cantilever and its length has been chosen small enough so that the amplitude of bending ξ' can be considered negligible compared with the amplitude of oscillation.

AMPLITUDE OF OSCILLATION

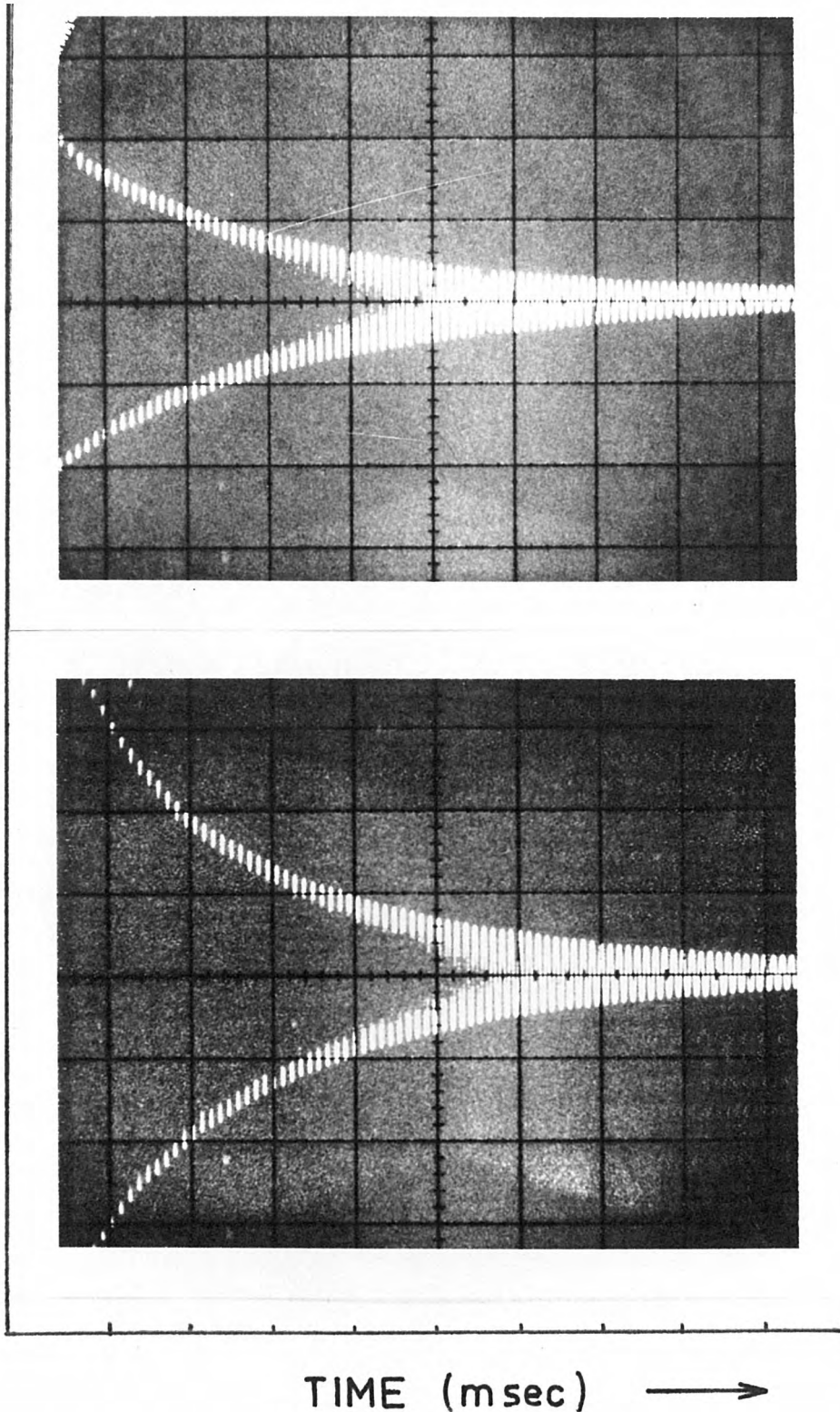


Fig. 2-8 Two typical patterns, obtained with a storage oscilloscope, showing the decay of amplitude of free oscillations of the piezoelectric element.

The piezoelectric element used is a Philips PXE 5 multimorph strip of 3.5 mm length, 0.67 mm thickness and 1.6 mm width. Two mm of its length were cemented with a composite adaptic of very high modulus (used as dental filling). From the available data⁷⁷ the expected fundamental frequency of resonance of the cantilever is of the order 10^5 Hz, which is well beyond the limits set in figure 2-5. On the other hand the amplitude ξ' resulted by an exerted force of 5000 dynes is less than 0.5% of a micron. This result was verified by experiment.

The application of a displacement of 4μ on a horse hair in a loop form of length 2 cm generates a force of about 4000 dynes, while a Lincoln fibre of the same (loop) length generates about 500 dynes. Thus the effect of the mass of the element as given by (2-22) is quite insignificant for frequencies up to 2 kHz.

However the piezoelectric element itself has a complex modulus which interferes with the measurement of the complex modulus of the sample. This effect would have to be calibrated out, if it proved to be significant. A first check of the order of magnitude of the element's loss angle was made by measuring the logarithmic decrement (log. dec.) from fig. 2-8, which shows the gradual decay in amplitude of vibration during a free oscillation of the element. The loss $\tan\delta_p$ is calculated as follows⁹⁸

$$\tan\delta_p = \frac{\text{log. dec.}}{\pi}$$

or alternatively

$$\tan\delta_p = \frac{1}{\pi f_0 \tau}$$

where f_0 is the resonant frequency of oscillation and τ the time constant of the decay of the amplitude of oscillation. From the above a value for δ_p of 1.2° with $f_0 = 9.2$ kHz at 25°C was estimated. Thus the interference of the measuring system is significant.

The complex modulus of the element is also dependent on frequency and temperature. One simple way of correcting for this interference is by the use of a sample of known complex modulus as reference. The electrical output of the element is in phase and proportional to its deformation, which in general lags behind the applied stress by an angle δ_p . Suppose the reference material acts upon the element with a stress

$$\sigma_r^* = \sigma_r \exp(i\omega t),$$

then the output would be

$$V_r^* = V_r \exp i(\omega t + \delta_p) \quad \delta_p < 0.$$

The stress and output are related as

$$V_r^* = N^* \sigma_r^* \quad (2-24)$$

where N is the transducer ratio:

$$N^* = N \exp (i\delta_p) \quad (2-25)$$

A similar relation holds for the test sample:

$$V^* = N^* \sigma^* \quad (2-26)$$

where

$$V^* = V \exp i(\omega t + \theta)$$

and

$$\sigma^* = \sigma \exp i(\omega t + \delta)$$

Solving equations (2-24) and (2-26) for σ^* we obtain

$$\sigma^* = \frac{V^*}{V_r^*} \sigma_r^* \quad (2-27)$$

If the reference material of modulus E_r and length l_r is considered practically elastic, its stress will be in phase with its displacement ξ_r^*

$$\sigma_r^* = \frac{E_r \xi_r^*}{l_r} \exp (i\omega t) \quad (2-28)$$

Therefore equation (2-27) becomes

$$\sigma \exp i(\omega t + \delta) = \frac{V \exp i(\omega t + \theta)}{V_r \exp i(\omega t + \delta_p)} \cdot \frac{E_r \xi_r}{\ell_r} \exp (i\omega t)$$

$$\sigma \exp (i\delta) = \frac{V}{V_r} \cdot \frac{E_r \xi_r}{\ell_r} \cdot \exp i(\theta - \delta_p) \quad (2-29)$$

From (2-29) we finally find

$$\delta = \theta - \delta_p \quad \text{and} \quad \sigma = \frac{V}{V_r} \cdot \frac{E_r \xi_r}{\ell_r} \quad (2-30)$$

Thus, in order to find the loss angle of a material we have to subtract from the measured angle θ the known (reference) angle δ_p . The modulus is found by the ratio V/V_r times a known constant C :

$$E = \frac{V}{V_r} C \quad (2-31)$$

$$\text{where } C = E_r \frac{\ell \xi_r}{\ell_r \xi}$$

since $\sigma = E \frac{\xi}{\ell}$ with ξ and ℓ referring to the test sample.

2.5 The Instruments Used

The measurement of strain did not present difficulties. A KAMAN-Multi-purpose Variable Impedance Transducer (KD-2300-1 type) was used. This provided exceptional accuracy for a non-contacting measurement of conductive surface motion. The most significant feature of this measuring system is its capability for highly linear calibration with almost any metal or alloy, whether flat or highly curved. The transducer consists of a variable impedance bridge with an active and a reference coil. Variation in impedance results from the eddy currents induced in nearby conductive surfaces. Sensitivity is therefore dependent upon the material and shape of the target. Its characteristics are as follows

Frequency Response 0 - 20 kHz (-1 dB point)
0 - 50 kHz (-3 dB point)

Transient Response 10 μ sec with no overshoot.

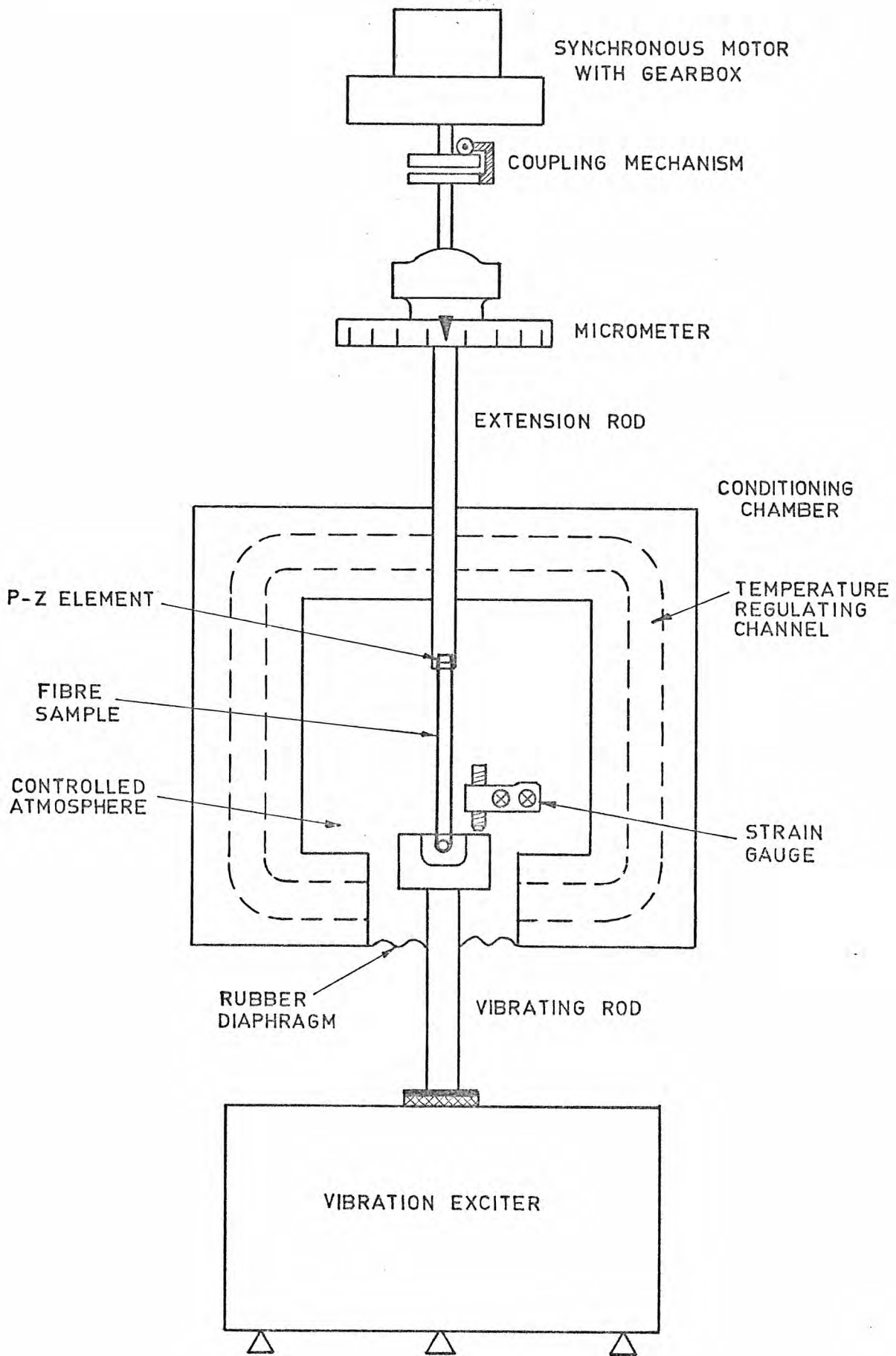


Fig. 2-9 Schematic diagram showing the relative positions of the extensometer, the conditioning chamber, the measuring gauges and of the vibration exciter.

Its approximate sensitivity with an aluminium target is $0.8 \text{ mV}/\mu$. An exact calibration was easily performed when required.

The fibre was clamped at the one end, while on the other end mechanical vibrations were applied by a vibration exciter (Bruel & Kjaer type 4809) via a pushrod (Figure 2-9). The strain gauge mounted close to the upper flat surface of the vibrating rod could detect the motion at that level. The piezoelectric element cemented at the other end on the extension rod could detect the a-c stress acted on it by the fibre. Any d-c extension could be applied via the extension rod, which was attached to a precise extensometer. The smallest graduation of the micrometer head of the extensometer was 10μ . It was found out that for fairly stiff samples (e.g. horse hair) the free end shifted in the direction of extension, but this could be detected very accurately by the d-c output of the strain gauge and thus a correction of the extension could be carried out accordingly. However, the latter correction was not necessary for fine fibres (e.g. Lincoln wool fibres). The extension could be applied either by steps manually or continuously at different rates by a synchronous motor coupled to the extensometer.

The design of the correct geometry for the vibrating pushrod encountered several problems, because it had to meet the following requirements: (a) to be light enough, so that the available power of the mechanical exciter could maintain a certain level of strain at higher frequencies; (b) to have high modulus and short length in order to avoid a longitudinal resonance. Such a resonance would make the measurement of stress and strain difficult, because the stress and strain are measured with respect to a reference signal from the electronic driver of the mechanical exciter, as will be shown later. On the other hand the length of the pushrod should be long enough to allow for the sample to be placed in a conditioning chamber; (c) to be symmetric, so that transverse vibrations would be

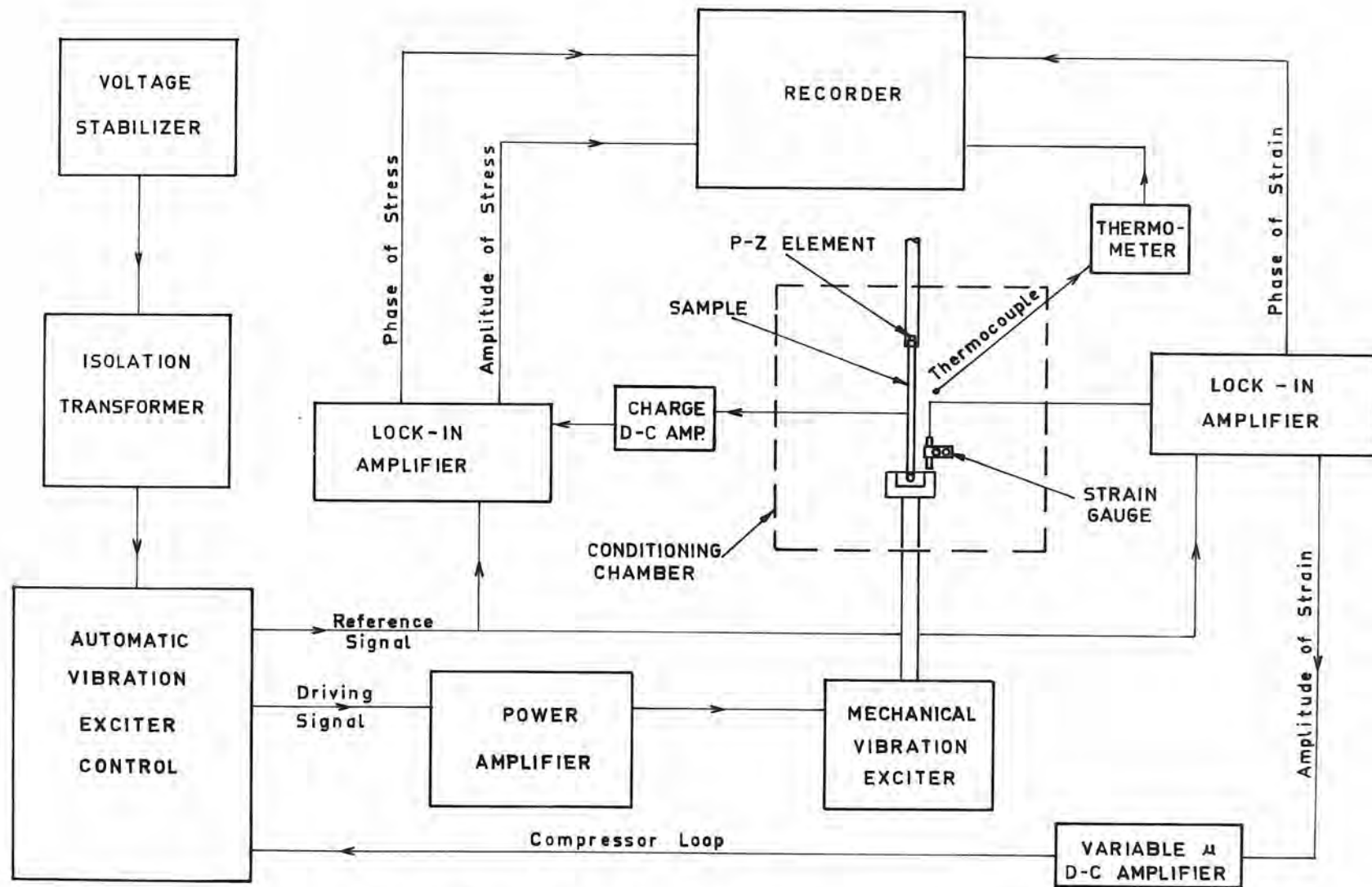


Fig. 2-10 General schematic diagram of the experimental apparatus.

avoided. However, the transverse vibrations could not be completely eliminated because the mechanical exciter itself had a small cross-motion, which, although it was a small percentage of the longitudinal motion, resulted in a considerable error in measuring the phase between the stress and strain. The compensation for this type of error together with errors from other sources will be discussed in a later section. Details about the pushrod is given in Appendix B along with the drawings of the conditioning chamber.

Figure 2-10 shows a general diagram of the instruments being used. The mechanical vibration exciter was driven via a power amplifier (BrueI & Kjaer type 2706) by an Automatic Vibration exciter control (BrueI & Kjaer type 1025). This allows for continuous scanning of frequency in the ranges: 0-5000 Hz, or 5-5000 Hz, or 5005-10000 Hz. The frequency scales are logarithmic. The maximum force available from the mechanical exciter is 44.5 Newtons. The moving element of the exciter was $m = 60$ gr and the vibrating rod had a mass of 13 gr, so the maximum acceleration that could be achieved was 609.6 m/sec^2 or 62.1 g.

The transducer ratio of the p-z element was found to be 2 V/Newton. The amplitude of vibration was kept low ($\approx 4 \mu$) so that linear viscoelasticity could be assumed to hold for the sample. This resulted in low levels of stress and strain signals. Successful measurement of such low level signals was obtained by the use of lock-in amplifiers. The lock-in amplifier had to be supplied, besides the measured signal, with a reference signal of the same frequency as the measured signal. Thus with a certain level of strain set, the strain signal could be used as reference input for the lock-in amplifier and the magnitude and phase of the stress signal could be measured. Two P.A.R. model 129 A two-phase/vector lock-in amplifiers were available. One unit would be sufficient except for the need of a minimum level

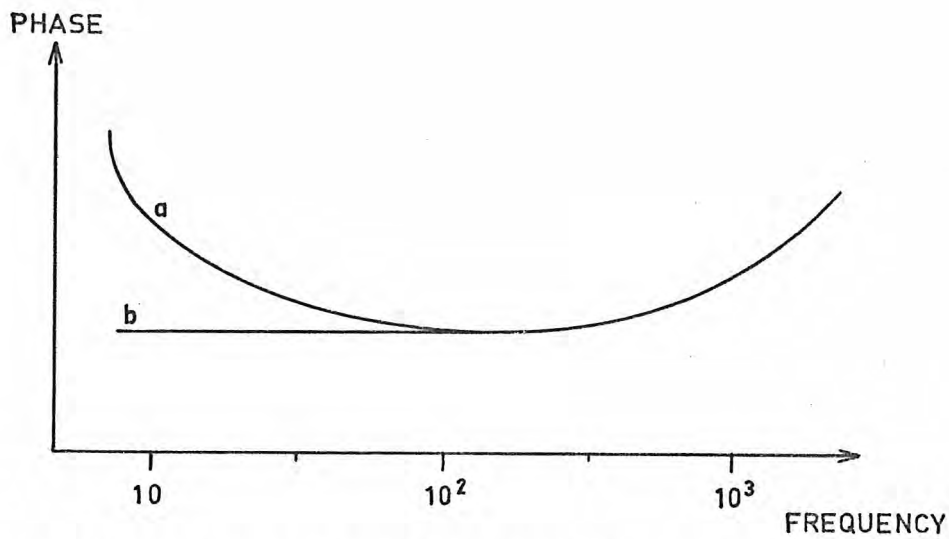


Fig. 2-11a The increasing values of the phase difference between stress and strain towards lower frequencies arise from leakages in the p-z element (curve a); this effect is eliminated by insertion of a charge preamplifier (curve b).

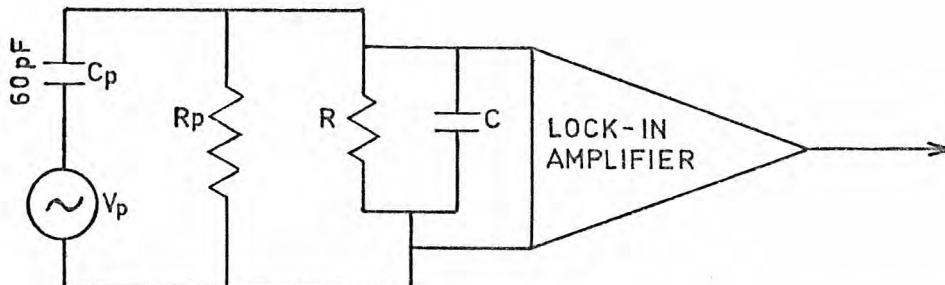


Fig. 2-11b Equivalent circuit diagram for the piezoelectric element and the lock-in amplifier.

reference signal, i.e. a voltage waveform having amplitude excursions of at least 5 mV on each side of the mean and crossing the mean only twice each cycle. For best results a 1 V rms sinewave is recommended as a reference. Such a signal is readily available at the electrical vibration exciter, which is of constant level (1 V rms) and of the same frequency as the driving signal. Thus by using the same reference signal simultaneously for the two lock-in amplifiers it is possible to measure separately the amplitude and phase of stress and strain relative to the common reference signal.

The outputs of the lock-in amplifiers are calibrated d-c voltages, which enable the difference of phase between stress and strain to be recorded directly on a multi-channel recorder alongside with the amplitude of stress and strain.

The measurement of output of the p-z element presented some difficulty. For low frequencies it was found that the phase of stress increases considerably (Figure 2-11a). This was found to be due to the relatively low input impedance of the lock-in amplifiers for low frequencies. Figure 2-11b gives an equivalent circuit for the piezoelectric element in connection with the lock-in amplifier. The input impedance of the lock-in amplifier is given as $R = 100 \text{ M}\Omega$, $C = 20 \text{ pF}$, while for the p-z element it is estimated⁷⁷ that $C_p = 150 \text{ pF}$ and $R_p = 10^{14} \Omega$. The value of R_p might be lower due to surface leakage, but it was found that $R_p \gg R$. Thus the amplifier does not "see" the signal V_p generated by the p-z element but the complex fraction

$$V = \frac{Z_{in}}{Z_{in} + Z_p} V_p = \frac{\omega R C_p}{\omega R (C_p + C) - i} V_p$$

The symbols Z_{in} and Z_p stand for electrical impedances in this case. The latter result modifies the expected mechanical loss angle by a term

$$\tan^{-1} \frac{1}{\omega R(C_p + C)} \quad (2-32)$$

which was in agreement with the experiment. This effect could be corrected by using a reference material, but it was desired to keep the phase characteristic as flat as possible, in order to avoid loss of accuracy, sensitivity and continuity, due to the necessity for continually adjusting settings on the various instruments.

From expression (2-32) there could be two alternatives for reducing the value of this correction considerably. (a) To increase C_p ; this suffers from the disadvantage of shunting (i.e. lowering) the magnitude of the signal. (b) To increase R ; this is generally difficult, because charge leakages could not be avoided very easily as well as high electrical noise. (c) To measure the charge rather than the voltage of the p-z element. This was successfully done by the use of a charge pre-amplifier before the lock-in amplifier.

The amplitude of strain could be kept constant by using the facility of electronic exciter control to compensate changes of a d-c signal. Thus a compressor loop was formed between the strain output of the lock-in amplifier and the compressor of the exciter control via a variable μ d-c amplifier for setting various constant level a-c strains.

2.6 Conditioning of the Sample

The apparatus so far described allows for the measurement of the complex modulus of a fibrous material at various extensions and frequencies. However the properties of polymers are dependent on temperature and humidity in many cases. The complex modulus of wool is very much dependent on the surrounding conditions as well as its previous history. Thus one has to precondition and condition the sample prior to any experiment. For this purpose a chamber to control the temperature

and humidity was designed and constructed.

2.6.1 Conditioning Chamber

Measurements at higher humidities are particularly difficult, because one has to keep not only constant temperature but also a homogeneous temperature throughout the chamber. This is because small local temperature deviations result in big humidity and even bigger regain variations for wool. The chamber must allow, while conditioning, for vibrations and various extensions to be applied to the fibre.

A diagram of the chamber is presented in fig. 2-9. The complete drawings are presented in Appendix B. The chamber was made out of a solid brass rod of 6" diameter. Brass was found as the most suitable material, partly because it has a high thermal conductivity, a factor which helps in maintaining uniform temperature, and partly because of its commercial availability and its relative ease of machining.

A cylindrical cavity was machined from the top. This was the humidity control portion of the chamber. Access to the humidifying part was obtained by opening the top cover, or through two small holes in the cover. Access to the sample was obtained through a window in the front. A rubber diaphragm around the vibrating pushrod ensured both freedom of oscillations and excellent sealing of the humidifying chamber. An "O"-ring also provides both sealing and freedom of movement for the extension rod.

Around the humidifying part there is a system of holes and cavities, which makes up a continuous pathway for circulation of air at the desired temperature.

Vacuum grease is used to block the two holes in the top cover as well as throughout the apparatus to ensure good sealing. The size of the chamber was made as small as possible, this being another factor contributing to the uniformity of temperature. The whole brass assembly

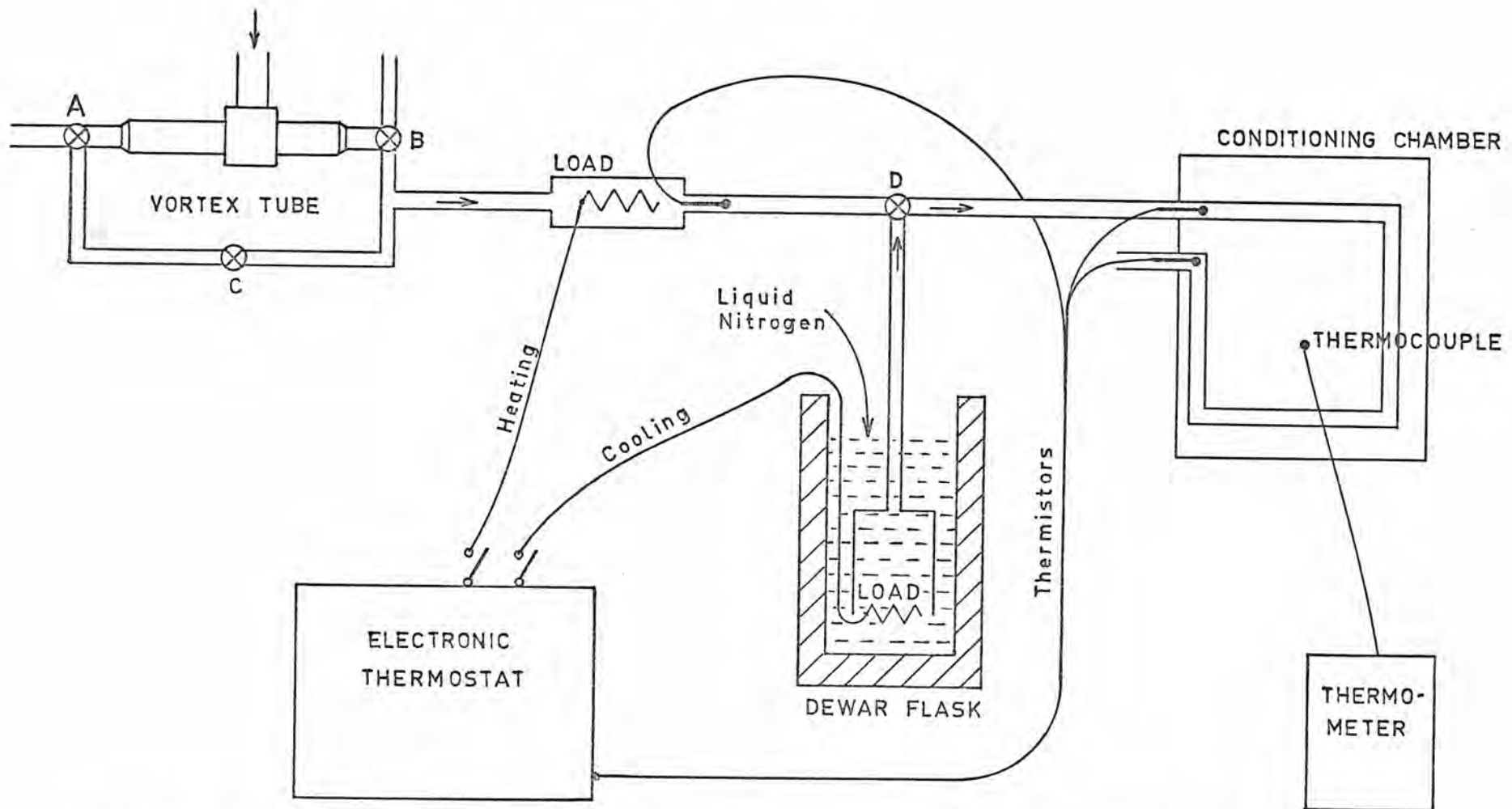


Fig. 2-12 Schematic diagram of the various instruments of the temperature control.

weighing 17 kg was mounted onto vibration absorbing felts, which acted also as good thermal insulators. The large mass of the chamber minimized the mechanical noise. Thick thermal insulation walls around and on top were cast in solid pieces from polyurethane foam.

2.6.2 Temperature Control

Air was used as the circulating medium in the chamber, the temperature of which was stabilized at the required temperature by an electronic thermostat (Fig. 2-12). For temperatures around or above room temperature, the air was first precooled below room temperature and then brought up to the desired temperature. For precooling a Vortex tube was used. This is a device, which was fed with compressed air and gave one cool and one hot output. The temperature difference between input and either of the outputs was dependent on the pressure of the input.

For temperatures below room temperature liquid nitrogen was used. The liquid nitrogen contained in a Dewar flask was boiled in a bell-like cavity and the cold gaseous nitrogen was allowed to circulate in the conditioning chamber. The rate of boiling was regulated by the electronic thermostat.

To achieve cooling or heating the valves A, B, C, D were appropriately used and the thermostat was turned on "cooling" or "heating".

Accurate temperature control involves two distinct problems: (a) reduction of both short and long-term fluctuations in temperature about a selectable control point, and (b) reduction or control of temperature gradients within the controlled space. The short-term variations of the circulating medium were evened out by the large heat capacity of the chamber.

The control system consists of a thermistor temperature sensor, the resistance of which is compared with a high stability reference resistor, whose resistance value can be varied to select the temperature at which both resistances are identical (Fig. 2-13). The thermistor and reference

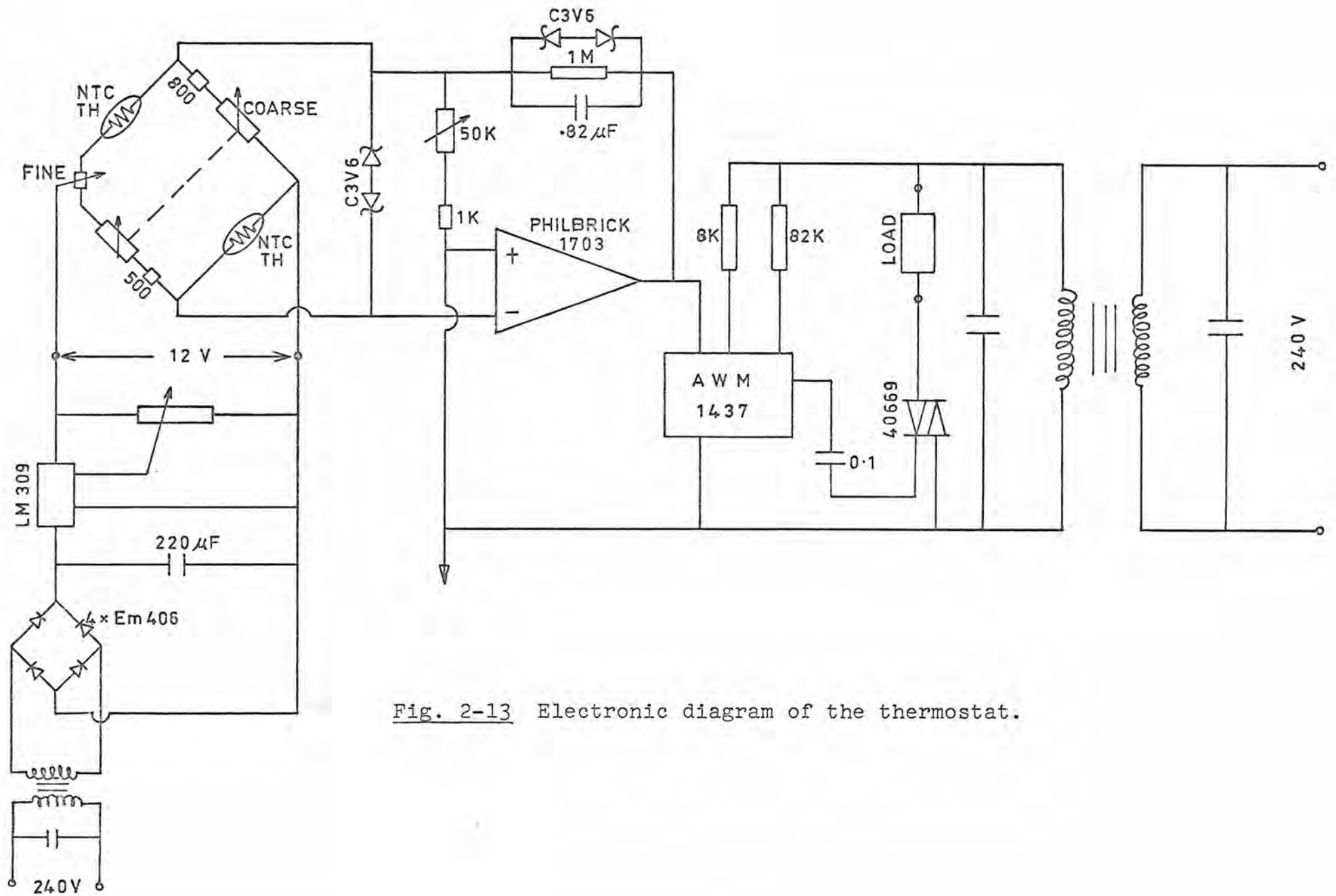


Fig. 2-13 Electronic diagram of the thermostat.

resistor are connected in a bridge circuit, the output of which is amplified by an inverting chopper stabilized operational amplifier to provide a d-c output that operates an AWM 1437 integrated circuit for the phase-controlled triggering of thyristors. Phase control is an ideal method of varying the power to loads with short time constants.

In operation, as the temperature of the thermistor increases, its resistance falls and the amount of current flowing in the heater load is reduced or vice versa. The sensor consists of three thermistors. One of them is placed immediately after the heating load, one at the input of the chamber and the third at the output of the chamber. The thermistor at close proximity to the source of heat input introduces a degree of anticipatory control. This anticipatory control effect coupled with the high gain and sensitivity of the system counteracts any fluctuation of temperature of the inflowing medium. The thermistor at the output tends to compensate for any variation of the heat losses throughout the chamber, thus contributing to the averaging out the long-term temperature fluctuations.

The achieved stability was within 0.1°C .

The temperature was measured with a thermocouple in connection with a calibrated electronic thermometer (Comark Electronic Thermometer Type 1605).

2.6.3 Humidity Control

The required humidity in the chamber could be obtained by inserting a preconditioned quantity of wool or with sulphuric acid/water solutions. Quick changes of solutions could be achieved with a syringe through the small holes on the top cover of the chamber.

For thermodynamic equilibrium the relative humidity above a solution is determined by the specific gravity of the solution. The

relationship between specific gravity of H_2SO_4/H_2O solutions and the corresponding relative humidity is given in Appendix C. The measurement of specific gravity could be performed easily and accurately with hydrometers.

For long-term measurements at constant temperature and relative humidity it was found satisfactory to use a quantity of wool as a buffer for stabilizing the relative humidity. Wool packed in perforated containers was preconditioned in sealed vessels containing saturated salt solutions. Saturated salt solutions were used in this case because they could be used repeatedly giving always the same relative humidity. The perforated containers with wool could fit the interior of the humidifying cavity of the chamber and could be transferred within 2-3 seconds from the vessel to the chamber, thus effecting a quick change of relative humidity. A determination of the necessary quantity of wool to keep a required relative humidity constant is presented in Appendix C. A table which relates relative humidity and saturated salt solutions is also presented in Appendix C. A minimum time for conditioning the buffer wool was found experimentally to be a week, but in practice it was left for over three months. The quantity of wool used was more than 30 grams.

In addition to the tests carried out on a fibre in a controlled atmosphere, it was found that experiments could be performed with the fibre immersed in a liquid provided that (i) the liquid used was not corrosive on the various parts of the chamber; (ii) the level of the liquid was kept just below the piezoelectric element. The vibrations were not affected by the presence of the liquid to any detectable degree.

2.7 Noise

Noise presented considerable problems. The sources of noise had to be identified and isolated appropriately. Two types of noise were present: mechanical and electrical.

2.7.1 Mechanical Noise

The mechanical noise was practically eliminated by mounting the strain gauge firmly in the conditioning chamber, which had thick walls, weighed 17 kg and sat on vibration absorption pads (felts). The piezoelectric element was also in the conditioning chamber, thus the main source for mechanical noise was the very small cross-motion of the pushrod.

2.7.2 Electrical Noise

The electrical noise sources were both mains noise and radiated noise. This problem was pronounced especially at the mains frequency (50 Hz). The electrical noise problem was solved by undertaking the following steps:

- (i) Using a mains voltage stabilizer for all instruments.
- (ii) The voltage stabilizer was followed by an isolation 240v-240v transformer with double insulation and an electrostatic shield between primary and secondary.
- (iii) The d-c power supplies for the charge preamplifier, the strain gauge and the d-c amplifier in the compressor loop had to be effectively isolated from amplifiers, in order to avoid the noise of 50 Hz via direct coupling.
- (iv) The various instruments were installed in a metallic cabinet for electromagnetic shielding.
- (v) Use of balanced signal shielded lines throughout (the amplifiers operating differentially).
- (vi) Use of a common earth for the various units. Special design techniques were employed to give a high degree of ground-loop signal rejection as recommended by the instrument manuals.

The various limitations imposed made it possible for the complex modulus for fibres to be measured in the frequency range of 6-1500 Hz.

2.8 Calibration of the Apparatus

The calibration of the strain gauge was performed by switching off the vibrations and mounting a practically solid material (e.g. a brass strip). By applying a known extension via the extensometer the d-c output was recorded. The d-c calibration obtained was assumed to hold for d-c strains in the frequency range 6-1500 Hz, because the minimum transient response time of the gauge is 10 μ sec.

The p-z element was calibrated by mounting a fine tungsten wire of 29 μ diameter. Tungsten has the highest elasticity of any metal⁸⁴ and the modulus of elasticity E has been determined as a function of temperature, for tungsten single crystal wires. It is well represented by the equation

$$E_T = E_0 \left[\frac{T_S - T}{T_S} \right]^{0.263} \quad (2-33)$$

where E_T is the modulus at a temperature T⁰K, $T_S = 3653^0$ K is the absolute melting point of tungsten, $E_0 = 40,000 \pm 1000$ kg/mm². The elastic modulus even for drawn wires varies from 34800 to 37300 kg/mm² at room temperature. From equation (2-33) we find that the modulus of tungsten varies by only 1.5% in the temperature range 200⁰K to 400⁰K. The effect of change of frequency should also be negligible.

The use of a reference material does not only enable the elimination of the effects of internal friction of the piezoelectric element (equation 2-30), it also excludes errors arising from the electronic equipment (e.g. amplifiers) as well as to a large extent from the mechanical cross-motion of the vibrating pushrod. Thus a zero level for the loss angle was established for different frequencies in the temperature range -50⁰C to +50⁰C.

For convenience the modulus was first measured at a single frequency and temperature and these values were used as reference for all other measurements. To fix our ideas, we note from equation (2-31) that the

modulus can be measured by knowing the geometry of the samples. This was done for a frequency $f' = 116$ Hz and a temperature $\theta' = 25^{\circ}\text{C}$. At this frequency and temperature the modulus is given by

$$E' = \frac{V'}{V_r'} C \quad (2-34)$$

and at any other frequency or temperature

$$E = \frac{V}{V_r} C \quad (2-35)$$

From (2-34) and (2-35) we get

$$\frac{E}{E'} = \left(\frac{V}{V_r}\right) / \left(\frac{V'}{V_r'}\right)$$

$$\therefore \frac{E}{E'} = \left(\frac{V}{V_r}\right) / \left(\frac{V_r'}{V_r}\right) \quad (2-36)$$

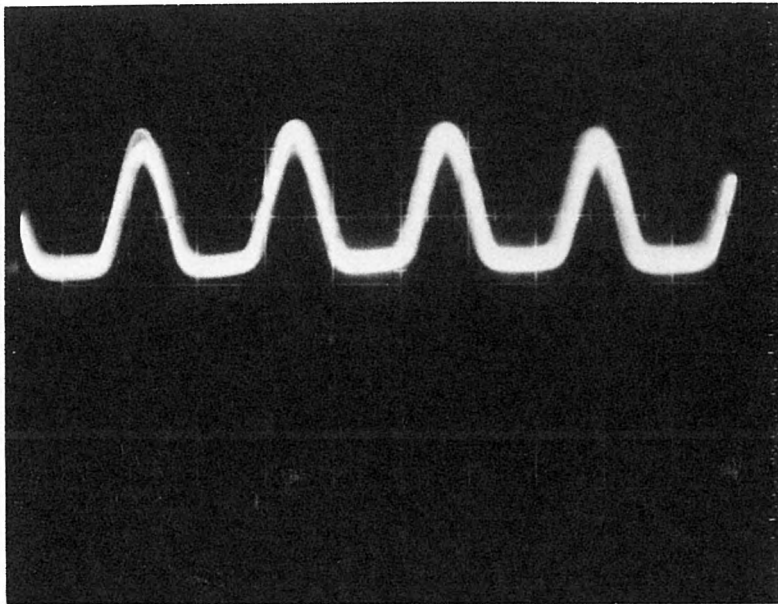
Thus by using as units the quantities E' , V' and V_r' we obtain

$$E = V/V_r \quad (2-36)$$

The relationship (2-36) is valid provided that V and V_r represent the stress output per unit strain output. In practice V and V_r represented only the stress output provided that the amplitude of strain was kept constant throughout an experiment.

The d-c extension of the fibre was found from the reading of the micrometer head and the d-c voltage output of the strain gauge. In the literature the zero point of extension is found by extrapolating the Hookean region of a stress-strain curve to zero stress. In our case this was not possible because the p-z element does not give a d-c output proportional to the stress. The small change of d-c output of the strain gauge gives a rough estimate of the stress on the fibre, but this was not calibrated. Zero extension was taken at that extension for which the sinewave of the a-c output of the stress was clipped as

a-c STRESS —→



TIME —→

Fig. 2-14 The stress signal due to the a-c strain. The signal is clipped for d-c strains lower than the amplitude of the a-c strain.

observed on an oscilloscope (fig. 2-14). When this occurs the d-c extension is of the order of the amplitude of the a-c displacement. The a-c displacement was around 4μ , which for a sample of 2 cm corresponds to a strain of 0.02%.

2.9 Errors

The errors in measurement of d-c extension arise from the position of zero extension, from the variation of length of the pushrods due to thermal expansion, and from a very small backlash of the extensometer. The overall absolute error in extension was limited to $\pm 0.05\%$ strain. For transient measurements at constant temperature and frequency the overall relative error of modulus was $\pm 1\%$ and of loss angle the absolute error $\pm 0.05^\circ$.

For measurements at varying temperature and frequency the error of modulus was $\pm 3\%$ and that of loss angle $\pm 0.1^\circ$.

The measurement of temperature was within 0.1°C .

The error of frequency was better than $\pm 1\%$.

The relative error in measuring time was significant for very short times (a few seconds), because there was an uncertainty of 2-3 seconds in defining the point of zero time.

2.10 Conclusion

The experimental technique developed in this project allows for the measurement of the complex modulus of fibrous materials under various conditions. The advantage of the technique is that once calibrated, it allows for continuous measurement of the complex modulus by continuously varying one or more parameters. Thus the following series of experiments can be performed :

Measurement of modulus and loss angle versus:

- (a) Time by abruptly changing the relative humidity at constant frequency, temperature and extension.
- (b) Extension at constant temperature, frequency and relative humidity. For fine fibres (e.g. Lincoln) extensions up to the breaking point can be reached.
- (c) Temperature at constant frequency, relative humidity and extension, in the temperature range -100°C to $+50^{\circ}\text{C}$.
- (d) Frequency at constant temperature, relative humidity and extension. This would be of great interest, if a transition could be detected. The frequency range is 6-1500 Hz.

CHAPTER 3

THE COMPLEX MODULUS OF KERATIN AGAINST EXTENSION

3.1 Introduction

In this chapter the author has reported experimental work carried out to study the effect of the extension of a wool fibre on the complex modulus of the fibre at different relative humidities and rates of extension. The change of the complex modulus with time for wool fibres in water at various extensions has been examined. The effect of extension cycling up to different strains has also been examined. Lastly the combined effect of strain and humidity cycling as well as the effect of extension at different frequencies of measurement has been checked. In each case some theoretical explanation of the results obtained has been provided.

3.2 Preparation of Samples

All the wool used in this series of experiments was from penned Lincoln sheep hand-fed for uniformity of growth of the fibres. These fibres were supplied by the Sheep Biology Laboratory of the CSIRO and had a cross-sectional area variance along their length of about 5%. They were designated SW351 for future identification. After a pre-cleaning with petroleum ether and drying, their diameter was measured and found to be around 45 microns. Medulla free fibres were chosen under a projection microscope. The fibres were rewashed thoroughly with petroleum ether to rid them of grease as well as of the cedarwood oil used for the microscope examination. Subsequently the fibres were left in room conditions for half an hour, then immersed in ethyl alcohol for one hour and finally held to form a loop in room conditions. A similar procedure has been used by various workers prior to physical

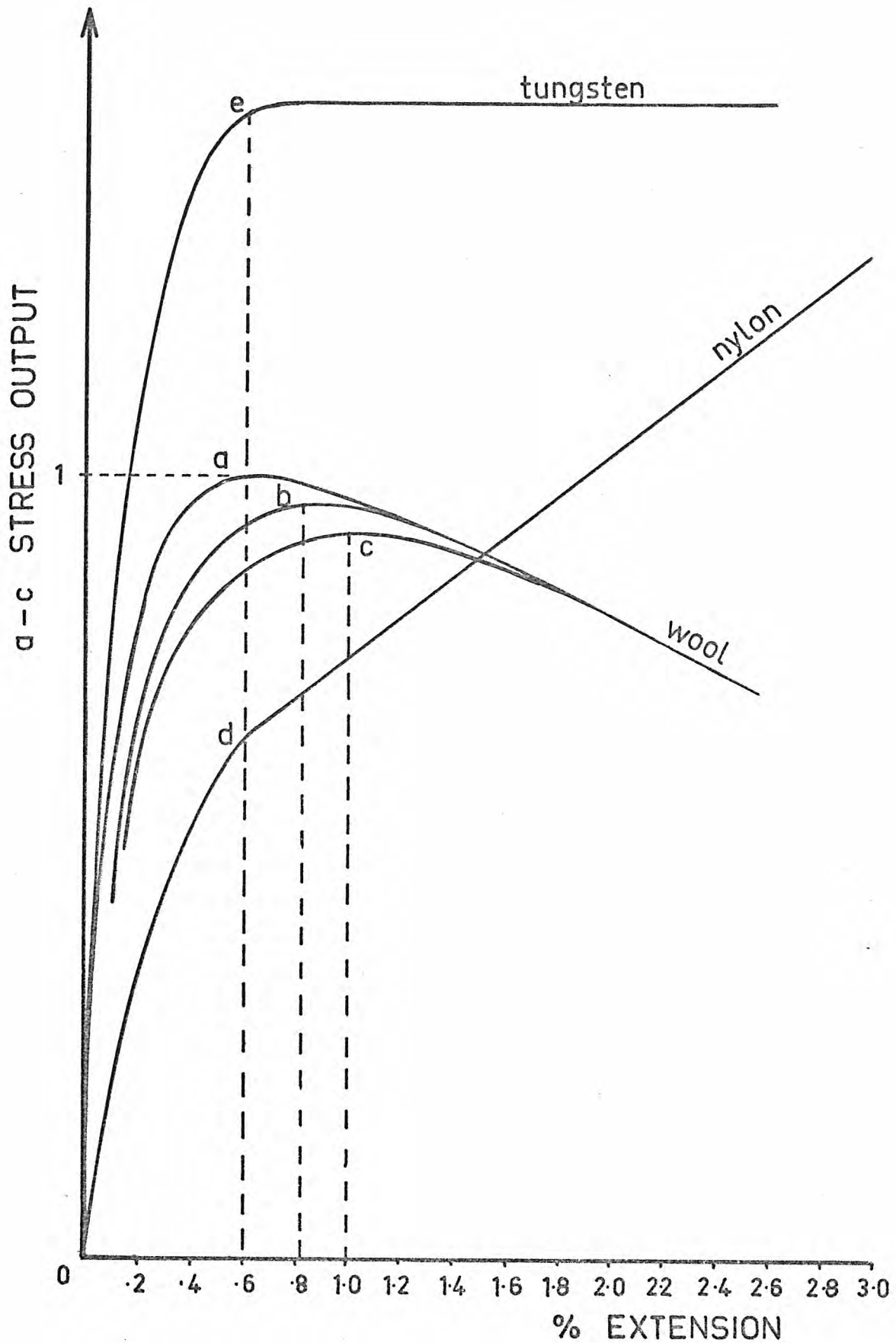


Fig. 3-1 The stress output at low extensions for wool (a,b,c), nylon (d) and tungsten (e). The stress scale for each of the three materials is arbitrarily chosen. The maximum value of curve (a) defines the unit modulus for the wool case.

and chemical tests of wool fibres. Araldite was used as adhesive for the loop. The loop length of the samples was maintained within (18 ± 0.2) mm. As each sample was being tested, an accurate loop length was obtained from the readings of the extensometer and the d-c output of the strain gauge. Except for the reference sample, for which a unit modulus is defined, as explained in the following section, the diameter of each fibre sample was not measured. All experiments in this chapter were carried out at 25°C and 116 Hz unless otherwise indicated.

3.3 Measurements at Low Extensions - Unit Modulus

It was found that the a-c output of the stress did not correspond to a tensile modulus for low extensions i.e. below 0.6% extension.

Regardless of the material tested the a-c stress output versus extension increased from zero up to a characteristic value at around 0.6% extension. Beyond this characteristic extension value the output could decrease, increase or remain constant depending on the material. In fig. 3-1 curves (a) for wool, (d) for nylon and (e) for tungsten wire depict these three cases. The monotonically increasing output up to the characteristic extension is attributed to the fact that the fibre is slack and thus the transverse waves prevail over the longitudinal. The velocity c of transverse waves is given by

$$c = \sqrt{T/\mu} \quad (3-1)$$

where T is the tension of the fibre and μ is its linear density. The tension increases monotonically from zero onwards, thus the a-c stress developed would increase correspondingly. Beyond a certain extension the longitudinal waves prevail and their velocity, which is characteristic of the medium is given by

$$c = \sqrt{E/\rho} \quad (\text{neglecting mechanical loss}) \quad (3-2)$$

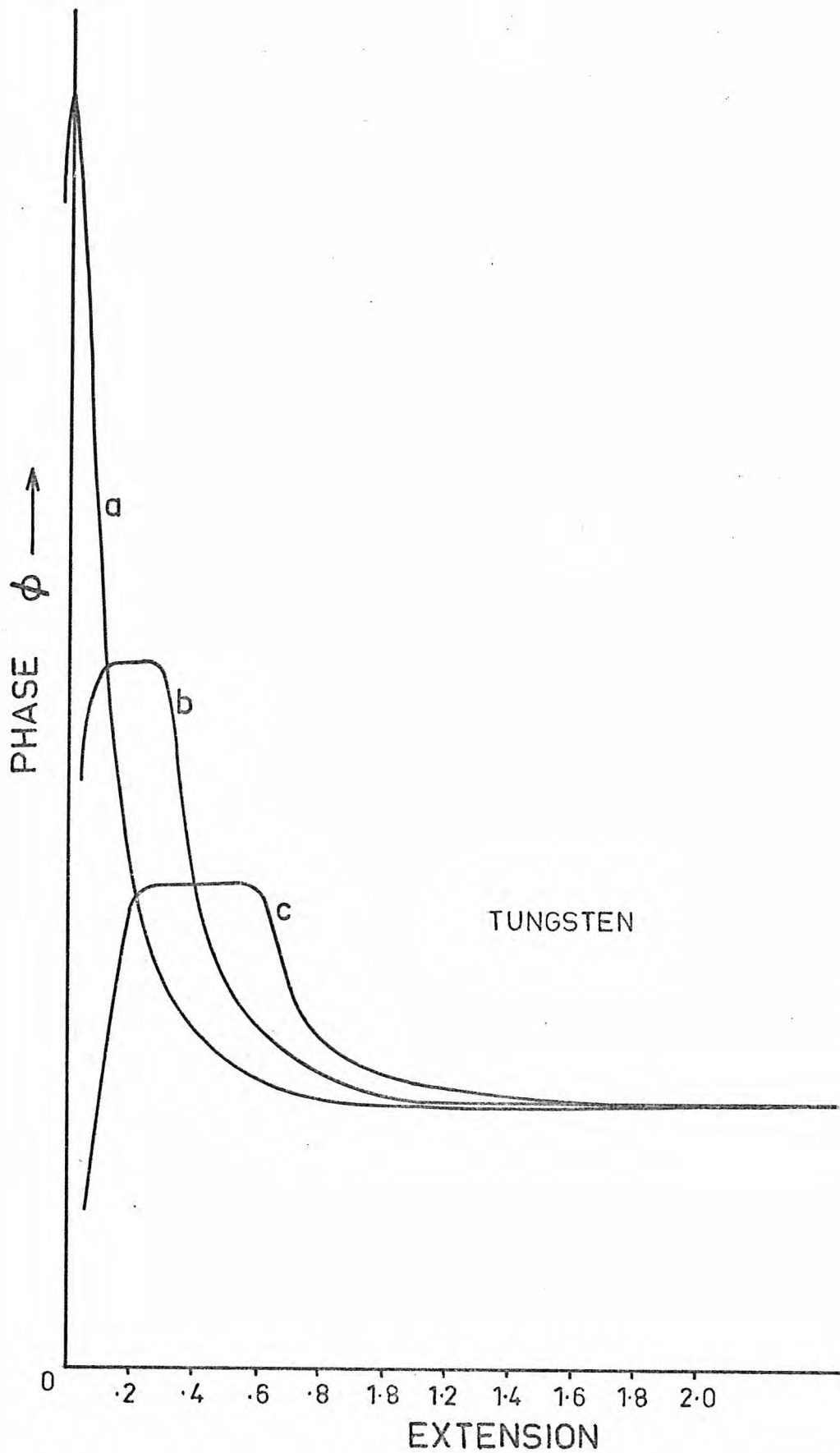


Fig. 3-2 The phase difference ϕ between stress and strain at low extensions for tungsten at three different amplitudes of oscillation, (a) 4 μ , (b) 16 μ and (c) 40 μ .

where E is the tensile modulus and ρ the density of the material. Therefore beyond this extension the a-c output is proportional to the tensile modulus, while below it the output corresponds to a decrimping as well as a bending of the fibre around the mounting points. For this reason extensions below 0.6% should not be considered true longitudinal strains; the correct strain is always less than the recorded extension, the error depending on the material and diameter of the fibre. It appears in fig. 3-1 that for the three different materials the point of inflection occurs at nearly the same extension. This has happened because of the definition of "zero" extension as described in section 2.8. For wool the modulus appears to decrease after the true strain region commences and thus a well defined peak results at 0.6% extension. The peak becomes broader with increase of a-c strain. Curve (a) in fig. 3-1 is for a 4μ amplitude of oscillation ($\approx 0.02\%$ strain), curve (b) for 16μ and (c) for 40μ . We observe that the maximum of the peaks moves to higher extensions, because the oscillating strain becomes comparable with the d-c strain.

A similar peak was found with sonic modulus measurements⁹⁵ at about 1% extension and was attributed to the structure of the material under test. Although a stiffening of the material could be present at low extensions, the author is of the opinion that such a property would be overshadowed by the straightening of the fibre. For wool in particular it was found from bending measurements⁷⁰ that the static modulus was constant for strains up to 0.3%, while from a theoretical investigation of the energy function and its second derivatives of the α -helix²⁴ the modulus should decrease from negative strains up to at least 4% strain.

The measurement of the phase difference ϕ between stress and strain of a tungsten wire is shown in fig. 3-2. Curves (a), (b) and (c) correspond to the three levels of amplitude of the oscillation i.e. 4, 16 and 40μ . The "zero" extension for curve (a) was defined

again as described in section 2.8' (see fig. 2-14). For "negative" extensions the phase (curve (a)) showed a sharp increase and above "zero" a sharp decrease up to 0.6% extension, where the phase approached the final value within 0.05° . The sharp decrease of phase can be explained according to formula (2-17) allowing the velocity c to vary according to equation (3-1). Beyond 0.6% extension where the longitudinal waves are dominant the phase measurement gives a true loss angle δ . The "zero" of curve (a) was used as "zero" for curves (b) and (c). For the latter curves we observe again an initial increasing part corresponding to the clipping of the stress wave, followed by a relatively flat portion and then a decrease towards the final value, which corresponds to higher extensions. The same general trend was observed for nylon, copper and wool fibres differing only near and above 0.6%, where the nature of the material determines the final value. Therefore the recorded changes of phase for low extensions should be attributed to the decrimping and mounting of the fibre. As a further check one fibre was observed closely while at low extension and it was noted that the fibre was slack.

The amplitude of a-c displacement was kept constant at 4μ throughout this work. It was found that the amplitude of 4μ was well within the region in which the oscillating stress is proportional to the oscillating strain. The observed maximum of a-c stress at 0.6% extension for wool in water was proven convenient to be used as a unit modulus for all the measurements taken in this chapter. This unit modulus was calibrated at 25°C and 116 Hz and it was found to be equal to $(2.0 \pm 0.2) \times 10^{10}$ dynes/cm².

In conclusion, the effect of strain on the complex modulus of wool could only be obtained beyond 0.6% extension bearing in mind what is meant by this extension.

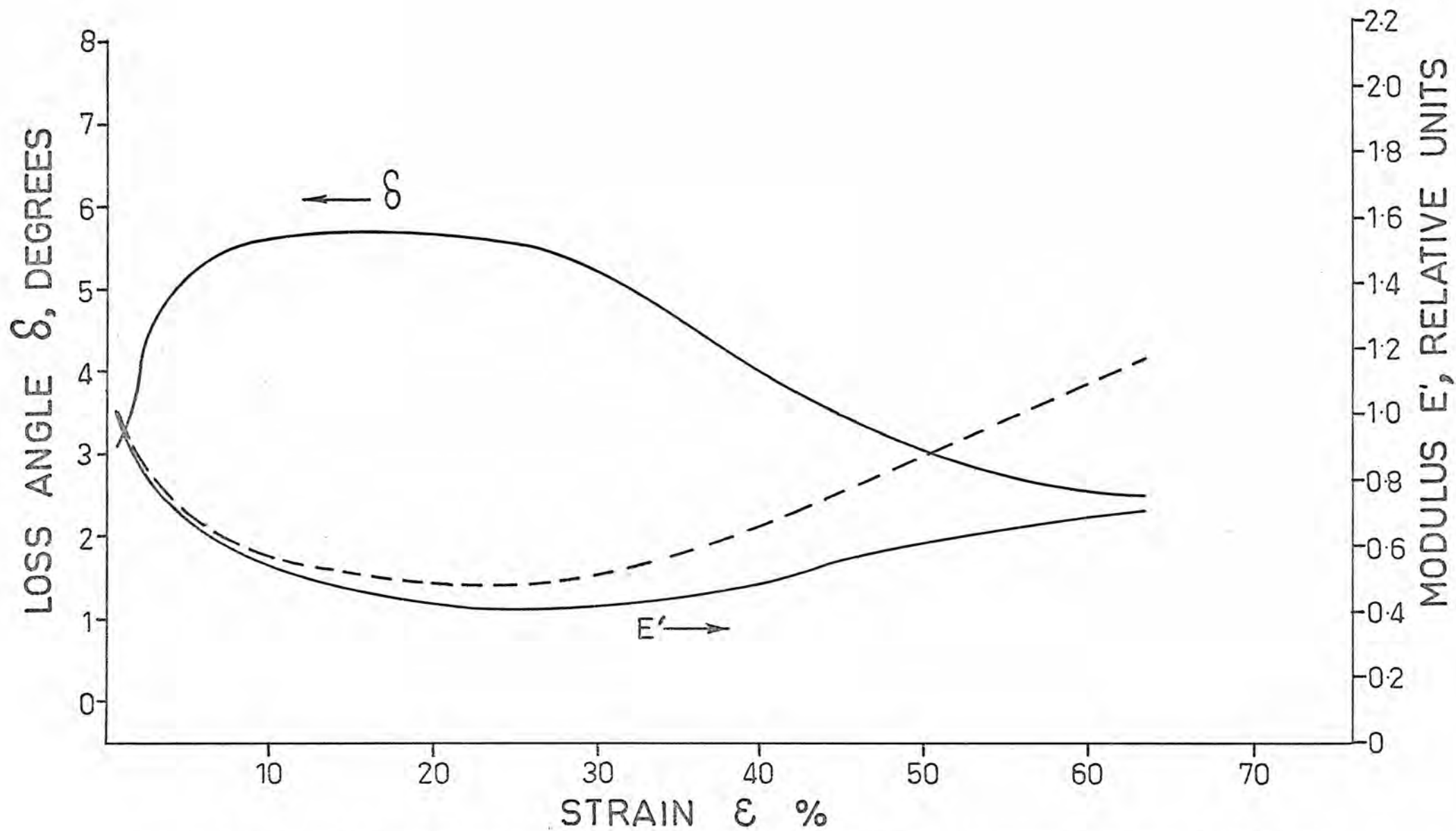


Fig. 3-3 The modulus E' and the loss angle δ against strain for wool in water at 116 Hz, 25° C and 0.18%/min strain rate. The broken line represents the corrected modulus.

3.4 The Effect of Strain on the Complex Modulus of Wool in Water

A Lincoln wool fibre was mounted slack on the tester and left in water for 24 hours. Then it was extended continuously up to the breaking point at a strain rate of 0.18% per minute. The modulus and loss angle were recorded simultaneously; the results are shown in fig. 3-3. The solid line for modulus is the direct output of the apparatus. However this must be corrected by a certain factor in order to take into account the variation of the cross-sectional area and the decrease of the oscillatory strain with the static strain ϵ as can be seen from the formula relating the modulus to the geometry of the fibre:

$$E = \frac{p\ell}{A\xi} \quad (3-3)$$

where E is the modulus, p the a-c force, A the cross-sectional area corresponding to the length ℓ and ξ the a-c displacement. The geometrical correction arising from the variation of the ℓ/A is dependent on the relative humidity surrounding the wool fibre. Below, two cases are considered, namely at 100% and 0% RH. At 100% RH the variation of the diameter with strain has been determined experimentally by Haly and Feughelman⁵⁵ and their results have been fitted in the present work by the parabola

$$d_V = 0.534 + 0.187\epsilon - 3.11 \times 10^{-3} \epsilon^2 \quad (3-4)$$

where d_V is the diametral variation in % and ϵ the static strain in %. Taking into account the relation (3-3) the geometrical correction factor g_1 at 100% RH is found to be

$$g_1 = \frac{1 + \epsilon/100}{(1 + d_V/100)^2} \quad (3-5)$$

For the case of 0% RH Haly and Feughelman checked the volume strain relationship of wool fibres and found no evidence of a measurable

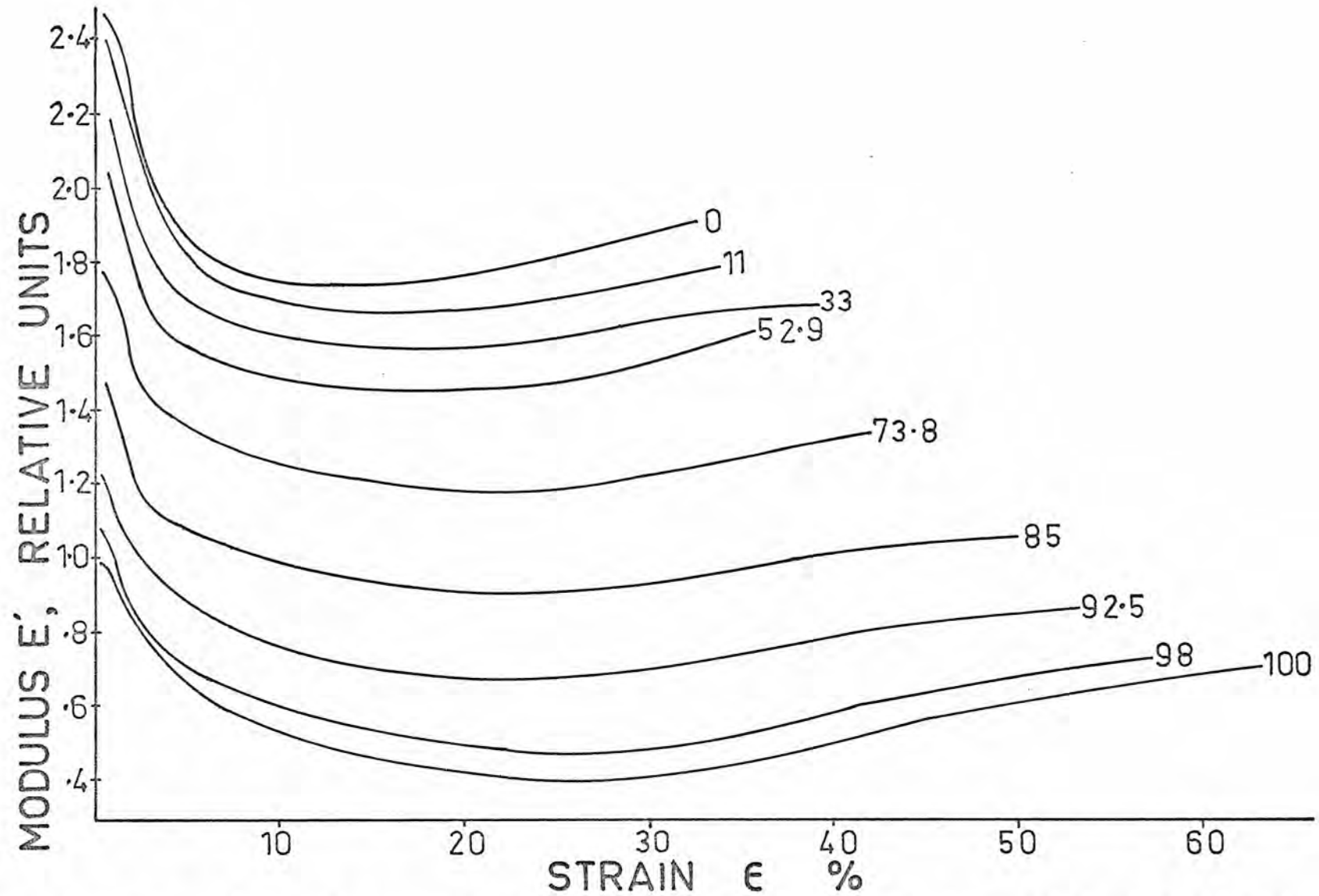


Fig. 3-4 The modulus E' against strain for different relative humidities as indicated on each curve.

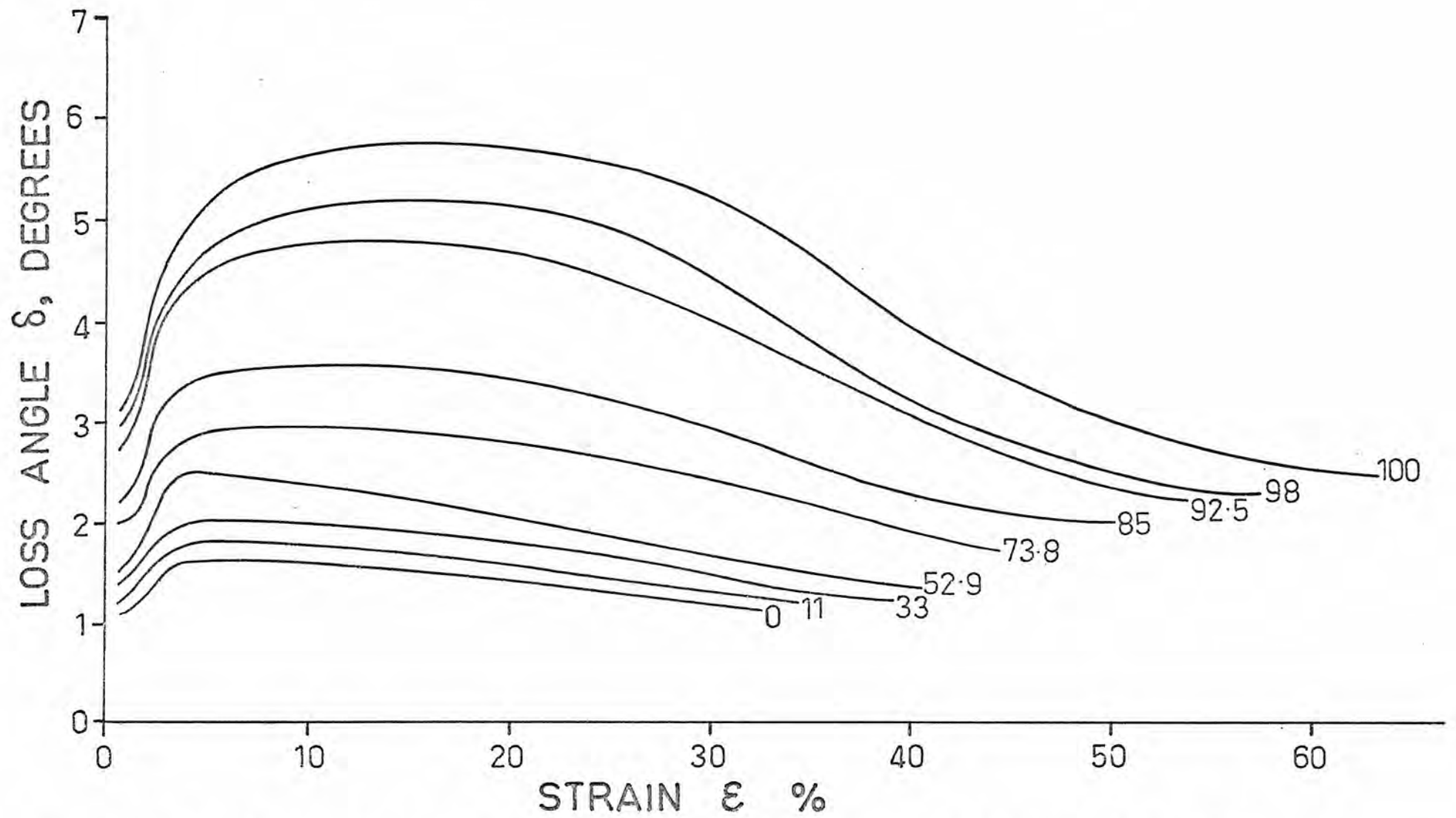


Fig. 3-5 The loss angle δ against strain for different relative humidities as indicated on each curve.

deviation from the constant volume relationship. Taking this into account the geometrical correction factor g_2 at 0% RH is easily found to be

$$g_2 = (1 + \epsilon/100)^2 \quad (3-6)$$

The broken line in fig. 3-3 shows the corrected modulus after effecting the correction g_1 . We notice that the modulus decreases up to about 22% strain and then increases gradually up to the breaking point (63% strain). The loss angle δ follows the changes of extension inversely to the modulus. The corrected modulus at the breaking point is higher than its initial value, while the loss angle is lower than its initial value.

3.5 The Effect of Strain on Complex Modulus of Wool at Different Relative Humidities

The modulus and loss angle versus extension were measured at various relative humidities. Prior to each test the fibres were mounted and left slack in 100% relative humidity for 24 hours, then dried for 24 hours and finally brought to the desired relative humidity during the following 24 hours. Conditioning the fibres of 100% relative humidity erases their "memory", so that their history becomes irrelevant and all fibres can be assumed to be in an identical initial state. In this way a comparison of the results becomes meaningful. After this treatment the fibres were extended at a rate of 0.18% per minute up to the breaking point and the modulus and loss angle were recorded. The results are shown in fig. 3-4 for the modulus and in fig. 3-5 for the loss angle. The dynamic moduli presented in this chapter are not corrected by the factor g_1 or g_2 unless otherwise indicated. The "zero" strain was set as defined in section 2.8 at each relative humidity. Measurements were taken at the following

relative humidities with the corresponding regains for the fibres as obtained from Appendix c.

RH	%	0	11	33	52.9	73.8	85	92.5	98	100
Regain	%	≈1	4.4	8.4	12	16.5	20	24	28.6	33

The dry atmosphere does not correspond to a completely dry fibre because of the possible presence of "incorporated water". The regain though must be very low ($\approx 1\%$)^{2,91}.

We notice that the modulus curves shift upwards with decrease of regain, the general shape of the curves remaining the same. However, there is an increase of the steepness of the initial part i.e. $< 5\%$ strain. Below 24% regain most of the initial change of modulus occurs within 3% strain i.e. within the Hookean region. It is also observed that the difference between the maximum recorded value of modulus at 0.6% strain and the minimum value of modulus at intermediate strains is almost independent of regain and equals approximately 0.6 units. The loss angle also retains the same general shape for all regains. The height, however, of the peak increases with increase of regain as does the width.

The general shape of the modulus curves for strains $> 1\%$ is in agreement with the result by Woo and Postle⁹⁵ who measured the sonic dynamic modulus of wool at discrete strains and room conditions.

3.6 The Effect of Rate of Static Strain at Different Relative Humidities

The rate of the static strain change was found to have a marked effect on the complex modulus of wool in water. The samples were left in water for 24 hours and then extended at three different rates of strain i.e. a very slow one of 0.023% per min., for which it took two days to break the fibres, a medium rate of 0.18% per min.

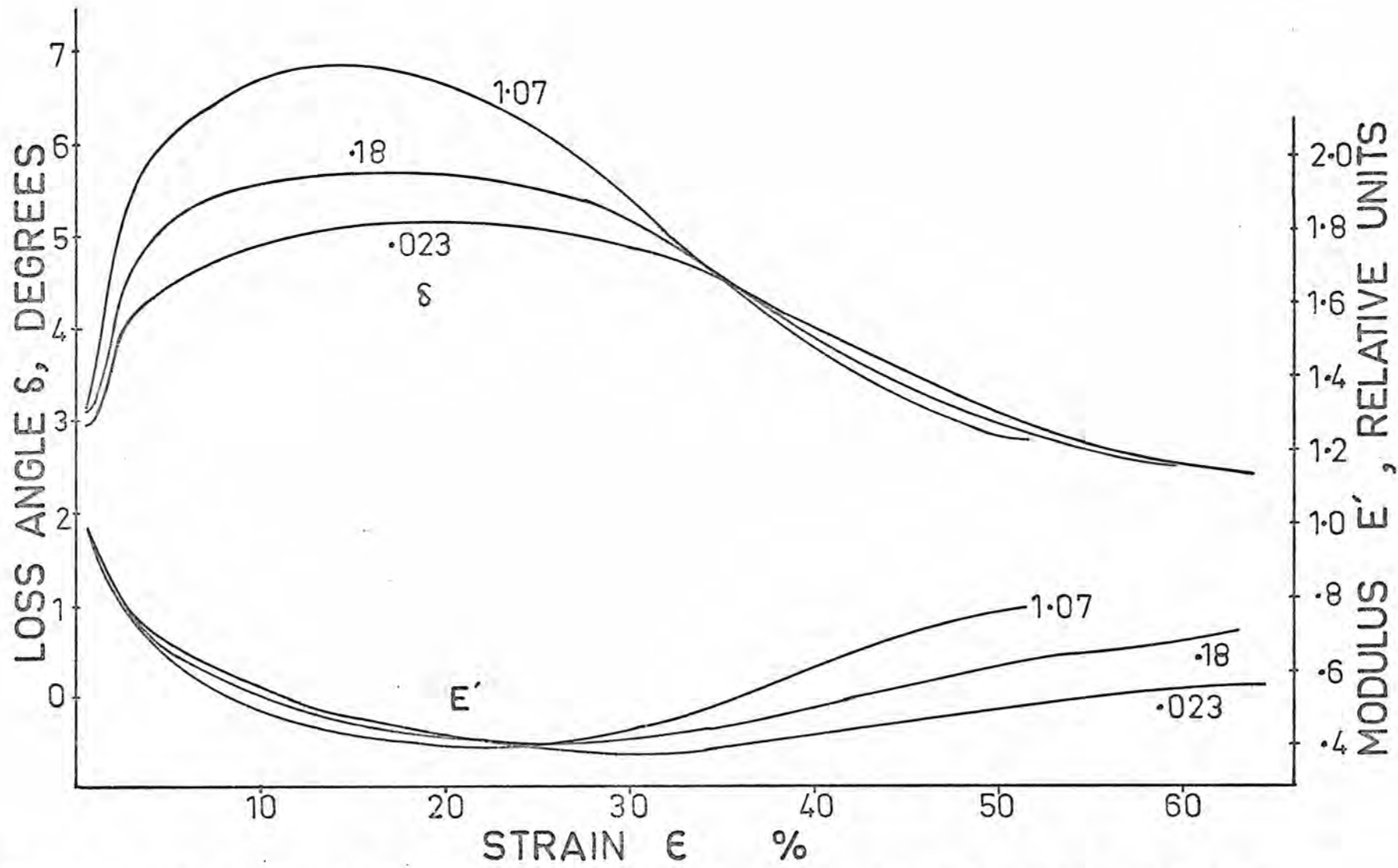


Fig. 3-6 The modulus E' and the loss angle δ against strain for wool in water at three different strain rates as indicated on each curve.

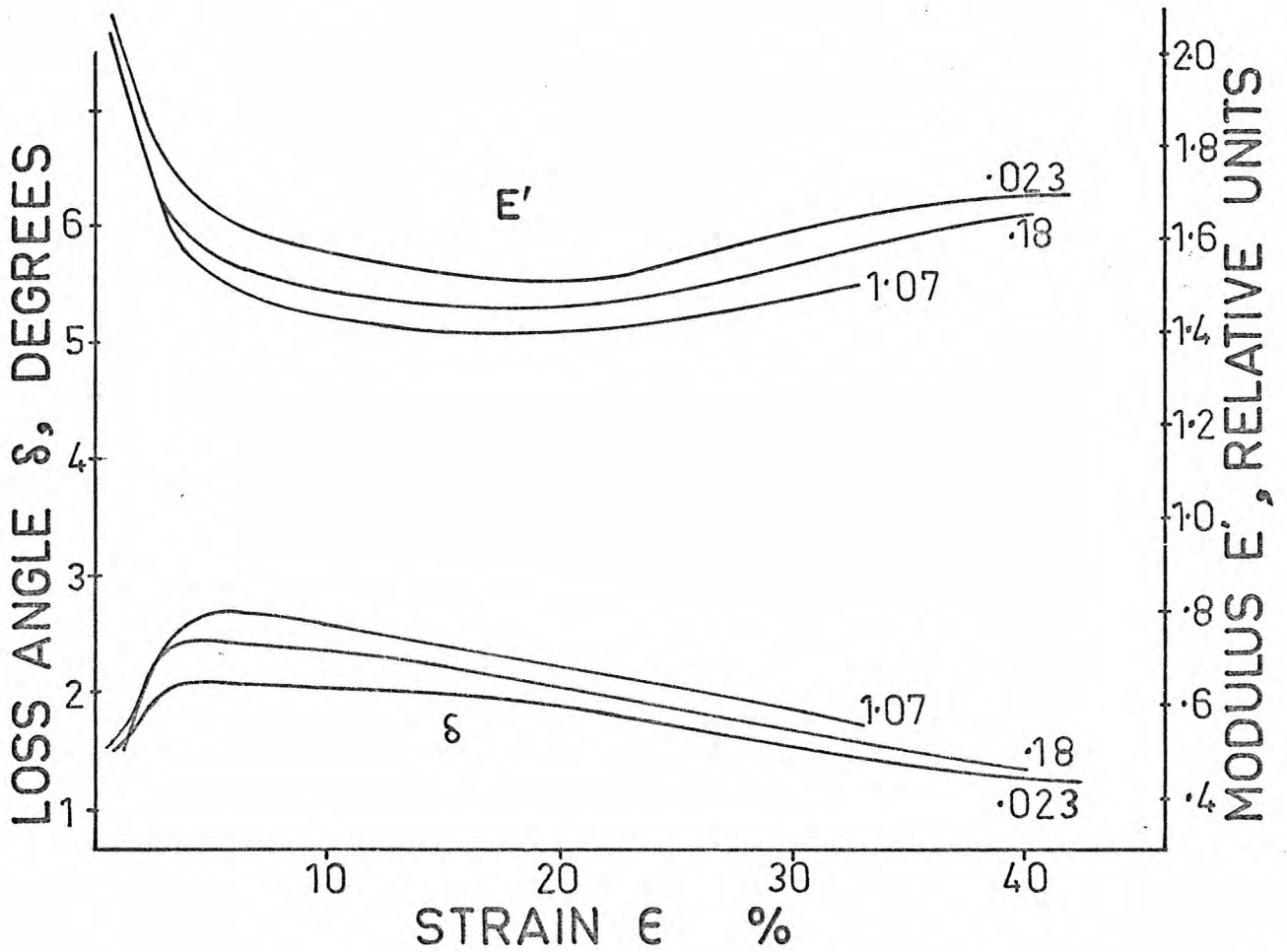


Fig. 3-7 The modulus E' and the loss angle δ against strain at 52.9% R.H., at three different strain rates as indicated on each curve.

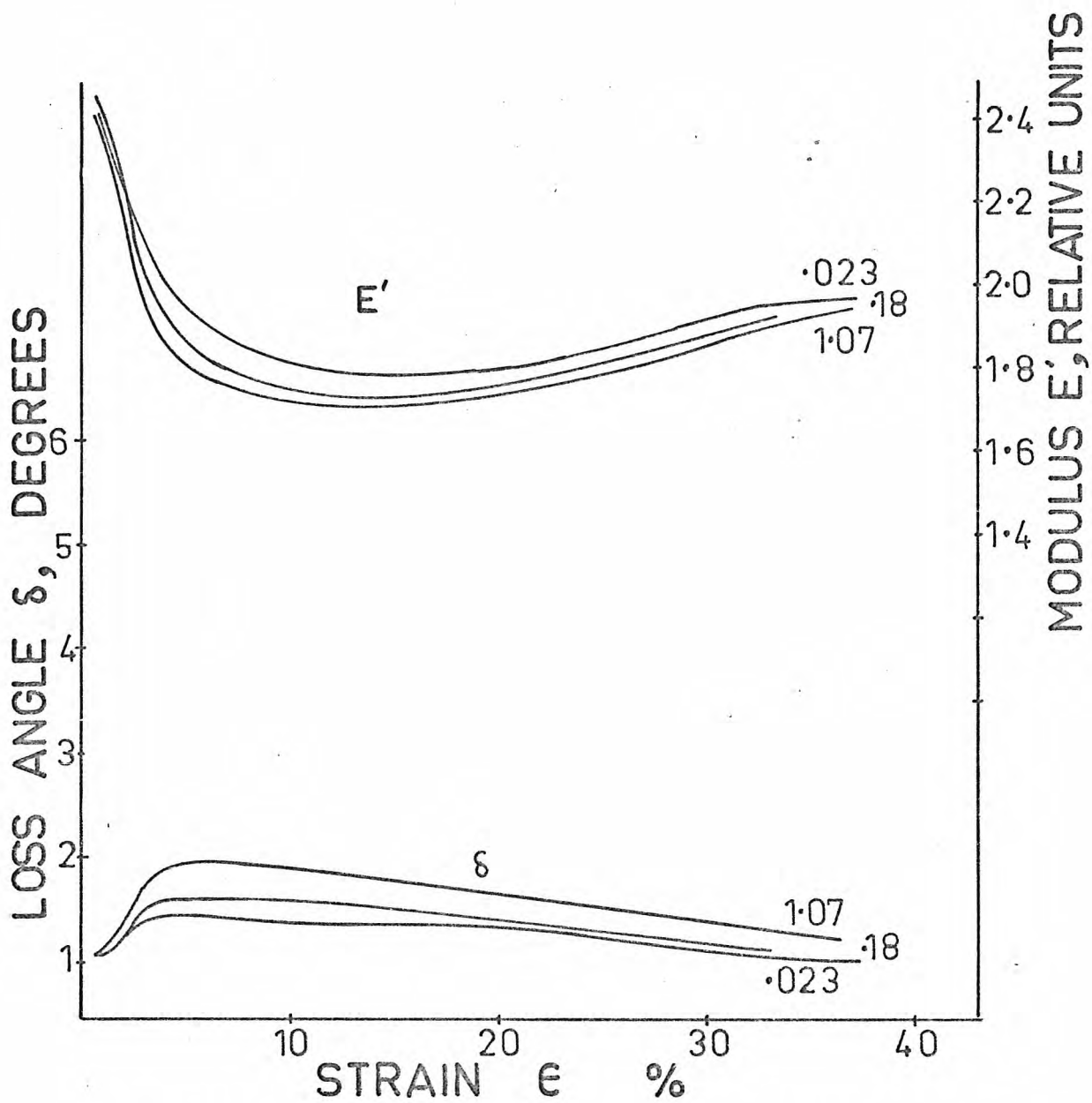


Fig. 3-8 The modulus E' and the loss angle δ against strain at 0% R.H., at three different strain rates as indicated on each curve.

(≈ 6 h to break the fibres) and a faster one of 1.07% per min ($\approx \frac{1}{2}$ h to break). The results are shown in fig. 3-6. The modulus reaches a lower value for a higher rate at lower strains; at higher strains the modulus attains a higher value for higher rates. The loss angle follows the inverse direction of these changes.

The effect of rate of strain was examined for fibres at equilibrium with 52.9% RH as well as 0% RH. The conditioning was performed as in the previous section. The results for 52.9% RH are shown in fig. 3-7 and for 0% RH in fig. 3-8. From these figures it seems that the effect of rate of straining becomes less significant at lower relative humidities. However it is clear again that the modulus achieves a lower value for a higher strain rate at all strains recorded. It is unknown what happens at very high strain, because the fibres break at lower extensions at lower relative humidities.

3.7 The Two Phase Model

On the basis of the above observations the change of physical behaviour of wool fibres with strain and relative humidity may be understood in terms of the two phase model. This model was originally proposed by Feughelman³⁰ to explain some mechanical properties of wool fibres. He considered a model fibre of circular section containing cylinders of phase C parallel to the fibre direction embedded in a matrix of phase M. According to that model, when the fibre is dry the mechanical properties of both phases are identical and for small extensions ($\approx 1\%$) also isotropic. Increase of relative humidity from 0 to 100% around the fibre progressively causes the phase M to swell isotropically. Phase C unstrained does not swell with increase of relative humidity. The increase of the relative humidity, and hence the moisture uptake of component M, reduces the mechanical moduli of this phase; phase C remains unchanged. The diametral dimensions of phase C are of molecular size. Finally it

was assumed that when the fibre is stretched, phase C becomes progressively accessible to moisture.

Although some of the above features of the model could be partly modified, it is generally accepted that the microfibrils embrace the organised and relatively water-impenetrable regions and hence may be thought of in terms of phase C; the matrix the disorganised and relatively water-penetrable regions of the keratin fibre may be thought of as phase M. Obviously a zone of gradation may exist between the two. Bendit¹¹ has shown that a large proportion of a microfibril is non-helical material. Further, side chains, which represent some 50% of the structure of keratin, whether attached to helical or non-helical material interact with water molecules. This means that only a fraction of the microfibrillar structure does not associate with water, namely the ordered helices together with their stabilizing disulphide bonds. However, the above gradation would not alter the points raised here in attempting to explain the experimental observations.

Two further assumptions, about the model, relating to the viscoelastic character of keratin are made in the present work. These are:

- (i) The phase C is practically loss free and therefore elastic at all strains and relative humidities.
- (ii) The phase M is characterised by a short-term relaxation process, for which the spectrum of relaxation times is practically invariant at all strains but dependent on the relative humidity and the rate of strain.

In the following subsections 3.7.1 and 3.7.2 a general discussion on the phase C and the phase M based on existing data and views is aimed at giving a preliminary justification of the above two assumptions and an understanding of structural changes during extension.

Subsequently the two assumptions are justified in their application in explaining the experimental results of this work.

3.7.1 The Phase C

Because of the crystalline nature of the microfibrils, they exhibit far less swelling and loss of mechanical stability due to the presence of water when compared to the matrix. The α -helices thus stabilize the structure longitudinally by mechanically opposing both extension and swelling. The stability of the α -helices and the stability of the microfibrils in the keratin structure are concomitant. The crystalline fraction of the microfibrillar structure accounts for the major portion of the equilibrium Young's modulus of 1.4×10^{10} dynes/cm²⁵⁰. A much smaller portion of this equilibrium modulus arises from the cross-linked network of protein chains, disulphide bonds together with possible stabilized units such as small globular proteins. This latter conglomerate of matter forms the matrix and the nonhelical microfibrillar material. The actual dimensions of a microfibril as seen under the electron microscope represents some 60% of a keratin fibre.

Electron microscope evidence^{59,78} suggests that the microfibrils are long and possibly run the full length of a cortical cell (c.100 μ). It follows that the extension of the fibre as a whole corresponds closely to the extension of the microfibrils. As the fibre is extended the α -keratin form is transformed into β -configuration, i.e. the α -helix is opened up into β -pleated sheet form. Quite a number of experiments point to the necessity of co-operative unfolding of the α -form in the intact α -keratin fibre. This necessity may arise from the environment in the fibre external to the α -helices. Haly's⁵⁷ results on reduced disulphide fibres, for example, suggest that the cystine link is involved in maintaining lateral mechanical co-operation

between the helices. This transformation starts from the beginning of the yield region up to the breaking strain. The situation thus arises, in which one ordered form (the α -) is transformed into another (the β -) and this means that the phase C remains practically elastic at all extensions, being under all conditions of strain the combination of two ordered forms α and β .

The assumption that the phase C remains practically elastic for all extensions can be criticised from the following observations. In a normal fibre extended in the yield region some α -keratin crystallites have been opened up and some β -keratin crystallites formed by the extension. In this process we may consider that α -crystallites go to a "liquid" or amorphous form, which may be considered as the activated state. Thus in addition to the presumed $\alpha \rightarrow \beta$ transition in the microfibrils there may also be α -crystallites \rightleftharpoons activated form \rightleftharpoons β -crystallites at mechanical equilibrium. Ciferri and Smith¹⁶ have set out the formal modifications resulting from the existence of three forms (α, β , activated) instead of two. On the other hand Bendit¹⁰ has emphasised that in the reversible $\alpha \rightleftharpoons \beta$ transformation produced by the isothermal extension of a wool fibre it cannot be assumed that there is a 1:1 conversion of molecular groups from α -form to β -form, because some of the newly created β -material may have been initially in a disordered form in the matrix. The existence of an activated state in the crystalline regions is tantamount with the creation of mechanically lossy material which contradicts the assumed elastic properties of phase C at all extensions. The activated material then becomes probably accessible to water. This is supported by the observed increase of diametral swelling against strain⁵⁵ which reaches a maximum (approx. 3%) around 25% strain. Further evidence is provided by Bendit et al⁸ who found that if wool were stretched at room temperature in D₂O by steps

of 1% up to an extension of 40% over a period of 8 hours and held at this extension for one day, then the exchange of hydrogen by deuterium in the peptide linkages was almost complete. It appears therefore that during extension of the wool fibres to 40% all the peptide linkages are able to enter into a hydrogen \rightleftharpoons deuterium exchange. This means that the whole of these fibres including the oriented regions is accessible to water. However, if the fibres were first stretched to 40% and relaxed in H_2O and then reacted to equilibrium with D_2O , only partial hydrogen \rightarrow deuterium exchange was observed. The same was observed with tests on fibres containing a large amount of β -keratin. From these observations by Bendit et al it is concluded in the present work that the accessibility of the phase C by water during extension is only transient i.e. a changing portion of the crystalline structure becomes only temporarily accessible to water and this portion is probably the material which exists in a disordered form between the α - and β -form.

In summary, the phase C, which unextended is in the α -form, when extended is in three forms : (a) unextended α -form, (b) extended β -form and (c) in an activated non-aligned form. The first two forms being crystalline can be assumed of small mechanical loss and therefore elastic. The form (c) can also be assumed as contributing negligibly in the mechanical loss of the phase C for either or both of the following reasons : 1) The form (c) constitutes only a small fraction of the total phase. 2) The α helix converting to the β -state requires a considerable amount of convolution of the peptide chains. Because this transformation occurs with little impedence (note: the small stress change in the yield region), it follows that only short chain portions of α -helix transform into the activated state and thence to the β state and that these short chain units are not impeded in their movement. It would therefore follow that the movement of the peptide chains in the activated state

are nearly loss free, especially in the time-scale of the present experiments.

The above discussion on the phase C seems to justify the first assumption made in section 3.7 i.e. that the phase C is practically loss free and therefore elastic at all strains.

One last point is made next concerning the stiffness of the phase C. The presence of the activated form (c), although it does not have a significant effect from the loss energy point of view, it may have a decisive effect on the stiffness of the phase, i.e. its modulus. The form (c) can disrupt the continuity of alignment and crystallinity and hence reduce the modulus considerably. The amount of form (c) is expected to increase with the rate of straining, hence resulting in a lowering of modulus with increase of rate of strain.

3.7.2 The Phase M

Consideration is now given to the mechanical behaviour of the phase M at varying extensions. The matrix is a cross-linked polymer held together by a network of polar bonds⁷¹ such as hydrogen bonds, salt-linkages and Van der Waals forces. It has been shown⁷¹ that the salt-linkages play a greater part in the mechanical stability of the matrix than they do in the whole fibre. As to what happens to these bonds and therefore to the matrix at high extensions can be understood from experiments on the torsional properties of single wool fibres⁷¹. The torsional properties in the main reflect the properties of the matrix. The conclusions arrived at from past work on torsion are assumed for the longitudinal extension of the matrix in the present work. Thus it is thought that the initial extension of the matrix strains polar bonds in the matrix network and, as the extension increases, some of these bonds break. As the extension increases further broken bonds reform on new sites. Eventually, as a large value of extension is reached, the rate

of breaking of bonds and the formation of new ones becomes equal and further extension does not produce an increase in stress. The matrix under these conditions is acting as a viscous solution and presumably would continue in this way with increasing extension until the cross-links and the backbone structure of the polymer forming the matrix approach full extension, or the deformation of other physical entities in the fibre, such as the microfibril, introduced opposition to the extension. The former effect, namely the opposition of the cross-links, backbone or entanglements limiting this viscous extension of the matrix has been demonstrated not to occur even at high extensions of the fibre. Invariably other effects external and parallel to the matrix intervene to limit further extension of the matrix⁵¹. This has been further demonstrated⁹⁹ in experiments on the lateral properties of keratin structures where it has been shown that at all lateral extensions in water up to break for porcupine quill and rhinoceros horn there is no indication of increasing stress level with extension that could be a result of crosslink, backbone or other limitations on the viscous flow of the matrix. (See Figure 1-4).

Disulphide bonds are an important component of the phase M and the mechanical and other effects of these crosslinks have been studied³. It has been found that any difference in disulphide crosslinking in the normal and sulfur-enriched fibres does not markedly affect the torsional behaviour of fibres because the larger proportion of the mechanical stiffness in torsion is governed by polar bonding and the effects on stiffness for differences in disulphide crosslinks could be masked. The disulphide bonds in the matrix can undergo reversible breakdown in the presence of water. The mechanism, sulphhydryl-disulphide interchange, however, involved in this breakdown does not occur to any significant extent in normal wool fibres at low extensions, for temperatures below 50°C.

For short times the stress relaxation of a strained matrix will be mainly due to the breakdown of polar bonds. Feughelman and Rigby²⁸ found that wool fibres immersed in water had a long-term and a short-term relaxation process at all extensions. The short-term process was associated with a relaxation time τ that depended very little on extension (between 5% and 25% strain) and also on temperature (between 5°C and 45°C). This relaxation time was found to be around 10 seconds. As pointed out earlier the characteristics of the matrix is that of a gel-like solid which under extension, because of polar bond breakdown, becomes a viscous solution, in other words goes from a "gel" to "sol" state. Under these conditions the mechanical characteristics of the matrix is independent of the extension. The results quoted from Feughelman and Rigby suggest that the stress relaxation of the wool fibre, being extension independent, is attributed to the matrix and hence the relaxation time of ≈ 10 seconds for the wet fibre stress-relaxing in the strain range of 5 to 25% can be attributed also to the matrix. That is, the basic structure of the matrix does not change but simply flows around the microfibrils and readjusts itself at any extension. This redistribution is characterised by the mean relaxation time $\tau \approx 10$ seconds, which corresponds to the short-term process. For lower relative humidities the relaxation times may become longer due to the lower mobility of the structure.

The fact that the short-term relaxation time is not constant beyond 25% strain may be attributed to the onset of other viscous flow effects due to the microfibrils or in the gradation region between the two phases associated with phenomena in the post-yield region. It is found⁴³ that when a fibre is stretched in water into the post-yield region (above 30% strain) and held extended, the resultant force-log (time) relationship shows three distinct regions. At room temperature

these three regions fall into periods (a) <0.1 minutes, (b) 0.1 min to 10 min and (c) >10 min. Wood showed that the first period is due to the breakdown of polar bonds, which therefore correspond to the matrix flow; the last period is due to scission of disulphide bonds. This disulphide bond breakdown is a result of sulphhydryl-disulphide interchange. This mechanism is confirmed by tests at low pH, at which sulphhydryl-disulphide interchange is prevented, and also tests with reduced wool fibres. Feughelman proposed⁴³ that during the intermediate period (b) the drop in value of force with time is due to disengagement between matrix and filament components of special zones in wool fibre structure.

The above discussion on the phase M seems to justify the second assumption made in section 3.7 i.e. that the phase M is characterised by a short-term relaxation process, for which the spectrum of relaxation times is practically invariant at all strains.

One last point need be made concerning the relative importance of each phase. The importance of phase M on C depends on the way we look at the material i.e. on the type of experiment that is carried out. For example, from room temperature up to 60°C it has been pointed out^{13,97} that the contribution of entropy to the mechanical properties of wool is negligible. The results obtained by Feughelman and Mitchell (May 1959) showed that at 10% strain the remanent (static) stress at a temperature 60° - 70°C has an elastomeric component less than 20% of the total stress and at 40% strain a component of about 50% (at 60° - 70°C there is a second order transition for the stretched wool fibre in water). However from a dynamic measurement point of view the importance of matrix becomes quite significant. In other words, the dynamic modulus at a sufficiently high frequency and at a given strain can be attributed mainly in the matrix, while the relative contribution of the crystalline phase decreases.

3.8 Application of the Two Phase Model

If a strain ϵ , which is a function of time and given by $\epsilon(t)$, is applied to a fibre, then the Boltzman superposition principle^{54,27} relates the stress on the fibre to the strain by

$$\sigma(t) = \int_{-\infty}^t \frac{d\epsilon(\tau)}{d\tau} [E_c(\epsilon) + E_m(t-\tau)] d\tau \quad (3-7)$$

In our experimental work

$$\epsilon(t) = \kappa t \quad (3-8)$$

where κ is the rate of strain applied to the fibre. The integration (3-7) contains two terms, one, E_c associated with the purely elastic character of the material, and the other, E_m , associated with the viscoelastic character of the material. The aim here is to perform the integration (3-7) by utilizing the two assumptions about the two phase model made in the previous section and show that the result is compatible with the existing experience. The term E_c , which is identical with the vector E_r in figure 1-6, is attributed to the phase C, while the term E_m (see figure 1-6) is attributed to the phase M. The integration (3-7) is performed in two steps in the following two subsections.

3.8.1. Integration of the Elastic Term

The two phases C and M are in parallel so that the stresses taken up by each phase must be added to give the resultant force on the fibre. If the strain is oscillatory, the addition of stresses must be made vectorially. A consequence of the assumption proposed in the previous section is that the vector for stress associated with the phase C must be in phase with the applied strain, since C is assumed mechanically elastic, while the vector for stress associated with the amorphous region M must lead the applied strain by an angle δ_m .

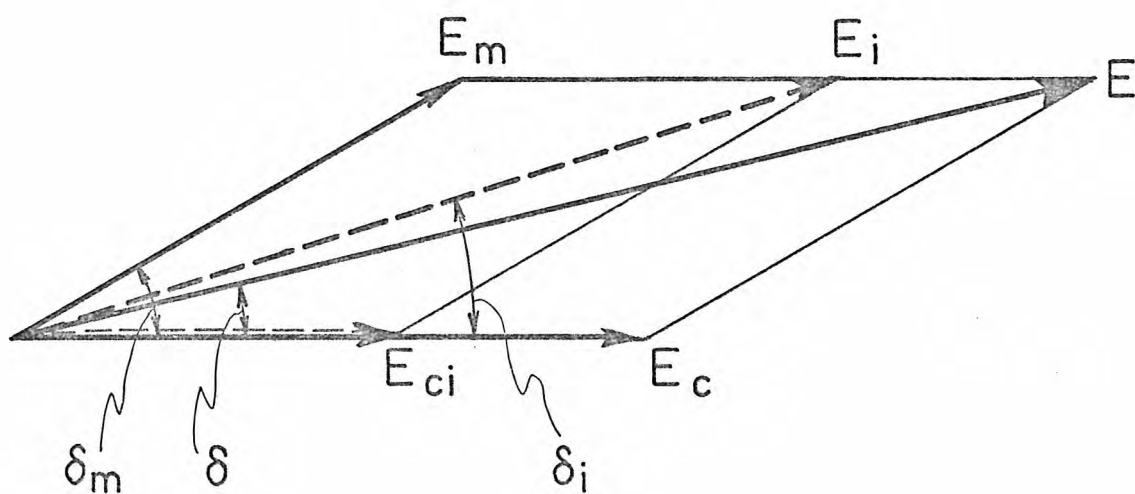


Fig. 3-9 Vector diagram for the moduli of the two phases and the fibre: E_c for the phase C, E_m for the phase M and E for the total fibre; δ is the loss angle for the fibre. At a different extension the E_m remains constant and $E_c \rightarrow E_{ci}$ and therefore $E \rightarrow E_i$ and $\delta \rightarrow \delta_i$.

The moduli (stress per unit strain) for the two phases and the fibre are shown in a vector diagram in fig. 3-9, where E_C is the modulus for the phase C, E_m the modulus for the phase M, E the resultant modulus for the fibre, δ_m the loss angle for the phase M and δ the measured loss angle for the fibre. It must be clarified here that the moduli for each phase refer to force per phase over the total cross-sectional area of the fibre. The correct moduli of each phase could be obtained if the relative fraction for each phase were known.

From the diagram the following relationships are derived

$$E_m = (E^2 + E_C^2 - 2EE_C \cos\delta)^{\frac{1}{2}} \quad (3-9)$$

$$\delta_m = \tan^{-1} [E \sin\delta / (E \cos\delta - E_C)] \quad (3-10)$$

and
$$E_C = [E^2 + E_m^2 - 2EE_m \cos(\delta_m - \delta)]^{\frac{1}{2}} \quad (3-11)$$

From equations (3-9) and (3-10) the magnitude E_m and loss angle δ_m of the complex modulus for the phase M can be obtained by evaluating the quantities involved at "zero" strain. The quantities E and δ are measured experimentally, while the unextended modulus E_C for the crystalline phase is given from the work of Feughelman and Robinson as $E_C = 1.4 \times 10^{10}$ dynes/cm². The latter value is the equilibrium modulus but it is equated with the dynamic modulus because of assumption (i) that the C region is elastic. Once the values for E_m and δ_m have been obtained at "zero" strain they can be used at other strains in equation (3-11) as constants (according to assumption (ii) with regard to the model) and the modulus for the crystalline phase can be calculated at all strains. The E and δ are available experimentally at all strains and in this way the results of fig. 3-6 for a wet fibre at three different rates of extension have been used to calculate the variation of modulus for the crystalline region. The results are shown in fig. 3-10 (bottom). The rate of strain is shown with each curve.

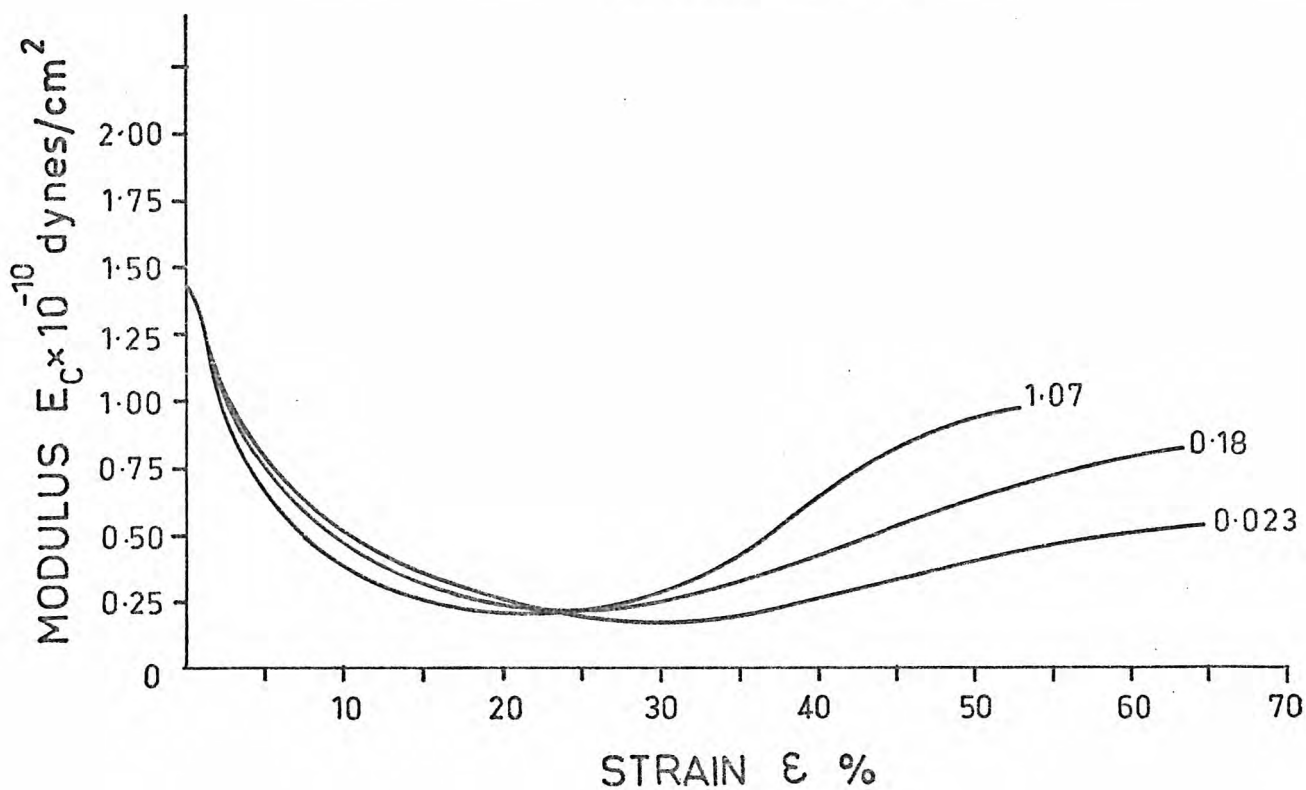
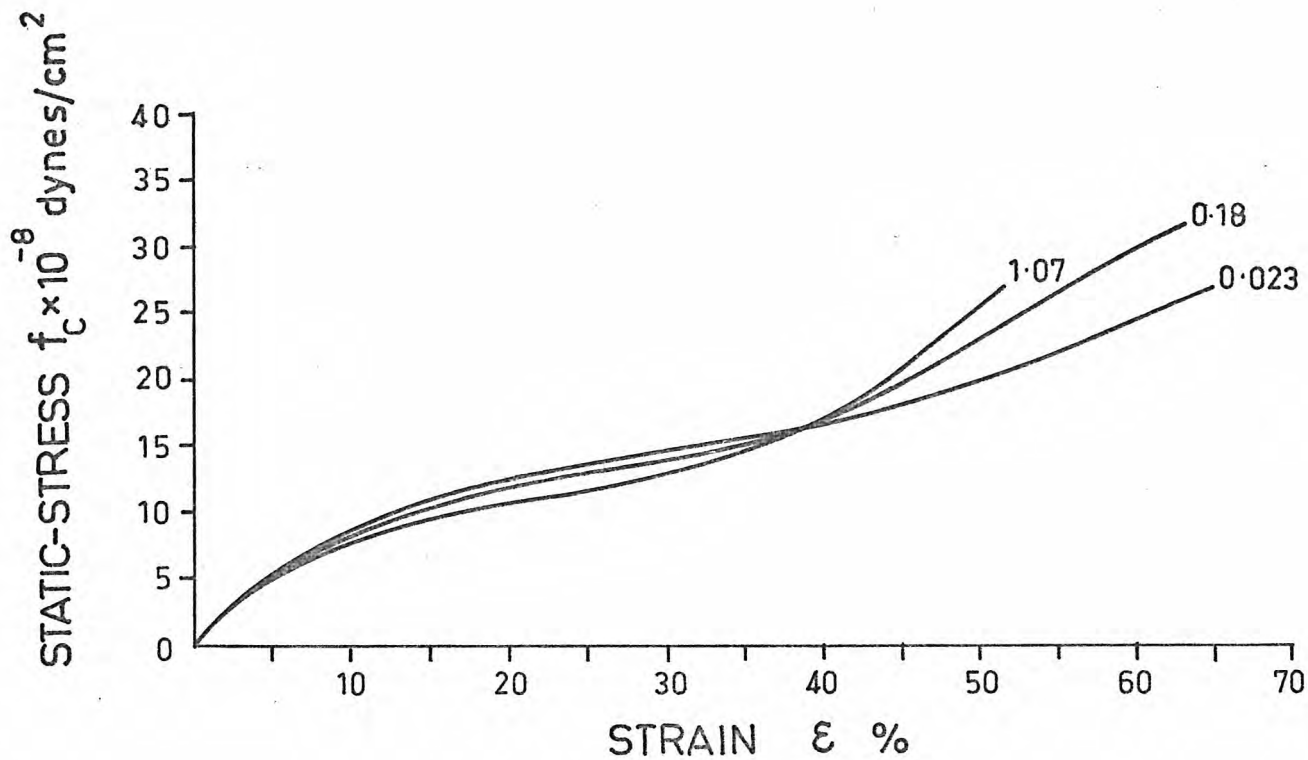


Fig. 3-10 The calculated modulus E_c of the phase C against strain for a wet fibre at three different strain rates as indicated on each curve (bottom). The calculated static stress-strain curves (top) by integrating the bottom curves.

Because the phase C has been assumed practically elastic, the modulus represents the slope of a static stress-strain curve. Therefore it is possible to obtain the static stress f_c - strain ϵ relationship for the phase C by integrating the modulus curve with respect to strain. The results of such an operation are presented in fig. 3-10 (top) for the three rates of strain.

It is observed that the static stress-strain curve thus derived presents the main characteristics of a stress-strain curve of a normal fibre. The Hookean, yield and post-yield regions are clearly present. The levels of stress are of the same order of magnitude as values published for keratin fibres^{66,99}. It follows that the stress-strain relationship for the phase C corresponds closely to the stress-strain relationship for a fibre as a whole in water. This result is compatible with the fact that the microfibrils are long and possibly run the full length of a cortical cell. The level of stress in the yield region however is lower for a higher rate of strain, which is contrary to established experience for the whole fibre. This probably arises from the fact that the phase M in parallel has not been taken into account. The lower stress in the yield region for the phase C is compatible with the fact that at higher rates of strain, with a concomitant increase of the rate of transfer of α -form material into extended β -form, the amount of material in the activated state between α and β must increase. The lower stress in the yield region of the stress-strain curve of the phase C for higher rates of strain reflects the presence in the C phase of more activated material.

The same procedure of integration was followed for a dry fibre; the modulus $E_c(\epsilon)$ for the C phase and the static stress-strain curves have been derived using the experimental results of fig. 3-8.

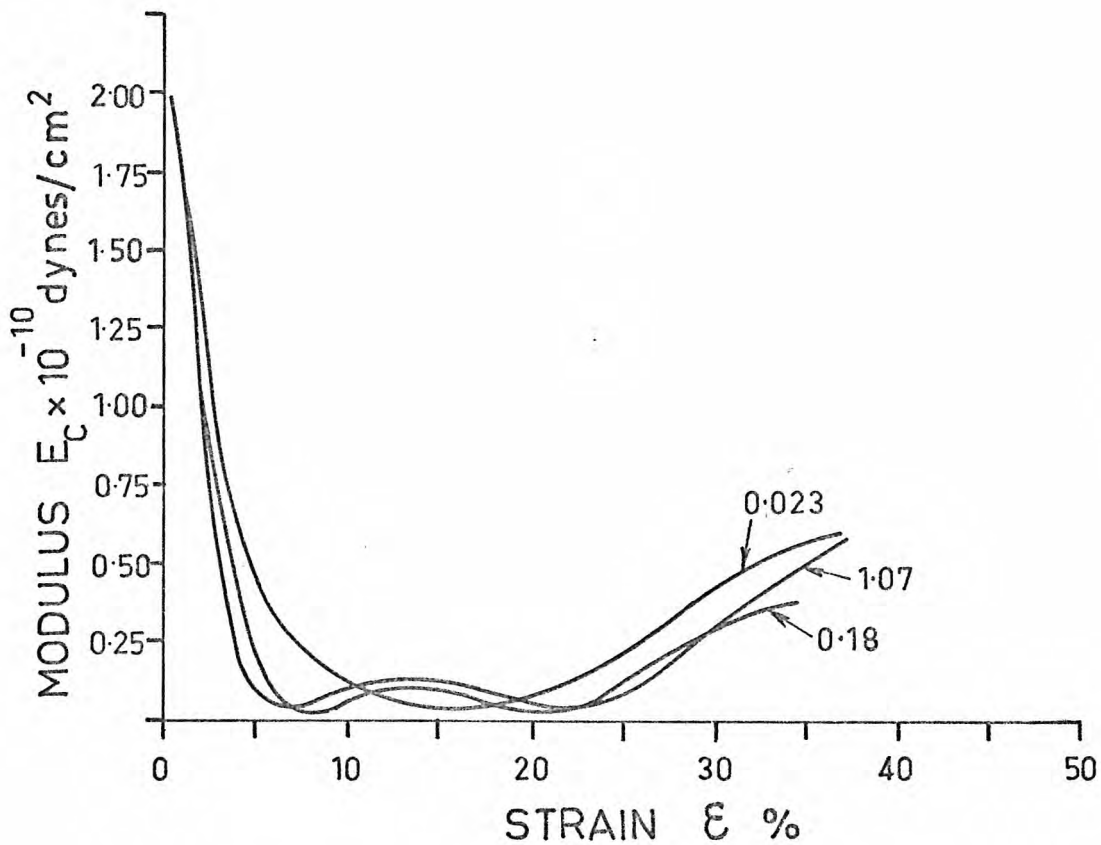
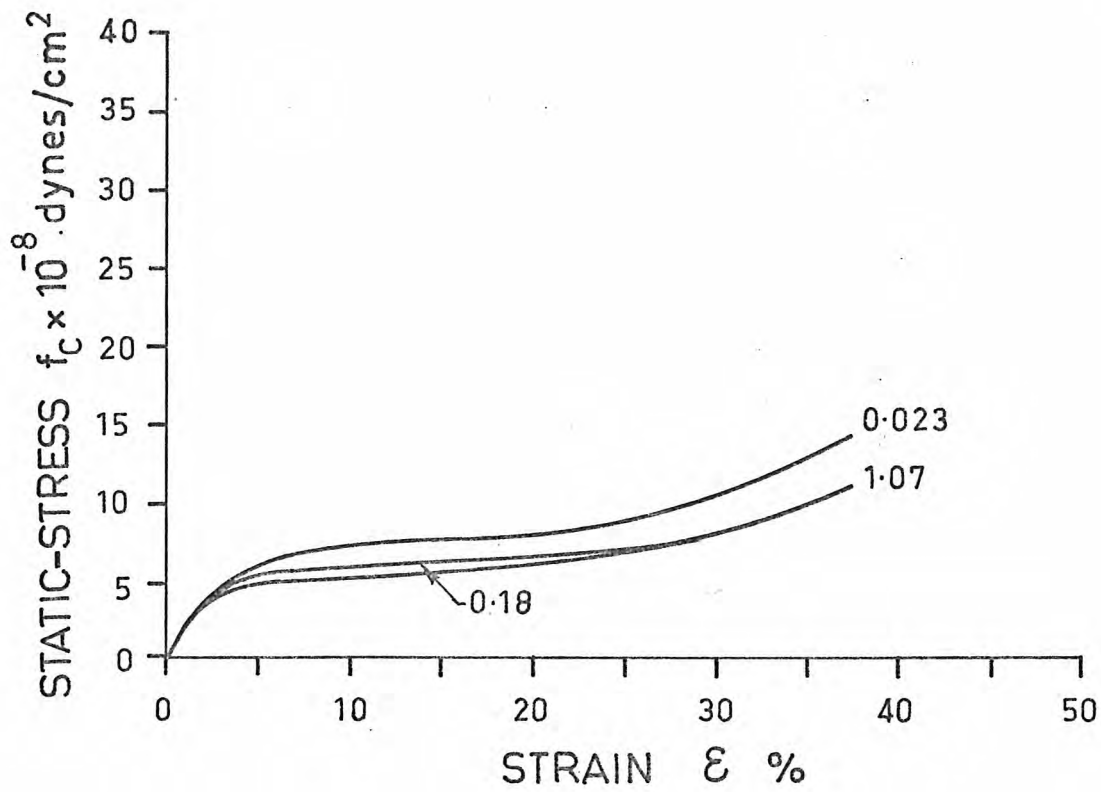


Fig. 3-11 The calculated modulus E_c of the phase C against strain for a dry fibre at three different strain rates as indicated on each curve (bottom). The calculated static stress-strain curves (top) by integrating the bottom curves.

The results from this procedure are shown in fig. 3-11. The general characteristics of the stress-strain curve for the C phase are similar as in the wet state. However, the Hookean, yield and post-yield regions can be distinguished more easily in the dry state; in addition, the level of stress in the yield region is somewhat lower and the turn-over points between the three regions occur at lower strains. These features are compatible with Bendit's¹⁰¹ X-ray evidence that in the process of unfolding from α - to β -form the transformation proceeds more rapidly at low than at high relative humidities; i.e. at a given strain, the transformation has proceeded further in the case of dry than that of wet fibres. This observation of Bendit's implies, therefore, that during extension more activated material is present in the dry than in the wet state and hence the modulus should be lower in the former than in the latter case.

It is noted at this point that the modulus $E_c(\epsilon)$ for the dry fibre has been multiplied by a factor of 1.35 to account for the reduction of the wet cross-sectional area due to the loss of water. The correction to compensate the effects of extensions was not carried out in order to make it easier to perform a comparison of the work in this section with results published by various other research workers.

3.8.2 Integration of the Viscoelastic Term

Consideration shall now be given to the integration of the viscoelastic term, namely the term corresponding to the phase M. The function $E_m(t)$ is unknown; however, as an approximation Feughelman and Rigby²⁸ used a simple exponential

$$E_m(t) = E_{m0} \exp(-t/\tau) \quad (3-12)$$

where E_{m0} is the difference between the initial and relaxed modulus; τ is some mean relaxation time. The integration of the second term of

equation (3-7) using the function (3-12) yields

$$f_m(t) = E_{m0} \kappa \tau (1 - \exp(-t/\tau)) \quad (3-13.)$$

which in connection with the strain function

$$\epsilon(t) = \kappa t$$

produces the static stress-strain curve for the phase M. The latter curve has the same shape as the curve (I) in fig. 1-4 for extension perpendicular to the growth of a porcupine quill. It is observed from (3-13) that the stress in the matrix M increases with increase of rate of strain, a feature that conforms with common experience. This increase should overcompensate for the decrease of modulus of the phase C. An approximate estimate of the equilibrium stress of phase M can be obtained by using the following values.

$$\kappa = 1\% \text{ per min} = 0.01 \text{ per min.}$$

$$\tau = 0.2 \text{ min} \quad \text{and}$$

$$E_{m0} = 2 \times 10^{10} \text{ dynes/cm}^2$$

The equilibrium value of stress (eq. 3-7) i.e. beyond about 1% strain is given by

$$E_{m0} \kappa \tau = 0.4 \times 10^8 \text{ dynes/cm}^2.$$

This value is not adequate to compensate for the decrease of the stress level of the phase C with rate of strain, which is approximately 2×10^8 dynes/cm² (fig. 3-10, top), although the order of magnitude can be considered satisfactory. The discrepancy is probably due to the oversimplified form of eq. 3-12 and the use of one relaxation time instead of a complete spectrum of relaxation times. The measurement of E_{m0} , performed by the present author using an "Instron", was also not very accurate. The oversimplifying assumptions about the two phase

model must also contribute to the discrepancy.

The above analysis based on the two phase model is further confirmed from the work of Feughelman and Druhala shown in fig. 1-4 that the longitudinal stress-strain relationship reflects the C region in the main, while the role of the M region is to add a component of static stress of the form of eq. (3-13) with an equilibrium value of $\approx 1.5 \times 10^8$ dynes/cm² at the given rate of extension (4% per minute).

3.8.3 Discussion on the Experimental Results

The two-phase structure with the assumptions proposed is obviously a first order approximation to the problem. No account is taken of the gradations that may exist between two such phases. However, simple as the structure proposed may be, it does give a satisfactory picture for the dynamic mechanical properties obtained in this work. Thus the variation of dynamic modulus against strain (fig. 3-4) is due to the C region and is practically independent of water content. The vertical shift of the curves is due to the M region, which is water penetrable. The dynamic modulus of the C region decreases initially and this is due to the unfolding of the α -helices and the formation of an activated state between the α and β form. The decrease of modulus is more abrupt at lower relative humidities and this can be explained by Bendit's χ -ray evidence¹⁰¹ as mentioned earlier. The α -form is eventually transformed with extension into the ordered β form and the modulus again increases. The loss angle variation is due to the combined interaction of the two phases C and M. The loss angle which arises from mechanical losses in the region M increases with increase of water content. This explains the vertical shift of the curves of fig. 3-5. The loss angle δ_m for the region M remains practically constant at any strain but the loss

angle for the whole fibre is determined by the relative moduli of each phase with respect to the other. For intermediate strains for which the C region has a low value of modulus E_{Cj} with respect to the M region of modulus E_m (see fig. 3-9) the phase δ_j for the fibre is higher. At very high strains, for which the modulus E_C is increased again, the loss angle for the fibre decreases correspondingly. In this way the maxima recorded for the loss angle can be explained in terms of the changing modulus of phase C. These maxima become more pronounced with increase of RH. In contrast, the amount of decrease with strain for the modulus is nearly independent of RH. These observations are a direct consequence of the mathematical analysis of the model presented previously.

The effect of rate of strain could be generally understood by a similar reasoning. A higher rate of strain of the fibre results in a greater amount of activated material in the phase C of the fibre. This means a reduction in the stiffness of the phase C with increase of this activated material; this reduction becomes prominent for extensions up to $\approx 20\%$ and is accompanied by an increase for the loss angle of the whole fibre.

It can be seen from fig. 3-6, 3-7 and 3-8 that at lower water content the effect of rate of strain tends to be more pronounced in the case of modulus measurement and less pronounced in the case of loss angle measurement. Increase of rate of strain for a fibre in the dryer case results in a greater amount of activated material in the C phase according to Bendit's X-ray data; it follows that the modulus of the phase C (and hence for the whole fibre) must show a pronounced drop with increase of rate of strain of the fibre for the dryer case. The phase difference, because it is already at a low level for the drier situation, does not change very markedly with change of strain rate.

From the above results it seems that the anisotropy at strains $>1\%$ in the fibre is diminishing for drier conditions but it is always present. It was proposed originally that the dry fibre is mechanically isotropic for low strains ($<1\%$). Makinson⁶⁵ has also shown that the elastic anisotropy is not very marked for dry keratin and she suggested that the anisotropy that does exist is to a large extent due to histological structure rather than molecular or near molecular structure. However from the present work it appears that the anisotropy could be due to molecular structure differences of the two phases especially for strains $>1\%$. Whether these differences are revealed or not depends on the mechanical properties which are considered and in particular the time scales of the experiment.

The modulus at very high strains ($>\approx 30\%$) is larger for higher rates of extension. This increase with strain rate at high extensions as well as the decrease at lower extensions ($\approx 20\%$) is associated with some relaxation processes possibly in the microfibrils. The elastic component E_c of the complex modulus has been considered as relaxation free up to now; the two phase model, as proposed in this work, cannot predict and does not explain the origin of relaxation processes. These are examined in experiments which follow in the next sections.

Regarding the effect of rate of strain the findings of Sikorski and Woods⁸³ should be mentioned. They found that the Young's modulus (slope modulus) varies linearly with \log (rate of straining). It will be shown in Chapter 5 of this thesis that such a relation holds over a considerable range of frequencies (or times) for a wet fibre in its Hookean region. In the present work an oscillatory strain is used to study the effect of the static strain. The oscillatory strain is very small (0.02%) and it should not affect the structure of the tested material, while the static strain is likely to alter the molecular structure of the material. In the case of keratin fibres

TABLE 3-1

The fibre and matrix complex moduli at different relative humidities.

RH %	F I B R E					M A T R I X			Fibre swelling factors
	E' * Relative Units	E' $\times 10^{-10}$ dynes/cm ² (corrected)	δ degrees	E'' $\times 10^{-8}$ dynes/cm ²	E'' $\times 10^{-8}$ dynes/cm ² (corrected)	E _m $\times 10^{-10}$ dynes/cm ²	E _m $\times 10^{-10}$ dynes/cm ² (corrected)	δ_m degrees	
0	2.485	6.72	1.10	9.54	12.90	3.57	4.83	1.53	1.352
11	2.42	6.34	1.20	10.14	13.28	3.44	4.51	1.69	1.310
33	2.22	5.63	1.40	10.85	13.76	3.04	3.85	2.04	1.268
52.9	2.06	5.06	1.55	11.14	13.68	2.72	3.34	2.35	1.228
73.8	1.78	4.20	2.00	12.42	14.64	2.16	2.55	3.30	1.179
85	1.49	3.40	2.25	11.70	13.34	1.58	1.80	4.24	1.140
92.5	1.22	2.67	2.70	11.49	12.58	1.04	1.14	6.32	1.095
98	1.07	2.23	2.95	11.01	11.49	0.74	0.77	8.50	1.044
100	1.00	2.00	3.10	10.82	10.82	0.61	0.61	10.27	1.000

* 1 Relative Unit = 2×10^{10} dynes/cm²

we have seen how the static strain and its first derivative affect the structure of the material.

To conclude this section an examination is made of the variation of the components of the complex modulus for the whole fibre and the phase M alone.

The components of complex modulus for the unextended fibre (at $\approx 0.6\%$ strain) taken from fig. 3-4 and 3-5 are given in table 3-1. The complex moduli for the matrix alone as calculated from equations (3-9) and (3-10) are given in the same table. The loss modulus was calculated from the equation

$$E'' = E \sin\delta$$

The magnitude of complex modulus and the in-phase component E' are practically equal, the difference being less than 0.05%. Where the moduli are indicated as corrected, the measured values have been multiplied by the correction factors presented on the last column of the table, in order to take into account the cross-sectional area variation due to desorption of water. These factors were calculated from data on diameter swelling given in reference (96).

3.9 Energy Considerations - Loss Modulus

A useful physical quantity is the energy ΔW absorbed by the fibre per cycle per unit volume. This is given by⁹⁸

$$\Delta W = \pi a^2 E \sin\delta = \pi a^2 E'' \quad (3-14)$$

The loss modulus E'' is thus a direct measure of the energy absorbed and therefore an indicator of possible molecular structure changes in the fibre. This modulus has been calculated against strain for wet and dry fibres at three rates of extension. The calculation was based on the data of fig. 3-6 and 3-8. To eliminate the effect of the change of cross-sectional area and oscillatory strain amplitude due to

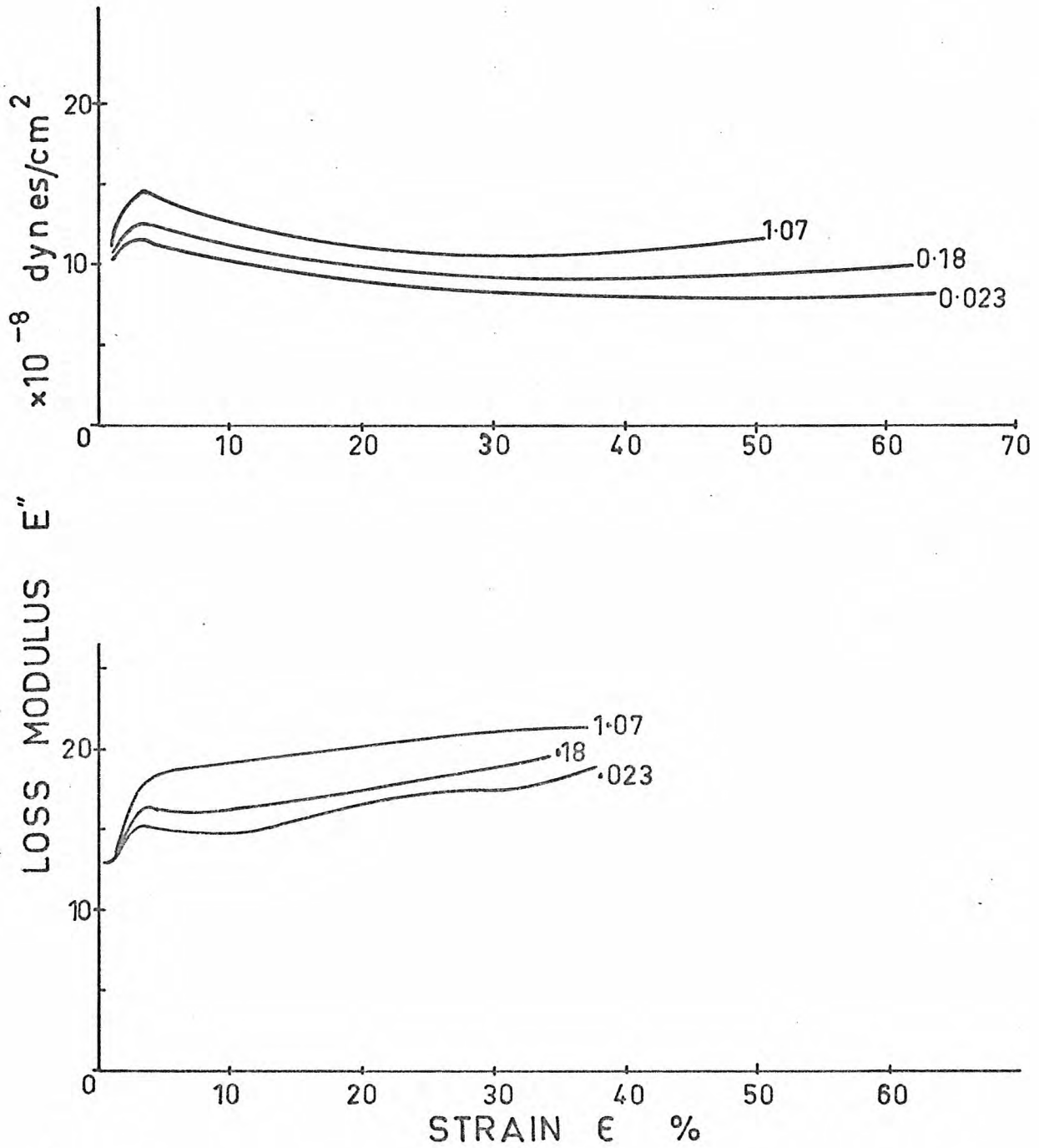


Fig. 3-12 The loss modulus E'' against strain for wet (top) and dry fibres (bottom) at three different strain rates as indicated on each curve.

extension, the moduli were multiplied by g_1 for the wet and by g_2 for the dry fibre (see eqs. (3-5) and (3-6)). The results are presented in fig. 3-12.

It is observed that the loss modulus is generally constant over a large region of strain. This is compatible with the two-phase model as proposed previously. That is, the phase M remains invariant and the energy absorbed by it must also remain invariant, while the phase C as elastic material does not absorb energy. Nevertheless, the loss modulus is not absolutely constant with strain; there is a variation within $\approx \pm 4\%$. Any deviation from the constant level is also a deviation from the two assumptions concerning the elasticity and the viscoelasticity of the model and its explanation must be sought in some structural change in the fibre. Thus the maximum of E'' around 3% strain could be explained as follows. When initially strained, the phase M, a crosslinked network of weak interactions, will progressively suffer bond breakdown followed by bond reformation (a gel-sol transformation). At an extension of a few percent a steady state is reached where bond breakdown and reformation become equal and further extension does not change the nature of the material as stated elsewhere. At this point the mechanical loss of the M phase material will reach a steady value. An increase in the rate of strain of the fibre will result in relatively faster bond breakdown and hence increase the loss modulus.

3.10 Measurement of Complex Modulus of a Fibre Relaxing in Water at Fixed Extensions

Several samples were tested in water, after having been left slack in water for 24 hours. They were extended at a rate of strain of 1.07% per min. up to strains of 5.4, 11, 15, 19, 29 and 39%, and held at these strains. The complex modulus was recorded while each

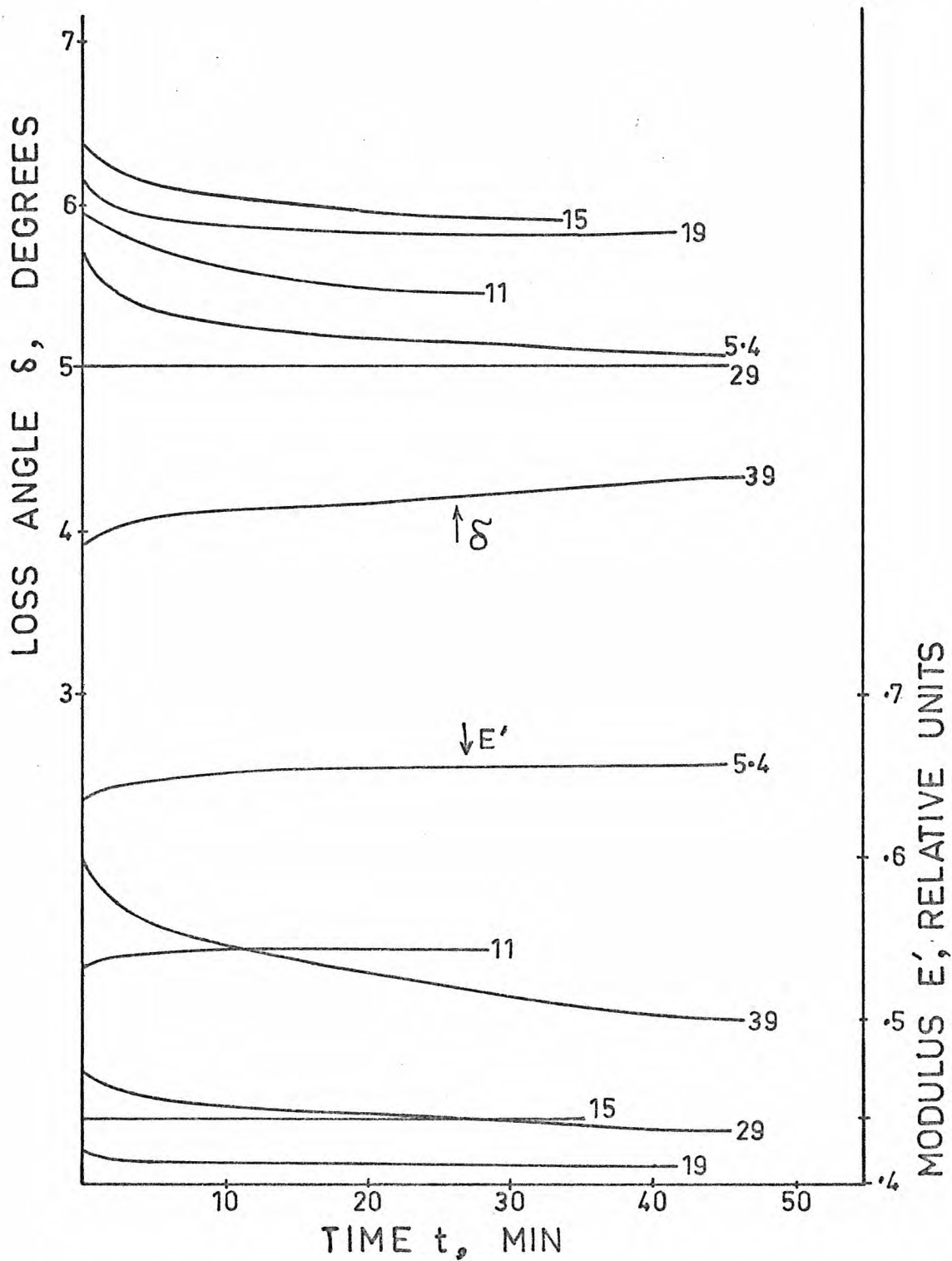


Fig. 3-13 The modulus E' and loss angle δ against time for wool fibres held extended in water at fixed strains as indicated on each curve.

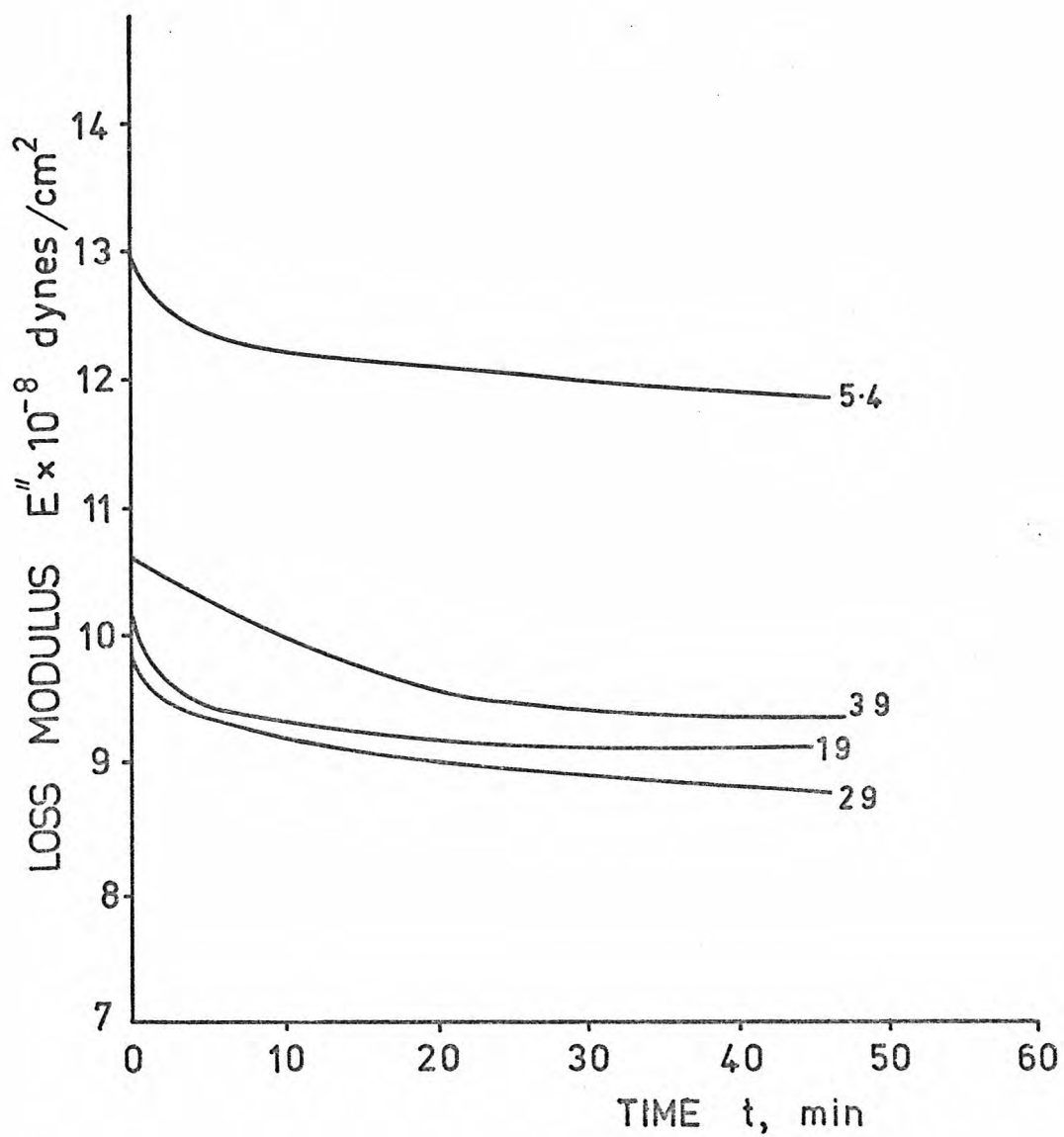


Fig. 3-14 The loss modulus E'' against time for wool fibres held extended in water at fixed strains as indicated on each curve.

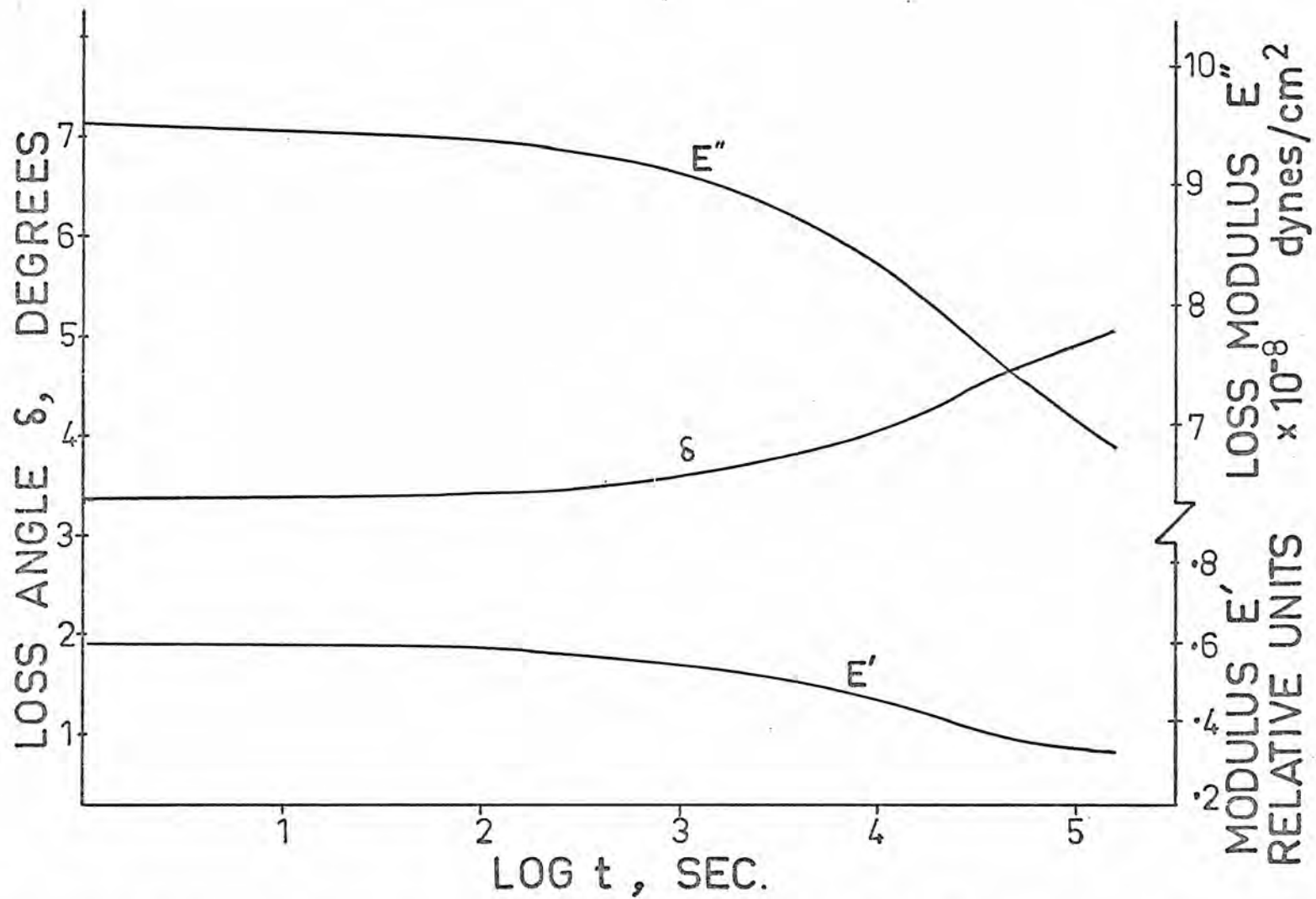


Fig. 3-15 The modulus E' , loss angle δ and loss modulus E'' against log-time for a fibre in water at 40% fixed strain.

fibre was relaxing for a period of time between 30-45 min.

This experiment revealed some remarkable properties of the modulus and loss angle of keratin fibres. While the fibre was relaxing, the modulus against time increased for fixed strains up to 15% and decreased for strains beyond 15% (fig. 3-13); at 15% strain the modulus remained constant. The loss angle behaves in an inverse manner to this. The value of the loss angle at fixed strain decreases with time for strains up to 30%. At 30% strain the loss angle remains constant with time. Beyond 30% strain the loss angle increases with time. At all fixed strains, however, the loss modulus decreases with time (see fig. 3-14); for the loss modulus only, the geometrical correction g_1 has been taken into account. Lastly, a fibre was tested in water over 48 h at 40% fixed strain; the modulus E' , the loss angle δ and the loss modulus E'' are plotted against $\log(\text{time})$ in fig. 3-15 and all these seem to indicate that the relaxation process is not completed even after a long period of time at this high extension (the g_1 correction for E'' has been effected). On the contrary, for fixed strains up to $\approx 20\%$ the relaxation seems to become completed within a few minutes. Thus, for lower fixed strains some short-term process is dominant, for higher fixed strains some long-term process is dominant, while for intermediate fixed strains both processes become apparent.

3.10.1 Discussion

An attempt to explain the above results is made below. Examination of the results expressed in fig. 3-13 suggests that at lower strains over a period of a few minutes bond reformation is taking place with time as indicated by the increasing modulus and the decreasing loss angle. At high strains bond breakdown is occurring with time as indicated by the reduction of modulus and the increase of loss angle. If the modulus change and the change in loss angle with

time occur due to structural changes in the same phase (C or M) of the fibre, the increase of modulus and decrease of loss angle should be concomitant. The steady value of loss angle with time occurring at 30% fixed strain should go with a steady value modulus at the same fixed strain. However, the modulus is steady with time at 15% fixed strain and hence suggests that the structural components, responsible for the change of complex modulus with time for the total fibre, do not exist in the same phase (C or M).

The two different relaxation processes (one for phase C, the other for phase M) are likely associated with the short-term and the long-term processes identified previously. It is suggested now that the long-term process occurs mainly in the C phase or in the zone of gradation between the two phases, while the short-term occurs in both phases. The suggestion that the long-term process takes place mainly in the C phase or in the zone of gradation between the two phases, is compatible with the idea that the backbone of the matrix does not "sieze up"⁵¹ but rather is characterised by short-term breakdown and reformation of polar bonds with low activation energy. Long-term relaxation processes are generally associated with crystalline structures, covalent crosslinks and macromolecules and hence it is reasonable to attribute the long-term relaxation process to the C phase or in the zone of gradation between the two phases. According to the above ideas and the properties of the two phases as described in the two-phase model (section 3.7) the short-term relaxation process may be due to polar bond breakdown and reformation in both phases and also it may be due to a partial reformation of the α - and β - form from the activated state between α - and β - form as supported by X-ray evidence¹⁰¹; the latter process must take place exclusively in the C phase.

In both short and long-term relaxation processes the magnitude of complex modulus change with time depends on the strain

and the rate of strain in general. In the present work with the rates of strain used the time required to break the fibre ranges between 30 min to 2 days. The short-term relaxation times are very much shorter than these times, so that the fibre is in a steady-state equilibrium after only a few percent strain. This means that the intensity of relaxation for the complex modulus is practically the same for all extensions and depends only on the rate of strain. On the contrary, the long-term relaxation times are longer or at least comparable to the time span of the extension experiments, therefore the intensity of complex modulus relaxation depends on both the strain and the rate of strain. It is suggested that both short and long term mechanisms operate at all extensions each possessing a different degree of relative importance. For lower strains the long-term process is insignificant so that the short-term becomes dominant. For higher strains the long-term process becomes overwhelmingly dominant.

The results of fig. 3-13 are compatible with the results of fig. 3-6, which show the effect of rate of strain. However, the amount, by which the modulus changes during relaxation at a fixed strain for a fibre after straining up to that strain at 1.07% per min, is considerably less than the difference between the moduli corresponding to the same strain on the modulus against strain curves at the two strain rates of 1.07% per min and 0.023% per min (see fig. 3-6). The same observation applies to the loss angle measurements. The explanation for this could be as follows. With a faster strain rate more α -helices are opened up at any particular extension so that, when the fibre is held at this particular extension, the modulus with time is always lower (or the loss angle with time always higher). The increase of the modulus (or the decrease of the loss angle) due to the short-term processes do not compensate the reduction of modulus (or the increase of loss angle) due to the increased opening up of the α -helices following

an increased rate of strain.

A closer consideration will now be given to what is possibly happening at high extensions in terms of the X-Y series zone model.

3.11 The X-Y Series Zone Model

In the microfibrils or in their immediate environment in the matrix it has been postulated by Feughelman and Haly^{29,34,51} that two types of zone exist in series (X and Y). These zones are present alternately along the microfibril. Both zones, it was proposed, consist of α -helices in an organised packed state. When the fibre is stressed the zones X open out prior to zones Y. These latter zones are possibly cross-linked to themselves and their surrounding matrix, and may have more bulky sidechains, which introduce steric hindrance and hence inhibiting unfolding. In this model the yield region of the load-extension curve of a wool fibre corresponds to the opening out of the X zones, and the post-yield region is the opening up of the Y zones. As a wool fibre in water at room temperature is extended from the yield region into the post-yield region there is a rapid stiffening of the fibre, the incremental (slope) modulus being an order of magnitude greater than in the yield region. There is however no discontinuity in the graph of X-ray intensity at 5.1 \AA^0 ^{9,39}, which shows a continuous decrease of crystalline α -keratin with increase of extension. The major part (approx. 2/3) of the α -type crystallinity is still present at the turnover from the yield to the post-yield region and a significant proportion is still present at extensions well into the post-yield region. The new opposition to extension arising in the post-yield region is due to bonds, which are either in the microfibrils still in the α -form or in the matrix immediately surrounding these microfibrils. Both of these possibilities have been speculated^{36,44,46,40,41,51}. However, there is general agreement that highly crosslinked structures

consisting of covalent cystine links between polypeptide chains play a major role in the mechanical properties of keratin fibres.

Examination of the static stress-relaxation in water of wool fibres for extensions in the yield⁹⁴ and post-yield regions⁴², has shown that sulphhydryl-disulphide interchange is at least in part responsible for long-term relaxation. For extensions in the post-yield region another mechanism of stress relaxation in addition to sulphhydryl-disulphide interchange has been proposed¹⁵. This mechanism is independent of pH and is not detectable for static stress-relaxation of fibres extended into the yield region. In terms of the series-zone model this mechanism may be interpreted as separation of the α -helices of the Y-zones from the component of the keratin structure, which provides the stiffening of the fibre, when extended into the post-yield region.

It is reasonable to assume that some gradation between the X and Y-zones exist. This means that some relaxations of the types described above does exist even at lower extensions. This is suggested by the gradual increase of dynamic modulus as high extension is approached. This increase of modulus can be explained by the formation of β -crystalline form as well as by the alignment of the sulphur-rich material associated with the Y-zones.

By consideration of both the two-phase model and the X- and Y- zones model it is possible to understand the behaviour of E' , δ and E'' . The behaviour at high strains in particular can be explained as follows. The decrease of E' at 40% (fig. 3-15) is attributed to a relaxation in the microfibril and is due most likely to disulphide bond scission. The crystalline structure is also affected by this scission, because the crystalline phase is directly dependent on disulphide bridges to provide stability to the structure⁴⁵. The weakening of the

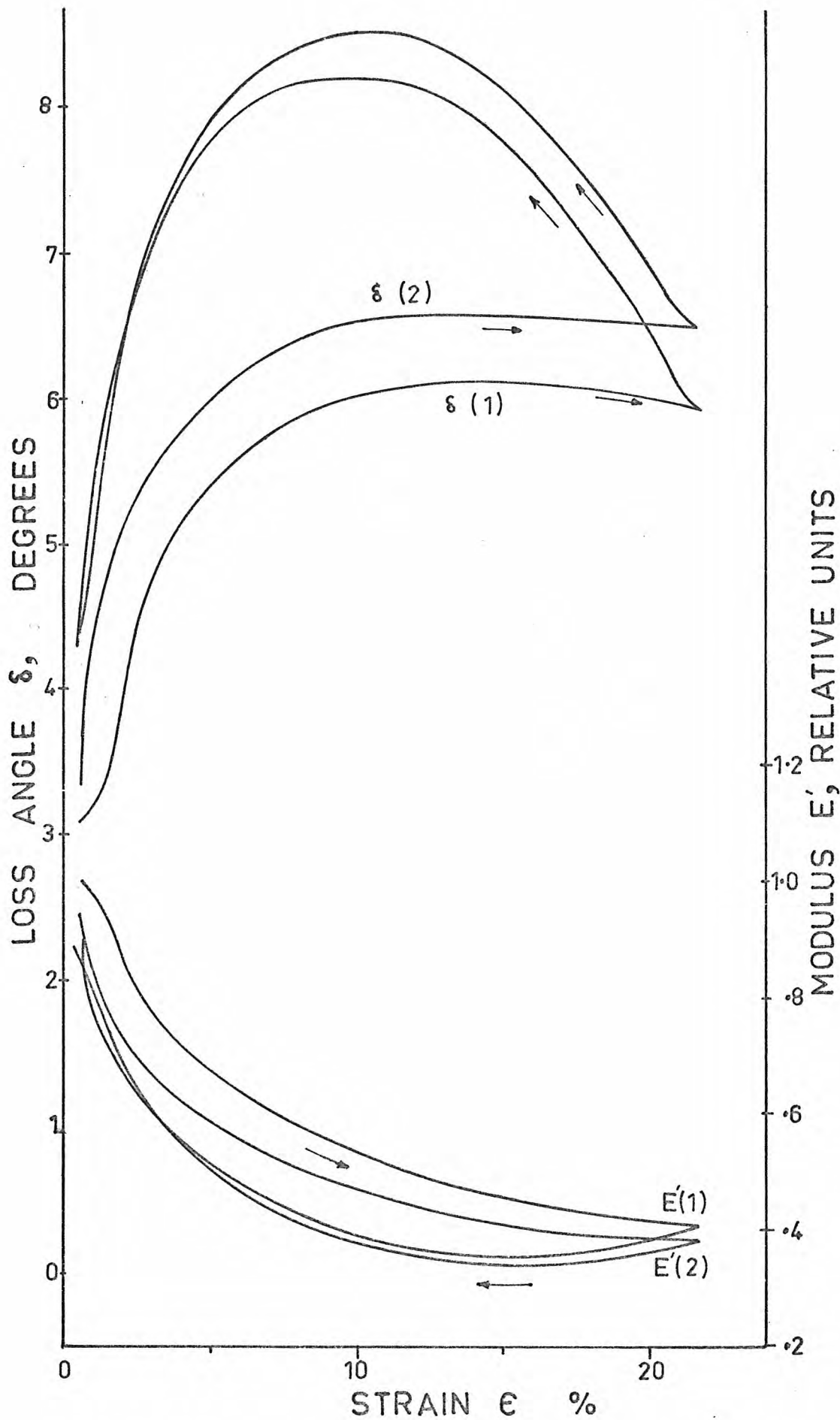


Fig. 3-16 The modulus $E'(1)$ and loss angle $\delta(1)$ for a wet fibre cycled up to an intermediate strain. The fibre was relaxed unextended for 24 h in water and the cycle was repeated resulting in $E'(2)$ and $\delta(2)$.

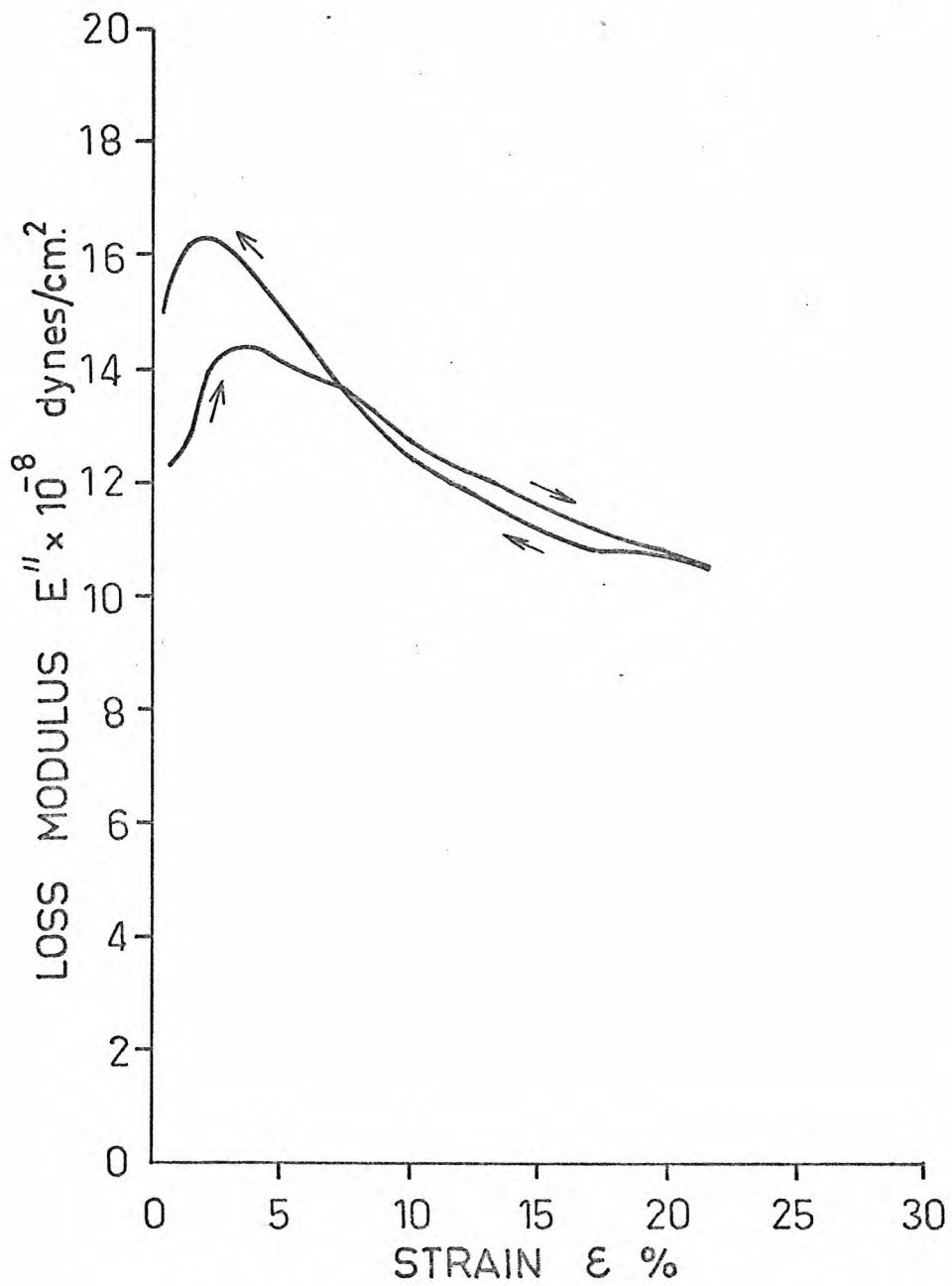


Fig. 3-17 The loss modulus E'' against strain for a wet wool fibre cycled up to an intermediate strain.

microfibrils renders the complex modulus of the matrix more prominent and this is demonstrated as an increase of the loss angle (fig. 3-15). The loss modulus E'' at high extensions increases with strain and rate of strain (fig. 3-12). The increase of strain and rate of strain creates more broken (most likely disulphide) bonds on free radicals, which are a source of mechanical loss. When the fibre is held extended at 40% strain the scission of bonds is accompanied by reformation of new ones in a relaxed state (most likely through sulphhydryl-disulphide interchange) and this implies less mechanical loss; as a result of this the loss modulus E'' decreases with time (fig. 3-15).

3.12 The Effects of Extension Cycling

A fibre was extended in water up to 22% strain at 1.07%/min and then released at the same rate of strain. The fibre was subsequently in water slack for 24h and the extension cycle was repeated. The modulus $E'(1)$ and loss angle $\delta(1)$ for the first cycling as well as $E'(2)$ and $\delta(2)$ for the second cycling are shown in fig. 3-16. It is observed that the results of the first cycling are mostly reproducible during the second cycling, which is in agreement with Speakman's finding⁸⁶ that, after extension of the fibres in water up to a strain of 34.5%, the load-extension curve was largely recoverable if the wool was relaxed in water at 18°C for 24h. During retraction the modulus is lower and the loss angle higher. The modulus exhibits a minimum during retraction, while the loss angle a maximum.

To better understand these results the loss modulus has been calculated for the first cycling and is shown in fig. 3-17; the correction g_1 (see eq. (3-5)) has been effected. The material seems to be less or equally lossy for first main part of the retraction, while the material becomes more lossy as retraction approaches its completion. The loss modulus does not vary as much as the E' and δ vary during the cycling.

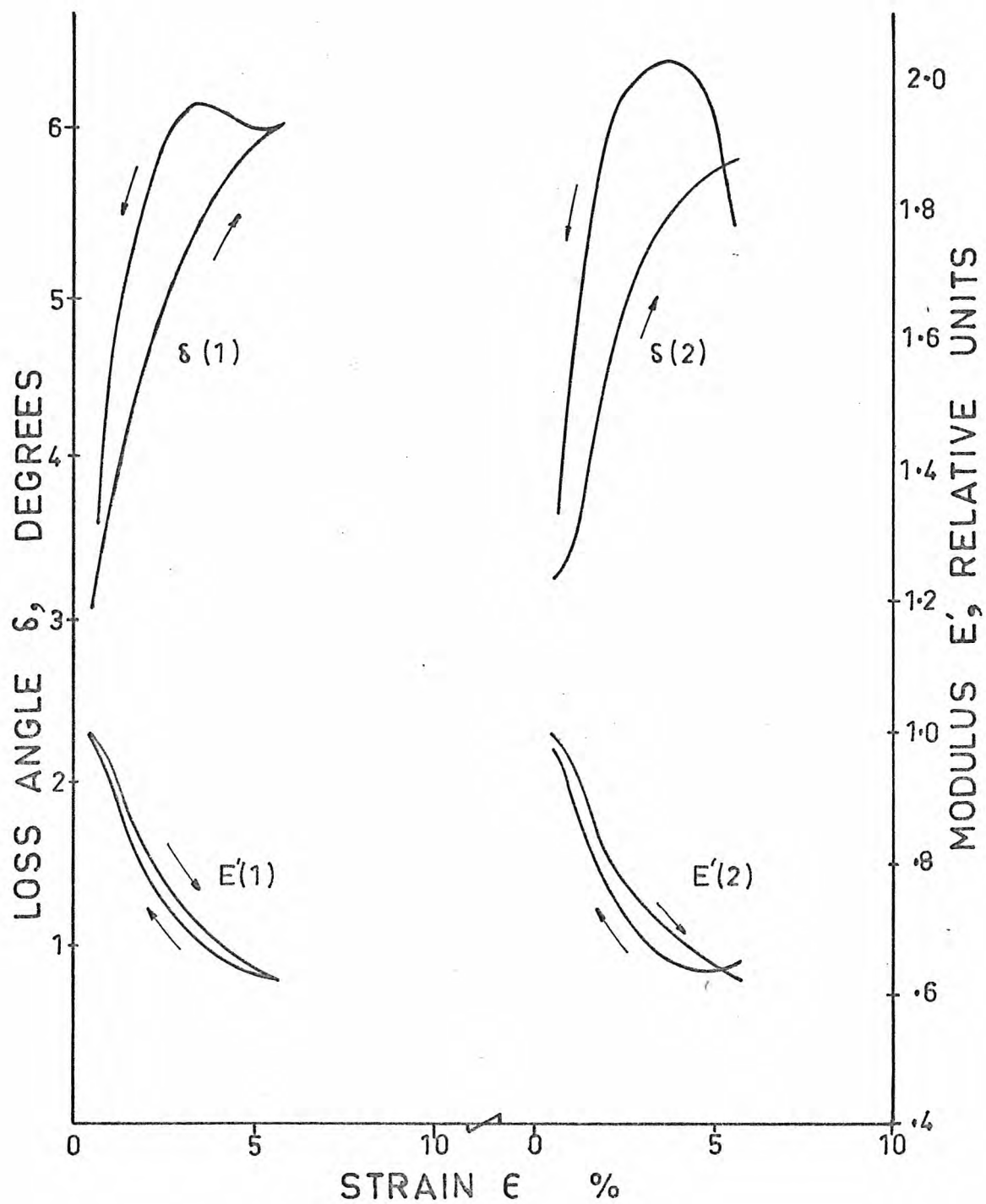


Fig. 3-18 The modulus $E'(1)$ and the loss angle $\delta(1)$ against strain for a wet fibre during the first cycle; $E'(2)$ and $\delta(2)$ are the same parameters during the second cycle, in which the fibre was relaxed at maximum extension for 30 min before retraction.

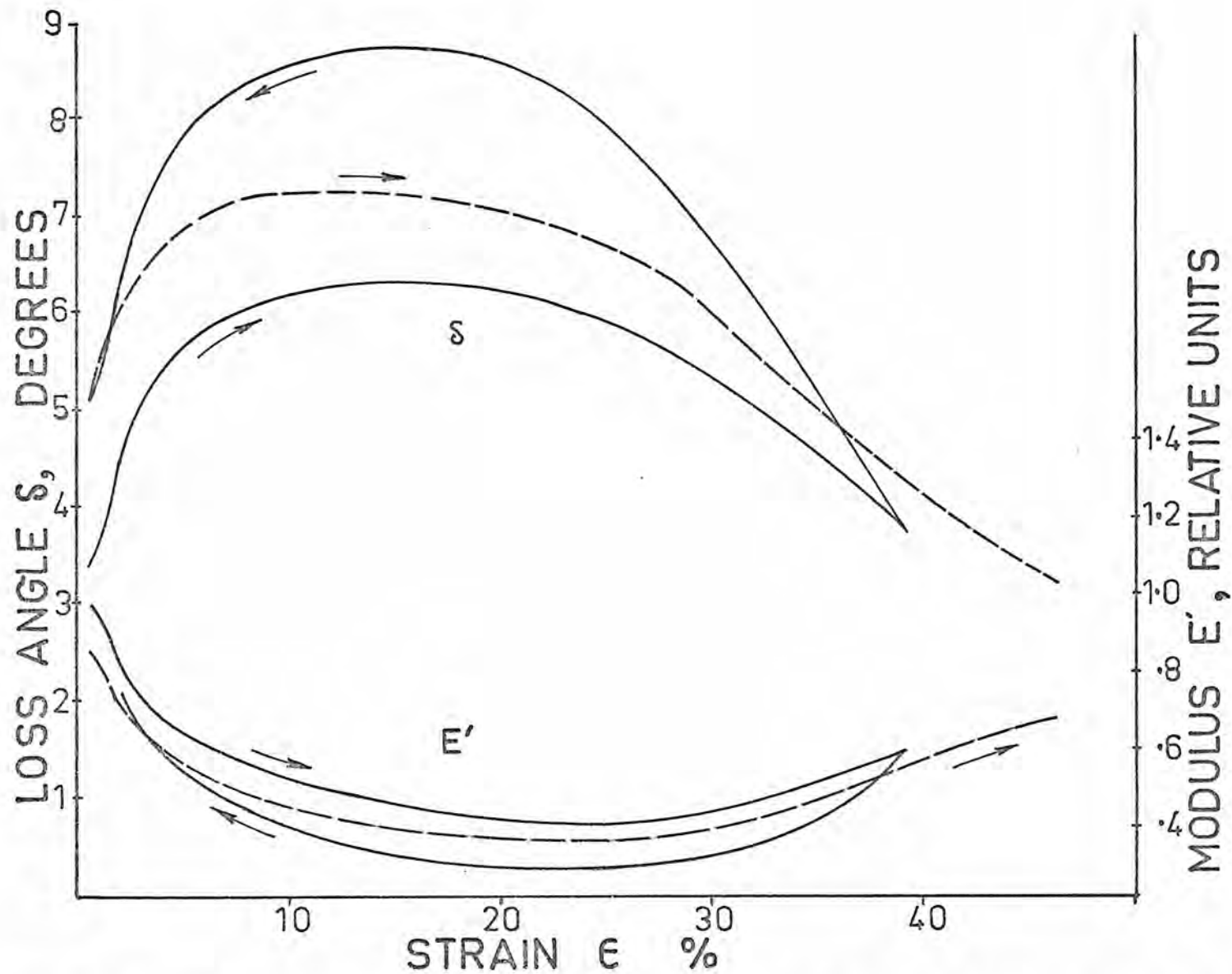


Fig. 3-19 The modulus E' and the loss angle δ against strain for a wet fibre cycled up to a very high strain ($\approx 40\%$, solid curves). The fibre was finally extended to break (broken curves).

The variation of E' and δ is obviously another manifestation of the two-phase model: the crystalline phase becomes weaker during retraction so that the amorphous region manifests itself as an overshoot in loss angle. The model of course again does not explain the causes of the weakening of modulus during retraction but rather demonstrates that such a weakening does take place. As to the causes of this weakening it can be speculated that it is due to a temporary slackening, distortion and disorientation of some structural units in the microfibrils. This process accumulates disordered material during retraction. Nearly all of this material returns back to order after the fibre is relaxed slack in water for 24h.

To further investigate the effect of extension cycling the following test was carried out. A wool fibre was extended in water up to 6% strain at a rate of 1.07%/min and then released at the same rate. No pronounced overshoot in angle $\delta(1)$ and no undershoot in modulus $E(1)$ was observed (see fig. 3-18) although the angle was higher and the modulus lower during retraction. Then the fibre was relaxed in water slack for 4h, a time during which the angle and modulus had practically recovered. Following this the same cycle was repeated, except that the fibre was held extended at 6% strain for 30 min and then retracted. This time the angle $\delta(2)$ showed a pronounced overshoot and the modulus $E'(2)$ showed an undershoot during retraction (see fig. 3-18). The same fibre was relaxed again in water for 4h and using the same rate of strain it was extended up to 40% strain, then retracted and finally extended to break without interruption of the cycling (see fig. 3-19). In fig. 3-19 the final extension to break is shown as a broken line and the rest of the cycle as a solid line.

In all cases of cycling, hysteresis is present in both modulus and loss angle measurements. The hysteresis becomes more pronounced with increase of strain and duration of time.

Some comments on the significance of the above results are made below. To start with, a clear distinction must be made between the "dynamic hysteresis" of fig. 3-18 and 3-19 as compared with the "static hysteresis" of a static stress-strain relationship¹⁰²; the dynamic hysteresis refers to a dynamic quantity (e.g. modulus or loss angle) being cycled against static strain, while the static hysteresis refers to a static quantity (e.g. stress) against static strain. The two types of hysteresis, if observed, imply basically different phenomena. To clarify this, consider the "standard linear solid" model (see fig. 1-7), which does have its characteristic static hysteresis but does not have a dynamic hysteresis. The static hysteresis is due to the viscoelastic character of the model. This viscoelastic character is invariant with strain and for this reason the complex modulus, which is a function of the viscoelastic constants of the model, must be independent of the state of strain (the springs and dashpot have invariant characteristic constants at all strains). A real material, however, in the present case wool, can present a hysteresis for the complex modulus as well (i.e. a dynamic hysteresis). This phenomenon cannot be regarded as a manifestation of viscoelasticity, but rather as indicating some structural change. To fix our ideas, static hysteresis can be due to both the viscoelasticity and the structural change (i.e. the change of this viscoelasticity) of the material, while a dynamic hysteresis reflects only the structural change in the material. The application of a very small oscillatory strain at any particular static strain is itself a cycling experiment and the complex modulus is a measure of the (purely dynamic) hysteresis corresponding to this small oscillatory strain. Because the oscillatory strain is very small, the complex modulus samples a region, over which the viscoelastic properties may be considered constant.

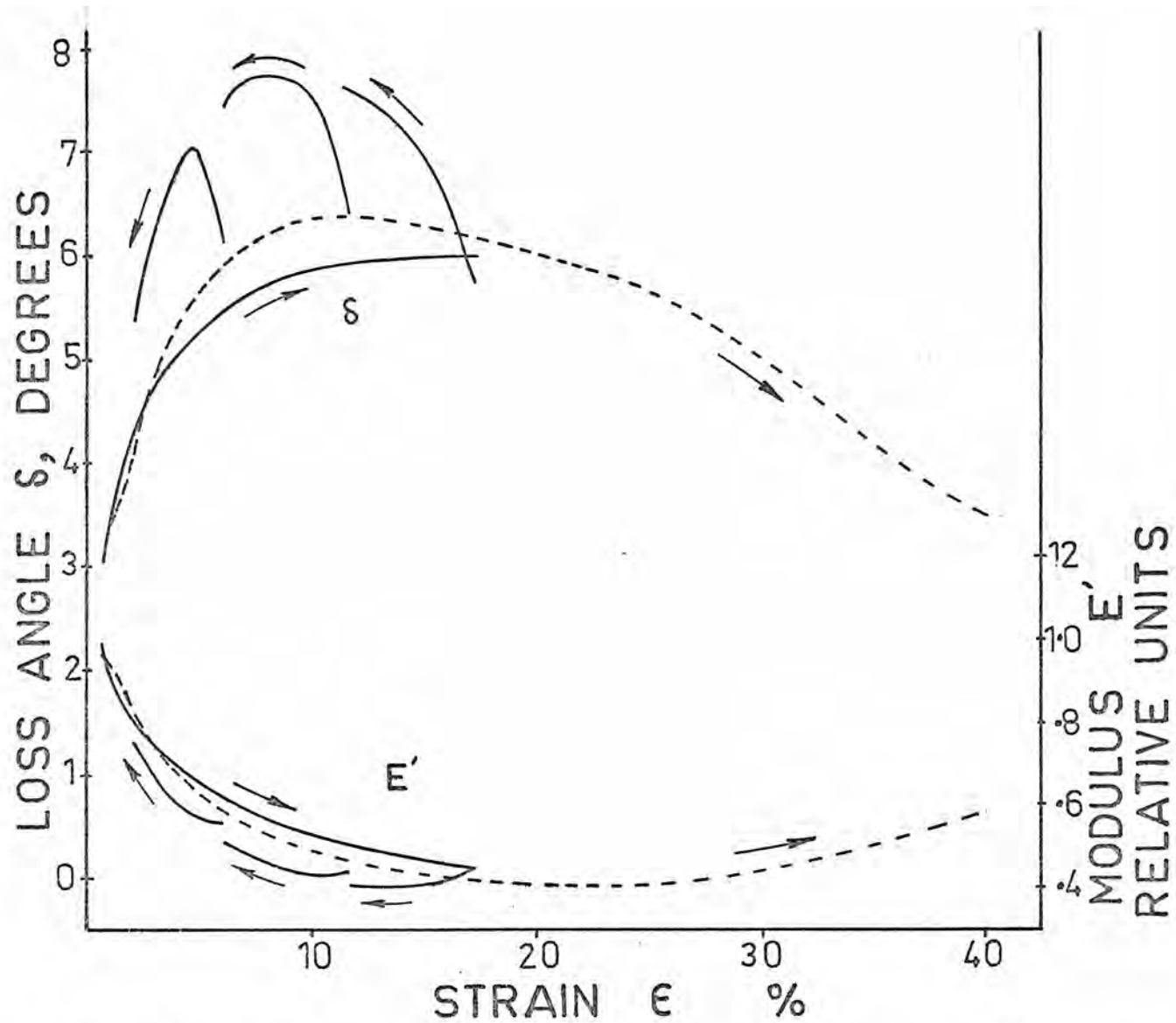


Fig. 3-20 The modulus E' and the loss angle δ against strain for a wet fibre extended up to 17% strain, held at this strain for 30 min and then retracted; the retraction was interrupted at fixed strains for 30 min relaxation intervals. After 24h in water the fibre was extended up to 40% strain (broken curves).

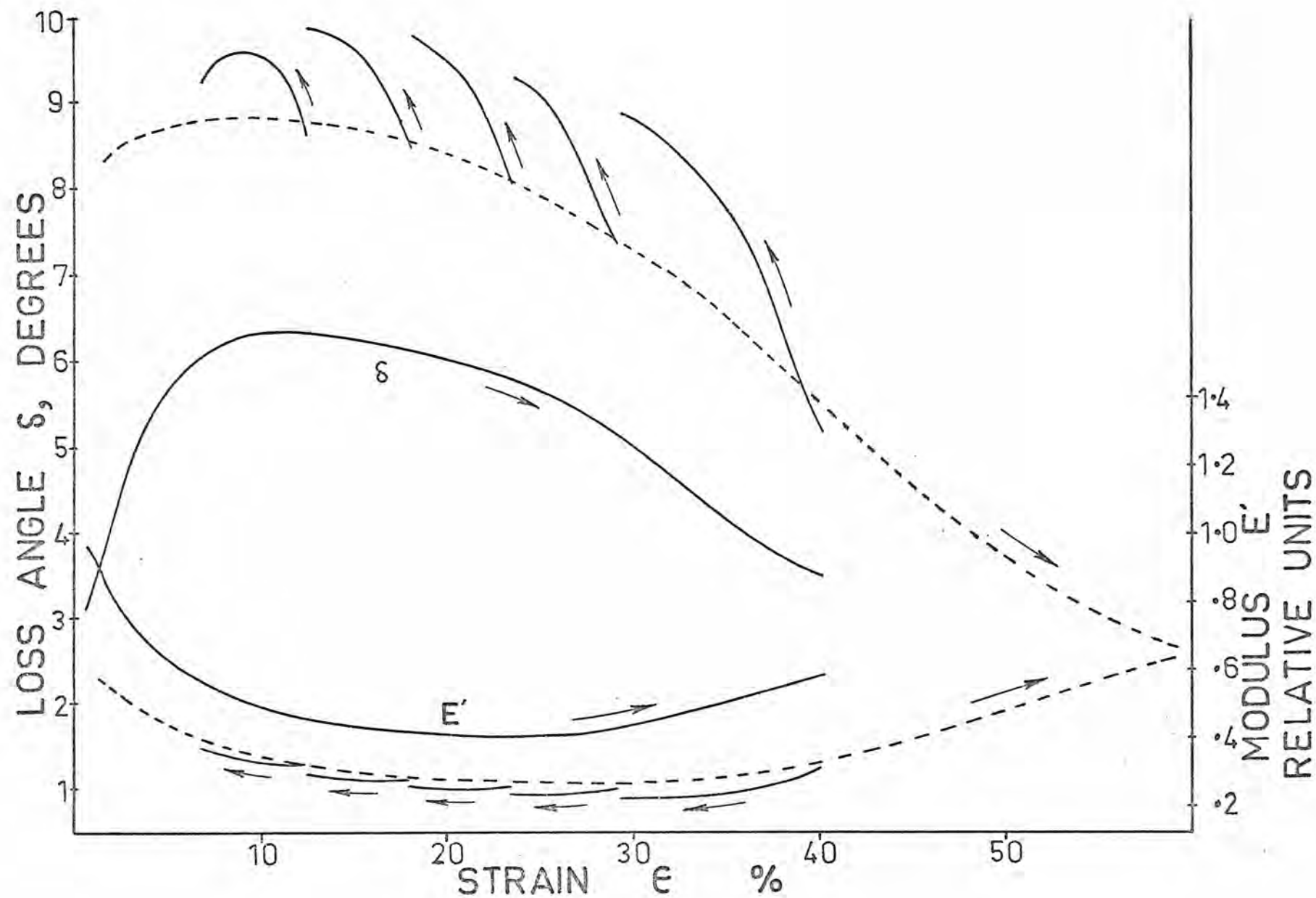


Fig. 3-21 The modulus E' and loss angle δ against strain for a wet fibre extended up to 40%, allowed to relax at this strain for 48h and finally retracted (solid curves); the retraction was interrupted at fixed strains for 30 min relaxation intervals. Upon completion of retraction the fibre was extended to break (broken lines).

With the application of a large static strain the material can change its structure and this change is revealed in the complex modulus.

The complex modulus alone cannot lead to the identification of the structural units responsible for the changes in the fibre; it can only serve as a general guide, which together with other physical and chemical properties can lead to such identification. It was pointed out previously that the microfibrils are weaker during retraction and this could be due to some distortion and disorientation of the α -helices. This distortion and disorientation of the α -form is likely to result from the reformation of bonds along the extended C phase, the reformation of bonds playing a stabilising role.

3.13 Relaxation During Retraction of an Extension Cycle

It was considered useful to examine the effect of relaxation during retraction on a cycling experiment for intermediate and high extensions. A wet fibre was extended in water up to 17% strain, at 1.07%/min, held at this extension for 30 min and then retracted at the same rate as follows. The retraction was interrupted at 10% strain at which strain the fibre was relaxed for 30 min, then again retracted to 5% strain, at which the fibre was again relaxed for 30 min and finally it was retracted close to 0.6% strain (a 10μ cohesive set⁴⁹ was observed). The results are shown in fig. 3-20. Following this the fibre was left slack in water for 24h and then extended up to 40% strain at 1.07%/min and held at this extension for 48h. The modulus and loss angle for this extension is shown in both fig. 3-20 (broken lines) and in fig. 3-21 (solid line). After the 48h relaxation the fibre was retracted, the retraction being interrupted for 30 min each time at the extensions shown in fig. 3-21. (Note: the final part of retraction is not shown due to a fault of the recorder). It was possible to retract the fibre down to 1.5% strain (cohesive set \approx 1%) from which with no relaxation it was

extended to break (broken line, fig 3-21).

It is observed from fig. 3-20 that at the fixed retraction strains the modulus and loss angle approach the values at the corresponding strain during extension. The change of modulus and loss angle with time at the fixed retraction strains are not shown, but they are similar to those of fig. 3-13 for lower fixed strains and they appear to have approached their equilibrium value in the 30 min allowed for relaxation. As the retraction of the fibre is resumed after the relaxation, the loss angle and modulus quickly approach the level, which they would have achieved if relaxation was not allowed during retraction. It is possible to understand this by considering that the effects of retraction tend to be cancelled during relaxation and vice versa, i.e. that the subsequent retraction tends to annul the effects of relaxation. It was suggested previously, that during retraction bond breakdown, distortion and disorientation of the microfibrils possibly occur; therefore during relaxation bond reformation and alignment of distorted and disoriented structures may occur, which during the ensuing new retraction again suffer breakdown and disorientation.

Finally, it is observed in fig. 3-21, that similar phenomena to those of fig. 3-20 take place, except that the retraction curves are permanently shifted away from the corresponding extension curves. This may arise from the irreversible structural changes occurring at the very high extension of 40% and the prolonged relaxation for 48h at this high extension.

3.14 The Effect of Strain at Various Frequencies

Two fibres extended to break in water at 0.18% per min strain rate, were oscillated at two different frequencies : 6 Hz and 1500 Hz. The results were only slightly different from those of fig. 3-3, the

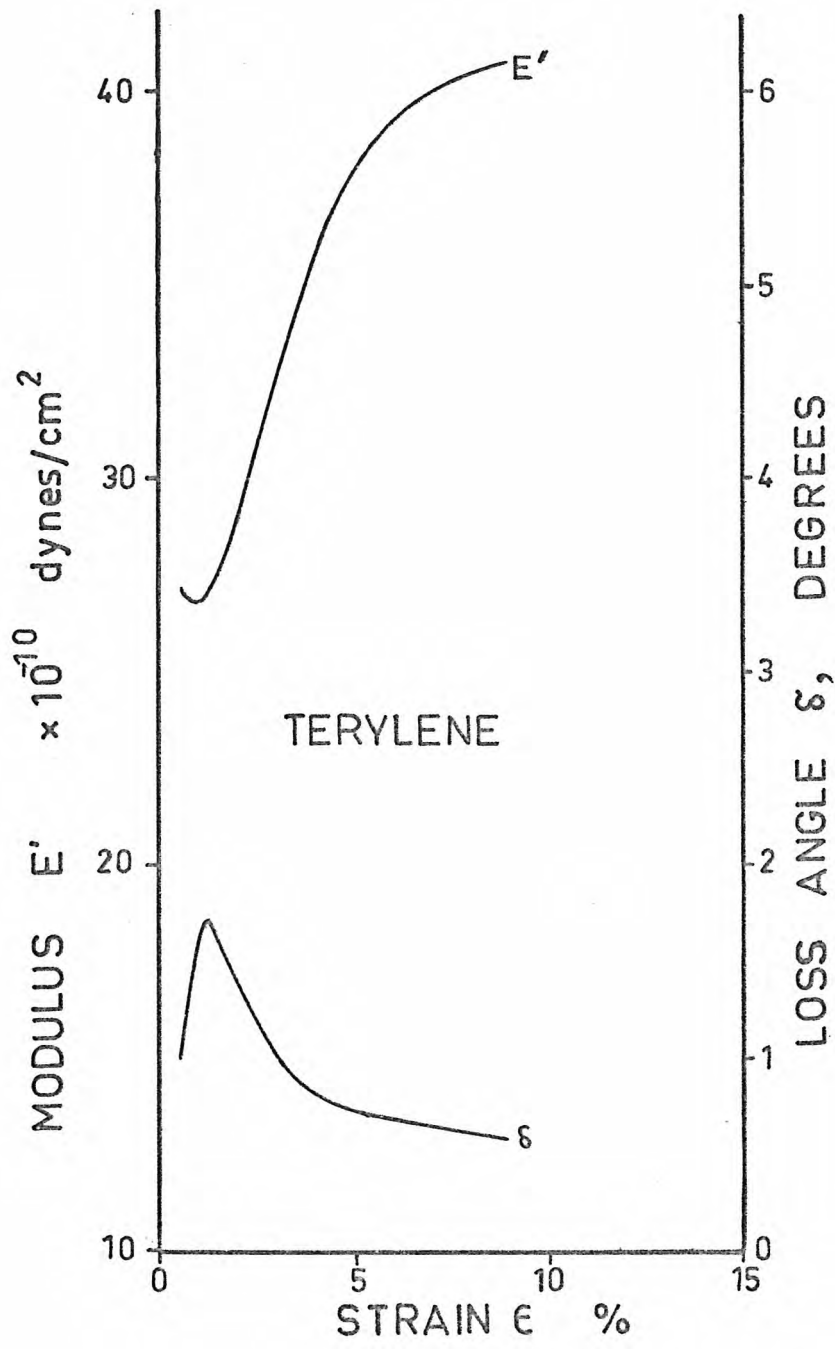


Fig 3-22 Plots of modulus E' and loss angle δ versus strain for a terylene fibre.

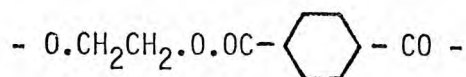
difference not allowing reliable interpretation in terms of structure or as an interfibre effect. Thus the effect of change of frequency in the frequency range 6 - 1500 Hz does not have any significant effect on the complex modulus as a function of strain for a wet fibre. The frequency-temperature effect is examined only in the Hookean region in chapter 5.

3.15 The Effect of Strain on Different Polymers

Three different types of polymers have been tested for comparison purposes. The modulus and loss angle against strain have been obtained at 25°C using a strain rate of 0.18% per minute. No geometrical correction has been taken into account.

3.15.1 Terylene

Terylene is a synthetic fibre produced from the polymer polyethylene terephthalate. The chemical constitution of the simplest fundamental unit of the Terylene polymer may be represented thus:



A single Terylene polyester fibre was tested in order to examine how its complex modulus varies with strain. The fibre was tested at room condition, because its modulus was found not to depend on relative humidity (its maximum regain being only $\approx 1\%$ at 100% RH¹⁰⁴). The modulus and loss angle against strain are shown in fig. 3-22. The modulus and loss angle are presented in absolute units.

The modulus decreases between 0.6% and 1% strain and then increases monotonically until the fibre breaks; the loss angle changes with extension inversely to the modulus. The variation of dynamic modulus of terylene beyond 1% at various strains obtained by measuring the velocity of sound waves and reported in Meredith's book¹⁰³ is in

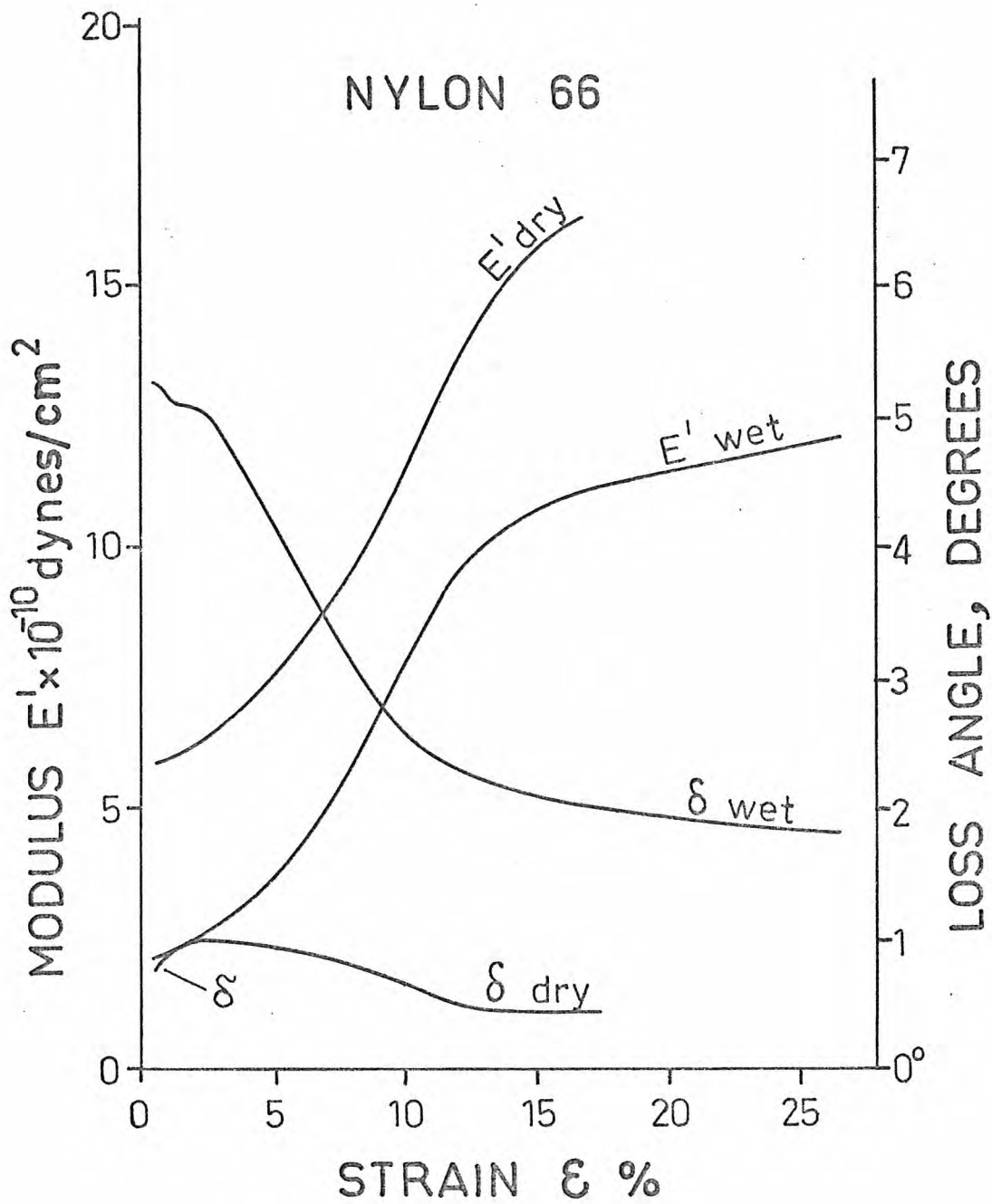
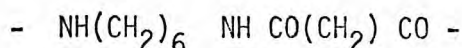


Fig. 3-23 Plots of modulus E' and loss angle δ versus strain for a wet and a dry nylon 66 fibre.

general agreement with the present results. However, the initial decrease of modulus with strain and the loss angle change over the complete strain range do not appear to have been previously reported.

3.15.2 Nylon

Nylon 66, a man-made fibre, was also tested. The basic molecular unit of nylon 66 is



Since its complex modulus was found to depend strongly on water content (which varies between 0% and >8% regain) two single fibres were tested, one at 0% RH, the other at 100% RH. The modulus and loss angle against strain are shown in fig. 3-23 for the two cases. The modulus at 100% RH increases initially slowly (up to 2% strain), between 2% and 15% more rapidly and finally again slowly; the loss angle follows inverse changes. The modulus curve at 0% has a higher value but follows the same general shape as that of 100% RH; the loss angle shows a very small maximum at 2% strain corresponding to the point of change in the rate of increase of modulus with strain. The variation of dynamic modulus for nylon fibres beyond 1% at various strains obtained by measuring the velocity of sound waves at room conditions and reported in Meredith's book is in general agreement with the present results. However, the remainder of these results does not appear to have been previously published.

3.15.3 Cupresa

Cupresa is the name of a high-grade continuous filament yarn made by the cuprammonium process by Farbenfabriken Bayer at Dormagen. The chemical constitution of the basic unit cuprammonium rayon molecule is represented by the same formula as that of all cellulose fibres, namely:

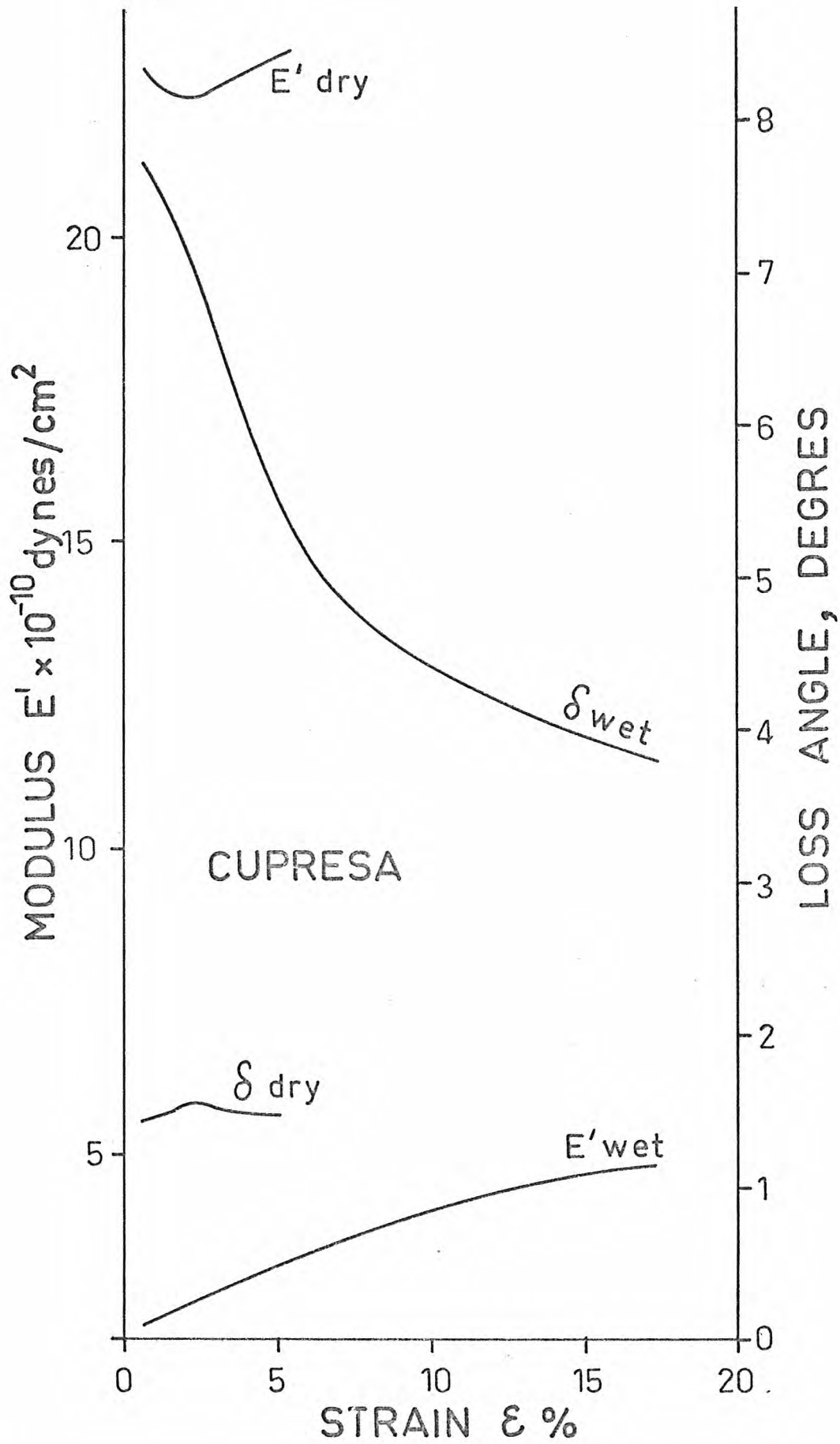
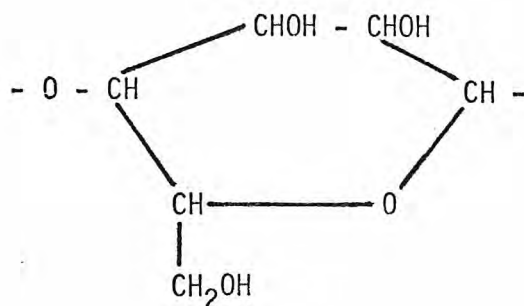


Fig 3-24 Plots of modulus E' and loss angle δ versus strain for a wet and a dry cupresa yarn.



Since its complex modulus was found to depend strongly on water content two filament yarns were tested, one at 0% RH and one at 100% RH. The modulus and loss angle against strain are shown in fig. 3-24 for the two cases. The modulus of the wet sample increases monotonically with strain while the loss angle changes inversely to the modulus. The modulus for the dry sample decreases up to $\approx 2\%$ strain and then increases; the loss angle presents an exceedingly small maximum at $\approx 2\%$ strain. The moisture uptake has a marked effect on the complex modulus.

3.15.4 Discussion

All the polymers tested show a general increase of modulus with extension except for low extensions ($\approx 2\%$). Nylon does not present a decrease of modulus for up $\approx 2\%$ strain but only a small increase instead; at $\approx 2\%$ strain the modulus of nylon shows a discontinuity in the rate of increase with strain beyond this point. Nylon, therefore, may have a similar behaviour with extension as cupresa and terylene except that the stiffening of modulus overshadows the weakening at initial extensions. The initial decrease of modulus may be due to the breakdown of weak interactions, while the increase of modulus with strain may result from the alignment of the macromolecules. A detailed interpretation of these experimental results concerning polymers other than wool is beyond the purpose of the present work.

3.16 Conclusion

The measurement of complex modulus of wool against extension has revealed important features of the structure of keratin. The modulus decreases with extension up to intermediate strain level and then increases gradually again. The loss angle follows the inverse to the modulus changes. The loss modulus, on the contrary, can be considered to be relatively constant with extension, showing only a small maximum around 3% strain and a slow increase at high strains. This sort of behaviour of the three components of the complex modulus has been explained mainly in terms of the two-phase model. The variation of the component E' reflects mainly the change of stiffness of the C phase. The variation of the loss angle of the fibre is also due to the change of stiffness of the C phase, the magnitude of the variation depending on the water content of the M phase. The very small variation of E'' with extension is in agreement with the viscoelastic properties postulated for the two phases, i.e. that the M phase behaves as a viscous liquid with constant viscoelastic parameters while the C phase is practically elastic at all extensions with varying stiffness. The two-phase model further has enabled the construction of the static stress-strain curve from dynamic data, this again justifying in the main the viscoelastic properties assumed for the model.

The increase of water content shifts the modulus curves to lower values, the magnitude of the variation of the modulus with strain not being practically affected. The loss angle curves are shifted to higher values and the magnitude of variation with strain increases, when the water content increases. This effect has also been explained in terms of the two-phase model.

The strain rate is a controlling factor of the intensity of

the structural changes occurring during extension. The relaxation of complex modulus with time at a fixed strain has revealed two relaxation processes, namely one short-term process present at all strains and a long-term process being dominant at high strains.

The extension cycling has revealed that during retraction the C phase is weaker at any particular strain than it is during extension at the same strain. This has been attributed to some distortion and disorientation of the α -helices during retraction. If the fibre is relaxed at a fixed strain during retraction the distortion and disorientation in the C phase tends to disappear with time.

The frequency change in the range 6 to 1500 Hz does not have any marked effect on the complex modulus as a function of strain.

Terylene, Nylon and Cupresa have also been tested and their complex modulus as a function of strain differs markedly from the results for keratin, indicating a basically different molecular structure.

CHAPTER 4

THE COMPLEX MODULUS DURING SORPTION

4.1 Introduction

Important phenomena during water sorption have been observed by various workers. In this chapter the dynamic mechanical properties of keratin fibres at a constant frequency and temperature have been studied during absorption and desorption. The effect on the complex modulus of an applied fixed strain on wool fibres during integral changes of relative humidity has been examined. Finally, the effect of regain cycling between wet-dry-wet states was tested.

All measurements in this chapter have been carried out at a constant temperature of 25°C and a constant frequency of 116 Hz (except in one case where $f = 84$ Hz).

4.2 Transient phenomena during absorption of water by keratin fibres

Mackay and Downes⁶² have shown that when a single wool fibre has its environment changed from dry conditions at about 0% relative humidity to highly moist conditions at 95% relative humidity the torsional rigidity falls rapidly to almost zero and then slowly increases until equilibrium at 95% relative humidity is attained. They also showed that the lowest value of rigidity is reached approximately when the fibre has attained maximum regain. Feughelman and Robinson³³ have also shown for a single wool fibre extended a few per cent, when it is taken from 0% R.H. into water (100% R.H.), that the longitudinal force in the fibre drops rapidly to a minimum and then increases slowly to come to an increased equilibrium value in water. The recorded minimum value of force in the fibre again corresponded to the time necessary for the fibre to reach maximum regain.

Nordon⁷⁵ has similarly shown from torsional measurements on wool fibres that when the relative humidity of the environment of a fibre is increased, the change results first in a reduction and then a partial recovery of the rigidity of the fibre.

The effect of changes in the relative humidity on the electrical conductivity and the dielectric constant of wool fibres were examined by Algie and Watt^{1,2}. They observed overshoots in the dielectric constant and conductance measurements vs time following step changes in relative humidity.

Watt⁹³ also reported overshoots in the length swelling accompanying the water absorption.

More recently Shishoo and Lundell⁸¹ using N.M.R. technique were able to demonstrate for some treated wools that the line width of the N.M.R. absorption, exhibits a minimum during the process of humidifying the wool fibres.

All these experiments suggest some structural change within the keratin structure produced by the front of moisture entering the wool fibre. In the present work further evidence for structural changes occurring in keratin fibres during moisture sorption is reported.

4.3 The Complex Modulus at Low Extensions Following Changes in Relative Humidity

Interesting phenomena have been observed during sorption in keratin fibres at low extension. In Chapter 3 the wool fibres tested could not however be examined at very low extension, i.e. below approximately 0.6% extension because of the fibre slackening. Because of this it was not possible to test a wool fibre held at 0.6% extension during a sorption experiment in which the fibre can swell longitudinally by as much as 1.4%. This difficulty was overcome by

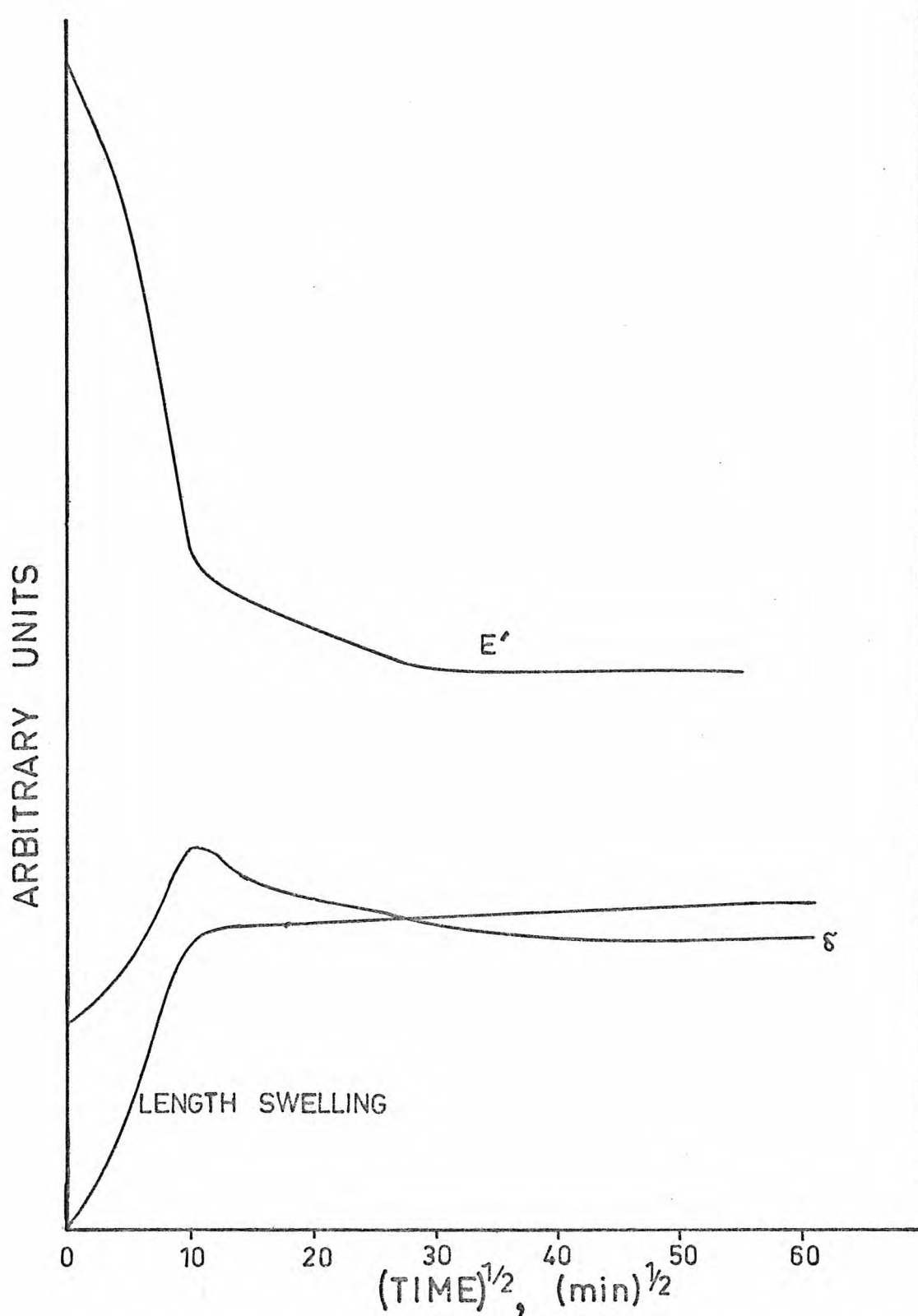


Fig. 4-1 The simultaneous change of modulus E' , loss angle δ and longitudinal swelling against $(\text{time})^{1/2}$ for horse hair at low extensions, during absorption from 0% to 85% R.H.

the use of horse hair samples, as is explained in the following subsection.

4.3.1. Tests on Horse Hair

The large diameter of a horse hair (around 190 μ) requires a large force to extend the fibre. This force is sufficiently large even at low extension to displace the vibrating (free) end of the fibre upwards by a large amount. This displacement of the free end can be as high as 500 μ until the "maximum" in modulus measurement at $\approx 0.6\%$ strain is reached (see fig 3-1). The last 200 μ or 300 μ of this displacement was found to correspond to a negligible true strain on the fibre because it followed the displacement of the clamped end very closely and the "maximum" in modulus measurement was nearly attained. This proved to be an advantage, allowing the performance of experiments at low extensions during sorption. Also, it allowed the simultaneous measurement of longitudinal swelling by recording the d-c output of the strain gauge.

A preliminary result on the loss angle and the swelling of a horse hair during sorption has been published by the author¹⁸. The loop length of the sample was 2 cm, its diameter 197 μ , the frequency of vibration 84 Hz and the amplitude of vibration 4 μ . The fibre was held at a low extension while the relative humidity was changed from 0% to 85%. The simultaneous change of modulus, loss angle and longitudinal swelling is shown in fig 4-1. The measured quantities have been plotted against square root of time, because this has been the practice by many workers for sorption experiments⁸⁹ (Fickian absorption gives a \sqrt{t} dependence). For convenience this practice also suitably compresses graphs over long periods. An observation of the graphs reveals two distinct regions for modulus change; the first region corresponds to a fast decrease up to about 100 min

followed by a slow decrease for the next 24 h. The loss angle increases during the first stage and then decreases slowly, while the longitudinal swelling has reached more than 90% of its total change within the first stage, followed by a very slow increase. A minute fraction of the loss angle overshoot could originate from the small slackening of the sample because of swelling (this small fraction is an artifact according to section 3.3 and fig 3-2). However, the overshoot in loss angle represents a genuine structural change in the fibre, otherwise the continuous swelling beyond the 100 min means an increasing slackening which should result in a continuous increase of the loss angle beyond the 100 min. Besides, it was checked and found that after the fibre was swollen, it still held very close to the "maximum" of modulus, a fact indicating that the fibre was still taut and the effect of slackening had not appeared.

More experiments were performed at a frequency of 116 Hz with horse hair under the conditions of low extension as outlined above. The fibre was conditioned in a dry atmosphere for 24 h and then an abrupt change of relative humidity was brought about from 0% R.H. to a relative humidity corresponding to one of the following regains : 4, 8, 12, 16, 20, 24, 28, 33%. Step changes of relative humidity were also performed between consecutive values of the above list. In all cases the general characteristics of the graphs in fig 4-1 were present.

The effect of tension on the sample was also examined: sometimes it was observed that the loss angle showed a new increase past the overshoot. This was dependent on the final value of relative humidity and/or the tension under which the fibre was held. This phenomenon was more pronounced with increase of either the tension or the final regain.

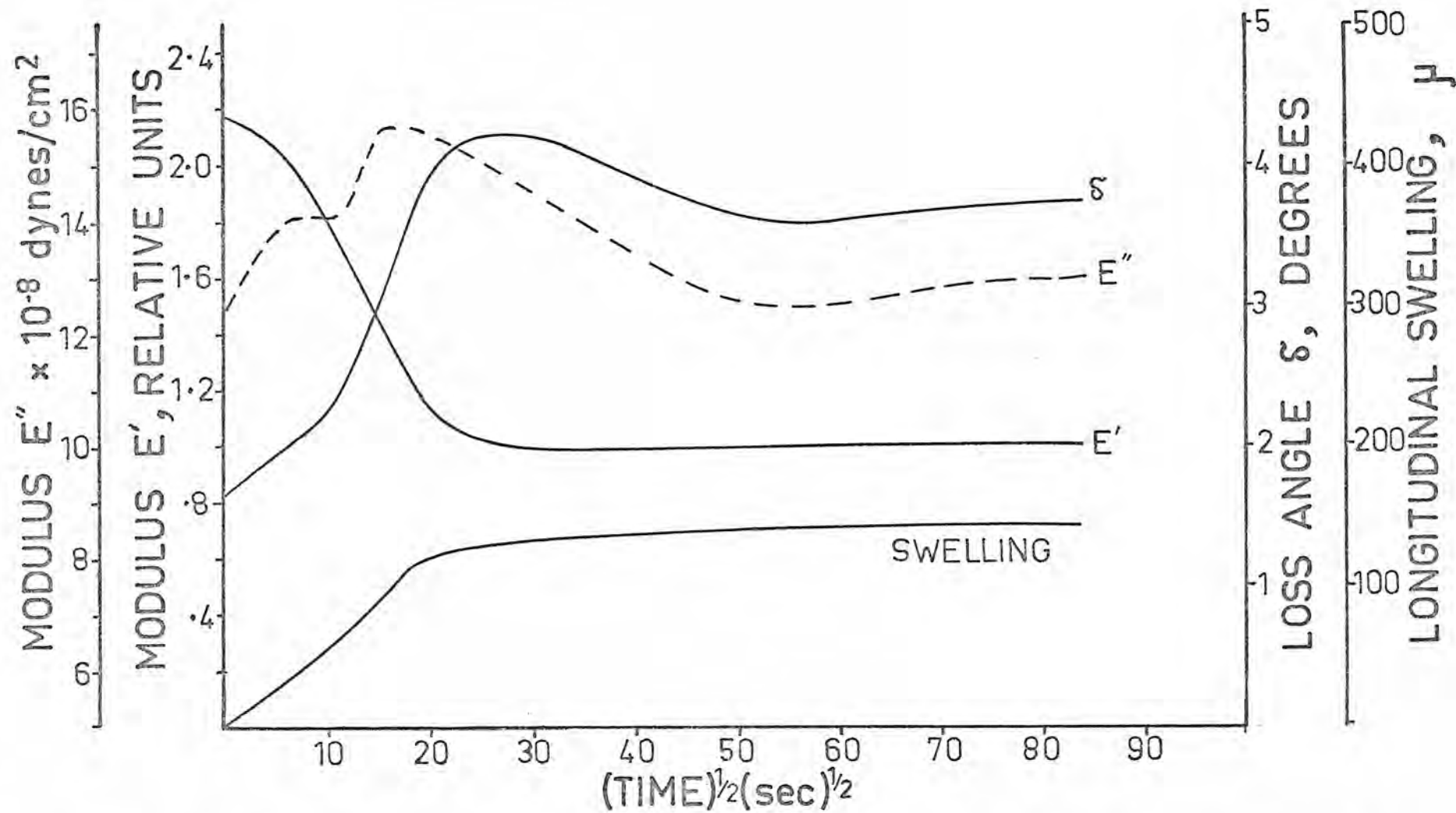


Fig. 4-2 The simultaneous change of E' , E'' , δ and longitudinal swelling against $(\text{time})^{1/2}$ for horse hair at low extensions, during absorption from 52.9% RH to wet condition.

When the tension (or extension) was sufficiently low the overshoot in loss angle was more pronounced, while the longitudinal swelling presented as well a small but well defined overshoot simultaneously with the loss angle. The increase of the intensity of the overshoot of the loss angle is believed to be at least partly an artifact (this was verified to be the case by increasing the tension, after sorption equilibrium was obtained, and showing that the loss angle decreased with tension - see section 3.3). The observed overshoot in longitudinal swelling is in agreement with the results by Watt.

Due to the above mentioned systematic errors in the apparatus at low extensions the exact values of the results obtained are not quoted. However, their relative magnitudes should be significant. One result believed to be accurate in absolute terms is quoted below. This result was obtained for a horse hair with 180μ (wet) diameter, 1.9 cm loop length, and a frequency of 116 Hz. The fibre was conditioned slack at 52.9% RH for 48 h then it was extended a little beyond the "maximum" of modulus and following this the chamber was flooded with distilled water. The results are shown in fig 4-2. In the same figure the calculated loss modulus E'' has been plotted. The two moduli, E' and E'' , refer to the wet cross-sectional area at all times. The loss angle curve shows a pronounced overshoot, and so does the loss modulus E'' . The modulus E' exhibits a very shallow undershoot. The longitudinal swelling is nearly completed a short time before the overshoot in loss angle occurs, while the undershoot in modulus E' occurs a short time after the overshoot in loss angle. Another feature of the loss angle and modulus curves is that they show an early inflection as a function of $(\text{time})^{1/2}$. With regard to the overshoot of the loss modulus E'' curve it should be pointed out that

this does not have a direct connection with possible structural changes, because a correction for the cross-sectional area variation, as the fibre swells, modifies significantly the shape of the curve. Such a correction is not attempted, of course, because the water content or a direct measurement of the fibre diameter against time could not be obtained. However, at the initial relative humidity i.e. at $t = 0$ sec and $RH = 52.9\%$, the correction factor is available in table 3-1 (it equals 1.228). The use of this factor raises the initial value of $E'' = 12.5 \times 10^8$ dynes/cm² to 15.4×10^8 dynes/cm², which is almost equal to the value at the overshoot (15.7×10^8 dynes/cm²). The equilibrium value of E'' of the wet fibre is lower than the initial equilibrium value at 52.9% R.H. and this change is in agreement with the general trend of change of E'' with R.H. as shown in table 3-1.

4.3.2 Tests on Lincoln Wool

Feughelman and Robinson⁴⁷ showed that the turnover point between Hookean and yield region on the stress-strain curve of a wet fibre occurs at the same absolute length at any relative humidity. This turnover point corresponds to the extension, at which the ordered α -keratin helices of the microfibrils in the wool fibres are just at the point of unfolding. This means that the extension of a fibre to a strain at the turnover point at all moisture contents brings the keratin structure to the same state of displacement. This observation led to the conduction of the following tests on the same single Lincoln wool fibre. The fibre was first conditioned at 100% R.H. and then extended to 0.6% strain (corresponding to the "maximum" of dynamic modulus). Following this the fibre was held at 0% R.H. for 24 h and then conditioned at a particular relative humidity X% for the next 6 to 8 h. Finally the atmosphere was brought to 100% R.H. again for

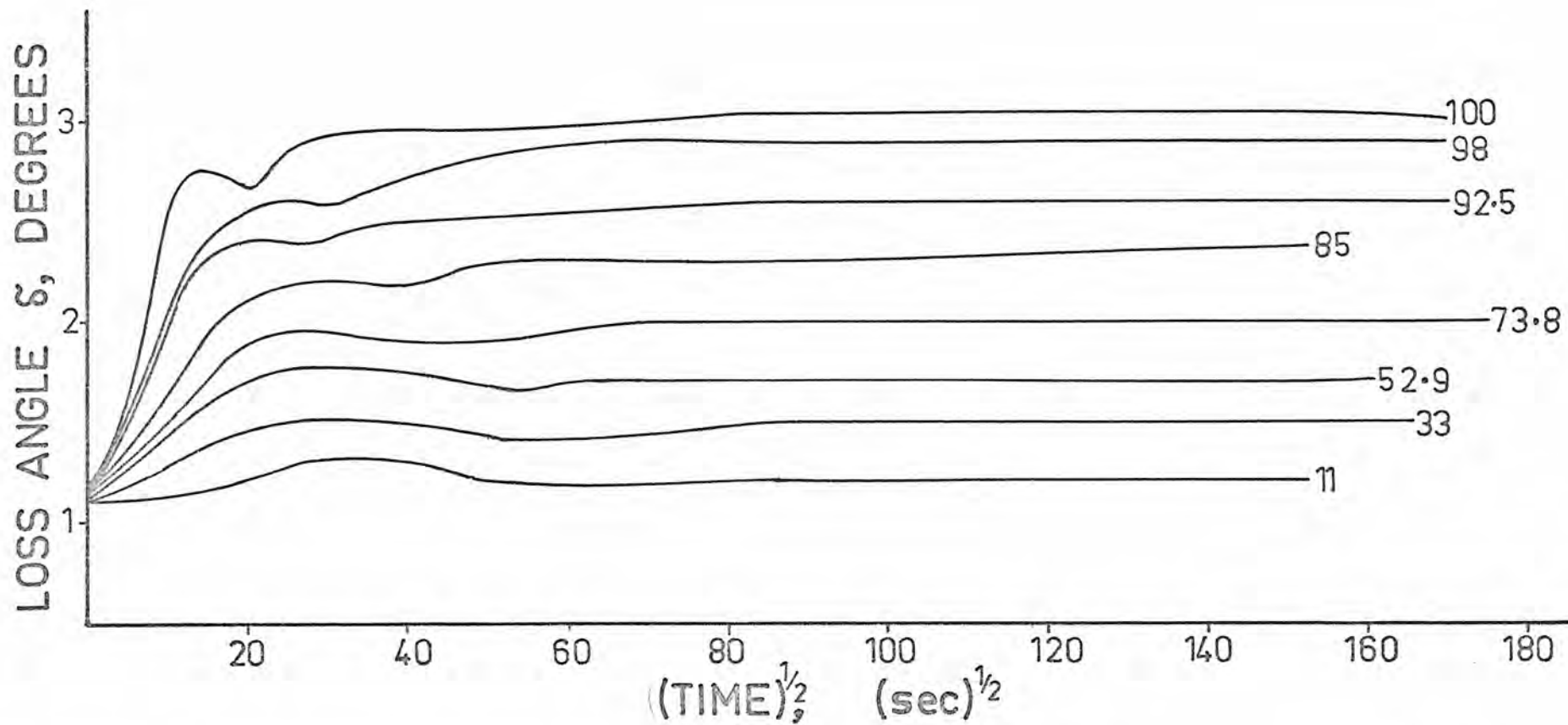


Fig. 4-3. The loss angle δ against $(\text{time})^{1/2}$ following a step change of relative humidity from 0% R.H. to a level shown with each curve.

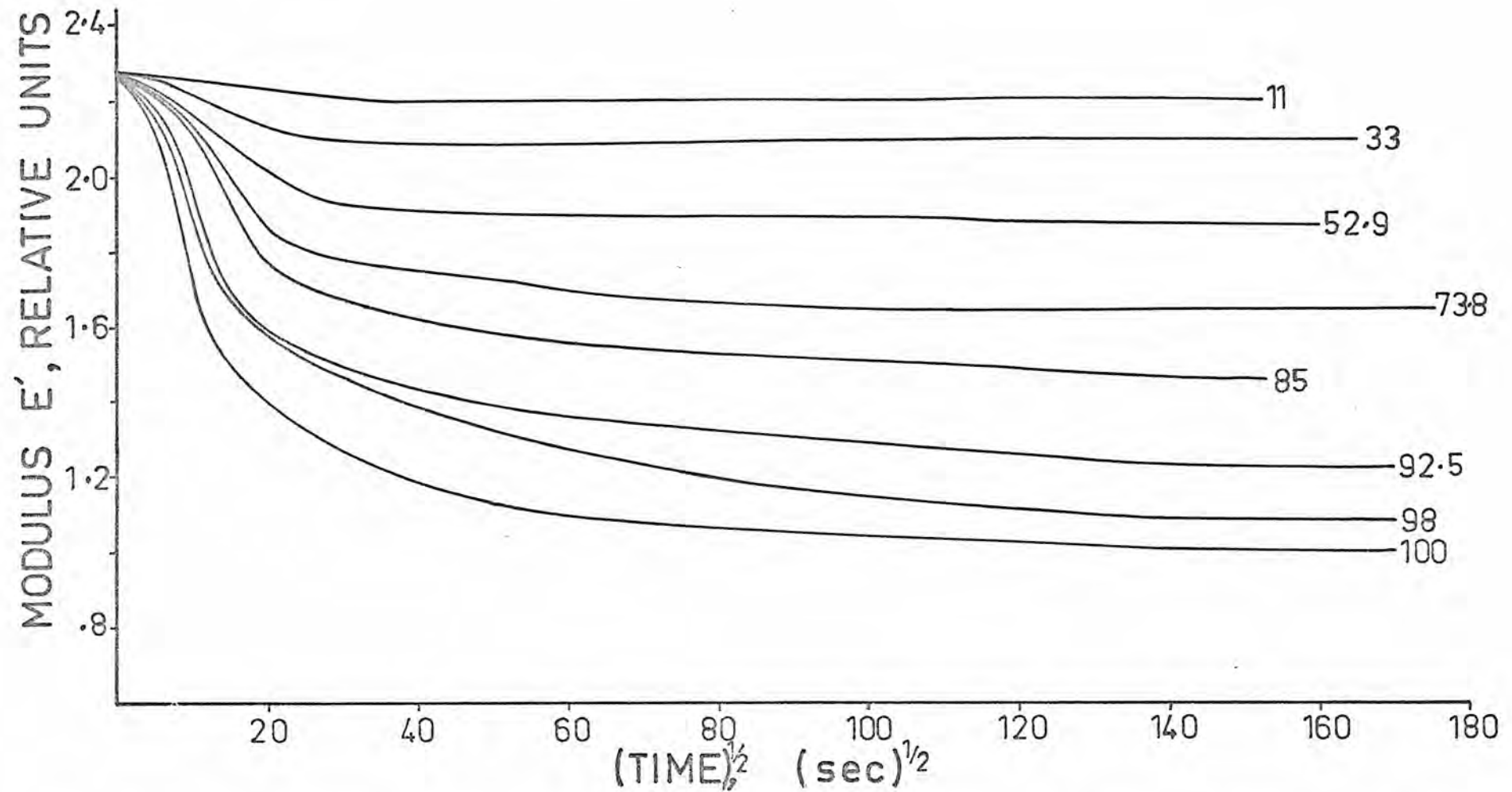


Fig. 4-4 The modulus E' against $(\text{time})^{1/2}$ following a step change of relative humidity from 0% to a level shown with each curve.

24 h in order to start a new conditioning cycle with a different X% R.H., which took on the following values : X% = 11, 33, 52.9, 73.8, 85, 98, 100%. During these tests the absolute length of the fibre was practically constant, a very small contraction of less than 0.1% occurring during drying (the fibre diameter was around 45 μ and the increase of tension during drying was not capable of contracting the fibre more than 0.1%). It was verified that the fibre was at the same state of strain, each time it was conditioned at 100% R.H. i.e. the modulus was always at its "maximum" value. The results thus obtained for the loss angle and modulus are shown in fig 4-3 and 4-4 correspondingly. These results confirm the ones obtained with horse hair. The overshoots as well as the secondary long-term increase in loss angle are again present. The overshoots, however, are of much less intensity probably because of the very early appearance of the secondary increase, which obscures the prominence of the overshoots. The graphs of fig 4-3 reveal the important feature that the overshoots occur at a shorter time and their width decreases with increase of relative humidity. The secondary increase in loss angle also occurs at a shorter time and becomes more intense with increase of relative humidity. The value of modulus for the dry fibre is approximately 2.3 relative units, a value somewhat lower than the recorded value of 2.45 relative units in chapter 3. Finally the early inflection on the loss angle and modulus curves as a function of $(\text{time})^{1/2}$ is again present.

4.4 Qualitative Explanation of the Results

The two-phase structure of keratin combined with the known change of modulus and loss angle with static strain as found in chapter 3, can give an adequate explanation for the transient phenomena reported in this chapter.

During absorption the water has a double effect on the structure of keratin fibres namely a weakening as well as a swelling effect. Because of the small size of water molecules, they can gain access to the internal structure of the phase M where, through their polarizability and ability to form polar interactions they distribute themselves in the fibre, so as to concentrate in regions of high electric field intensity. The molecules of water concentrate around accessible charged and polar groups and, being highly polarizable, tend to attenuate the electric fields associated with these groups. The result is to reduce the interaction between neighbouring polar groups, that is to produce shielding. The overall effect of the water is to moderate and average out the internal electric fields in the fibre. The swelling of the wool fibre due to the presence of water is extremely marked. The longitudinal and lateral swelling for the fibre from the dry to the wet state are about 1.2% and 16% respectively⁸⁵. Feughelman and Nordon³⁸ calculated that the matrix alone should swell volumetrically by a considerable degree equivalent to a purely 42% lateral change. Phase M tends to swell isotropically. However, phase C being much stiffer than phase M confines the swelling of the phase M in the lateral direction. This means that phase C will have high forces in the extension direction applied to it by phase M. The extension of phase C corresponds to the extension of the whole fibre. It is proposed now that the α -helices in the phase C of an unextended fibre are strained during absorption and subsequently retract slowly back to their natural length. The transient extension of the C phase implies a transient decrease of its modulus according to fig 3-10 or 3-11 (bottom). This transient decrease of modulus E_c amounts to about 10% (corresponding to about 1.2% strain). A qualitative presentation of the components of the complex modulus is shown in fig 4-5. The

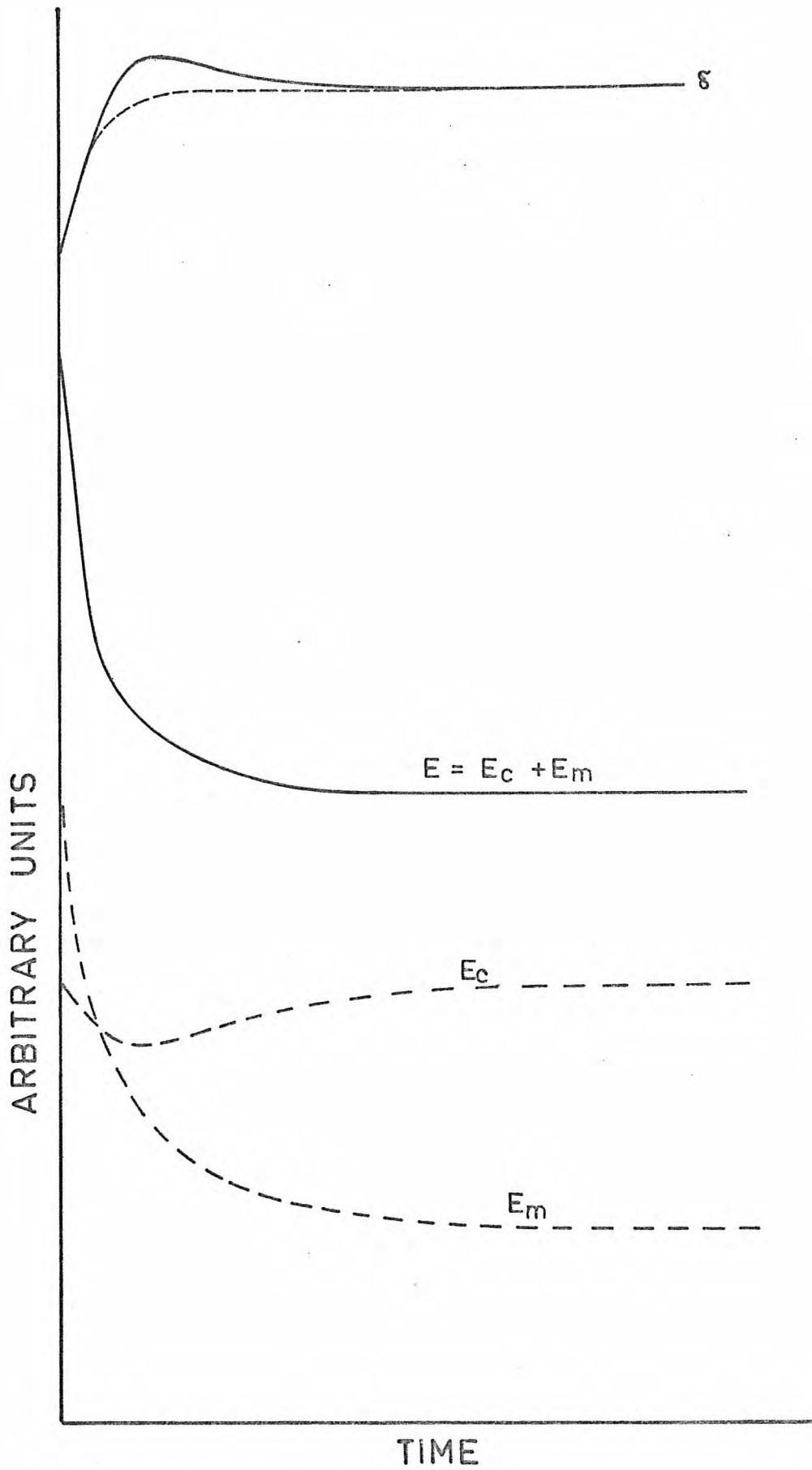


Fig. 4-5 A qualitative representation of the simultaneous change of E_c , E_m , E and δ with time for a keratin fibre after a step change of relative humidity.

modulus E_m (curve E_m) of the phase M should be a monotonically decreasing curve corresponding to the continuous weakening effect as the water penetrates this phase. The modulus E_c of the phase C shows an undershoot corresponding to the straining of the α -helices. The curve $E = E_c + E_m$ is the modulus of the total fibre and has the same characteristics as the experimentally obtained curves. The undershoot in E_c occurs when the swelling i.e. the absorption is nearly completed. At this point of time the modulus vector for phase M (see fig 3-9) has reached nearly its final value and therefore the loss angle for the total fibre would also have reached closely to its final value as shown by the broken curve for δ . However, because of the undershoot of E_c the loss angle should exhibit a value in excess of the expected (solid curve δ). From this point onwards the modulus vector for the phase C starts increasing slowly as the phase retracts and this means that the loss angle must decrease accordingly. The above qualitative analysis provides one possible mechanism responsible for the overshoot of the loss angle curve for the whole fibre. That is, the overshoot implies a transient extension of the microfibrils accompanied by breakdown and reformation of bonds, probably of the hydrogen bonds within the α -helices. However, polar bond breakdown and reformation takes place in the matrix as well, as the water front penetrates this phase. In other words, the matrix passes through a gel-sol-gel state during absorption, which could result in a maximum of energy absorption and might show up as an overshoot in loss angle. Although structural changes do take place in both phases, it is proposed here that the structural changes mainly in phase C, are responsible for the overshoot in loss angle for the whole fibre. The change of δ with time during absorption confirms previously expressed ideas³⁸ that a maximum of bond-breakdown and reformation is in progress in the fibre structure just as maximum swelling is reached.

At this stage the structure is at its maximum mobility. Beyond this point in time the structure comes progressively to equilibrium with the rate of bond breakdown and reformation considerably reduced and with more bonds unbroken the behaviour of the fibre becomes more elastic.

The results of tests on Lincoln wool fibres can be explained by using the mechanisms proposed above. The occurrence of the overshoots in loss angle at shorter times and the concomitant decrease of their width with increase of relative humidity is due to the faster penetration of water into the structure on the one hand and the faster relaxation of the structure on the other. The retraction of the α -helices extended due to the swelling action of water in the matrix is facilitated by the plasticizing action of water; again, due to the plasticizing effect of water the reformation of broken bonds in the amorphous region takes place at a shorter time.

The secondary increase in loss angle with time observed during tests on horse hair and Lincoln wool fibres could be attributed to the progressive weakening of the phase C due to long-term bond breakdown within this phase or interactions between this phase and phase M. Also, in part this slow increase of loss angle may result from second stage sorption of water⁹⁰.

The temperature rise because of heat evolution during absorption of water by keratin fibres is not believed to be responsible for the appearance of the overshoots in loss angle for the following reasons: firstly, the rise of temperature around the fibre implies a decrease of relative humidity and hence would result in a decrease in loss angle and not the increase obtained at the overshoot; secondly, it will be shown in chapter 5 that the loss angle for a wet or nearly wet fibre decreases with increase of temperature, again in

contradiction to what happens at the overshoot; thirdly, the heat effects should be minimal during the experiment in which water was used to change the relative humidity from 52.9% to 100% (see fig 4-2).

4.5 Corroborative Evidence from Published Work

All avenues of investigation likely to contribute to the ultimate interpretation must be explored. There is much experimental evidence in published works, which is compatible with the results presented in this chapter and supports the proposition given here, and vice-versa. Some of this evidence is given below.

4.5.1 Experiments with D₂O

For wool fibres placed into D₂O about 70% of the amide hydrogens are replaced by deuterium. The unexchanged hydrogens belong to the peptide chains of the ordered α -helices³⁸. Haly and Feughelman showed that by drying and wetting wool fibres in D₂O five hundred times about 90% of the amide hydrogen in the peptide chains is replaced by deuterium. This result indicates that during the sorption process from dry to saturation a transient increase of accessibility of the wool fibre occurs. Such a transient increase of accessibility would result from a sorption process causing increase of accessibility in the phase C by bond weakening or disruption followed by a return to equilibrium accessibility by bond reformation. This finding is in direct agreement with the proposal that the α -helices are extended as the water front penetrates the structure and afterwards they retract back to their equilibrium length.

4.5.2 Stresses Developed Due to Regain Change by Absorption

When a fibre is held extended in the Hookean region at any constant relative humidity, the stress developed relaxes always to an equilibrium value corresponding to a modulus of 1.4×10^{10} dynes/cm²⁵⁰.

The relaxation time varies between 5.2×10^2 min for a dry fibre and 6.6×10^{-1} min for a wet fibre⁵⁰ (relevant experiments are reported in chapter 5). The relaxation occurs in the phase M and the equilibrium value of stress reached in all cases is due to the phase C. Thus the stress sustained by each phase depends on the time scale of the experiment as well as on the regain of the fibre. For a wet fibre it can be said that the static stress is nearly completely attributable to the phase C, while at lower water content the matrix plays an increasing role. If, now, an initially dry wool fibre held at 1.5% strain is conditioned for 11 min at 49% R.H. and subsequently placed in water, the stress passes through a minimum level, which is more than 30% lower than at the final equilibrium level⁵⁸. By the time the undershoot in stress occurs the water uptake is nearly completed and the fraction of stress supported by the phase M is negligible. Besides, a wet matrix can under no conditions support a stress of such level equal to the amount, by which the stress increases with time after the undershoot occurs. Thus, on the basis of the two-phase model for a wool fibre, the minimum in stress during absorption would be interpreted to mean that for a short time there is a decrease in the stress supported by the phase C. This decrease may indicate a transient opening up of the C structure. It was mentioned in an earlier section that during a change from 0% to 94% R.H. the torsional rigidity of the fibre also falls rapidly and then slowly increases until the equilibrium rigidity at 94% R.H. is reached⁶². If, as proposed by Feughelman³¹, for a fibre being twisted most of the shear strain is taken up by the M phase and the torque due to the fibre is controlled by the shear properties of the M phase, the latter phase passes through a gel-sol-gel state during absorption and thus it is partly responsible for the undershoot in stress observed.

4.5.3 Kinetic Studies of the Wool-Water System

Kinetic studies of the wool-water system have been undertaken by various workers^{21,91,63,93,89,92}. It has been observed that small changes in relative humidity cause sorption and desorption processes which occur in two distinct stages. The second stage is much longer in duration than the first and occupies some hours. The first stage is associated with a diffusion mechanism, which may be in accordance with Fick's law^{21,92}, while the second stage is associated with some structural relaxation mechanism. Both absorption and desorption to and from high water concentrations in wool is anomalous⁹² i.e. does not obey Fick's law. The distinguishing features of this anomalous sorption are that the uptake curve shows an inflection as a function of $(\text{time})^{1/2}$ and the initial rate of desorption is faster than the initial rate of absorption. An additional deviation from Fickian behaviour are the concentration overshoots on absorption, which are only observed with final relative humidities above 80%. All the above anomalous features of the variation of water content with time observed during absorption bear a great similarity with those observed for the variation of the complex modulus during absorption. The mechanisms proposed to explain the behaviour of complex modulus can be readily used to explain the sorption features as well. That is the phase M alone with an absence or a minimum of backbone constraints may absorb water according to Fick's law; however, the existence of the C phase opposes the absorption of water by opposing the swelling effects of the water (Le Chatelier principle). Increased constraints to swelling reduce the water absorption and a removal of swelling constraints allows increased absorption. In keratin the main constraint to swelling are the ordered α -helices, which are extended during the first stage of absorption; following this stage, they retract and gradually release the phase M from constraints. This relaxation of

the phase C is responsible for the second stage of absorption. The relaxation times of the phase C depends on the water content in the fibre, which acts as a plasticizer. A large change of relative humidity causes both the diffusion and relaxation mechanisms to act simultaneously with the result that the sorption becomes characteristically "anomalous".

Other workers in their kinetic studies of the wool-water system have come to general conclusions, which corroborate the views expressed in this work. Thus, Bagley and Long⁴ considered the second stage to be additional desorption or absorption resulting from the slow rearrangement of interchain bonds brought about by the change of penetrant concentration during the first stage. Barkas suggested⁵ that sorption hysteresis is dependent on the mechanical hysteresis; from this Watt concluded for the wool-water system⁹¹ that no hysteresis is shown on desorption from the quasi-equilibrium prior to second stage sorption but considerable hysteresis is exhibited on desorption after second stage absorption, that mechanical rearrangement of the fibres does not occur during first stage absorption but coincides with second stage absorption. Watt⁹¹, using the hypothesis that the second-stage absorption occurs as a result of the stresses set up in the wool fibre by the first-stage absorption showed quantitatively that his data on the relative size of the second-stage absorption is consistent with the idea of an osmotic balance between the expansion pressure of absorbed water and the cohesive forces of the fibre. Fujita, Kishimoto and Odani⁵³ showed that when a polymer was partially crystalline the curve of moisture uptake against $(\text{time})^{1/2}$ assumed a non-Fickian sigmoid shape at high initial penetrant concentrations. This anomalous sorption appears to be concomitant with a non-absorbing stiff phase in the presence of an absorbing weaker phase.

Further corroboration is derived from studies of the longitudinal swelling of keratin fibres during absorption. Watt⁹³ reported from a series of interval absorption steps at high humidities, where the fibre length undergoes a transient increase that:

- (i) the length reaches a maximum value more quickly than the water content;
- (ii) this maximum is reached more quickly with increasing humidity;
- (iii) the magnitude of the transient elongation decreases above 90% Relative Humidity;
- (iv) the time required for the length to drop to the equilibrium value decreases as saturation is approached.

Later, Mackay and Downes⁶³ using an improved sorption vibroscope reported the existence of undershoots with time on the desorption curve, when a small change of relative humidity is applied. The transient length changes following abrupt humidity changes are evidently associated with disruption in the phase C⁹³. The features of length swelling listed above are in excellent agreement with the observations made on the overshoots in loss angle during the tests of Lincoln fibres as reported earlier.

In the above, only a few examples were chosen to demonstrate the validity of the suggestions made to explain the behaviour of the dynamic mechanical properties of keratin fibres during absorption. Further, a large range of published data (ranging from the electrical properties of keratin to the variation of the diffusion constant with regain, to the variations in the equilibrium weight of wool at zero humidity etc.) can be re-examined in the light of the interaction of the two phases of keratin; however, this goes beyond the scope of the present work.

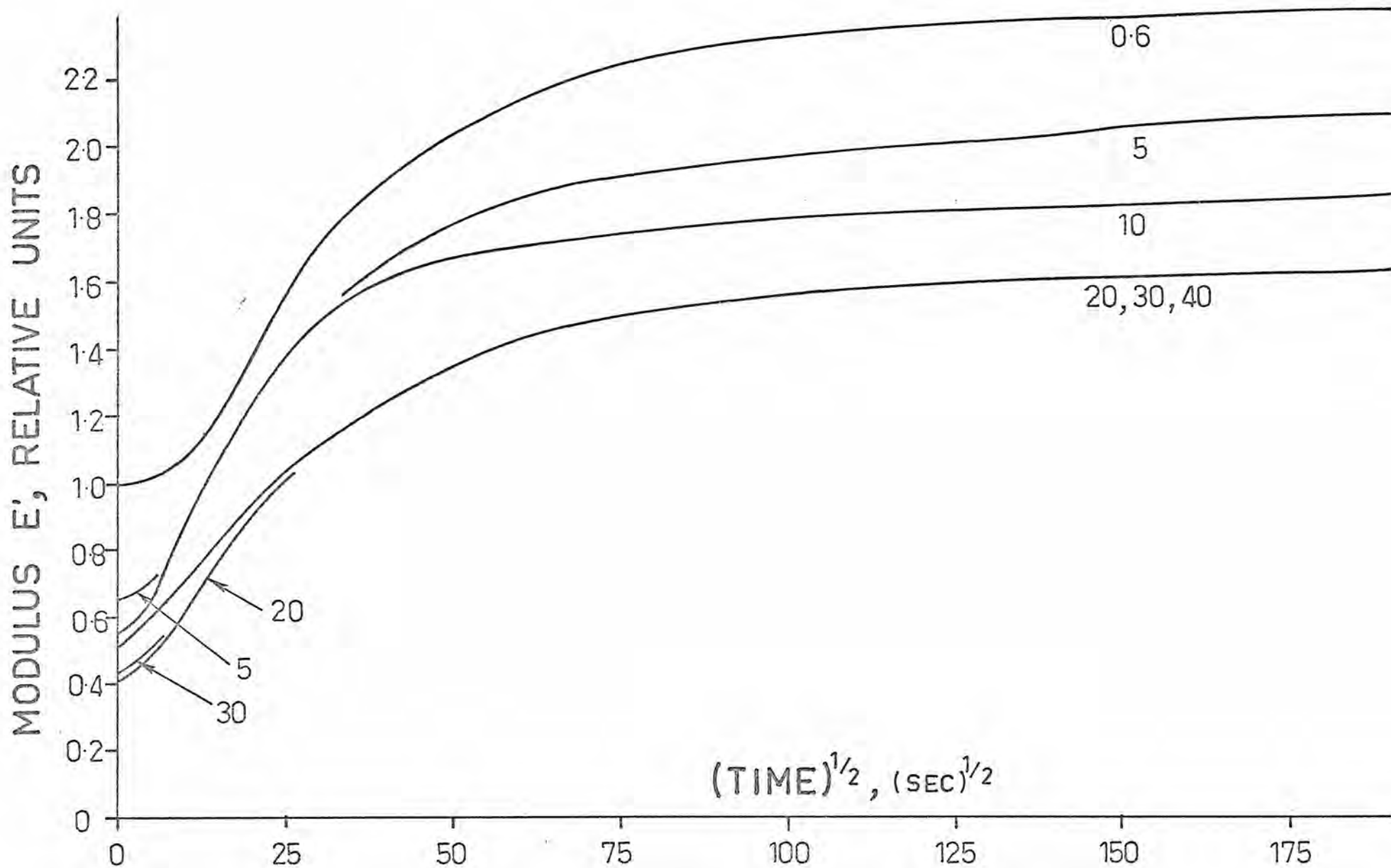


Fig. 4-6 The modulus E' against $(\text{time})^{1/2}$ for fibres during desorption from 100% R.H. to 0% R.H. for different fixed extensions of each fibre shown with each curve.

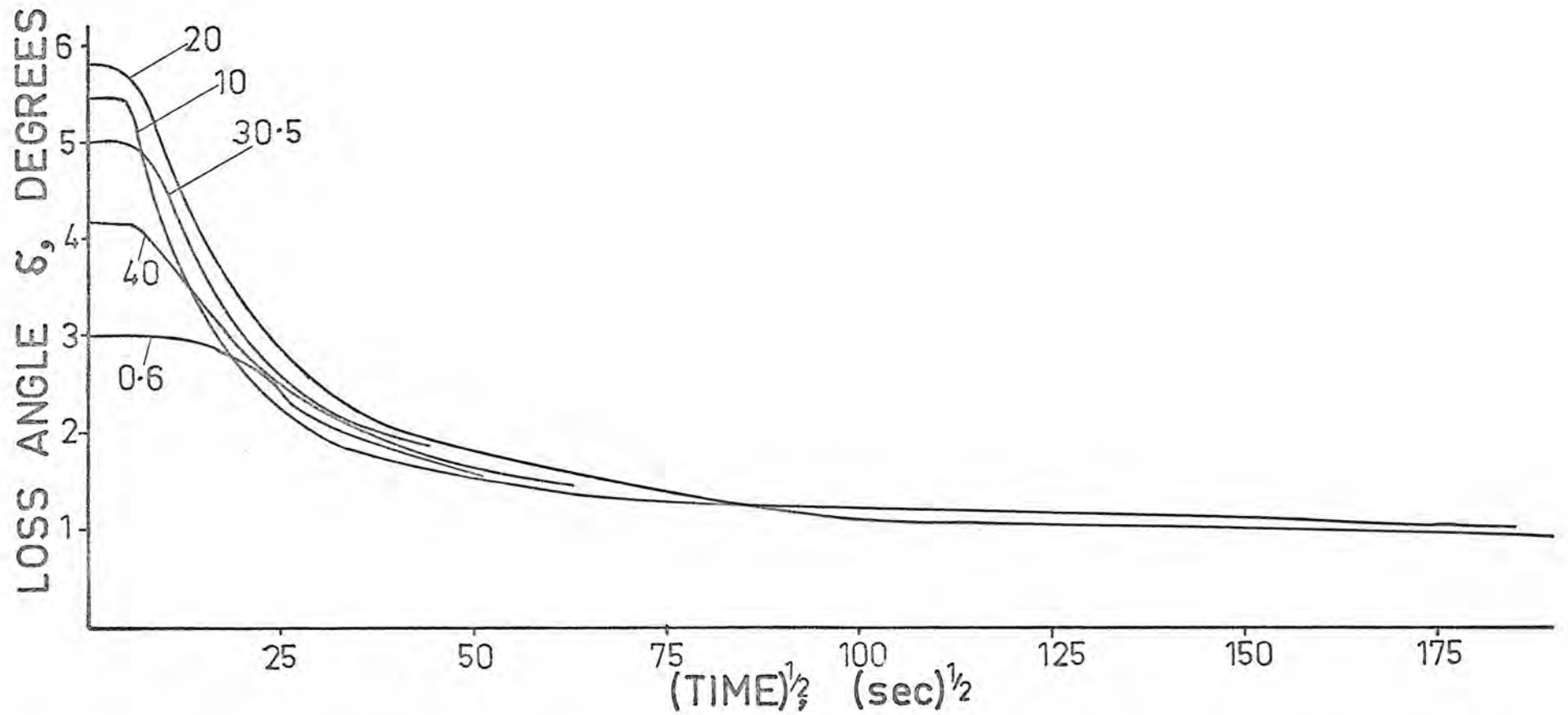


Fig. 4-7 The loss angle δ against $(\text{time})^{1/2}$ for fibres during desorption from 100% R.H. to 0% R.H. for different fixed extensions of each fibre shown with each curve.

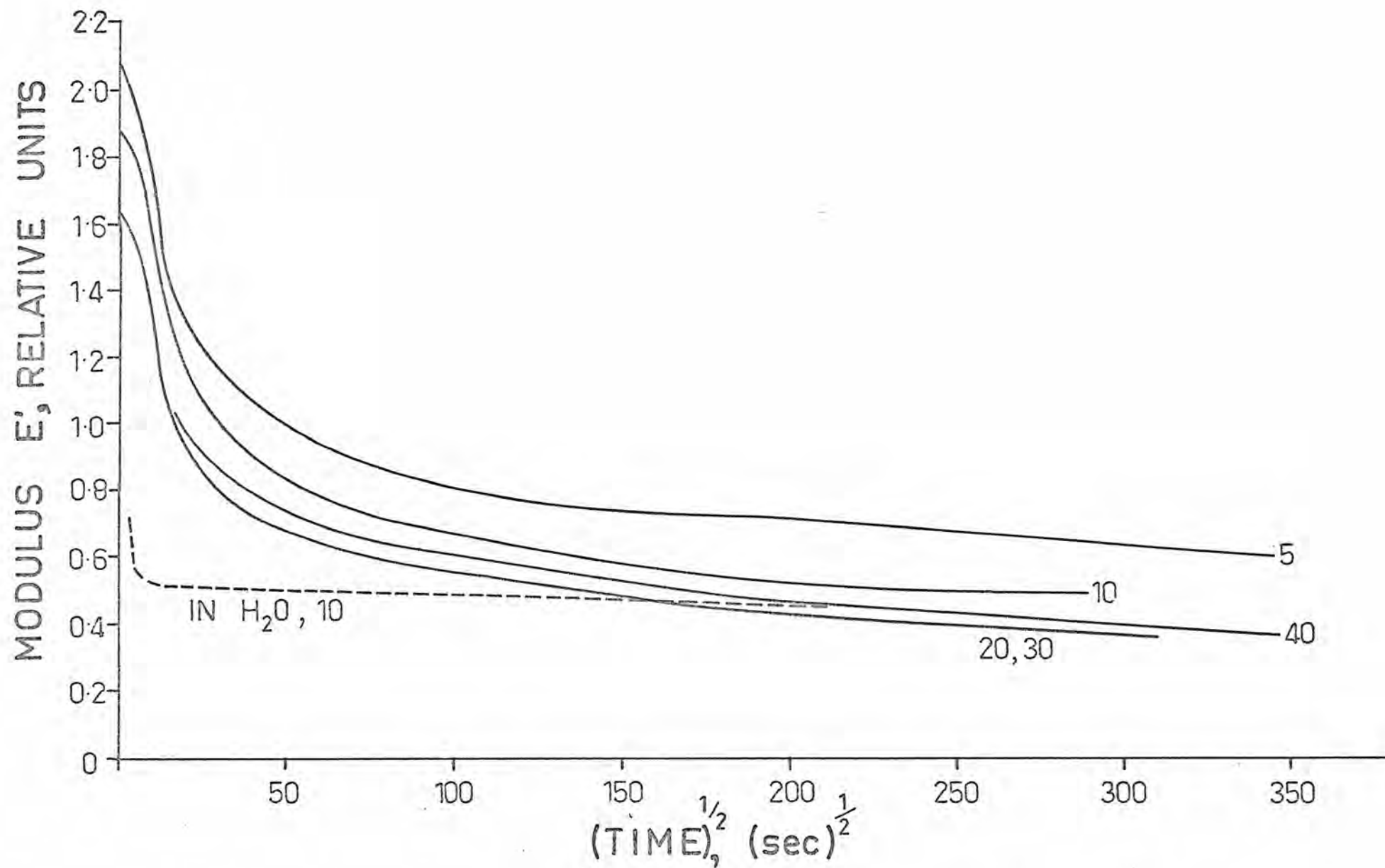


Fig. 4-8 The modulus E' against $(\text{time})^{1/2}$ for fibres during absorption from 0% R.H. to 100% R.H. for different fixed extensions of each fibre shown with each curve.

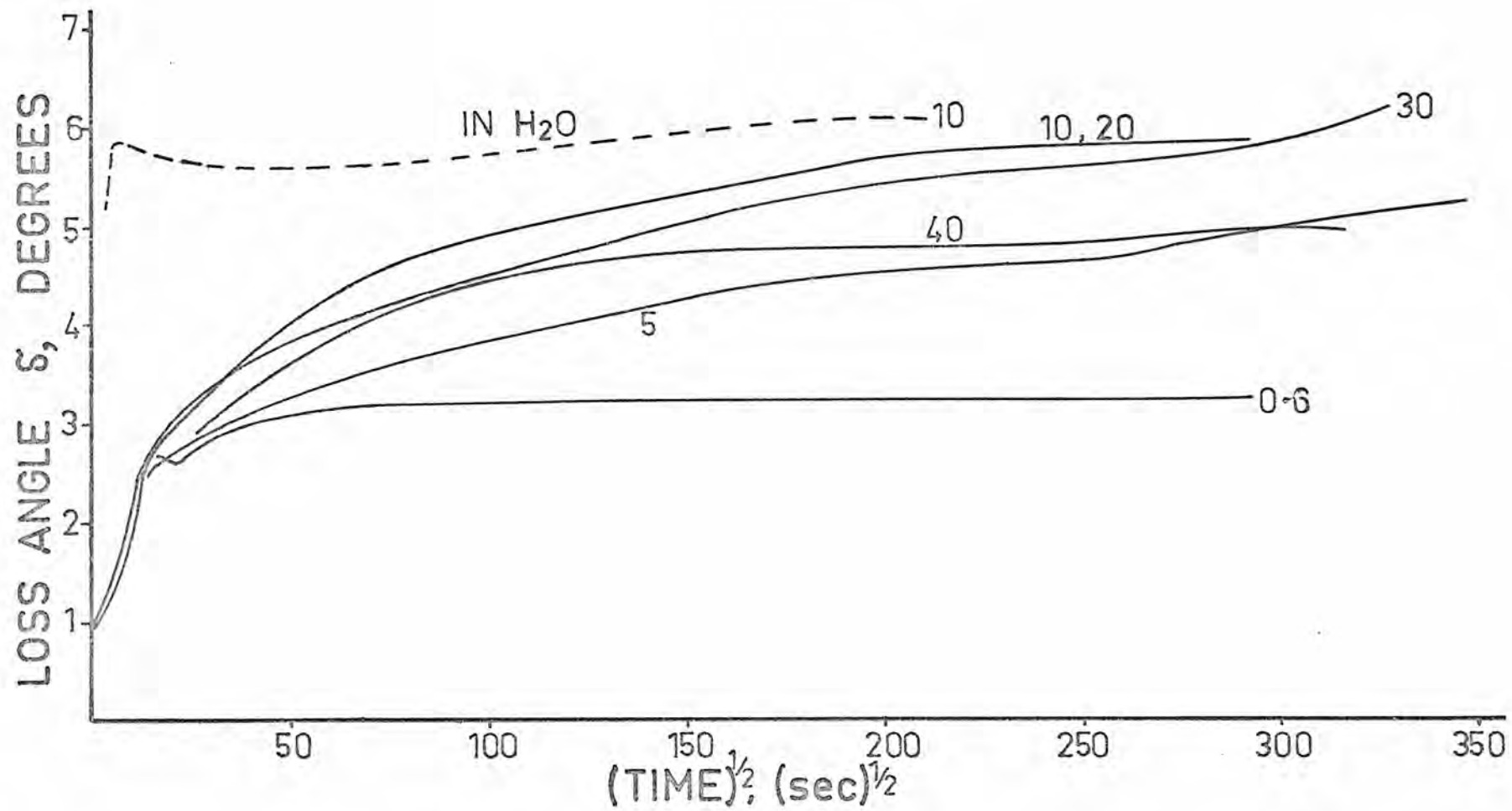


Fig. 4-9 The loss angle δ against $(\text{time})^{1/2}$ for fibres during absorption from 0% to 100% R.H. for different fixed extensions of each fibre shown with each curve.

4.6 The Complex Modulus During Absorption and Desorption at Fixed Extensions

Up to this point the complex modulus has been examined only during absorption at low extensions of the keratin fibres, however, it was considered important to investigate the variation of complex modulus at different constant extensions during both absorption and desorption. These measurements, it was expected, would yield more information on the structural changes within the fibre with increase of extension.

Lincoln wool fibres were used for the tests. Prior to the test each fibre was conditioned slack at 100% R.H. for 24 h and then extended to X% strain at a strain rate of 1.07% per minute. The fibre was held at this extension X% for 30 min after which the relative humidity was changed to 0%. The modulus and loss angle were recorded during desorption until they seemed to have reached an equilibrium value. The drying lasted for 24 h and subsequently the relative humidity was changed back to 100%. The modulus and loss angle were again recorded until they again appeared to have reached an equilibrium value. Six fibres were tested using the above procedure, the value of the constant strain X being 0.6, 5, 10, 20, 30, 40% respectively. The modulus and loss angle during desorption are shown in figures 4-6 and 4-7 correspondingly with the percentage of the constant strain X indicated with each curve. The modulus and loss angle during absorption are shown in figures 4-8 and 4-9 in the same way. One more Lincoln wool fibre held at 10% fixed strain was treated as above, except that the final conditioning to 100% R.H. was performed by introducing water into the chamber and not by saturating the atmosphere with vapour. The result during absorption is shown with broken lines in figures 4-8 and 4-9. Finally, one Lincoln wool fibre underwent the following treatment: it was conditioned slack at

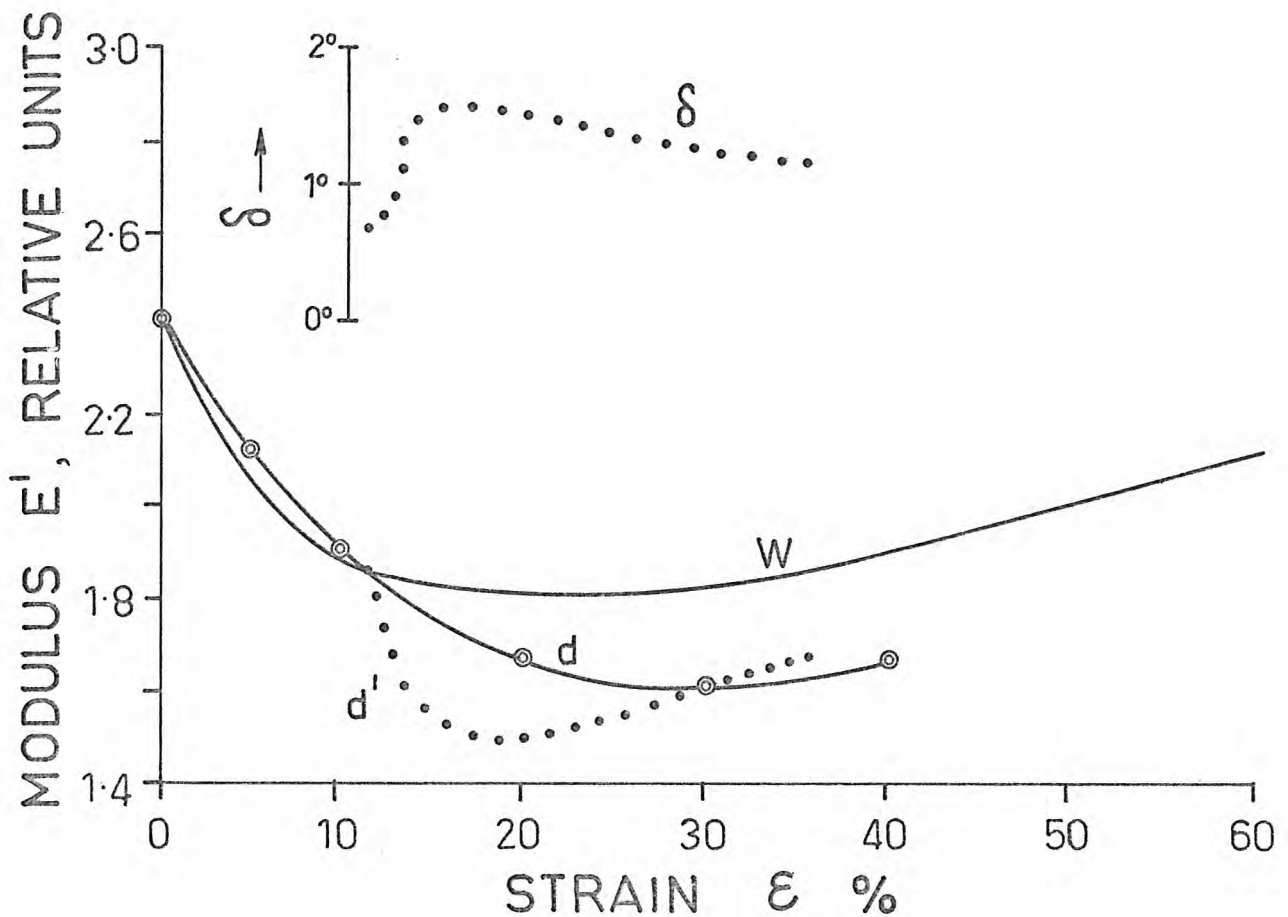


Fig. 4-10 The modulus versus strain for Lincoln wool fibres under the following conditions:

Curve (d), the modulus of a dry fibre after extension in water to the plotted strain.

Curve (w), the modulus of a wet fibre, for which a fixed vertical shift has been applied to equate the modulus at zero strain ($\approx 0.6\%$) with that of the dry fibre of curve (d).

Curve (d'), the modulus of a dry fibre extended dry to various strains greater than 11%, after the fibre had been previously extended wet to 11% strain and dried.

The loss angle for the fibre corresponding to the conditions for curve (d') is plotted as curve (δ).

100% R.H. for 24 h, then extended to 11% strain at 1.07% per min and held at 11% strain for the following 30 min. Subsequently, the fibre while held at the fixed strain was dried for 24 h and eventually it was extended to break in dry conditions by using a strain rate of 1.07% per minute. The modulus and loss angle with strain during the final extension in dry conditions are shown in figure 4-10 with dotted curves. Observations and discussion of these results follow.

4.6.1 Desorption

It is observed that the modulus during desorption generally increases with time to some equilibrium value depending on the fixed strain at which the fibre is held. Wherever portions of the various curves almost overlap with one another, the curves have been drawn discontinued for clarity. The exact equilibrium values of modulus for dry fibres at various constant strains is shown as curve (d) in figure 4-10 from which it is observed that the equilibrium dynamic modulus decreases with strain up to 20% and beyond that it remains practically constant. During desorption the loss angle decreases with time and it reaches practically the same low level regardless of strain.

The curve (d) for modulus in fig. 4-10 has the same general shape as the one for modulus against extension for a wet fibre. (See fig. 3-4 for a wet fibre). A comparison of the shape of this wet curve neglecting the absolute level, redrawn as curve (w) with the curve (d), is shown in fig. 4-10. The curve (w) has been plotted so that the initial level at zero strain coincides with curve (d). It is observed that the two curves are close to each other for fixed strain up to $\approx 15\%$. This implies that the phase C remains basically unaltered upon drying the fibre from the wet state for fixed strains

up to $\approx 15\%$. Beyond this strain the phase C appears to be weaker upon drying, which is compatible with the fact that the modulus decreases with time when a wet fibre is held at a fixed strain higher than $\approx 15\%$ (see section 3.9). Thus the effect of the phase M upon drying a wet fibre is as follows. It raises the modulus of the total fibre by a component which is practically invariant with strain; this component corresponds to the increase of modulus of the M phase itself.

The conclusion from the similarity of curves (d) and (w) is further supported by the behaviour of modulus E' (curve d') and loss angle δ (curve δ) against extension as shown by the dotted curves of fig. 4-10. This result was obtained by continuously extending a dry fibre from 11% strain up to the breaking point, after the fibre was extended at a fixed strain (11%), at 100% R.H., relaxed for 30 min and subsequently dried at 0% R.H. The dotted curves present all the characteristics of a normal unextended dry fibre (see fig. 3-4) with an abrupt decrease of the dynamic modulus and a corresponding increase of the loss angle. The marked increase of the initial slope of the curve (d') as compared with the slope of the curve (d) at 11% strain arises from the fact that the opening up of α -helices for the case of curve (d') is inhibited by a dry matrix which would result in more α -helices opening up to obtain the same strain level. For a dry fibre α -helices do not open up completely into β configurations because of steric hindrances; hence more helices must be partially unfolded to obtain the same strain when compared with the unfolding of α -helices to β chains in a wool fibre extended in water⁹. The fact, however, that the loss angle (curve (δ)) starts from the same low value as that of an unextended fibre needs closer consideration. Upon drying a fibre from the wet state at any fixed extension, the loss angle achieves the same final low value as that of an unextended dry

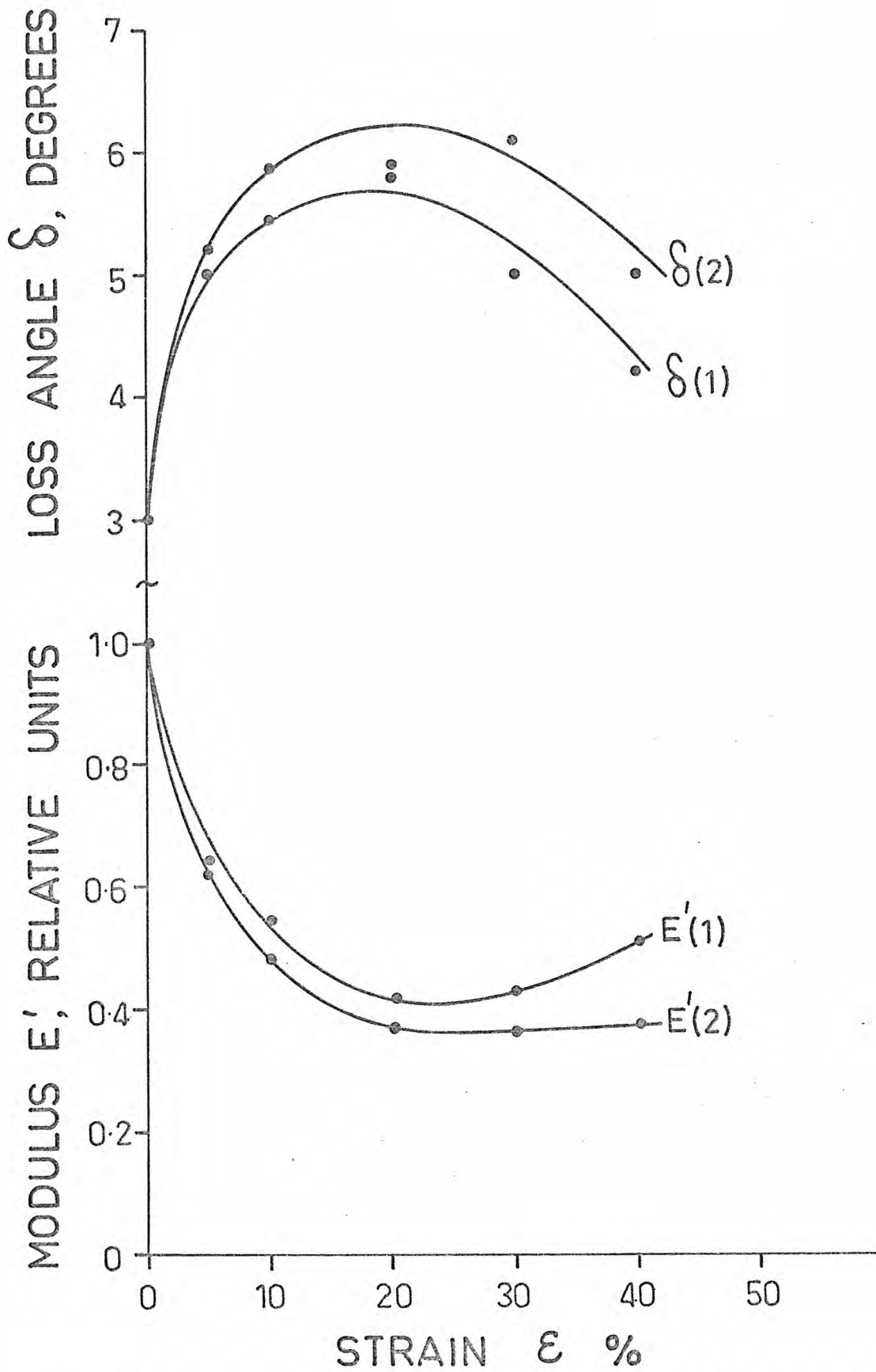


Fig. 4-11 The equilibrium dynamic modulus $E'(2)$ and loss angle $\delta(2)$ against strain for a fibre at 100% R.H. and the modulus $E'(1)$ and loss angle $\delta(1)$ against strain just before desorption, at 100% R.H. (see text).

fibre, as pointed out earlier. This suggests that the structural state of the wool fibre dried from the wet condition at any extension is similar to the initial state of the unextended dry fibre. As far as the matrix is concerned drying from the wet condition at any strain certainly achieves a dry matrix set in a state similar to an unextended dry fibre. Further extension of this latter set fibre when dry will create stresses in a network of bonds similar to that when straining an unextended dry fibre.

4.6.2 Absorption

It is observed that the modulus during absorption generally decreases with time to some equilibrium value depending on the fixed strain, at which the fibre is held. Wherever portions of the various curves almost overlap with one another, the curves have been drawn discontinued for clarity. The equilibrium values of modulus at 100% R.H. have been plotted with (fixed) strain as curve $E'(2)$ in fig. 4-11; for comparison the modulus just before desorption is also plotted with (fixed) strain as curve $E'(1)$. During absorption the loss angle generally increases with time (fig. 4-9) to some equilibrium value depending on the fixed strain at which the fibre is held. The loss angle against (fixed) strain is also plotted in fig. 4-11 for just before commencement of desorption (curve $\delta(1)$) as well as when equilibrium was nearly achieved at 100% R.H. after absorption (curve $\delta(2)$). From fig. 4-11 it is observed that in general $E'(2) < E'(1)$ and $\delta(2) > \delta(1)$ and the inequality becomes more pronounced with strain. The important feature, though, is that the fibre recovers, in the main, its previous structural state, as though the desorption cycling had no major effect, except for the inequalities stated above. When the relative humidity is changed from 0% to 100% using water vapour, the loss angle change with

(time)^{1/2} shows an abrupt increase and subsequently a slow increase. The magnitude and speed of the abrupt increase is almost independent of fixed strain, while the slow increase is strongly dependent on the fixed strain. When from 0% R.H. the fibre (at 11% fixed strain) is wetted with water the loss angle shows a pronounced overshoot and finally it increases again by a small amount and slowly, as shown by the broken line in fig. 4-9. The latter result proves that the overshoots observed at low extensions are genuine and that the structural behaviour of keratin during absorption is similar at higher extensions. However, the structural changes during absorption depend strongly on the way the conditioning of the surroundings is performed. Thus the overshoots in loss angle were not observed, when water vapour was used, probably because the secondary slow increase overshadows a possible tendency for an overshoot. This secondary slow increase is probably of the same origin as the one described during absorption at low extensions. In summary, there are three phenomena occurring during absorption: one responsible for the initial abrupt increase of loss angle, a second responsible for the decrease of loss angle after the overshoot occurs and a third responsible for the secondary increase in loss angle. Their relative importance depends on the path the environmental changes follow.

The main factor likely to be decisive on the structural behaviour of keratin during absorption is the heat evolution. The important role of temperature in the wool-water sorption system is not always fully appreciated. Two examples may serve to emphasize the magnitude of the effect²²: (1) if the water content of a wool sample near saturation is changed under adiabatic conditions by 1%, then the temperature of the sample will change by about 12°C (2) in a system initially containing water vapour at saturation

pressure at 20°C, if the temperature is increased by 1°C while the vapour pressure is maintained constant, then the relative pressure is reduced to 94% and the corresponding equilibrium water content of wool is reduced from 33% to about 26%. When keratin absorbs water vapour, the total quantity of heat liberated consists of the heat of condensation of the water vapour plus the heat of reaction of the water with keratin. The heat of reaction varies with the water content of the keratin. When the dry keratin is saturated (33%) from the liquid phase the heat evolved amounts to approx. 220 cal/gr of wool⁷², while the heat of absorption from the vapour phase is 660 cal/gr of wool. It appears thus that the heat effects are minimized, when the water is absorbed from the liquid phase, both because the heat evolution is considerably less and because of the higher heat capacity of the water.

A considerably higher rate of water absorption (e.g. in water) results in a considerably higher rate of swelling i.e. in a higher rate of extension due to swelling. In chapter 3 it was found that the rate of extension is responsible for significant structural changes in the fibre. This observation provides an explanation for the different behaviour of the dynamic mechanical properties of keratin during absorption from the liquid as against the vapour phase.

4.7 Conclusion

It has been observed that, when the relative humidity around a keratin fibre is increased abruptly by any given amount the loss angle goes through a maximum value with time, while the rate of change of the modulus shows a sharp discontinuity at the time of the maximum of the loss angle. These phenomena appear, when the fibre is held at a low fixed extension. They are also present

when the fibre is held at a higher fixed strain provided that the relative humidity increase is extremely fast and the temperature effects are eliminated; such is the case, for example, when the fibre is immersed into water. This characteristic change of the complex modulus with time has been interpreted to mean a general increase of mobility in keratin at the molecular level. This mobility must take place in both phases: the phase M must be at a maximum mobility, since it has to accommodate its marked swelling mainly in the lateral direction, the longitudinal swelling being inhibited by the C phase. The latter phase C also passes through a state of maximum mobility, since it undergoes a transient extension by the swelling forces of the M phase. Thus the transient increase of mobility of the structure of the whole fibre combined with the transient weakening of the C phase result in the maximum of the loss angle and the abrupt change of the rate of decrease of modulus with time.

When a keratin fibre at a fixed strain is dried from the wet state, the modulus increases to a value above that, which it would have, if the fibre were extended in the dry state to the particular fixed strain; the loss angle decreases correspondingly to the value, which the unextended dry fibre has. These observations have been suggested to mean that the dried fibre at the fixed strain has less α -helices opened out than it would have if the fibre was extended in the dry state from zero up to this particular strain. This particular effect arises from the steric hindrance to unfolding of α -helices when a fibre is extended in the dry state as against extension of the wet state. This hindrance means that to obtain the same strain level more α -helices have to be unfolded,

Finally, it has been found that, when a wet fibre is dried

and then rewetted, while it is held at a fixed strain, the fibre achieves, in the main, the same structural state as in the original strained wet case; the modulus, however is a little below and the loss angle a little above their corresponding values in the initial wet case.

CHAPTER 5

THE TIME-TEMPERATURE DEPENDENCE OF THE COMPLEX
MODULUS OF KERATIN FIBRES

5.1 Introduction

The complex modulus tester developed and described in Chapter 2 has been successfully used to study the dynamic modulus of keratin fibres versus frequency at various temperatures. Horse hair and Lincoln wool have been tested for various water contents.

5.2 The Modulus of Keratin Fibres as a Function of Time

Feughelman and Robinson⁵⁰ have found that wool fibres behave as linear viscoelastic materials at all water contents for extensions up to 1% in the Hookean region. On this basis they measured the stress relaxation at various humidities at an extension of 0.8% above the zero length of the fibre at the test humidity. Measurements at each humidity were carried out on four fibres for periods of up to 4 - 5 days. In their work they reported the stress decay, based on the wet cross-sectional area, as a function of log-time in minutes.

In the present work the above results were used to find the relaxation modulus as a function of time in seconds; correction factors for the variation of the cross-sectional area due to swelling at various humidities were taken from reference (96). Figure 5-1 shows the values of relaxation modulus calculated in this manner at relative humidities of 0%, 32%, 65%, 91% and 100% (wet), at 20°C. Each curve is the average for four fibres at each humidity. The rate of extension up to 0.8% strain was at 10% per min. An examination of the figure suggests that curves at all relative humidities may come together after a long period and may be asymptotic to a value of about 1.4×10^{10} dynes/cm².

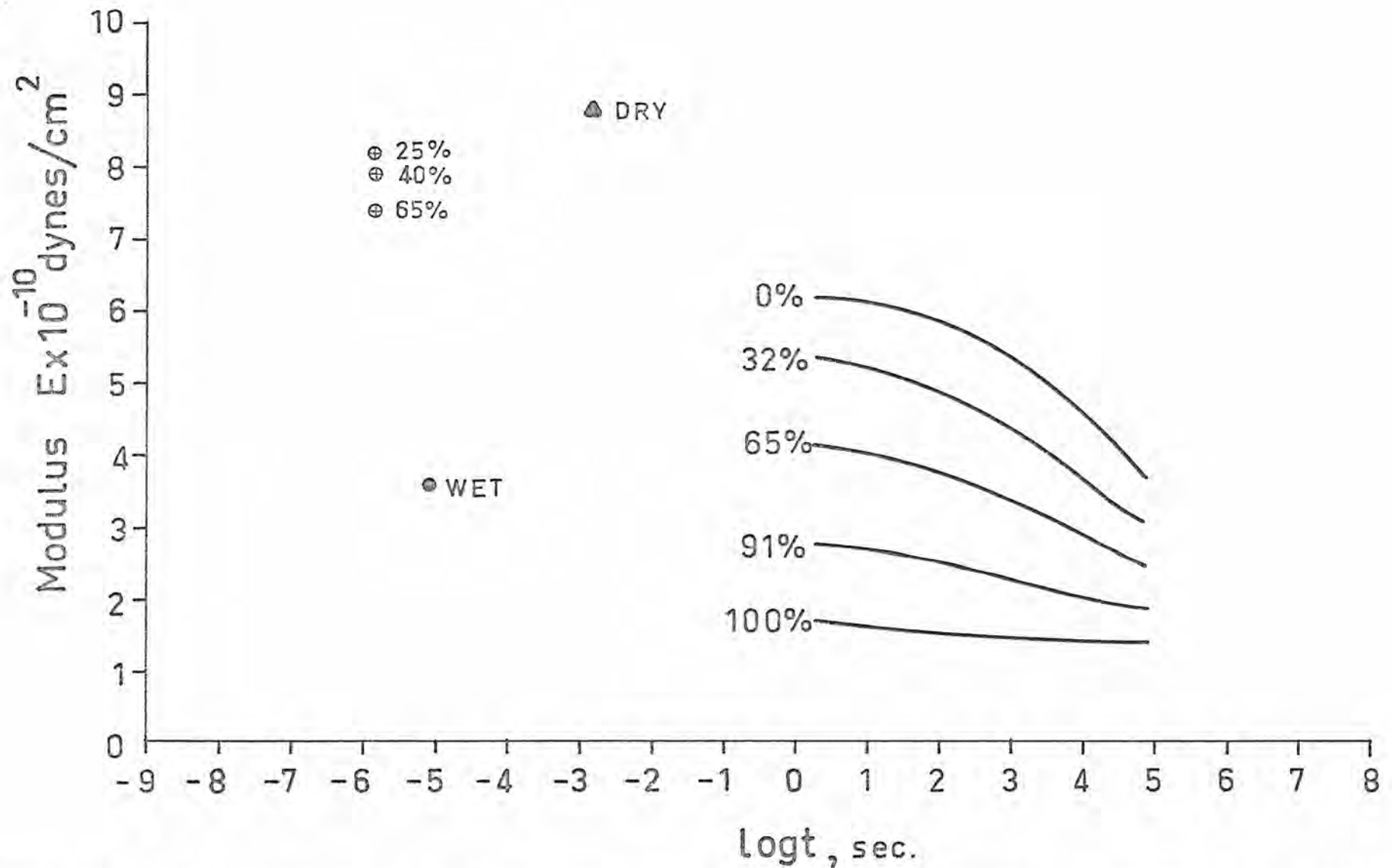


Fig. 5-1 Published results on the modulus of α -keratin plotted against log-time, t in seconds. \oplus by Chaikin, \bullet by Mason, \blacktriangle by Druhala, solid curves by Feughelman.

However, it was impractical to demonstrate this more clearly for long enough periods at 20°C. The time invariant component of modulus was attributed primarily to the microfibrils, while the relaxing component to the matrix, which can be plasticized by water. This proposition is further supported by recent measurements of modulus of rigidity by Stootman⁸⁷. It is evident that a major relaxation process occurs within the laboratory time scale and for this a pseudo-time constant τ was obtained by Feughelman and Robinson at each relative humidity corresponding to the time, at which the stress has fallen to a value half way from the initial value. However, it seems that at the higher relative humidities we are looking at the "tail" of the relaxation of modulus. This view is supported by measurements of dynamic modulus at very short times using different techniques.

Mason⁶⁸ obtained a value of 3.5×10^{10} dynes/cm² for the modulus of horse hair in water at 20 kHz using a wave propagation technique. He also measured the modulus of Lincoln wool at a strain rate of 0.001 sec⁻¹ and found it to be 1.8×10^{10} dynes/cm². Although this corresponds to an equivalent increase in time by a factor of over 10^7 , the two values of modulus differ only by a factor of 2. Chaikin and Chamberlain¹⁴ using a similar technique measured the modulus of human hair at 100 kHz for 25%, 40% and 65% R.H. and found that water had little effect on modulus. They reported values of (8.2 - 7.9 - 7.4) $\times 10^{10}$ dynes/cm² respectively.

In order to compare the dynamic measurements with those obtained by relaxation techniques the transformation of frequency to time was obtained using the method of Ninomiya and Ferry²⁷.

$$E(t) = E'(\omega) - 0.40E''(0.40\omega) + 0.014E''(10\omega) \Big|_{\omega = 1/t} \quad (5-1)$$

where $\omega = 2\pi f$ and f the applied frequency. In practice it was found that

$$E(t) \approx E'(\omega) \Big|_{\omega = 1/t} \quad (5-2)$$

Using 5-2 to relate dynamic and relaxation moduli Mason's result is shown in fig. 5-1 together with Chaikin's for three relative humidities. Comparing the two points it seems that there must be an unusual decrease of modulus at 100 kHz and 65% to the modulus at 20 kHz and 100% R.H., if we wanted to have a smooth increase of the wet modulus for shorter times. This observation remains to be explained. Makinson⁶⁵ reported a value of 1.01×10^{11} dynes/cm² for rams horn and 1.09×10^{11} for rhinoceros horn at 5 MHz in room conditions. However, these values refer to the dilatational modulus c_{11} , which is somewhat higher than the longitudinal dynamic modulus depending on the Poisson's ratio. Makinson reported that the dynamic modulus should be 17% less than the dilatational modulus of isotropic solids with Poisson's ratio 0.25. However, the lack of information on the dependence of the Poisson's ratio on the water content makes the estimation of the dynamic modulus from the dilatational modulus impossible. Druhała²³ found a value of 8.8×10^{10} dynes/cm² for dry horse hair, at 110 Hz. As can be seen there is a considerable gap of information for the modulus of keratin at short times. In this work it has been possible to look at relatively short times for modulus and an important gap of information to be filled and comparisons with existing data to be made.

5.3 Experimental Results

A horse hair fibre, medulla free, washed with petroleum ether was tested at frequencies between 6 and 1500 Hz in the temperature range 0.2°C - 45°C. The average diameter of the dry fibre measured at 10 different points was found to be 155 μm. Horse hair was chosen in this experiment, because it produces a high a-c output from the piezoelectric element, thus minimizing the effects of background noise.

TABLE 5-1

Ratios of the dry/wet a-c force for horse hair at constant a-c strain.

Temp. °C Frequency Hz	0.2°	5°	10°	15°	20°	25°	30°	35°	40°	45°
5	2.310	2.405	2.482	2.600	2.703	2.719	2.826	2.898	3.019	2.997
9	2.270	2.364	2.482	2.554	2.641	2.692	2.802	2.886	2.953	2.967
17	2.260	2.341	2.461	2.550	2.622	2.675	2.765	2.808	2.887	2.923
32	2.211	2.307	2.426	2.496	2.593	2.651	2.723	2.774	2.878	2.903
61	2.188	2.287	2.379	2.480	2.546	2.593	2.681	2.728	2.808	2.837
116	2.160	2.245	2.350	2.412	2.487	2.569	2.633	2.707	2.735	2.756
218	2.111	2.210	2.293	2.353	2.446	2.499	2.578	2.628	2.694	2.724
413	2.081	2.180	2.262	2.322	2.398	2.455	2.533	2.604	2.642	2.669
785	2.056	2.138	2.234	2.298	2.344	2.404	2.514	2.561	2.615	2.625
1480	2.045	2.131	2.198	2.297	2.340	2.384	2.483	2.503	2.566	2.574

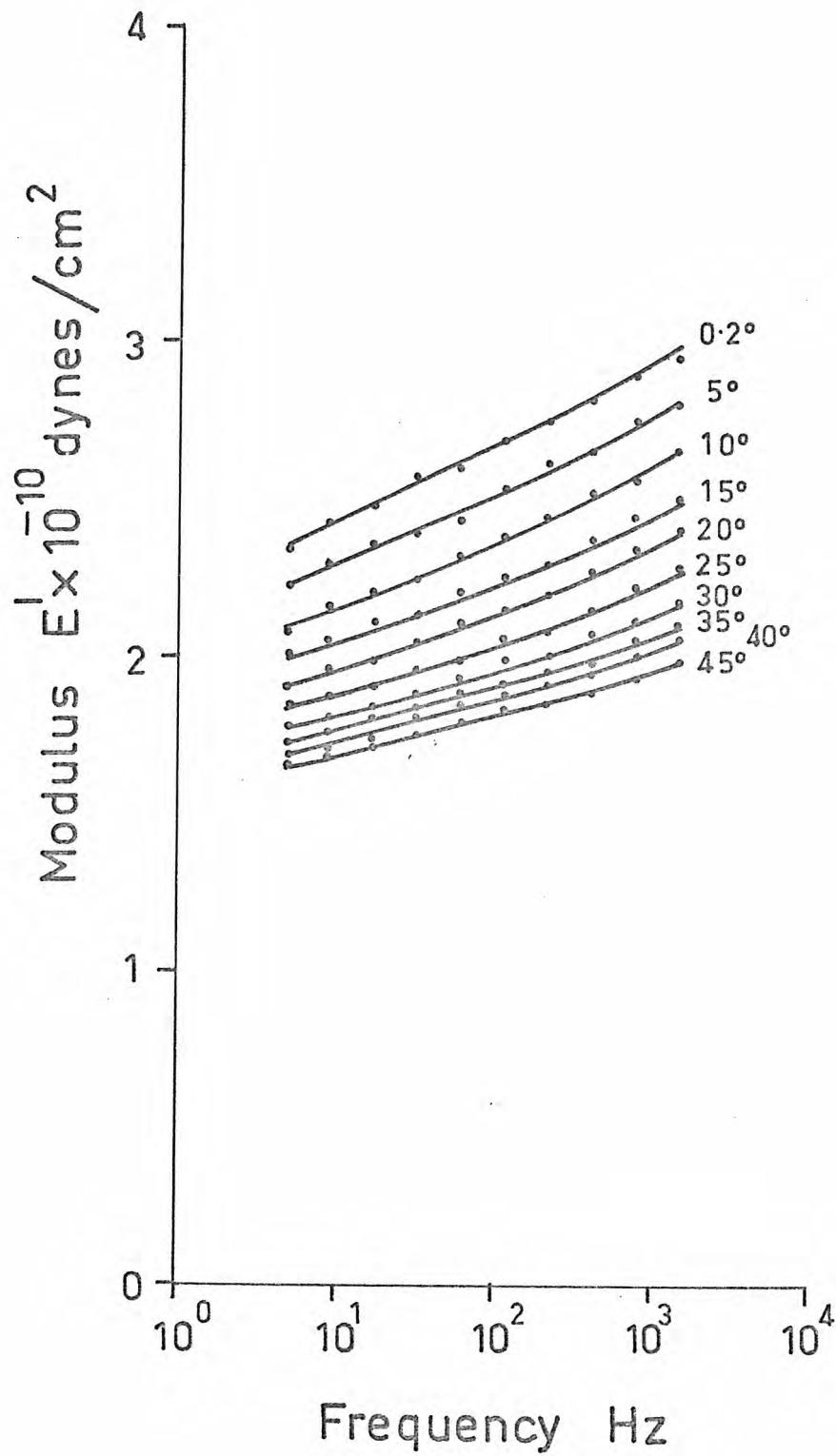


Fig. 5-2 The modulus E' of α -keratin plotted against frequency on a log-scale at different temperatures as shown with each curve.

The fibre was left in distilled water in the conditioning chamber overnight and then tested in water by scanning the frequency, while keeping the temperature constant. This was repeated for various temperatures starting from 45°C and decreasing the temperature by steps of 5°C. The lowest temperature achieved was 0.2°C, close to the freezing point of water. The use of water was the only way to ensure 100% R.H. around the sample. The use of saturated vapour was shown to be impractical, not giving reproducible results. The results for the dynamic modulus are presented in graphical form in fig. 5-2. Those for the loss angle are given as a "master curve" in the following section, because they are relatively too scattered to give a clear picture as for the modulus in fig. 5-2. The fibre was then dried in a dry atmosphere for 48 h and tested over the same frequency and temperature range. The results are given in table form (table 5-1) as ratios of the dry over the wet force amplitude at a fixed strain amplitude. The ratios to be ratios of moduli need to be corrected for cross-sectional area swelling, the correction factor being 1.352. The importance of these ratios resides in the fact that they are independent of the calibration of the apparatus and refer to the same fibre. The loss angle varies very little, indicating a slight increase towards higher frequencies and lower temperatures, but this being uncertain due to the considerable scatter of the experimental points.

Lastly, Lincoln wool fibres were tested for relative humidities of 0%, 32%, 65%, 91% and 100%, at a constant frequency of 116 Hz, at 20°C. The conditioning procedure was chosen in a way to be practical with the present experimental technique on the one hand and to be as close as possible with the one followed by Feughelman and Robinson on the other hand. That is, the fibres were left slack for 24 h at 100% R.H. and 20°C, then dried and finally brought up to the required

relative humidity. (Feughelman and Robinson were relaxing the fibres between tests by leaving them for 1 h at 52°C in water prior to conditioning at the required relative humidity; but it has been shown that the same effect is achieved if the fibres are left at 100% relative humidity at room temperature for 24 h⁸⁶). The reason for using a Lincoln fibre in this test was that it required considerably less time for conditioning, while the moduli for wet horse hair and Lincoln wool did not differ more than the experimental error of the apparatus. The results from this test are given in table 5-2.

TABLE 5-2

R.H. %	Ratios of a-c forces (dry/wet)	Correction factors for swelling	Corrected moduli $\times 10^{-10}$ dynes/cm ²	Loss Angle, Degrees
0	2.45	1.352	7.08	1.0
32	2.27	1.270	6.17	1.5
65	1.90	1.202	4.88	2.0
91	1.48	1.105	3.49	2.4
100	1.00	1.00	2.14	2.9

In the table are given the measured ratios of dry/wet a-c force, the correction factors used for swelling, the corrected moduli and the loss angle. The coverage of a wider range of humidities and temperatures is left for future work.

5.4 Analysis of the Results

From fig. 5-2 it can be seen that there is an overall change in the slope of the modulus-frequency curve as the temperature varies. At high temperatures the value of the slope is low, while around 5°C the slope has achieved its maximum value. This behaviour is as would be expected from a viscoelastic material, in which the processes are

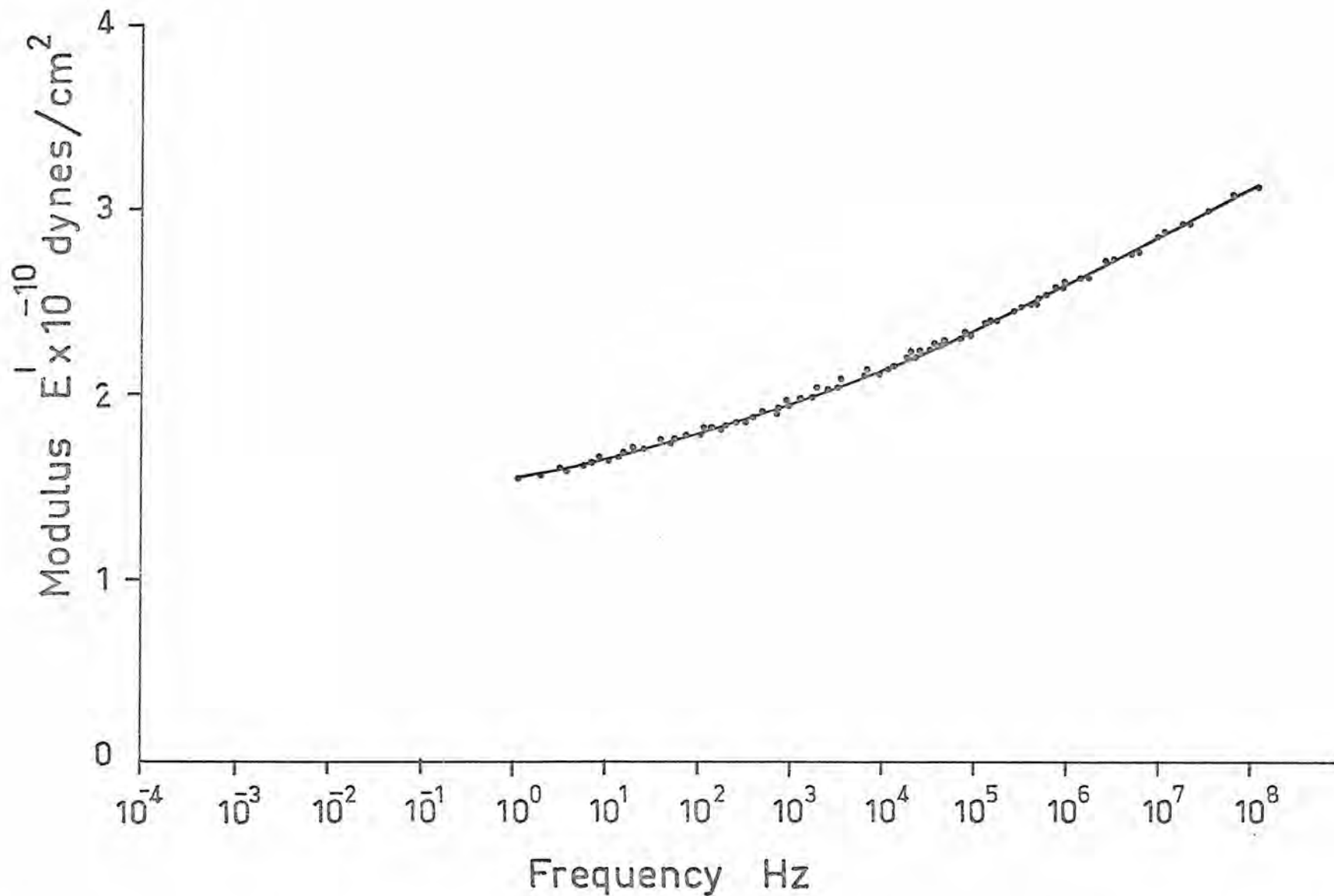


Fig. 5-3 The "master curve" for modulus obtained by plotting the data of fig. 5-2 with reduced variables, representing the behaviour of modulus of α -keratin over an extended frequency scale at 20 °C.

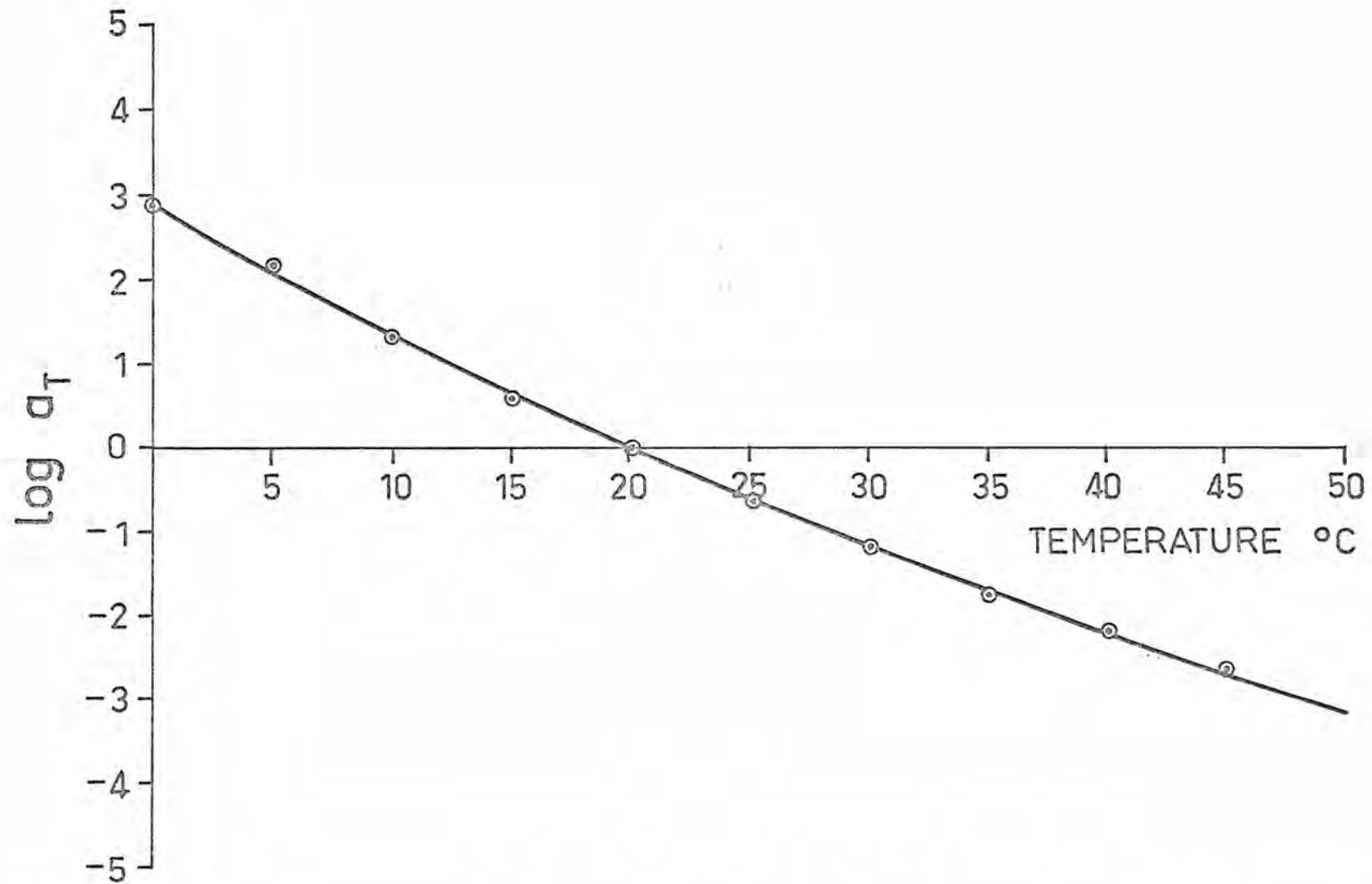


Fig. 5-4 Temperature dependence of the shift factor a_T used in plotting fig.5-3. Points chosen empirically; curve, from equation (5-4).

activation controlled (as described by Williams, Landel and Ferry²⁷). To analyse the results the assumption is made that the time-temperature equivalence of W.L.F. holds for this case. From this it follows that it is possible to produce a "master modulus curve" by choosing one particular temperature and applying a horizontal shift on a logarithmic time scale to make the modulus curves for other temperatures join as smoothly as possible onto the curve at this particular temperature; 20°C was chosen as the reference temperature here. The molecular theories of viscoelasticity suggest that there should be an additional small vertical shift factor $T_0\rho_0/T\rho$ in changing from the actual temperature T° K and density ρ to the reference temperature T_0° K and density ρ_0 . This is taken into account here; the correction factor can be expressed equivalently as

$$[1 + \beta(T - T_0)] \frac{T_0}{T} \quad (5-3)$$

where β is the coefficient of thermal expansion, which has been taken from Mason's work⁶⁷ to be equal to $5 \times 10^{-4} \text{ deg}^{-1}$. From the results in fig. 5-2 the modulus master curve obtained is shown in fig. 5-3. The shift factors $\log a_T$ are given in table (5-3) and plotted against temperature in fig. 5-4.

TABLE 5-3

T $^\circ\text{K}$	$T_0\rho_0/T\rho$	$\log d_T$	ΔH_a k cal
273.2	1.062	2.90	56.1
278	1.046	2.15	54.1
283	1.030	1.32	52.3
288	1.014	0.60	50.6
293	1.000	0.00	49.1
298	0.986	-0.63	47.7
303	0.972	-1.20	46.3
308	0.958	-1.76	45.1
313	0.945	-2.20	44.0
318	0.933	-2.65	42.9

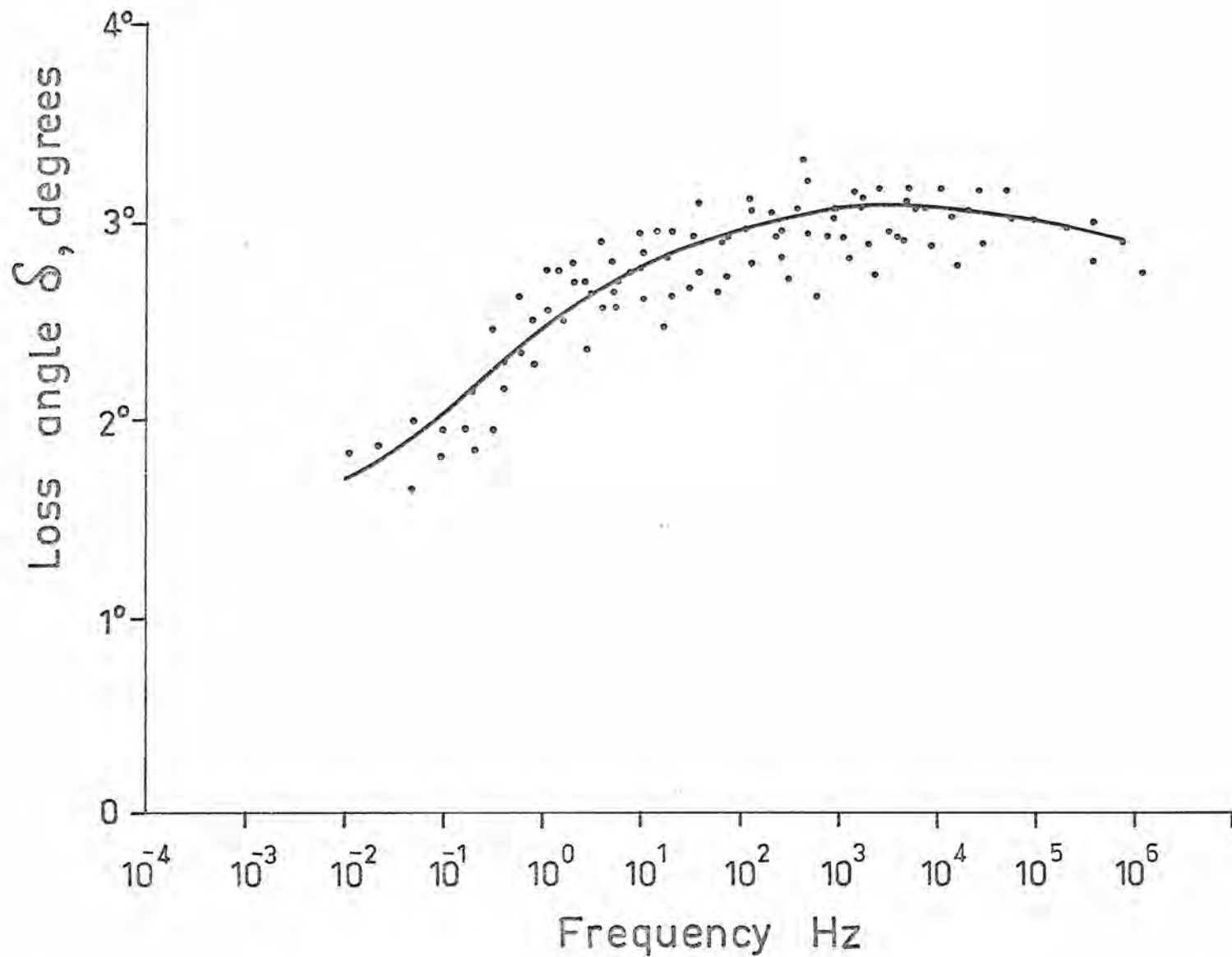


Fig. 5-5 The "master curve" for loss angle obtained by using the shift factors a_T in table 5-3, representing the behaviour of loss angle of α -keratin over an extended frequency range at 20 °C.

Thus starting from a complicated dependence of modulus on both temperature and frequency, these two variables have been separated to give a function of frequency alone and one of temperature alone. The choice of T_0 , the reference temperature, is of course arbitrary and a matter of convenience.

An important criterion of the applicability of the technique of forming the reduced curve is that the shapes of the original curves at different temperatures must match over a substantial range of frequencies. This appears to hold in the present case. One other general criterion is that the same values of a_T must superpose all the viscoelastic functions. Unfortunately, the measurement of the loss angle (which is a viscoelastic function) resulted in a considerable scatter of points, which did not allow a reliable independent estimation of the factors a_T . Because of this the assumption is made that the viscoelasticity of the keratin fibre complies with the W.L.F. theory and the shift factors obtained from the modulus measurements are used to construct the "master curve" for the loss angle. The result is presented in fig. 5-5.

One further criterion²⁷ for the viscoelastic behaviour of the fibre is that the temperature dependence of a_T must take a reasonable form consistent with experience. This criterion, the form of $\log a_T$ as a function of temperature, has been applied. The relation of $\log a_T$ to temperature is a smooth curve with no gross fluctuations or irregularities. The curve was fitted with the empirical values to an expression which has proved to be widely applicable for other polymers:

$$\log a_T = -c_1(T - T_0)/(c_2 + T - T_0) \quad (5-4)$$

For this purpose $(T - T_0)/\log a_T$ was plotted against $T - T_0$ and fitted with a "least-squares fit" straight line. From the slope s and the

intercept i of the line two empirical constants were calculated

$$c_1 = -1/s \quad (5-5)$$

$$c_2 = -i/s \quad (5-6)$$

Finally the function given by equation (5-4) was plotted with the calculated coefficients $c_1 = 19.5$ and $c_2 = 155.5$. This is shown with a solid line in fig. 5-4. The values for c_1 and c_2 compare well with those obtained for other polymers²⁷ indicating the reasonableness of the assumptions for the W.L.F. technique (e.g. 2-EthylHexyl with $c_1 = 20.2$ deg, $c_2 = 119.9$ deg and $T_0 = 284^{\circ}\text{K}$).

Equation (5-4) is one form of the W.L.F. equation, in which the reference temperature T_0 is often the glass transition temperature of the polymer.

The glass transition temperature is usually defined in terms of a kinetic process involving volume contraction at an arbitrary but convenient time interval. The volumetric transition reflects the temperature, below which the collapse of the free volume is very slow and the rates of relaxation processes, which are determined by the free volume, are also considerably reduced.

From fig. 5-5 it appears that there is a maximum of the loss angle δ at a frequency around 10 kHz at 20°C . To deduce a frequency dependent transition temperature corresponding to the loss maximum, one has to consider the loss modulus E'' , for which the maximum lies to the right of that of δ on the frequency scale. This difference on the frequency scale usually amounts to a few decades²⁷. From table 5-4, in which the values of E'' are given, it appears that the latter difference must be greater than three decades.

TABLE 5-4

log f in sec	E'x10 ⁻¹⁰ dynes/cm ²	δ degrees	E''x10 ⁻⁸ dynes/cm ²
-2.0	1.54	1.7	4.57
-1.5	1.60	1.83	5.11
-1.0	1.65	2.02	5.83
-0.5	1.72	2.25	6.76
-0.0	1.78	2.45	7.62
0.5	1.86	2.63	8.53
1.0	1.95	2.75	9.37
1.5	2.04	2.87	10.23
2.0	2.14	2.95	11.03
2.5	2.25	3.02	11.87
3.0	2.35	3.05	12.52
3.5	2.47	3.07	13.27
4.0	2.60	3.07	13.94
4.5	2.74	3.05	14.60
5.0	2.86	3.01	15.04
5.5	3.00	2.95	15.46
6.0	3.14	2.88	15.80

From the W.L.F. equation, an apparent activation energy for viscoelastic relaxation can be calculated formally as²⁷

$$\begin{aligned} \Delta H_a &= R \, d \ln a_T / d(1/T) \\ &= 2.303 R \, c_1 c_2 T^2 / (c_2 + T - T_0)^2 \end{aligned} \quad (5-7)$$

This quantity increases rapidly with decreasing temperature. The calculated energies are given as a last column in table (5-3) and their values compare well with those of typical polymers (see Ferry).

5.5 Comparison with Published Data

One aspect of the dynamic measuring technique has to be considered, before any comparison is attempted, in order to establish the thermodynamic conditions, under which an experiment is to be conducted. In particular, it must be clarified whether we have adiabatic or iso-

thermal conditions.

It has been found²⁷ that thermal equilibrium with the surrounding medium will not occur for frequencies that exceed the order of

$$f_1 = K/C_p \rho x^2 \quad (5-8)$$

where K is the thermal conductivity, C_p the heat capacity per gram at constant pressure, and x the thickness of the sample.

On the other hand, at very high frequencies the wavelength becomes so short that thermal conduction prevents development of temperature gradients within a cycle (along the direction of propagation of the wave) and the deformation is again isothermal. The critical frequency for the second case is

$$f_2 = E'C_p/6\pi K \quad (5-9)$$

Haly and Snaith⁵⁸ have reported values of specific heat for wet and dry keratin between (0.3 → 0.5) cal gr⁻¹ grad⁻¹ and from reference (96) we have for thermal conductivity $K = (4.6 \rightarrow 7) \times 10^{-4}$ cal cm⁻¹ sec⁻¹ grad⁻¹ and $\rho = (1.268 \rightarrow 1.304)$ gr/cm³. From equation (5-8) we have approximately

(i) for Lincoln wool with a diameter = 45 μ

$$f_1 = (54 \rightarrow 73) \text{ Hz}$$

(ii) for wet horse hair with diameter = 180 μ

$$f_1 = (3.4 \rightarrow 4.9) \text{ Hz}$$

From equation (5-9) we find that f_2 is of the order 10^{11} Hz. Obviously the only transition of interest in the present work is f_1 . We can conclude that for horse hair the measurement of modulus can be considered adiabatic in the frequency range used and similarly in the case for Lincoln wool at 116 Hz. However the relations (5-8) and (5-9) give only the orders of magnitude for the two characteristic frequencies, because the transition from isothermal to adiabatic con-

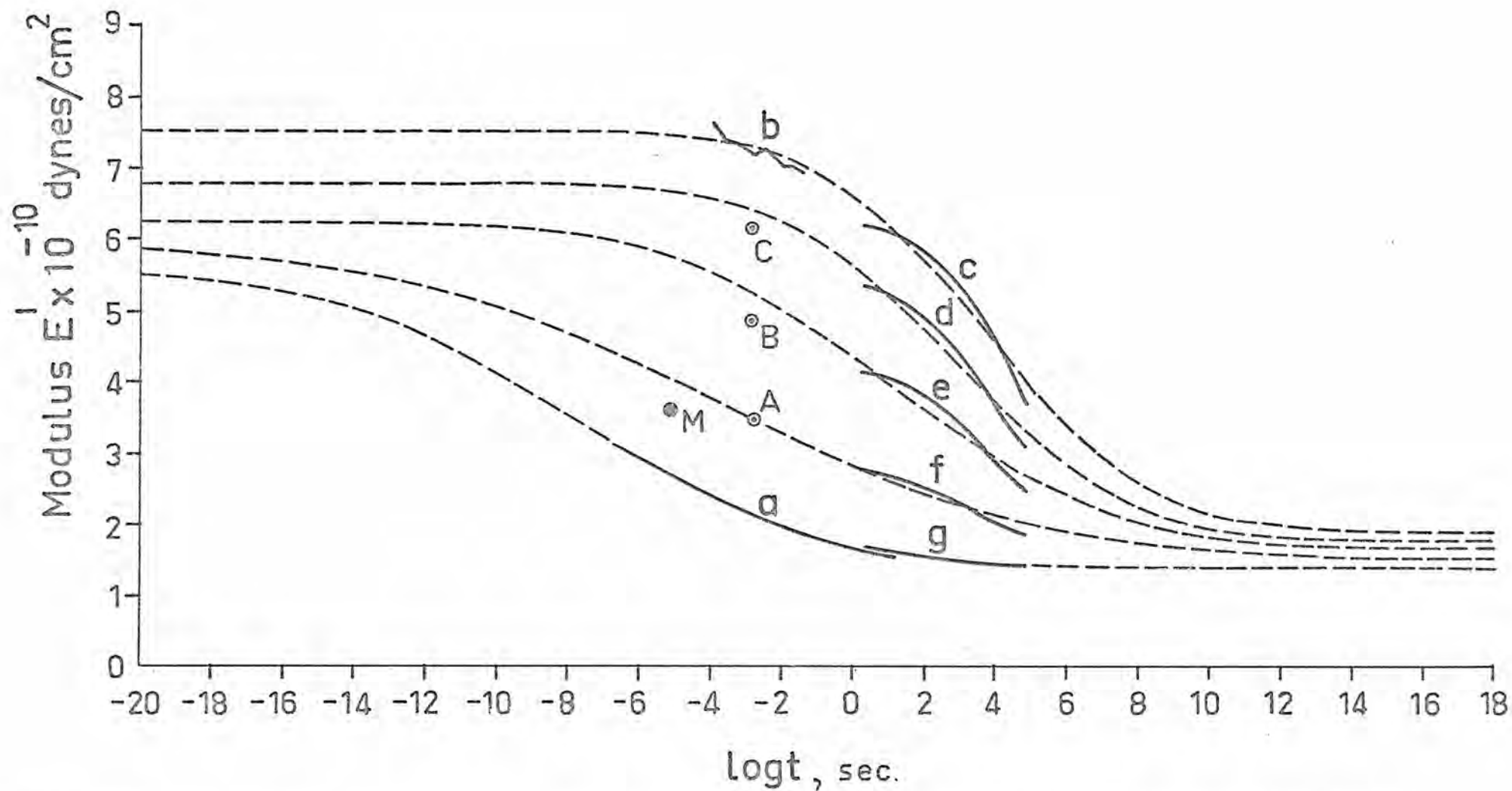


Fig. 5-6 The modulus E' vs time in sec on a log-scale: Solid curve (a) for wet keratin, solid curve (b) for dry and points A,B,C for intermediate relative humidities (see text) have been obtained in the present work. Solid curves (c),(d),(e),(g) and point M have been replotted from fig. 5-1. The broken curves are the theoretical fits.

ditions is gradual. Therefore it is possible that the experiments were conducted partly under isothermal conditions. The difference however between adiabatic E_{ad} and isothermal E_{is} moduli is in practice negligible. This can be shown to be the case by using the formula²⁷

$$E_{ad} = E_{is} + \left[\left(\frac{\partial E}{\partial T} \right)^2 \frac{T}{C_a \rho} \right] a^2 \quad (5-10)$$

where a is the strain, C_a the heat capacity per gram at constant strain. The above formula holds for the case in which the modulus E is directly proportional to T . Although this is only approximately true in our case, we can use it to show that the difference between adiabatic and isothermal moduli is very small. From Feughelman's work⁴⁸ the factor $\partial E/\partial T$ for a 10% per min strain rate is 1.1×10^8 dynes cm^{-2} grad^{-1} , or from the present work at 116 Hz is 1.9×10^8 dynes cm^{-2} grad^{-1} . Using the latter value and $a = 0.02\%$ we find the second term of equation (5-10) to be of the order 10^4 dynes/ cm^2 , which is really negligible relative to E_{is} .

Another point in the comparison of published data on keratin is that various authors have used different types of keratins as well as different techniques. The latter is more likely to give different results than the former. This however, still remains to be resolved.

We now proceed to compare the experimental data obtained for this thesis with the results of others. The curve of fig. 5-3, the modulus master curve for wet keratin, has been replotted on a log-time scale in fig. 5-6 as a solid curve (a). The moduli for intermediate regains are shown as points A, B, C taken from table 5-2. The modulus for the dry horse hair is shown as solid curve (b) for times corresponding to frequencies between 6 Hz and 1500 Hz only, at 20°C; the data have been taken from table 5-1. The conversion of frequency to time was made by using the relation (5-2). The results by Feughelman and Robinson have been plotted in the same fig. 5-6 as solid curves (c),

(d), (e), (f), (g) for 0%, 32%, 65%, 91% and 100% R.H.; Mason's point (M) for wet keratin is also shown.

The curve (a) matches curve (g) very well; it does not, however, agree too well with Mason's point. Mason's results, however, over seven decades of time show a similar change of modulus to that obtained in this work. Only the absolute value of modulus differs. The curve (b), lastly, for the dry fibre does not seem to match the corresponding curve (c) too well.

To better understand the above observations a closer look at the role of water in keratin must be made.

Water in keratin can be considered as a plasticizer which associates with the polymer. The effect of plasticizers generally is to lower the temperature of the glass transition by making it easier for changes in molecular conformation to occur. Plasticizers make the loss peak broader and this broadening depends on the nature of the interaction between the polymer and the plasticizer. Thus, because of the strong interaction between water and keratin, a very broad loss peak is expected to be observed. It is found that this is the case as shown in fig. 5-5.

In the case of an ideal plasticizer in a polymer the initial (unrelaxed) modulus for very short times and the final (relaxed) modulus for very long times are independent of the plasticizer content provided the plasticizer does not swell the polymer. The question now arises whether this is applicable with the keratin-water system. From existing data (Druhala²³) it is expected that the relaxation of the water itself would show up as well the relaxation of other small units of the main chain. Thus a considerable portion of the relaxation spectrum of times for the main chain must overlap with the relaxation spectrum of smaller units and that of the water. Druhala found that the water loss maximum occurs for 18% regain in the fibre at -95°C and

at 110 Hz, and is much less well defined than for the lower water contents. This is because of a transition at a higher temperature occurring in the vicinity of 0°C. This transition probably arises from the motion of bulky side chains. Drahula also found that the modulus of the keratin water system for temperatures below the transition temperature for the water loss is higher at higher water contents, because of the contribution to the modulus of the water per se. This could partly explain the very high modulus reported by Makinson and Chaikin, since their results were at very high frequencies.

5.6 Theoretical Fit

In the following an attempt is made to fit the results obtained by the author along with the ones of Feughelman and Robinson by use of a relaxation function derived from a log-normal distribution of relaxation times " τ ". The same function was used successfully by Stootman⁸⁷ to fit his data on the modulus of rigidity. The distribution function is given by

$$F(\tau) d\tau = \frac{1}{\beta\sqrt{2\pi}} \exp \left[-\frac{(\ln\tau - \alpha)^2}{2\beta^2} \right] d\ln\tau \quad (5-11)$$

which satisfies the condition

$$\int_0^{\infty} F(\tau) d\tau = 1$$

where α is the mean $\langle \ln\tau \rangle$ and β is the width of the distribution. Gross⁵⁴ gives the normalized relaxation function $\psi(t)$ as

$$\psi(t) = \int_{-\infty}^{\infty} F(\tau) \exp(-t/\tau) d\tau \quad (5-12)$$

By applying the transformation

$$\frac{(\ln\tau - \alpha)^2}{2\beta^2} = u^2$$

and combining equations (5-11) and (5-12) we obtain

$$\psi(t) = \frac{1}{\sqrt{\pi}} \int_{-\infty}^{\infty} \exp \left[-u^2 - t \exp \{ -u\beta/2 + \alpha \} \right] du \quad (5-13)$$

If E_i is the initial (unrelaxed) modulus and E_f is the final (relaxed) modulus, then the modulus $E(t)$ as a function of time is given as follows

$$E(t) = (E_f - E_i) \psi(t) + E_f \quad (5-14)$$

Equation (5-14) can be made to fit the experimental data and depends on four parameters, i.e. E_i , E_f , α and β . The parameters E_i and E_f were fixed and the α and β were calculated via a computer program (used by Stootman⁸⁷) for the best fit using the method of "least squares". The parameter E_f was taken to be equal to 1.4×10^{10} dynes/cm² for the case of 100% R.H., while for the other relative humidities the above value was multiplied by the correction factors of table 3-2 to allow for diametral swelling. The parameter E_i was fixed as follows. Initially, the program was run for only one fixed parameter i.e. $E_f = 1.9 \times 10^{10}$ dynes/cm² corresponding to the relaxed modulus for dry keratin and the initial dry modulus E_i was predicted to be equal to 7.5×10^{10} dynes/cm². This value was taken as the value to which all the moduli would converge for very short times regardless of the water content; but to allow again for diametral swelling the above value was divided by the correction factors of table 3-2, in order to fix the initial modulus for the program at the corresponding relative humidities. The fixed pairs of E_i and E_f for the different relative humidities are given in table 5-5. In the same table the calculated parameters α and β for the distribution function are given. These values for α and β apply for the variable $\ln \tau$ and, since the results of other workers are usually plotted against $\log_{10} \tau$, an additional two columns are given in the table, where the values of α and β have been converted to this variable.

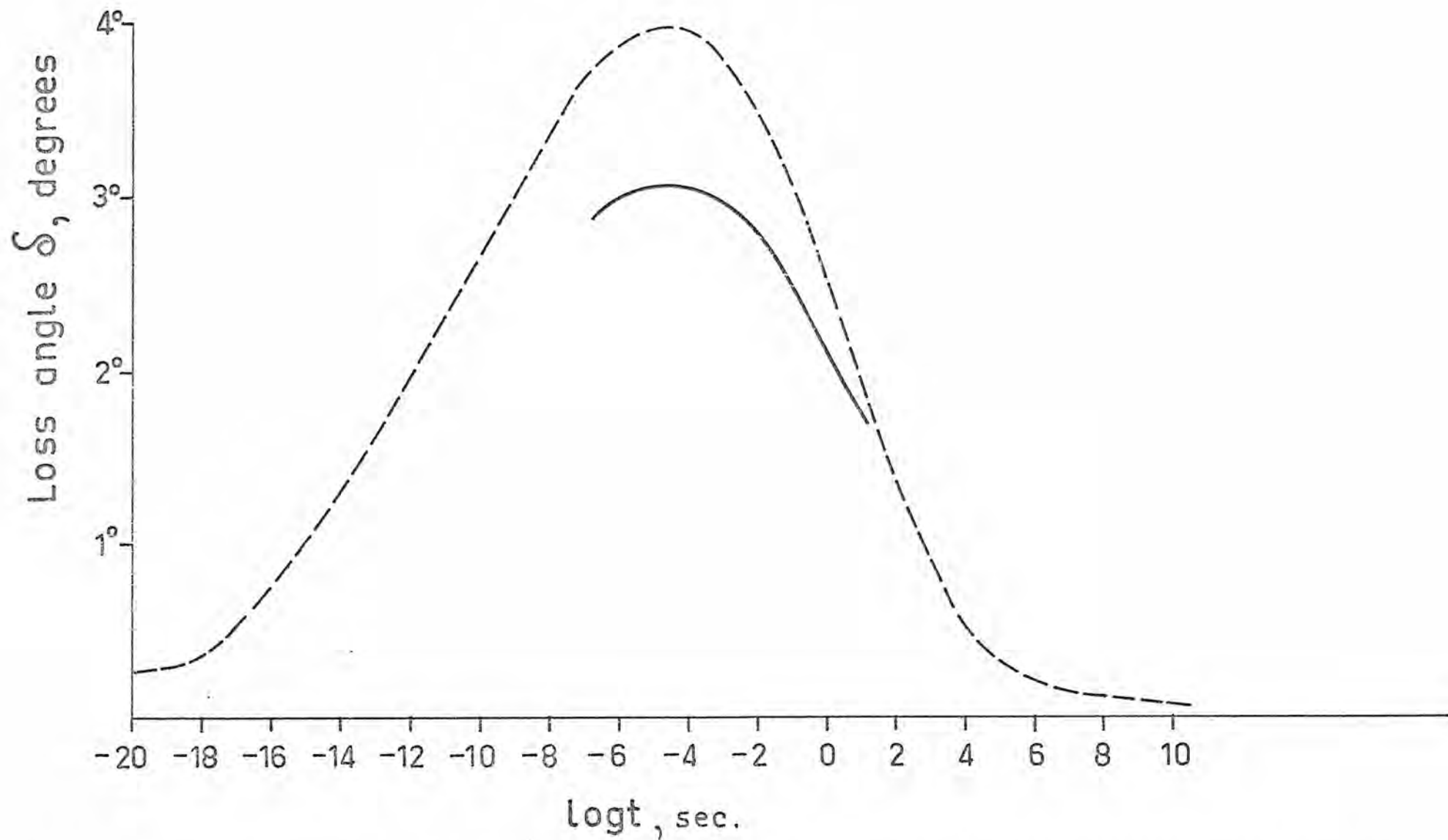


Fig. 5-7 The loss angle vs time in sec on a log-scale for wet α -keratin obtained experimentally (solid curve) and predicted from the theoretical fit for the wet case in fig 5-6 (broken line).

TABLE 5-5

R.H.(%)	$E_i \times 10^{-10}$ dynes/cm ²	$E_f \times 10^{-10}$ dynes/cm ²	α	β	$\alpha/2.303$	$\beta/2.303$
0	7.50	1.90	9.18	8.54	3.99	3.71
32	6.79	1.78	7.23	8.90	3.14	3.86
65	6.24	1.68	3.06	11.51	1.33	5.00
91	5.91	1.55	-8.37	16.37	-3.63	7.11
100	5.55	1.40	-17.36	12.19	-7.54	5.29

5.7 The Loss Angle

It is possible to calculate the loss angle from the theoretical fits in fig. 5-6 by using the formula⁹⁸

$$\tan \delta = -\frac{\pi}{2} \frac{d \ln E'}{d \ln \tau} \quad (5-11)$$

In this work the loss angle has been calculated from the curve corresponding to 100% only in order to compare it with the experimentally obtained loss angle as shown in fig. 5-5. Thus in fig. 5-7 the experimentally obtained loss angle has been replotted as a solid curve together with the calculated loss angle (broken curve) using eq. (5-11).

5.8 Discussion

When a polymer is subjected to an oscillatory strain at a particular frequency and temperature, the material absorbs a certain amount of energy per cycle per unit volume. This energy is absorbed by specific structural units of which the time of response is equivalent to the applied frequency. McCall¹⁰⁵ has classified the various relaxation processes or absorption bands as follows:

- (i) Primary main chain motion in crystals.
- (ii) Primary main chain motion in amorphous materials.
- (iii) Secondary main chain motion in crystals.
- (iv) Secondary main chain motion in amorphous materials.

- (v) Side group motions.
- (vi) Impurity motions.

The results in fig. 5-6 are indicative of a major relaxation process occurring in the keratin structure. This process is characterized by a mean relaxation time varying by more than 11 decades, when the atmosphere surrounding the keratin is varied between dry and wet conditions. The width of the distribution function of the relaxation times is large and varies considerably with relative humidity. The figures for α and β given in table 5-5, however, must not be considered as the final and accurate characteristic constants for keratin, but because of the following, only a reasonable approximation :

The theoretical fit is satisfactory but not excellent, because the experimental data have been obtained using different techniques, for different fibres under non-identical conditions. The application, for example, of a step function of strain is not identical as the application of a sinusoidal strain. Besides, the application of a step function of strain in practice is inevitably accompanied by an error in the definition of zero time. Furthermore the initial structural condition of keratin, when starting an experiment, has not been identical in all cases and this is of great importance when testing keratin. The dry or near dry fibre, for example, may not be in an internal stress-free condition, or in other words the fibre may be at a different state of "ageing" prior to a test. The results by Feughelman and Robinson, thus, were obtained after 17 hours of equilibration following drying from the water saturated state, while relaxation effects still occur after 10^9 seconds, i.e. after 32 years, in the dry fibre. In addition to these observations it must be clarified that the theoretical fits in fig. 5-6 for very short times are meaningless: by the time the visible region is reached (very high frequencies) all molecular absorption bands are past and any energy

absorption arises simply from electronic polarization. Furthermore in the short time range, where molecular absorption is possible, the fits should not vary as smoothly as predicted, because of special absorption bands due to small side chain units or the reorientation of the water molecules themselves (see Druhala²⁴).

The fits for times greater than approximately 10^{-7} sec are believed to represent reality closely. They appear to have the characteristics describing a typical viscoelastic material. This is further supported by the close agreement of the two curves for loss angle in fig. 5-7. For viscoelastic materials if one viscoelastic function is known all the others can be calculated⁵⁴ from the known one. The relaxation process indicated by the abrupt change of slope of the curves in fig. 5-6 is thought to arise from the primary main chain motion in the M phase for the following reasons. In general, the longer and more ordered the structural units are, the larger will be their relaxation times, therefore the large relaxation times for low relative humidities must be characteristic of macromolecules. These relaxation times for the macromolecules change markedly because of the action of water. The modulus relaxes with time to an equilibrium level of 1.4×10^{10} dynes/cm² which does not change at ambient conditions in the laboratory time scale. The latter equilibrium value of modulus has been attributed mainly to the C phase. Algie found (private communication) that the relaxation in the C phase (which he terms α - process) for wool fibres in water at 20°C has a relaxation time of 100 hrs at 100°C. From this fact he calculated a relaxation time of 10^{10} years at 20°C using an activation enthalpy of 77 Kcal/g-mole. Therefore if the main chain relaxation does not occur in the C phase in the laboratory time scale, the main chain motion, to which the results of fig. 5-6 have been attributed, must occur in the M phase.

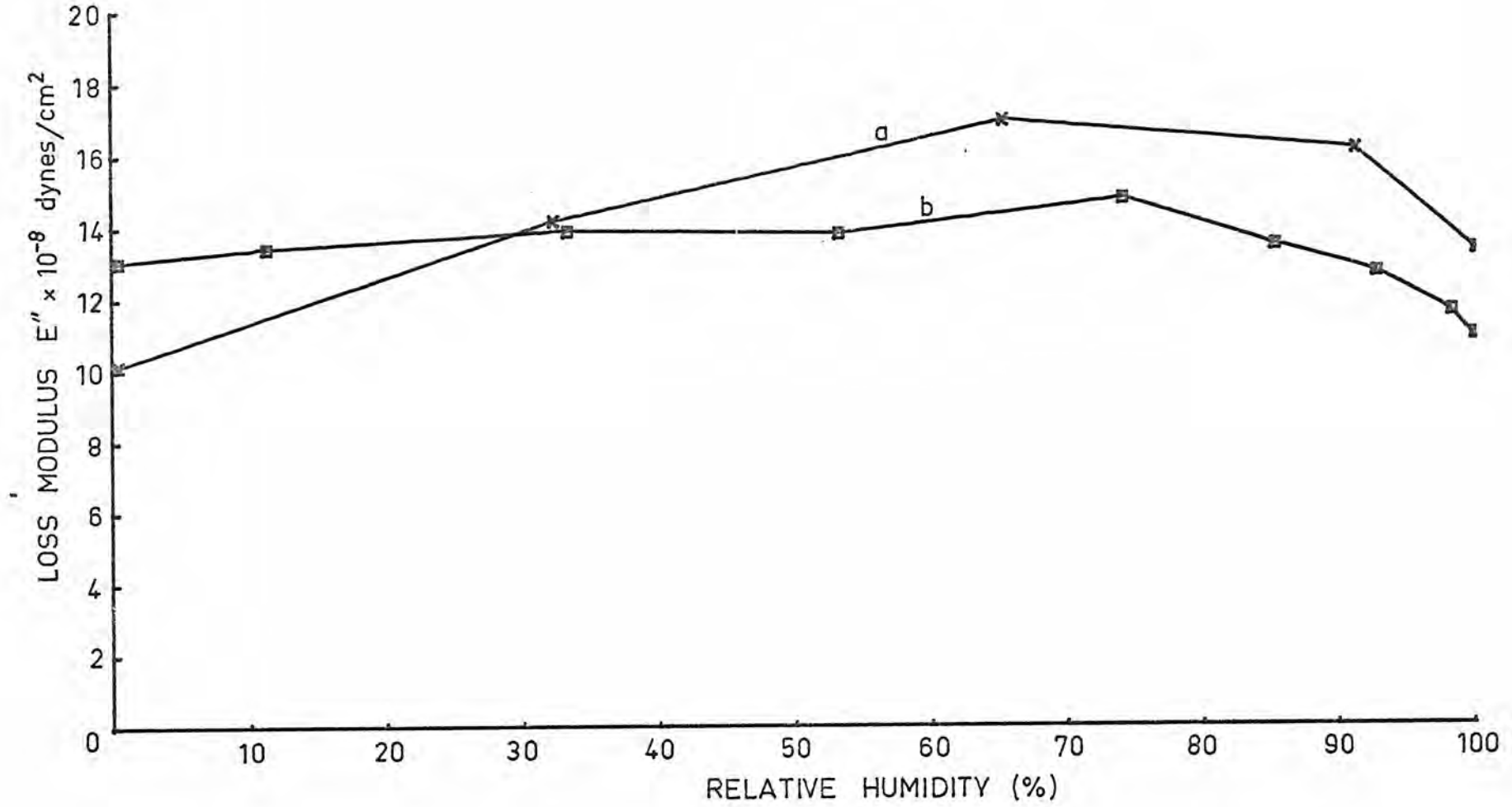


Fig. 5-8 The loss modulus E'' against relative humidity in % for keratin at 116 Hz and 20 °C. Curve (a) predicted from the theoretical fits in fig. 5-6; curve (b) plotted from experimental data in table 3-1.

The marked effect of the water being absorbed in the M phase is further corroborative evidence of the above suggestion.

To close this section some more observations are made. In table 3-1 of chapter 3 the loss modulus E'' is presented as a function of relative humidity. From this it is observed that the loss modulus has a maximum value around 80% R.H. From table 5-5 it is observed that the parameter β has also a maximum value around 80% R.H. (if plotted). Numerous workers have also observed a marked change of many mechanical properties of keratin around 80% R.H. (e.g. regain vs R.H.). Therefore there might be a correlation between E'' and β . This, however, is not necessarily the case, since E'' is essentially a function of time and as such, if E'' is plotted against relative humidity, the plot will vary with the time at which E'' is measured. The loss modulus E'' can be derived from the modulus E' (see fits in fig. 5-6) at a fixed time for different relative humidities using the relationship (5-11). Curve (a) in fig. 5-8 is the loss modulus against relative humidity for $\tau = 10^{-2.8}$ sec (i.e. $f = 116$ Hz) derived from the fits in fig. 5-6. Curve (b) in the same figure is the loss modulus against relative humidity taken from table 3-1. The two curves having been constructed quite independently, compare with each other satisfactorily. This is another indication that the theoretical fits for the modulus are close to reality.

Lastly, the comment is made that Sikorski and Woods⁸³ have reported that the Young's modulus varies linearly with $\log(\text{rate of straining})$. From fig. 5-6 it is observed that these findings hold for a few decades of time only and not over the complete time range, in which the modulus curve has a sigmoidal shape.

5.9 Conclusion

A relaxation process with a very broad spectrum of relaxation

times has been found for wet keratin. The modulus and loss angle have been measured experimentally in the time range between $10^{-6.8}$ and $10^{1.2}$ seconds by varying the frequency from 6 to 1500 Hz and the temperature from 0° to 45°C and employing the W.L.F. principle. The experimentally covered times consist only part of the whole spectrum of times of the relaxation process. For this reason the present results have been combined with results of others and all these have been fitted with a theoretical function of modulus. Some measurements of complex modulus have been performed at different relative humidities and a theoretical modulus as a function of time has been derived in the same way. The relaxation process established depends markedly on the relative humidity. With increase of relative humidity the relaxation times decrease by more than 11 decades and the width of the distribution function of the relaxation times varies considerably. This process was attributed to the M phase.

The results of this chapter further confirm that keratin at very low extensions ($< 1\%$) behaves as a viscoelastic material.

C H A P T E R 6

CONCLUSION

6.1 Summary

In this thesis the studies have been chiefly concerned with the dynamic mechanical properties of single keratin fibres. A substantial part of this research was involved with the design and construction of a dynamic mechanical tester for the measurement of complex modulus of fibrous samples.

The complex modulus of keratin fibres has been measured under varying extension, relative humidity, temperature, frequency and time.

The experimental results thus obtained were explained in terms of the keratin structure, enabling a clearer understanding of the general behaviour and properties of this biopolymer.

6.2 The Experimental Technique

A dynamic mechanical tester for the measurement of the dynamic modulus and the loss angle of fibrous samples has been developed. The technique is based on the application of forced vibrations. The main problem was the measurement of the a-c stress at high frequencies, the highest frequency used successfully being 1500 Hz and achieved by the use of a p-z element as a force measuring device. The lowest frequency used was 6 Hz and was limited by the electronic equipment available. The tester comprised a device for the conditioning of the sample at a specified relative humidity and temperature as well as an extensometer for the application of varying strains.

6.3 The Keratin as a Viscoelastic Material

The keratin consists of two phases; the phase C which is relatively water impenetrable and phase M which is relatively water penetrable and swells with water content. The experimental results on the complex modulus with varying temperature and frequency combined with experimental results of other workers point to the fact that the phase M may be characterized by a viscoelastic rate process associated with the main chain motion. This process has a very broad spectrum of relaxation times and depends strongly on the water content. The combined results at different relative humidities have been fitted by a theoretical function of modulus against time based on a log-normal distribution function of relaxation times. The width parameter of the latter function varies between 3 to 7 decades of time, while its mean varies by more than 11 decades of time. This marked change of the relaxation times is caused by the plasticizing effect of water in phase M. In the laboratory time scale the invariant component of the modulus of the total fibre in ambient conditions has been attributed to the phase C and has a value of 1.4×10^{10} dynes/cm². The value of the unrelaxed modulus for a dry keratin fibre may be more than 7.5×10^{10} dynes/cm².

6.4 The Keratin Under Extension

The complex modulus of keratin fibres has been examined with varying strain and rate of strain and the results obtained were explained by applying the two phase concept. The modulus of the fibre decreases with extension up to approximately 20% strain and then increases again. The loss angle follows changes inversely to the modulus. These changes for the modulus and loss angle become more pronounced with increase of strain rate. To explain these results it was assumed that the phase C

remains essentially elastic at all strains, while the phase M undergoes a gel-sol transformation within the first few percent strain and remains in the sol state at all subsequent strains. The sol-gel transformation is characterized by a mean relaxation time of the order of 10 sec and is practically invariant with strain. The extension cycling experiments revealed that during retraction the phase M again undergoes a gel-sol transformation while an extra portion of the C phase becomes disoriented and distorted resulting in a further weakening of the overall structure. The change of the complex modulus with time at a fixed strain, relative humidity, temperature and frequency has also been examined. This showed that the assumptions made about the two phase model are a good approximation at least in the time scale used for the experiments in the present work.

6.5 Transient Phenomena in Keratin

The complex modulus of keratin fibres with time has been measured after effecting an abrupt change of relative humidity at a fixed strain, temperature and frequency. These measurements showed that the loss angle exhibits an overshoot while at the same time the modulus has a marked discontinuity in its rate of change. These phenomena were related with structural changes occurring in the keratin fibre. These changes occur mainly in two stages. During the first stage the changes are caused by the swelling action of the water; this stage practically ends when the water content has approached its final value. During the second stage a rearrangement of the molecular structure takes place as a result of the changes brought about during the first stage; namely, the swelling of the phase M causes a transient extension of the phase C and a concomitant transient weakening of this phase. At the time of the loss angle overshoot the whole fibre

structure is in a state of maximum mobility. The interaction of the two phases can give a satisfactory explanation of the experimental results obtained.

6.6 Future Work

The conclusions about the keratin structure arrived at in the present work could be further studied with the use of the experimental technique developed in this work. The studies presented in this thesis of the measurement of complex modulus of keratin fibres especially during continuous extension and sorption, represent a pioneer piece of work and a large body of work remains to be done in this field.

In general, much of what has been carried out by numerous workers in the study of the properties of keratin fibres under different conditions can be repeated with the simultaneous measurement of the complex modulus.

In particular, to further elucidate the two phase structure of keratin, the fibres can be tested after having undergone special chemical or other treatment, which affect selectively one or other phase, or bring about a known or hypothetical change in the keratin structure. The use of alcohols, varying pH, or setting treatments are only a few examples. Such experiments are likely to reveal still unknown features of the keratin structure or to confirm or reject certain views about keratin.

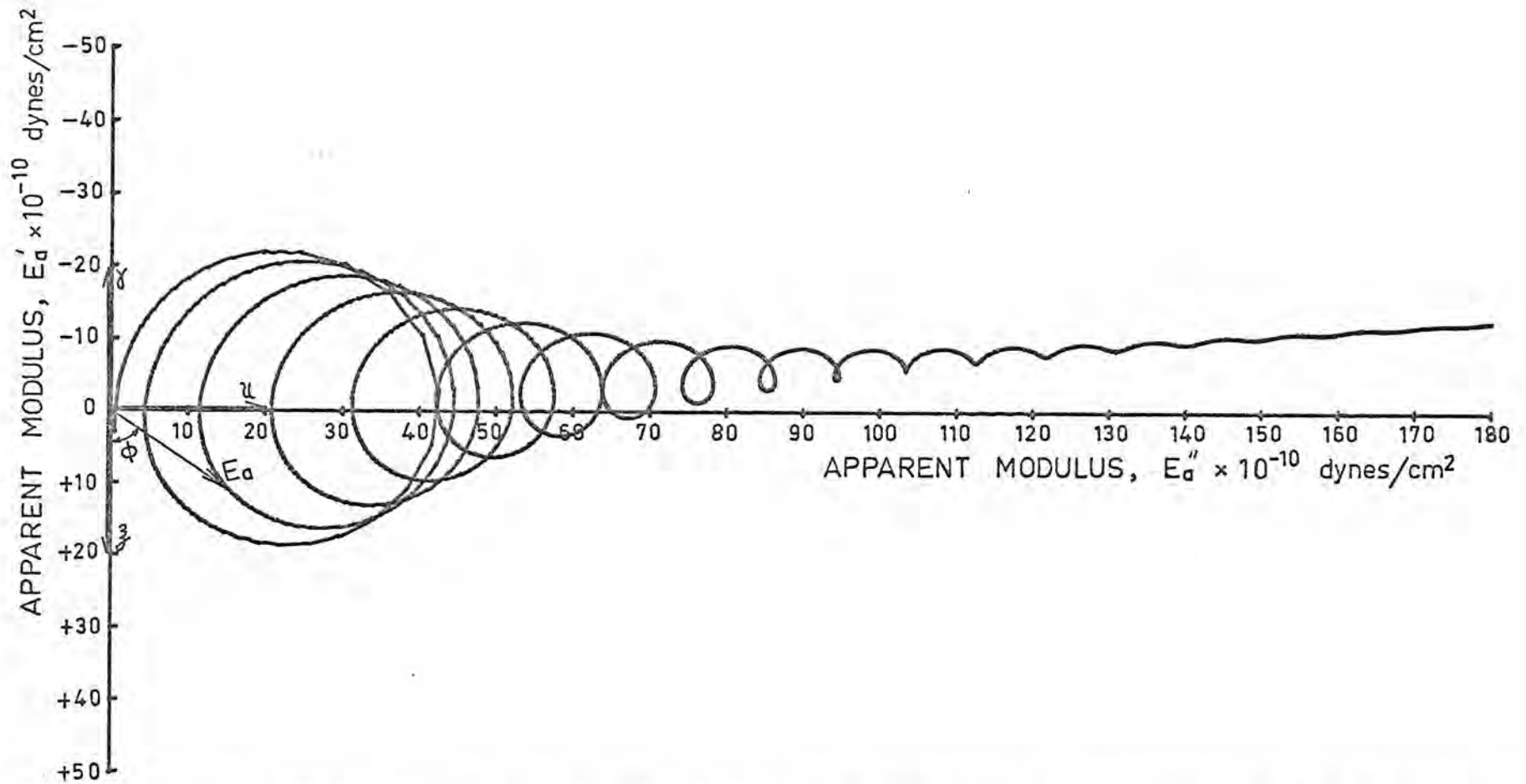


Fig. A-1 The vector diagram for the displacement ξ , velocity u , acceleration γ and apparent modulus E_a at a particular frequency. When the frequency varies, the end of the vector E_a traces the spiral locus shown. The components of E_a in phase and in quadrature with the displacement can be measured on the vertical and horizontal axes respectively.

APPENDIX A

The Apparent Modulus

In chapter 2 the magnitude $|\frac{\sigma^*}{\xi^*}|$ of stress per unit displacement and the angle ϕ between the stress and displacement are calculated. The vector diagram for the displacement ξ , the velocity u and acceleration γ is shown in fig. A-1. The vector for stress per unit strain $E_a = |\frac{\rho \sigma^*}{\xi^*}|$, corresponding to a particular frequency, with its angle ϕ is also shown in the diagram. If the frequency varies from 0 Hz up to 150 kHz the end of the vector E_a will trace the locus given in the diagram. The locus is drawn for $c = 1500$ m/sec, $\delta = 8^\circ$, $l = 10$ cm and $\rho = 1.3$ gr/cm³; the two components $E_a \cos\phi$ and $E_a \sin\phi$ of the quantity E_a are measured in dynes/cm². The quantity E_a is an apparent modulus, which for sufficiently low frequencies (see relationship (2-18)) is

$$E_a = E \sqrt{1 + D^2} \approx E \text{ for small } \delta$$

$$\text{where } D = \frac{1}{2} \tan\delta \text{ and } E = \rho c^2$$

while for very high frequencies:

$$\lim_{f \rightarrow \infty} E_a = \omega l \rho c \sqrt{1 + D^2}$$

The apparent modulus, therefore, equals the actual modulus of the material for sufficiently low frequencies.

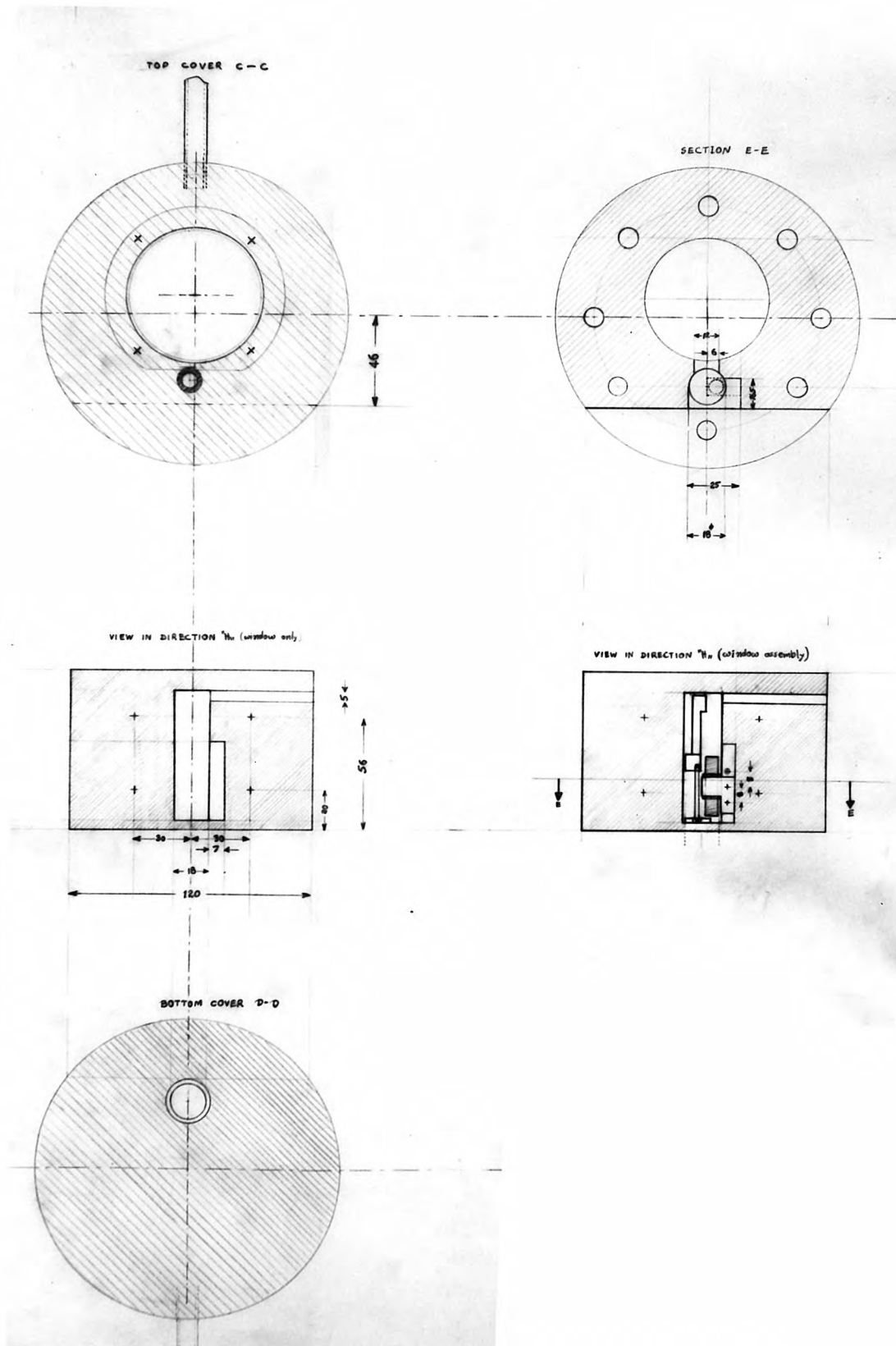


Fig. B-1b Drawings of the conditioning chamber.

BRASS EXTENSION ROD

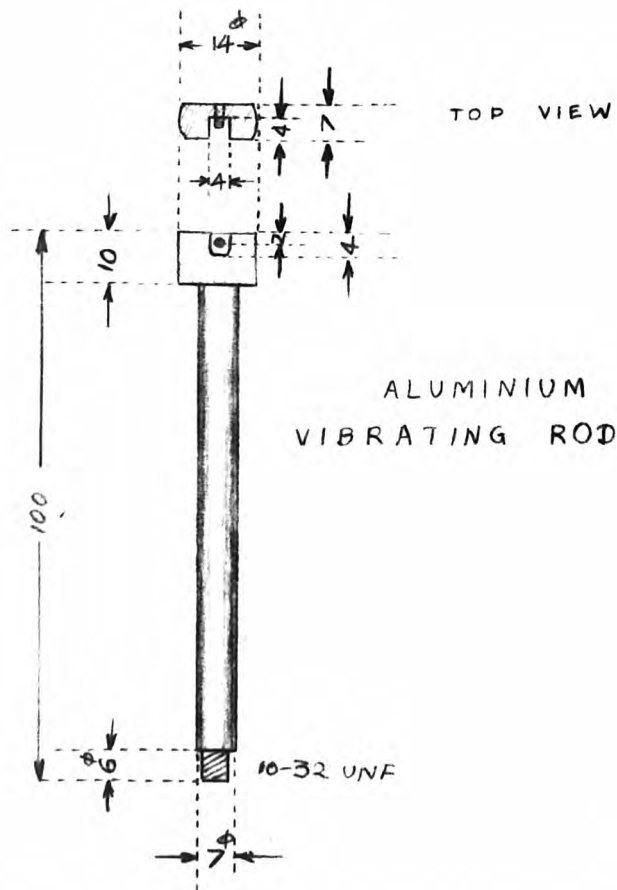
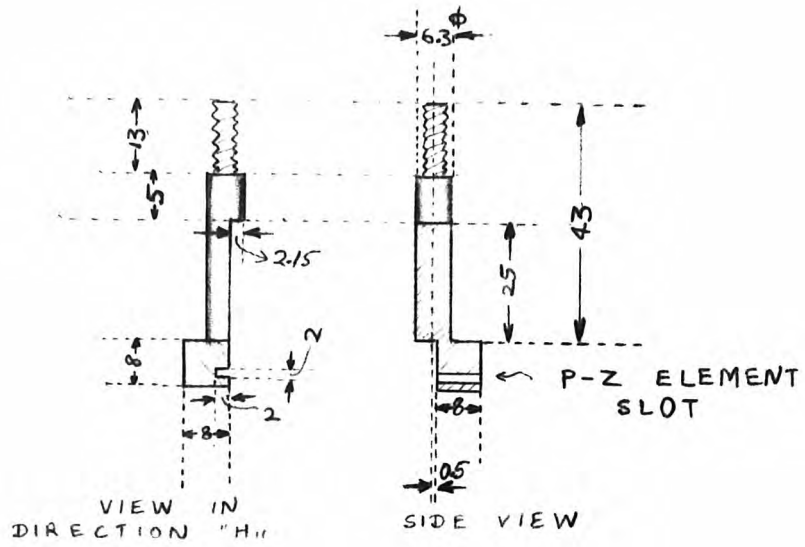


Fig. B-2 Drawings of the extension and vibrating rods.

APPENDIX B

Drawings of Apparatus

In fig. B-1a and B-1b the detailed drawings of the conditioning chamber are presented.

Figure B-2 shows the exact drawings of the extension and vibrating rod.

All dimensions are given in millimetres.

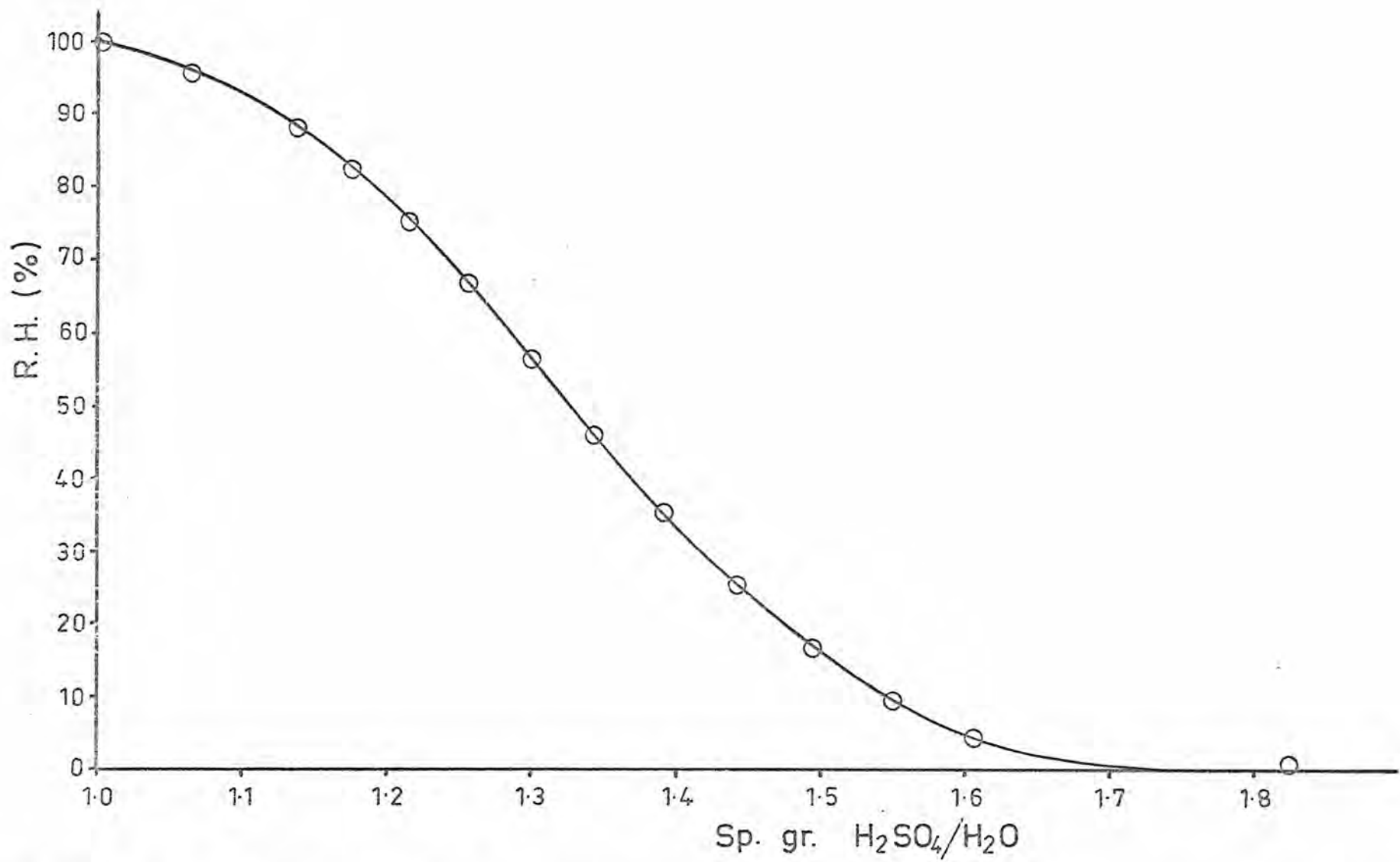


Fig. C-1 Plot of the equilibrium relative humidity above a sulfuric acid/water solution against specific gravity of the solution

APPENDIX C

C.1 Solutions for Maintaining Constant Relative Humidity

In the following table the relative humidity corresponding to each saturated salt solution at 25⁰C is given. The data have been taken from reference (76).

Solid Phase of Salt	Per Cent R.H.
K ₂ Cr ₂ O ₇	98
NH ₄ H ₂ PO ₄	93
KNO ₃	92.5
(NH ₄) ₂ SO ₄	81.1
NH ₄ Cl	79.3
NaCl	75.3
NaNO ₃	73.8
NaBr.2H ₂ O	57.7
Mg(NO ₃) ₂ .6H ₂ O	52.9
MgCl ₂ .6H ₂ O	33
LiCl .H ₂ O	11.1

To obtain relative humidities other than the ones given in the above table, sulphuric acid/water solutions were used. The relative humidity corresponding to a particular H₂SO₄/H₂O solution was determined from measurements of the specific gravity of the solution using data relating relative humidity to specific gravity. The relationship between specific gravity of the solution and relative humidity is presented in fig. C-1; the data have been taken from reference (76).

C.2 Calculation of the Required Quantity of Buffer Wool

A satisfactory way to conduct measurements at constant relative humidity is to use a certain quantity of wool as a buffer. The wool buffer is transferred quickly into the chamber after it has been conditioned in a separate vessel. Following are calculations for the approximate amount of wool required to keep the regain in wool within a specified small range.

For this case the ideal gas equation of state is sufficient as can be easily shown. For n moles of water vapour within the chamber of initial free volume V_i , initial partial vapour pressure P_i and initial temperature T_i we have

$$P_i V_i = nRT_i \quad (C-1)$$

while for the initial state of the total atmosphere within the chamber we have

$$PV_i = (n+n') RT_i \quad (C-2)$$

where P is the total pressure (ambient) which remains constant and n' is the effective number of moles of the dry atmosphere. If the temperature is increased to T_f , there will be an extra amount of vapour Δn , which has evaporated from the buffering wool. For the final state of equilibrium the corresponding equations will be (total pressure is constant)

$$P_f V_f = (n+\Delta n) RT_f \quad (C-3)$$

$$PV_f = (n+\Delta n+n') RT_f \quad (C-4)$$

The simultaneous solution of the equations (C-1), (C-2), (C-3) and (C-4) yield for the final relative humidity in the chamber

$$RH_f = \frac{(RH_i P_{s_i} V_i + RT_i \Delta n) P}{(P V_i + RT_i \Delta n) P_{s_f}} \quad (C-5)$$

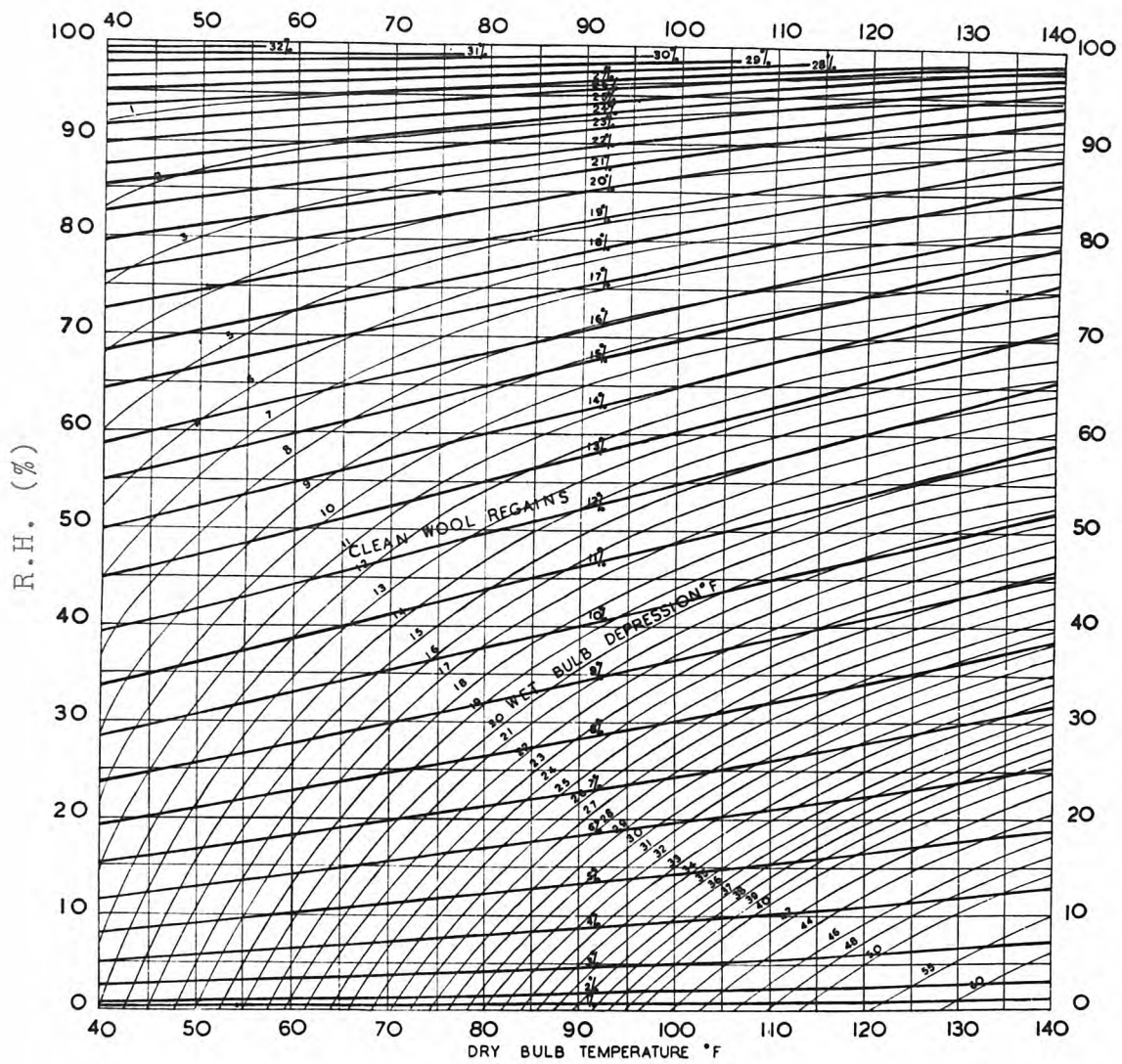


Fig. C-2 Nomogram for equilibrium regain in wool.

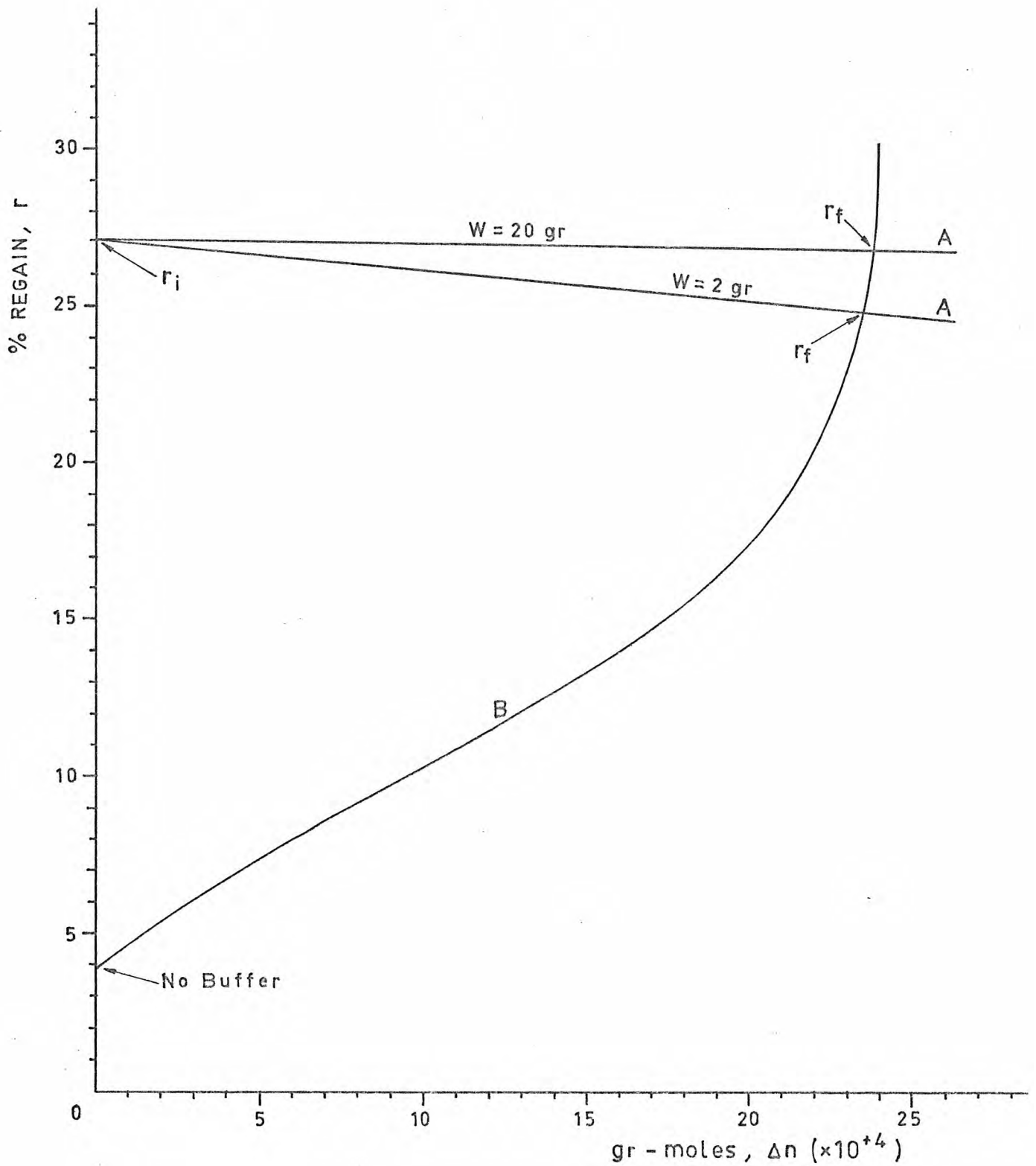


Fig. C-3 The simultaneous solution of equations (C-6) (curves A) and (C-8) (curve B) for the regain r against Δn . The two curves A correspond to two different amounts of buffer wool of 2 gr and 20 gr.

where P_{si} and P_{sf} are the saturation vapour pressure at the initial and final temperature, RH_i and RH_f the initial and final relative humidity, which is defined as

$$RH = \frac{P_i}{P_{si}}$$

If the weight of dry wool is W grams, with initial regain r_i , the regain r at a different temperature will be

$$r = r_i - \frac{1800}{W} \Delta n \quad (C-6)$$

The curves of fig. C-2 give the graphical relation between RH , T_f and r^{96}

$$r = r(T_f, RH) \quad (C-7)$$

The RH is a function of n and T_i given by (C-5), therefore

$$r = r(T_i, T_f, \Delta n) \quad (C-8)$$

The common solution of (C-6) and (C-8) yields the required final regain. This can be done graphically since the function (C-8) is not given analytically. In fig. C-3 the relationships (C-6) and (C-8) have been plotted versus Δn and their common intercept gives the final regain.

The values of the various parameters used for these plots are

$T_i = 294^{\circ}K$	$P_{si} = 25.05 \times 10^3 \text{ dyn/cm}^2$	$RH_i = 0.95$
$T_f = 333^{\circ}K$	$P_{sf} = 199.2 \times 10^3 \text{ dyn/cm}^2$	$r_i = 27\%$
$V_i = 270 \text{ cm}^3$	$P = 10^6 \text{ dyn/cm}^2$	$R = 8.31 \times 10^7 \text{ erg.mol}^{-1} \text{ gr}^{-1}$

By choosing different values for W for the straight line (C-6) we find for each case how much the initial regain changes. For the graph we have taken $W = 20 \text{ gr}$ for which the change of regain is only 0.2% or $W = 2 \text{ gr}$ for which the change of regain is 2%. If there is no buffering wool, the final regain in a single fibre in the given initial volume could be 3.7% i.e. a change of 23.3% regain.

REFERENCES

1. Algie, J.E., Text. Res. J., Vol. 34 No. 6, June 1964.
2. Algie, J.E., and Watt, I.C., Text. Res. J., Vol. 35, No. 10, October 1965.
3. Armstrong, L.D. and Feughelman, M., Text. Res. J., Vol. 39, No. 3, pp. 261-272, March 1969.
4. Bagley, E. and Long, F., J. Am. Chem. Soc., 77, 2172 (1955).
5. Barkas, W.W., "Swelling Stress in Gels", Forest Products Research Special Report, No. 6, H.M.S.O. (1945).
6. Becker, G.W., Materie Plastice ed. Elastomeri, 35, 1387 (1969).
7. Bendit, E.G., Nature 179, 535 (1957).
8. Bendit, E.G., Feughelman, M., Fraser, R.D.B., and MacRae, T.P., Text. Res. J., Vol. XXIX, No. 3, March 1959.
9. Bendit, E.G., Text. Res. J., 30, 547, 1960.
10. Bendit, E.G., Text. Res. J., 30, 547 (1960).
11. Bendit, E.G., Text. Res. J., 38, 15 (1968).
12. Bendit, E.G., and Feughelman, M., Encyclopedia of Polymer Science and Technology, Vol. 8, pp. 1-44, 1968.
13. Bull, H.B., J. Am. Chem. Soc., 67, 553, 1945.
14. Chaikin, M., and Chamberlain, N.H., J. Text. Inst., T25 (1955).
15. Chapman, B.M., and Feughelman, M., J. of Polymer Science: Part C, No. 20, pp. 189-199 (1967).
16. Ciferri, A., and Smith, K.J., Jr., J. Polymer Sci., A, 2, 731 (1964)
17. Crick, F.H.C., Acta. Cryst., 6, 685 (1953); Crick, F.H.C., Acta. Cryst., 6, 689 (1953).

18. Danilatos, G.D., and Feughelman, M., Text. Res. J., Vol. 46, No. 11, November 1976.
19. Dobb, M.G., Fraser, R.D.B., and MacRae, T.P., III^eme Cong. Intern. Recherche Textile Lainière (Paris) 1, 95 (1965).
20. Dobb, M.G., Nature 202, 804 (1964).
21. Downes, J.G., and Mackay, B.H., CSIRO Wool Conference, W/D. 131, July 19, 1955.
22. Downes, J.G., and Nordon, P., Nature, Vol. 203, No. 4946, P. 719.
23. Druhala, M., and Feughelman, M., Colloid & Polymer Sci., 252, 381-391 (1974).
24. Druhala, M., PhD Thesis, UNSW, Australia, 1973.
25. Dunlop, J.I., and Teasdale, D., Research Memorandum, No. 23, "Determination of Compressive Bulk Modulus of Fibrous Masses from Acoustic Impedance Measurements, School of Physics, UNSW, Australia, 1973.
26. Farrant, J.L., Rees, A.L.G., and Mercer, E.H., Nature 159, 535 (1947).
27. Ferry, J.D., "Viscoelastic Properties of Polymers", John Wiley & Sons, Inc.
28. Feughelman, M., and Rigby, B.J., Proceedings of the Intern. Wool Text. Re. Conference, Australia, 1955.
29. Feughelman, M., and Haly, A.R., Text. Res. J., 28, 453, 1958.
30. Feughelman, M., Text. Res. J., Vol. XXIX, No. 3, March 1959.
31. Feughelman, M., J. Appl. Pol. Sci., Vol. II, pp. 189-191, Sept-Oct 1959.
32. Feughelman, M., Text. Res. J., Vol. XXIX, No. 12, December 1959.
33. Feughelman, M., and Robinson, M.S., J. Appl. Polymer Sci., 1, 371-372 (1959).

34. Feughelman, M., and Haly, A.R., *Biochim. Biophys. Acta*, 1959, 32, No. 2, 596.
35. Feughelman, M., and Haly, A.R., *Kolloid-Z*, 168, 107 (1960).
36. Feughelman, M., and Haly, A.R., *Colloque Structure de la Laine*, Paris, July 1961, 159, (Institute Textile de France).
37. Feughelman, M., and Haly, A.R., *Text. Re. J.*, Vol. 32, No. 3, March 1962.
38. Feughelman, M., and Nordon, P., *Applied Polymer Science*, Vol. VI, No. 24, pp. 670-673, Nov-Dec 1962.
39. Feughelman, M., *Nature*, Vol. 200, No. 4902, pp. 127-129, October 12, 1963.
40. Feughelman, M., *Text. Re. J.*, 33, 1013-1022, 1963.
41. Feughelman, M., *Text. Re. J.*, Vol. 34, No. 5, May 1964.
42. Feughelman, M., *Illene, Congr. Intern. Recherche Textile Lanière*, Paris, 1965.
43. Feughelman, M., *III International Wool Textile Conference*, Vol. 1, No. 45, p. 619, Data: 29 Jun - 9 Jul 1965.
44. Feughelman, M., *Text. Res. J.*, Vol. 36, No. 3, March 1966.
45. Feughelman, M., *Nature*, Vol. 211, No. 5055, pp. 1259-1260, September 1966.
46. Feughelman, M., and Reis, P.J., *Text. Res. J.*, Vol. 37, No. 4, pp. 334-336 (1967).
47. Feughelman, M., and M.S. Robinson, *Text. Re. J.*, Vol. 37, No. 6, June 1967.
48. Feughelman, M., and Robinson, M.S., *Text. Re. J.*, Vol. 39, No. 2, pp. 196-198, Feb 1969.
49. Feughelman, M., and Mitchell, T.W., *Text. Re. J.*, Vol. 39, No. 12, pp. 1162-1163, Dec 1969.

50. Feughelman, M., and Robinson, M.S., Text. Re. J., Vol. 41, No. 6, pp. 469-474, June 1971.
51. Feughelman, M., Applied Polymer Symposium, No. 18, 757-774 (1971).
52. Fraser, R.D.B., MacRae, T.P., Rogers, G.E., "Keratins Their Composition, Structure and Biosynthesis", Charles C. Thomas Pub., USA, 1972.
53. Fujita, H., Kishimoto, A., and Odani, H., Progr. Theoret. Phys. (Japan), Suppl. No. 10, 210 (1959).
54. Gross, B., "Mathematical Structure of the Theories of Viscoelasticity, Paris, Herman & Cie Editeurs, 1953.
55. Haly, A.R., and Feughelman, M., J. of Text. Inst., Vol. 51, No. 12, December 1960.
56. Haly, A.R., and Feughelman, M., Text. Re. J., Vol. 31, No. 2, Feb. 1961.
57. Haly, A.R., Text. R.J., 35, 889 (1965).
58. Haly, A.R., and Snaith, J.W., Biopolymers, 6, 1355, 1968.
59. Jeffrey, G.M., Sikorski, J., and Woods, H.J., Proc. Intern. Wool Text. Conf., Australia, F130 (1955).
60. Kinsler, L.E., Frey, A.R., "Fundamentals of Acoustics", John Wiley & Sons, Inc., New York/London.
61. Long, F.A. and Di Pietro, A.R., Abstracts, 128th Am. Chem. Soc. Meeting, Mineapolis, Minn., Sept 1965.
62. Mackay, B.H. and Downes, J.G., J. Appl. Polymer Sci., 2, 32-38 (1959).
63. Mackay, B.H., and Downes, J.G., J. of Text. Inst., Vol. 60, No. 9, 378-394, September 1969.
64. McCrum, N.G., Read, B.E., and Williams, G., "Anelastic and Dielectric Effects in Polymeric Solids, Wiley, New York, 1967.

65. Makinson, K.R., Aust. J. Biol. Sci., 7, 336 (1954);
8, 225-287 (1955).
66. Mason, P., Text. Re. J., Vol. 34, No. 9, September 1964.
67. Mason, P., Text. Re. J., Vol. 34, No. 11, November 1964.
68. Mason, P., Kolloid Z. uZ. Polymere, 202, 139 (1965).
69. Mason, P., Kolloid Z. uZ. Polymere, 218, 1, 46-52 (1967).
70. Mitchell, T.W., and Feughelman, M., Text. Re. J., Vol. 35,
No. 4, April 1965.
71. Mitchell, T.W., and Feughelman, M., Text. Re. J., Vol. 30,
No. 9, September 1960.
72. Morrison, J.L. and Hanlan, J.F., Nature 179, 528 (1957).
73. Morton and Herle, "Physical Properties of textile fibres",
Butterworth & Co. Ltd., and the Textile Institute, 1962.
74. Newns, A.C., Trans. Faraday Soc., 52, 1533 (1956).
75. Nordon, P., Text. Res. J., 32, 560-568 (1962).
76. Pande A., "Modern Hygrometry", Bombay, Somaiya, 1970.
77. Philips Data Handbook, Components and Materials, Part 4b,
October 1973.
78. Rogers, E.G., Ann. N.Y. Acad. Sci. 83, 378, 1959.
79. Rogers, E.G., and Filshie, B.K., in R. Borasky, ed. Ultra-
structure of Protein Fibres, Academic Press Inc. New
York, 1963, p. 123.
80. Ryder, M.L., and Stephenson, S.K., "Wool Growth", Academic
Press, London-New York, 1968.
81. Shishoo, R., and Lundell, M., Text. Re. J., 42, 285-291, (1972).
82. Sikorski, J., and Woods, H.J., L. of Text. Inst. 51, T 506
(1960).

83. Sikorski, J., and Woods, H.J., Leeds Philosophical Soc., (Scientific Section), Proc. V.5, Pt 4, 1950, 313-7.
84. Smithells, C.J., "Tungsten", Chapman & Hall Ltd., London.
85. Speakman, J.B., J. Soc. Chem. Ind., 49, 209T (1930).
86. Speakman, J.B., J. of Text. Inst, 1927, 18, T 431.
87. Stootman, F., PhD Thesis, UNSW, Australia, 1977.
88. Ward, I.M., "Physical Properties of Solid Polymers", Wiley-Interscience, London 1971.
89. Watt, I.C., Text. Re. J., Vol. 30, No. 6, June 1960.
90. Watt, I.C., Text. Re. J., Vol. 30, No. 9, September 1960.
91. Watt, I.C., and Kennett, R.H., Text. Re. J., 30, 489 (1960).
92. Watt, I.C., and Algie, J.E., Text. Re. J., Vol. 31, No. 9, September 1961.
93. Watt, I.C., Text. Re. J., Vol. 35, No. 12, December 1965.
94. Weighmann, H., Rebenfeld, L., and Dansizer, C., Text. Re. J., 36, 535 (1966).
95. Woo, J.L., and Postle, R., J. of Appl. Polymer Sci., Vol. 18, pp. 589-613 (1974).
96. "Wool Research", Vol. 3, Testing and Control in the Wool Industry, Wool Industries Research Association, Torridon, Headingley, Leeds 6.
97. Woods, H.J., Nature 164, 34 (1949).
98. Zener, C., "Elasticity and Anelasticity of Metals", Chicago Press, Chicago, Illinois, USA.
99. Feughelman, M., and Druhala, M., Proceedings of the 5th International Wool Textile Research Conference, Vol. II, September 1975, Aachen.
100. McMahon, G.B., and Watt, I.C., Text. Re. J., Vol. 35, No. 1, January 1965.

101. Bendit, E.G., Text. Re. J., Vol. 30, No. 8, August 1960.
102. Feughelman, M., J. Macromol. Sci-Phys., B7(3), 569-582 (1973).
103. Meredith, R., "The Mechanical Properties of Textile Fibres", North-Holland Publishing Company, Amsterdam, 1956.
104. Moncrieff, R.W., "Man-Made Fibres", Heywood Books - London.
105. McCall, D.W., U.S. N.B.S. Special Pub. 301, "Molecular Dynamics and Structure of Solids" by R.S. Carter and J.J. Rush (1969).